Wave attenuation due to vegetation: Duursche Waarden (case study)

M. de Bruijn

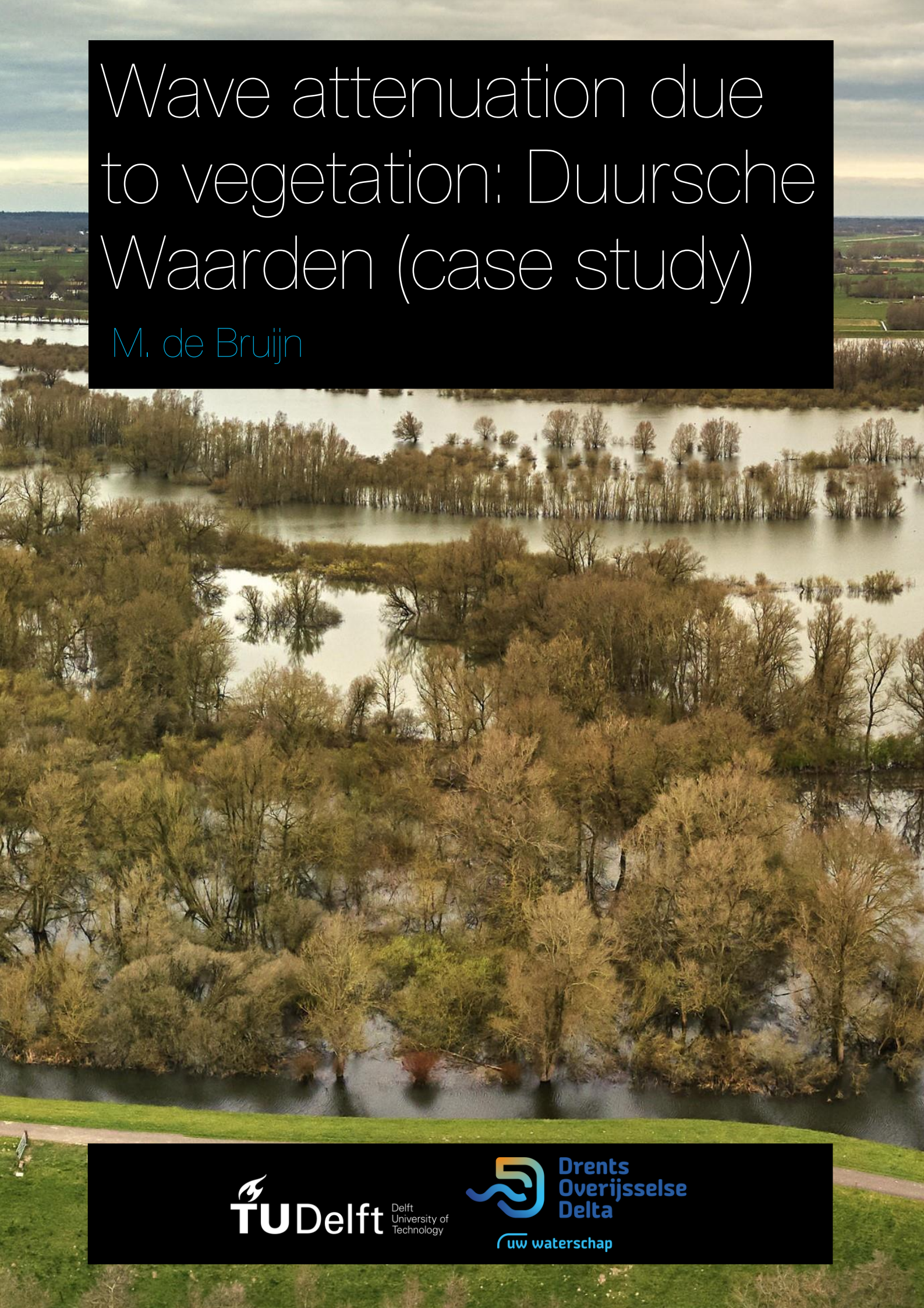

TU Delft Delft University of Technology

Drents Overijsselse Delta

uw waterschap

Wave attenuation due to vegetation: Duursche Waarden (case study)

By

M. de Bruijn

in partial fulfilment of the requirements for the degree of

Master of Science
in Civil Engineering

at the Delft University of Technology,
to be defended publicly on Monday November 2, 2020 at 11:45 AM.

Student number: 4395298
Project duration: March, 2020 - November, 2020
Thesis committee:

Dr. ir. B. Hofland,	TU Delft (chair)
Dr. ir. R.C. Lindenbergh,	TU Delft
Dr. Ir. B. van Wesenbeeck	Deltares
Ir. S. Kalloe,	TU Delft
J. Gruppen	WDOD

This thesis is confidential and cannot be made public until November 31, 2021.
Cover: Drone footage of Duursche Waarden in March, 2020

Abstract

Conventional dike reinforcement measures do not take vegetation into account, while vegetation contains wave damping properties. Reasoning for this is that vegetation in general is seen as temporary and hence may be removed in the future. In this case study for the Dutch waterboard WDOD, the wave damping properties of vegetation in a floodplain along the river IJssel (Duursche Waarden) are studied. Duursche Waarden consists of mostly willow species and is adjacent to a dike. It is part of Natura2000 and hence it is a protected vegetation area and not considered to be temporal.

A general approach is developed for similar sized (riparian) forests as Duursche Waarden (1.1 km^2) to map the vegetation and obtain the vegetation parameters. This approach is also applied to Duursche Waarden. First of all the different vegetation areas within the riparian forest are identified with the help of aerial photos and field observations after which they are prioritised with the help of a Multi Criteria Analysis. The prioritised vegetation areas are divided into uniform and non-uniform areas and studied in detail. Uniform and non-uniform areas are distinguished based on tree species, structure, height and density with the help of field observations, aerial photos and airborne Light Detection and Ranging (LiDAR) data. A representative distribution of the vegetation parameters over the different vegetation areas is obtained with the help of one method.

The vegetation parameters interesting for wave damping are the frontal area per volume and the bulk drag coefficient of leafless vegetation. Leafless vegetation is of interest since most extreme storms occur in winter. On top of that leaves seem to have insignificant contribution to wave damping in the full scale physical experiments of white willow trees conducted in the Delta Flume at Deltares. These experiments were performed in 2018. A new definition is introduced for the frontal area per volume. The frontal area density distribution over the height is estimated with the help of point clouds retrieved from TLS measurements and validated with hand measurements and studies of similar vegetation. Two methods are used in estimating the frontal area with the help of literature: the alpha shape and grid method. These methods are used for merged point clouds from Multiple Scanning Stations (MSS) and a point cloud from a Single Scanning Station (SSS). The SSS method includes a shadowing correction factor. Finally, the values of the frontal area per volume are chosen based on assessing the outcomes of the MSS method, SSS method and hand measurements. The bulk drag coefficient is estimated using selected values from literature. Dense vegetation contains relatively higher values for the vegetation parameters than sparse vegetation. This will result in more wave energy dissipation and hence more wave damping for dense vegetation.

The frontal area per volume of sparse to moderate dense woody vegetation (values on average of about 0.01-0.20 m^{-1}) in uniform areas is believed to estimated best and most efficiently with the MSS method. In non-uniform areas hand measurements are believed to be estimated best and most efficiently by hand measurements. The frontal area per volume of dense woody vegetation (values on average greater than 0.20 m^{-1}) is most uncertain. Therefore, both hand and TLS measurements (with the SSS method) should be used to estimate the frontal area per volume.

The wave attenuation by vegetation is estimated using the numerical wave model SWAN 1D and 2D computations including and excluding vegetation using the obtained vegetation parameters. No currents are included. Hydraulic conditions of Hydra-NL calculations using Bretschneider are used for both SWAN 1D and 2D computations. A comparison between Hydra-NL and SWAN 1D computations including model uncertainty for exactly the same conditions show similar outcomes for SWAN. SWAN 1D computations showed wave attenuation due to vegetation with a magnitude of 0 to about 44 cm for all dike locations adjacent to Duursche Waarden.

SWAN 2D computations without vegetation show significantly lower outcomes than 1D computations without vegetation: on average about 12 cm. This difference is explained by refraction and directional spreading resulting from the spatial variability in water depth and fetch of the studied area. Therefore the studied area is believed to be better described by 2D computations. One combination of the wind direction and water level is proven to be governing for all dike locations. Following 2D computations, the failure mechanism ‘erosion of the outer slope’ with a return period of 66666 year results in an estimated maximum wave height of 77 cm for dike locations adjacent to Duursche Waarden. This is a reduction of about 23 cm compared to the results of Hydra-NL. Indicative calculations suggest that dike reinforcements are still needed at Duursche Waarden.

The wave damping is estimated to be 16 to 24 cm at dike locations adjacent to relatively large vegetation areas of sparse to dense vegetation. Dike locations at which the significant wave height is the greatest are called critical dike locations. The wave damping for these critical dike points is estimated to vary between 4 to 7 cm. In a report by Deltares an overview is made of promising wave damping foreshores in the Netherlands. Rough estimations show possible wave damping at Duursche Waarden of about the same order of magnitude as found in this study. Also studies on similar vegetation show significant greater values for the wave damping, suggesting rather conservative than optimistic outcomes in this study.

Preface

This thesis has been produced as final work to fulfil my Master in Science program in Hydraulic Engineering at the Delft University of Technology. This work is carried out for the waterboard 'Waterschap Drents Overijsselse Delta'. I first want to thank my thesis committee of the Technical University of Delft: Bas Hofland, Roderik Lindenbergh and Su Kalloe. I am grateful for your help in these special COVID-19 days. Even though we almost always met by Zoom or Teams the collaboration was amazing. Thank you Bas Hofland for our discussions and sharing your knowledge. Also thanks to Roderik Lindenbergh for helping me with the TLS measurements and sharing your knowledge in writing a scientific report. Special thanks to my daily supervisor Su Kalloe for helping me with field observations, answering all my questions and transferring your enthusiasm for this topic. Also thanks to Bregje van Wesenbeeck for sharing her knowledge on the 'Building with Nature' concept and to Jan Gruppen of the waterboard for the enjoyable collaboration and always willing to help me. I definitely cannot forget my girlfriend, two brothers, parents and grandma. Thank you for your unconditional love and support of the previous months.

Max de Bruijn
Delft, November 2020

Table of contents

1 Introduction

This chapter provides a project description, problem description, research questions and the research approach.

1.1 Project description

The Netherlands is a low-lying, flood-prone country. In 1953 the southwest of the Netherlands was hit by disastrous floods and in the early 1990s the banks nearly bursted of rivers in the province Limburg. The Netherlands want to prevent these kind of events to happen and therefore the Delta Programme exists. Under the Delta Programme the government has collaborations with residents, businesses, knowledge institutes and NGOs. It sets out plans annually to protect the country from flooding, mitigate the impact of extreme storms and secure supplies of freshwater (Rijkswaterstaat, 2019).

The largest execution programme of the Delta Programme is the Dutch Flood Protection Programme (HWBP). This is an alliance between regional waterboards and Rijkswaterstaat. The programme focusses on flood-prone stretches in coastal zones and riverine areas of the Netherlands. The goal of the programme is to reinforce all primary flood defences in an efficient way by 2050 (Alliantie van waterschappen en Rijkswaterstaat). In 2012 HWBP concluded that about 264 primary flood defences with a length of 780 km through the whole country need to be reinforced in order to withstand (nearby) future conditions (Waterschap Drents Overijsselse Delta, 2019). Currently, the length of the required primary flood defence reinforcements has even increased more.

The regional waterboards manage about 90% of the primary flood defences. 'Waterschap Drents Overijsselse Delta' (WDOD) is one of the regional waterboards and is responsible for 29 primary flood defences (primarily dikes) with a length of 180 km. Thirteen projects will be finished in the period 2014-2050. One of the thirteen projects is 'Project IJsseldijk Zwolle-Olst'. This is a trajectory with 29 km of dike that needs to be reinforced. It contains rural area, but also more densely populated areas. Besides, it contains a lot of cultural history and ecological value. The primary flood defences are assessed by the regional waterboard. In the trajectory Zwolle-Olst the considered flood defences are dikes. The dikes are assessed on multiple failure mechanism. Four of these are a problem in the concerning trajectory: macro stability, height (overflow and wave overtopping), revetment of the dike and piping. The load on the dikes is depending on many variables to be discussed later.

The focus in this research is on Duursche Waarden in the trajectory Zwolle-Olst. Duursche Waarden is a nature reserve in a floodplain of the river IJssel. A secondary channel of the IJssel is connected with the floodplain. Over the years Duursche Waarden has made a transformation. Due to a decrease in biodiversity in the Netherlands a nature policy plan has been made 30 years ago with the goal to increase again the biodiversity. This resulted in the current image of Duursche Waarden which consists of areas covered with grass, shrubs and small alluvial forests (Wageningen University & Research, 2007). Duursche Waarden is part of the Natura 2000 (N2000). N2000 is a European network of protected nature reserves. In these reserves certain animal species and their natural habitat are protected to keep the biodiversity at a certain level or to increase it (Natura 2000). Hence this is the goal for Duursche Waarden as well.

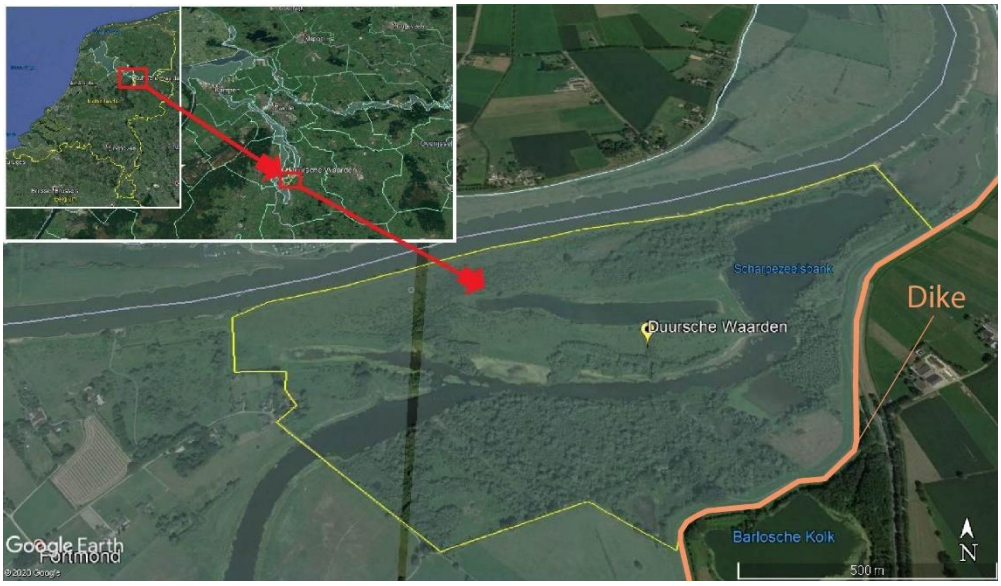

Figure 1.1: Location Duursche Waarden

Floodplains in front of a river dike can reduce the incoming wave load by dissipating energy by means of wave breaking and bottom friction (Vuik, 2019). Vegetation will increase the energy dissipation even more by means of blocking waves which will decrease the wave load. Duursche Waarden is located in a floodplain and contains different forms of vegetation: grass lands, riparian forests and shrubs. The presence of the riparian forest and shrubs in combination with a shallow foreshore suggest there will be wave attenuation in the Duursche Waarden. However, the HWBP does not take into account vegetation on floodplains and this can result in unnecessary costs.

Many studies are spent on wave attenuation by vegetation since (Dalrymple, et al., 1984). From there on it was recognized that that drag forces due to pressure differences cause most dissipation due to vegetation in wave energy. The diameter of the stem b_v, the amount of stems per area N and the bulk drag coefficient $\tilde{C}_D$ are found to be important parameters in wave attenuation by vegetation in later studies (e.g. (Kobayashi, et al., 1993), (Mendez, et al., 2004) and (Suzuki, et al., 2011)). Together they form the so called vegetation factor: $V_f = b_v N \tilde{C}_D$.

Currently nature-based solutions or solutions including the 'Building with Nature' concept are increasingly promoted (Vuik, 2019). This concept integrates (processes of) nature in the design of hydraulic engineering projects and allows design and nature to be sustainable and adaptable (Ecoshape). In this way the riverine or coastal ecosystems benefit while also the impact of extreme weather conditions is reduced. Nature-based flood defences can stand alone, but can also function in combination with engineered defences. The perfect example for this is a floodplain in front of an engineered dike as the floodplain reduces the wave impact on the dike. This research hopes to contribute in showing the efficiency and possibilities of wave attenuating, vegetated foreshores. Hopefully one day, the use of vegetation on foreshores will be a widely used method to reduce wave load and will be an example of a both ecological value gaining and economical attractive solution.

1.2 Problem description

The dike reinforcements located at Duursche Waarden are based on hydraulic conditions obtained from a legally prescribed probabilistic model. However, these hydraulic conditions do not include the effect of the vegetation on the governing waves. Reasoning for this is that vegetation in general is seen as temporary and hence may be removed in the future. If this happens the design of the dike may not hold anymore and therefore this conservative approach has been chosen.

As stated before the Duursche Waarden is part of N2000 and therefore it is very unlikely any vegetation will be removed in the future. The magnitude of wave attenuation due to the vegetation can result in a reduced reinforcement of the dike and hence is of economic interest. Besides, if vegetation is proven to damp waves and can be quantified this could be widely used in the future to incorporate nature in designs for flood defences. This concept of 'Building with Nature' adds ecological value to the area and can reduce the dimensions of flood defences like dikes.

1.3 Research questions

Main research question:
How can one accurately account for the wave attenuation by vegetation on flood safety for the dike's failure mechanism 'erosion of the outer slope' due to wave attack?

Sub research questions:

- How are the vegetation areas going to be mapped and what vegetation areas will result in most wave damping?
- How can the vegetation parameters for the most interesting vegetation areas be obtained?
- What is the estimated wave height and attenuation for the critical dike locations?
- How can the wave damping capacity effectively be monitored?

1.4 Research approach

First of all it is of great importance to understand the design criteria for the reinforcement of the dikes. Based on WBI (Wettelijk Beoordelingsinstrumentarium), the legal Dutch guidelines for assessment of primary flood defences, the failure probability for the failure mechanism is determined. The waterboard WDOD did some initial computations using statistical data of the discharge, wind speed and directions with the program Hydra-NL which uses the empirical formulas of Bretschneider. These initial computations resulted in different hydraulic conditions (wind speed, wind direction and water level) for dike locations at Duursche Waarden. These hydraulic conditions will be used in this study.

The theory behind wave attenuation due to vegetation will be considered with the help of a literature study. The goal is to understand what parameters of the vegetation are of interest and what these vegetation parameters depend on. This knowledge was crucial in order to set up an efficient field work program to collect the right vegetation data.

A new definition is introduced of the spatial frontal area distribution. Then based on the governing wind directions obtained from Hydra-NL a Multi Criteria Analysis (MCA) is set up to predict the most wave attenuating vegetation areas. Methods for uniform and non-uniform vegetation areas are described to make a clear plan of the types and density of tree species in the prioritised vegetation areas. This is done with the help of observations during field trips, drone footage, Google Earth images and AHN 3. A clear distribution of the vegetation parameters over Duursche Waarden can be retrieved based on the plan of different tree species. Finally the results of hand measurements and ranges of the bulk drag coefficient are discussed.

The frontal area (per volume) of leafless vegetation is an important parameter that can be obtained from different types of measurements. First of all, leafless vegetation is of interest since most extreme storms occur in winter. On top of that leaves seem to have insignificant contribution to wave damping in the full scale physical experiments of white willow trees conducted in the Delta Flume at Deltares (Wesenbeeck, et al., 2020 (to be published)). These experiments were performed in 2018. Hand measurements, pixel image analysis of photographs, AHN 3 (Actuele Hoogtebestand Nederland 3) point cloud data and Terrestrial Laser Scanner (TLS) measurements were considered to estimate the frontal area. Pixel image analysis of photographs is hard to use in field experiments due to the uneven background, with AHN 3 point cloud data the pursued accuracy of millimetres cannot be achieved and with hand measurements the frontal area only up to an height of two metres can be estimated. TLS measurements generate 3D point clouds consisting of millions of (xyz) points with an accuracy of millimetres in only a few minutes. Therefore TLS measurements have been used to estimate the frontal area. Also hand measurements have been done in order to check whether TLS results are of the same order of magnitude.

Possible errors in TLS measurements for estimating the frontal area are evaluated. Hereafter, different techniques of estimating the frontal area and studies on similar vegetation are discussed. Then two methods in estimating the frontal area are compared. With the help of mainly one method the frontal area is estimated for uniform and non-uniform parts based on TLS measurements with Multiple Scanning Stations (MSS). Then the frontal area is estimated with the help of a TLS measurement with a Single Scanning Station (SSS) in combination with a shadowing (error in TLS measurement) correction factor. Outcomes of TLS measurements with MSS and SSS for the frontal area (per volume) are compared. Based on the hand measurements outcomes of MSS or SSS are going to be used in estimating wave attenuation due to vegetation.

The wave attenuation is estimated with the help of a hydraulic numerical model. The goal of using a numerical model is to see the damping influence of vegetation on the significant wave height. Multiple models are available for estimating the wave propagation on a foreshore, and hence can also be used on a floodplain. Models such as SWAN, XBeach and SWASH have their own characteristics and processes taken into account. The ability of taking into account the vegetation is of great importance in choosing the right numerical model for this study. As all three models enable to describe the present vegetation in quite some detail, all three models would satisfy. However, XBeach and SWASH are not used since both are not used for formal safety calculations. In contrast, SWAN is suited and used in formal safety calculations and will therefore be used as numerical model for estimating the wave height and damping. SWAN is efficient and can be used for the short-crested wind-generated waves on floodplains. In SWAN VEG wave energy dissipation over a vegetation field with vegetation parameters varying over depth is possible. More information on SWAN can be found in Appendix SWAN.

The governing hydraulic conditions (and effective fetches for 1D computations) of Hydra-NL are used for all SWAN computations. First of all, a SWAN 1D computations are compared with Hydra-NL (Bretschneider) computations. This gives insight into the differences between SWAN and Hydra-NL. A 2D grid of the bottom level is made and a line is drawn in the governing wind direction to get a representative bottom level for the 1D computations. Then for all dike locations adjacent to Duursche Waarden SWAN 1D computations are made with and without vegetation in order to estimate the wave damping due to vegetation. Hereafter SWAN 2D computations with and without vegetation are done to include spatial variety in depth and fetch. Finally a SWAN 2D sensitivity analysis is carried out for different water levels, wind speeds and vegetation parameters based on relevant studies and hand measurements. This gives more insight into the contribution of these parameters in wave attenuation due to vegetation.

Finally, a general approach is developed for similar sized (riparian) forests as Duursche Waarden (1.1 km^2) to map the vegetation and obtain the vegetation parameters.

In Figure 1.2 a schematic overview of the research approach is illustrated. The arrows from one box to another mean that information is needed from one box in order to start the plans in the other box. The arrows in both directions between ‘Vegetation’ and ‘TLS measurements’ symbolise on one hand the comparison between the outcomes of the TLS and hand measurements and on the other hand that the vegetation should be mapped first in order to know of what and where the TLS measurements should be done.

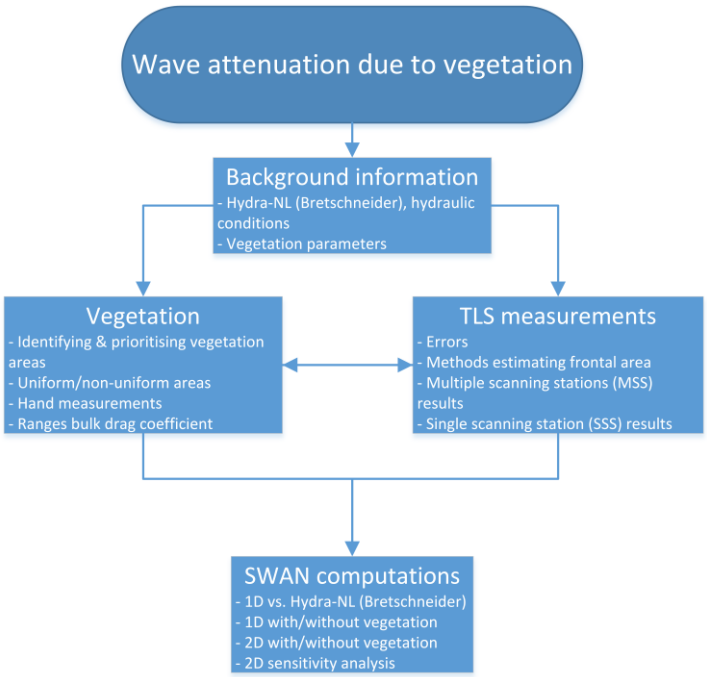

Figure 1.2: Schematic overview of the research approach

2 Background information

This chapter provides information on the hydraulic conditions used for Duursche Waarden and treats the vegetation parameters important for wave attenuation due to vegetation.

2.1 Hydraulic conditions Duursche Waarden

This thesis is officially started in early March, 2020. The regional waterboard WDOD just completed one of the four stages in this dike reinforcing project: the exploration stage. This is the first of the 4 different stages:

- Exploring
- Plan elaboration
- Realization
- Aftercare

In the exploring stage all the primary flood defences have been analysed in the trajectory Zwolle-Olst. The primary flood defences in this trajectory are dikes and hydraulic works/structures. Trajectory Zwolle-Olst is part of the dike trajectory Salland (53-2). For this and many other trajectories a maximum allowable failure probability is set which is based on estimated economical damage and amount of deaths. The maximum allowable failure probability for the dike trajectory Salland is 1/3000 per year (Overheid). Within the dike trajectory every 200 meter a dike location is defined which is assessed on several failure mechanisms. In case several consecutive dike locations have similar characteristics and surrounding environment, they can be assessed in the same way which saves computation time. These are called dike segments and consist of approximately 1-10 dike locations. One of these dike locations is an output point ('uitvoerpunt' in Dutch) and represents the dike segment. Hence, the calculations for a dike segment are done with such an output point. The dike segments in trajectory Zwolle-Olst are assessed on the failure mechanisms height (critical discharge due to wave overtopping), piping, macro stability and erosion outer slope (due to wave attack on revetment):

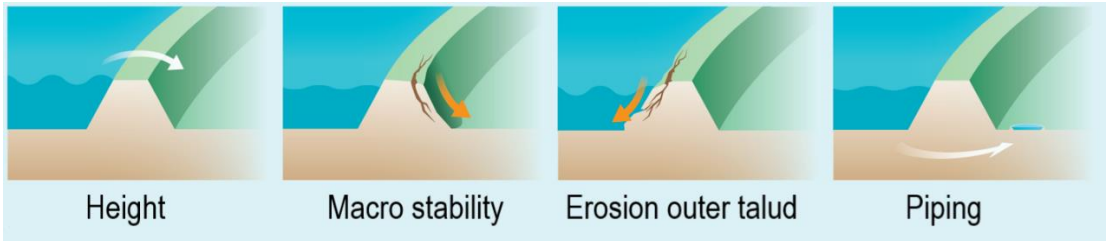

Figure 2.1: Failure mechanisms trajectory Zwolle-Olst © WDOD

Concerning the dike adjacent to Duursche Waarden two failure mechanisms are identified which lead the need of dike reinforcement: piping and erosion outer slope (due to wave attack on revetment, GEBU). Both failure mechanisms are assessed individually. The focus with piping is on the hydraulic head at the inner and outer slope, which means especially the water level is of importance. A critical hydraulic head difference leads to the transport of water and sand particles under the dike and this results into instability of the dike. The failure mechanism erosion outer slope is mainly caused by wave attack. In case a critical cyclic wave load on the dike is reached this results in erosion of the outer slope and hence instability of the dike. The combination of water level and wave characteristics is of importance for this failure mechanism and is also the most interesting for this research on attenuating waves due to vegetation.

As mentioned above four failure mechanisms are assessed in the dike trajectory Salland. The maximum allowable failure probability is divided over these failure mechanisms. Each failure mechanism has a fixed part of the 1/3000 per year failure probability of Salland (Rijkswaterstaat, Deltares en VNK2, 2013). A fault tree is presented in Figure 2.2 containing the fixed probabilities (Rijkswaterstaat, Deltares en VNK2, 2013). For erosion of the outer slope due to wave attack on grass (GEBU) at Duursche Waarden this failure probability is 4.5% of 1/3000 per year: 1/66666 per year (see Appendix Calculation GEBU Duursche Waarden for calculation).

Only two out of four failure mechanisms are identified for the dike adjacent to Duursche Waarden. This does not result in the division of 1/3000 per year over two failure mechanisms, but still the fixed values are used as determined in (Rijkswaterstaat, Deltares en VNK2, 2013). The dike reinforcements are meant to withstand extreme conditions in 2075. Only statistical data is available for 2050 and 2100. This means that first separate calculations are done with the corresponding statistical data in order to get the hydraulic conditions of 2050 and 2100, which is done with the program Hydra-NL. Then with the help of linear interpolation the hydraulic conditions of 2075 are obtained.

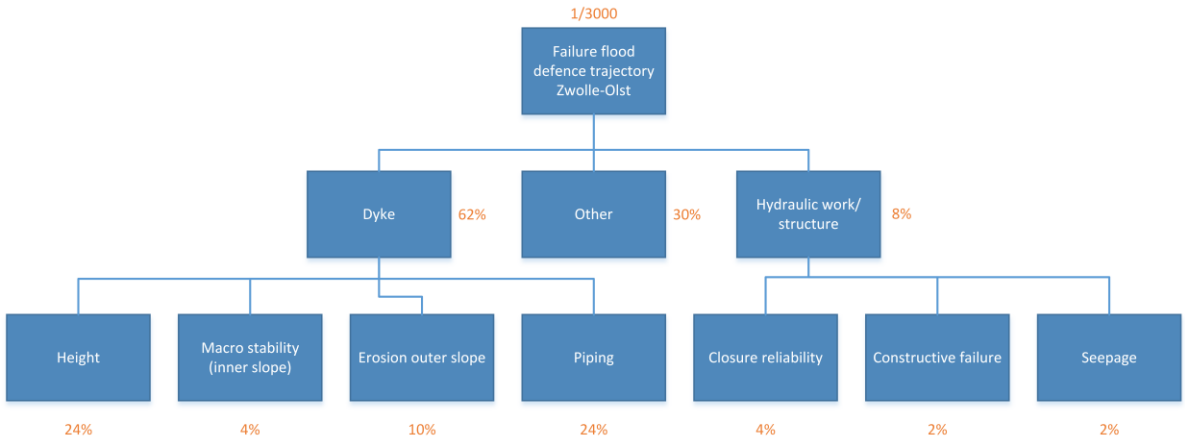

Figure 2.2: Fault tree trajectory Zwolle-Olst

Hydra-NL is doing the calculations with a dataset corresponding to a half year of winter. The dataset contains exceedance probabilities of the discharge of the IJssel, water level of the Lake IJssel ('IJsselmeer') and wind speed. Also the instantaneous wind direction and storm duration probabilities are incorporated. The dataset is divided into six periods and each period contains one extreme storm. Each period takes 30 days and is simulated with the above described parameters. Usually a storm is build up to a certain peak, then stays constant at this peak for a while and gradually ends. This results in a trapezoidal shaped storm. In order to simplify modelling a block shaped storm a used. In order to compensate for the build-up and gradual ending in the 'trapezoidal storm', the 'block storm' contains a longer peak duration, see Figure 2.3.

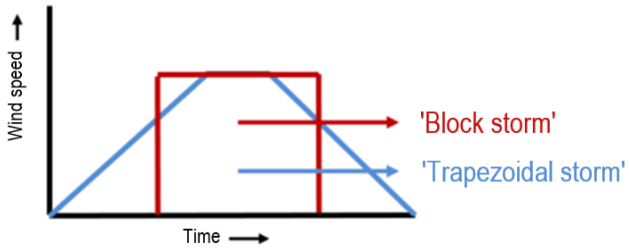

Figure 2.3: Storm schematization © WDOD

In a calculation of such a block storm many parameters and processes are included. First of all geometry parameters are fixed such as: foreland, slope, crest height of the dike, dike orientation in degrees North, roughness. The type of revetment on the dike in combination with wave height, wave period and angle of incidence result in coefficients for determining the wave height. Extrema discharge of the IJssel, water level of the IJssel Lake, water level rise of Lake IJssel due to climate change (+ 0.25 m) and an upper limit of the wind speed (50.00 m/s) is incorporated. Uncertainties concerning water level, wave height and wave period are also taken into account (see Appendix Hydra-NL).

The phenomena storm surge of the IJssel Lake is take into account as well. Besides the water level due to river discharge also storm surge influences the water level. In case of a Western wind, the IJssel Lake is pushed towards the river IJssel causing water level rise for a certain length of the river. The storm surge barrier Rampspol ('Rampspolkering') influences this water level rise too. It is located downstream of Duursche Waarden, near the IJssel Lake. Hydra-NL makes calculations with an open and closed storm surge barrier Rampspol. In case the IJssel Lake is pushed towards the river IJssel the Rampspol will close. The result is that more water is pushed towards the river and hence an higher water level is expected upstream (also at Duursche Waarden). An higher water level allows the development of higher waves, because the waves are less depth-limited. Therefore it makes also sense that an open Rampspol contributes minimal to the failure probability of dike segments (~ 1%) and hence only the scenario of a closed Rampspol will be considered. A failure probability of the Rampspol is also taken into account in Hydra-NL.

The failure mechanism 'erosion outer slope' depends mainly on two hydraulic conditions: water level and wave characteristics (disregarding the strength of the soil in the dike and the revetment on the dike). These hydraulic conditions are a result of stochastic variables used in Hydra-NL at which especially river discharge and wind (speed and direction) play a significant role. For every part in the trajectory Zwolle-Olst the balance between probability space of river discharge and wind differs. Downstream of the IJssel the water level is highly influenced by the wind pushing the water into the IJssel, while more upstream the water level is mainly influenced by the river discharge (leaving less probability space for the wind). For every entered water level (with steps of +0,5 m) Hydra-NL is looking for the maximum wave impact. This is a combination of the wave height and period which can be determined at the entered water level for a specific dike segment with corresponding river discharge and wind

parameters. The distribution of the probability space over the stochastic variables in Hydra-NL and the entered water level determine the wave characteristics. The result is an interplay between the water level and wave characteristics and results in the combination of water level and wave characteristics that damage the outer talud most and hence are governing.

The governing wave height and period are expressed in Strength S [-] that stands for the impact on or strength of the wave on the dike. The wave characteristics depend on multiple aspects: effective fetch, wind speed, wind direction and water depth. The effective fetch is a weighted average of all projections on the chosen wind direction within a chosen amount of degrees (see Appendix Hydra-NL). The water depth (with steps of +0.5 m) and the effective fetch are fixed parameters. Besides the limiting factor of the water depth, the wave characteristics are mainly depending on the wind speed. The wind speed takes most of the probability space of the wave characteristics and are based on historical data of airport Schiphol. This is a conservative assumption since Schiphol is located closer to the coast than the trajectory Zwolle-Olst and hence gives higher wind speeds.

In total sixteen wind directions are defined, but only a few are of interest for the dike adjacent to Duursche Waarden. In case the wind direction is offshore, the wind direction is not taken into account. Of the remaining wind directions, SW (225 °N) until N (0 °N), only a few will be interesting since they involve a relatively large water depth and effective fetch. With the help of Bretschneider's formulas (Rijksoverheid) the wave height and period of every wind direction is determined in Hydra-NL:

$$H_s = \frac{0.283u^2 v_1}{g}\tanh\left(\frac{0.0125}{v_1}\left(\frac{gf}{u^2}\right)^{0.42}\right) \quad v_1 = \tanh\left(0.530\left(\frac{gd}{u^2}\right)^{0.75}\right) \tag{2.1}$$

$$T_s = \frac{2.4\pi u v_2}{g}\tanh\left(\frac{0.077}{v_2}\left(\frac{gF}{u^2}\right)^{0.25}\right) \quad v_2 = \tanh\left(0.833\left(\frac{gd}{u^2}\right)^{0.375}\right) \tag{2.2}$$

In which g is the gravitational acceleration [m/s^2], H_s the significant wave height [m], T_s the significant wave period [s], u_w the wind speed at an height of 10 meter [m/s], h the assumed average water depth over the water surface of the wind direction [m] and F the effective fetch [m].

Furthermore the following relationships hold for this case:

$$T_p = 1.08T_s \tag{2.3}$$

$$T_{m-1,0} = T_p/1.1 \tag{2.4}$$

$$H_{m0} = H_s \tag{2.5}$$

With T_p the peak period [s], $T_{m-1,0}$ the spectral wave period [s] and H_{m0} the spectral wave height [m].

The water depth, effective fetch and wind directions with corresponding wind speed and exceedance frequency for 2050 and 2100 can be seen in Appendix Hydra-NL for every output point (representing one dike segment). The calculated wave height and period is at the location of the toe of the dike. Influence of the river current is neglected in determining the wave characteristics. The different dike locations and segments adjacent to Duursche Waarden is shown in Figure 2.4, including the result of the governing hydraulic conditions for the different dike segments. In Table 2-1 the hydraulic conditions of the output points adjacent to Duursche Waarden following Hydra-NL are shown.

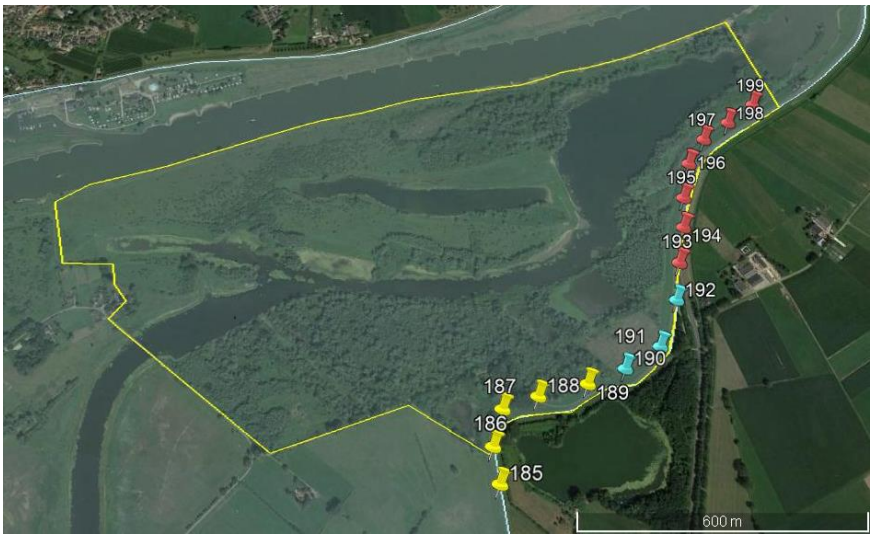

Figure 2.4: Dike locations adjacent to Duursche Waarden

Dike segment	Output point	Water level [m +NAP]	$H_{m0,toe}$ [m]	T_p [s]
185-189	185	5.70	0.915	3.85
190-192	190	5.70	0.995	3.975
193-199	193	5.64	0.96	3.94

Table 2-1: Hydraulic conditions of the different dike output points following Hydra-NL

For an overview of the way Hydra-NL makes calculations see Appendix Calculation steps.

2.2 Wave attenuation due to vegetation

The considered part is a floodplain located in Duursche Waarden. Therefore, the theory of wave propagation and characteristics on a foreshore will be used for Duursche Waarden. This theory is needed in order to understand the outcomes of numerical models such as SWAN. The most important characteristic of a wave are the wave height (H) and the wave period (T). The wave height is defined as the vertical distance between the top and the trough between two zero-crossings in a wave field. The wave period is defined as the horizontal distance between two downward zero-crossings. Different mechanisms will be discussed that will affect the wave height at a foreshore, especially the effect of vegetation and what vegetation parameters are of importance for determining attenuated waves.

2.2.1 Linear waves

Wave motion can be described by the continuity equations and the Navier-Stokes equation of motion. Problems arise when these equations have to be solved. Therefore Linear Wave Theory (LWT) provides an excellent alternative. In LWT a couple of assumptions are made. The most important are:

- Linearized surface boundary
- Horizontal and impermeable bottom

Neglecting non-linearities is a good approximation for not too steep waves in deep water ($ak << 1$) and small amplitude waves in shallow water ($a << h$ for kh is small) with a the wave amplitude [m], k the wave number [rad/m] and h the average water depth [m] (Bosboom, et al., 2015).
Wind generated waves in rivers will behave as surface gravity waves at the free surface. Gravity is the restoring force. An approximation fur such wave is a linear sine wave. This results in the following formulation (Schiereck, et al., 2016):

$$\eta = a \sin(\omega t - kx) \tag{2.6}$$

In which η is the water surface elevation [m], ω the wave frequency [rad/s], t the time [s], k the wave number [rad/m] and x the distance along x-axis in wave propagation [m].

According to LWT, for a linear sine wave the relation between wave frequency ω, the wave speed c and wave number k is:

$$\omega = \sqrt{gk \tanh\ kh} \tag{2.7}$$

$$c = \frac{gT}{2\pi} \tanh kh = c_0 \tanh kh \tag{2.8}$$

With g gravitational acceleration [m/s^2] and T the wave period [s]. This relation is called the dispersion relation. The magnitude and shape over the depth of horizontal orbital velocities over the depth are of importance for determining wave attenuation by vegetation. Horizontal orbital velocities are characterised differently for deep, transitional and shallow water. The orbital velocity is schematised in the next figure:

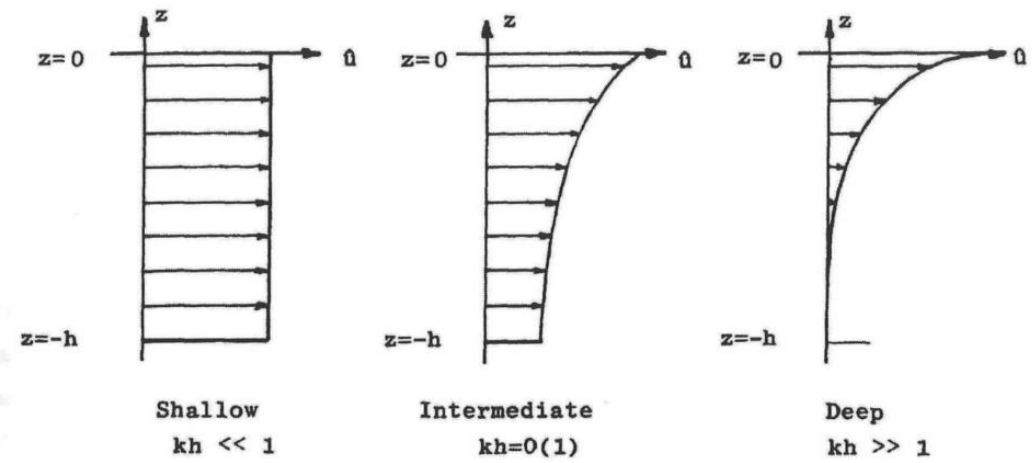

Figure 2.5: Horizontal orbital velocity profiles according to LWT (Bosboom, et al., 2015)

The horizontal orbital velocity is generally described by:

$$u(t) = \hat{u} \cos \omega t \tag{2.9}$$

In which $\hat{u}$ is the amplitude of the horizontal orbital velocities [m/s]:

$$\hat{u}(z) = \omega a \frac{\cosh k(h+z)}{\sinh kh} \tag{2.10}$$

In which h is the water depth [m] and z is a point along the z-axis where $z = 0$ is at the still water level and $z = -h$ is at the bottom.
For shallow water ($kh \ll 1$) the depth-uniform velocity amplitude [m/s] is simplified to:

$$\hat{u} = \frac{\omega a}{kh} = c\frac{a}{h} = \sqrt{gh}\frac{H}{2h} \tag{2.11}$$

In which H is the wave height [m].

2.2.2 Energy dissipation

Wave attenuation by vegetation originates from loss of energy in wave groups: energy dissipation. The energy in cross-shore direction to the toe of the dike is constant in case of no losses:

$$\frac{\partial F}{\partial x} = \frac{\partial (E * c_g)}{\partial x} = 0 \tag{2.12}$$

In which F is the wave force [N], E the wave energy [J/m^2] and c_g the wave group speed [m/s].
The wave energy E is expressed as:

$$E = \frac{1}{8}\rho g H^2 \tag{2.13}$$

In which ρ water density [kg/m^3] and H the (significant) wave height [m]. The wave group speed depends on the relative depth. Three categorisations are made: shallow water, intermediate/transitional water depth and deep water.

Energy dissipation is generally caused by white-capping (D_{wc}), bottom friction (D_{bf}), depth-induced breaking (D_{dib}) and due to vegetation (D_{veg}). These are all negative terms in the energy balance. There can also be a positive contribution to the energy balance by input of wind (S_{in}). This gives the following one-dimensional energy balance (Bosboom, et al., 2015):

$$\frac{\partial(E * c_g)}{\partial x} = S_{in} - D_{wc} - D_{bf} - D_{dib} - D_{veg} \tag{2.14}$$

Dissipation on vegetated foreshores or floodplains will be dominated by bottom friction, depth-induced breaking and vegetation (Bosboom, et al., 2015). Energy input of wind is generally neglected for relatively small foreshores. In this case the wave energy dissipation due to vegetation is of most importance.

2.2.3 Vegetation parameters

Most of the literature about wave attenuation use (Dalrymple, et al., 1984) as a starting point. This scientific paper will therefore be elaborated in more detail.

2.2.3.1 Background vegetation parameters

In (Dalrymple, et al., 1984) a model for calculating the combined refraction/diffraction of monochromatic linear waves is developed, including a term that counts for the dissipation of wave energy. Wave calculations are performed for a localized area of dissipation, based on a friction model for a spatial distribution of rigid vertical cylinders (or submerged trees).

(Dalrymple, et al., 1984) saw the interaction of waves with vegetation as energy that is dissipated due to work done by waves on the vegetation. The bed is assumed to be rigid and impermeable, since Linear Wave Theory or also called Airy wave theory (Bosboom, et al., 2015) is used. The conservation of energy equation is:

$$\frac{\partial(Ec_g)}{\partial x} = -\epsilon_v \tag{2.15}$$

In which E is the wave energy/unit area = $\frac{1}{2}\rho g a^2$ [J/m^2], ρ the fluid density [kg/m^3], g the gravitational acceleration [m/s^2], a the wave amplitude [m], c_g the wave group velocity [m/s] and ϵ_v the time-averaged energy dissipation due to vegetation [J/m^2].

A popular method of expressing wave dissipation is suggested by (Dalrymple, et al., 1984). Energy losses are calculated as actual work carried out by vegetation due to plant induced forces acting on the fluid expressed in terms of a (Morison, et al., 1950) type equation. In this equation the forces induced by a solid body (piles) in oscillatory flow are described and consist of two parts: an inertial (F_I) and drag force (F_D). The Morison equation is defined as follows:

$$F = F_D + F_I = \frac{1}{2}\rho \tilde{C}_D A|u|u + \rho C_m V \frac{\partial u}{\partial t} \tag{2.16}$$

In which F is the total force [N], F_D the drag force [N], F_I the inertial force [N, $\tilde{C}_D$ the drag coefficient for a singular element [-], A the cross-sectional area of the body perpendicular to the flow [m^2], u the horizontal flow velocity in oscillatory flow [m/s], C_m the inertia coefficient [-], V the body's volume [m^3]. In this method vegetation motion such as vibration due to vortices and swaying is neglected.

Only the drag force causes energy dissipation and is therefore of interest. The drag force can be divided into two components: drag force due to bottom friction and pressure difference. The drag force due to pressure differences is much larger than the drag force due to bottom friction. Therefore only the first is considered. This drag force can be seen as fluid resistance acting opposite to the motion of the wave-induced current. Based on this approach the time-averaged energy dissipation due to vegetation is defined as follows:

$$\epsilon_v = \overline{\int_{-h}^{-h+s} Fu\, dz} \tag{2.17}$$

In which s is vegetation height [m], the over-bar represents the time averaging of the energy dissipation term and F is the horizontal component of the force acting on the vegetation per unit volume [N/m^3]. Swaying motion and inertial forces are neglected and results in the following expressions of F by (Dalrymple, et al., 1984):

$$F = \frac{1}{2}\rho C_D A u|u| \tag{2.18}$$

In which C_D is the drag coefficient (constant over depth), A is the area of the cylinders perpendicular to the horizontal flow [m^2/m^3] and u is the horizontal velocity due to wave motion [m/s].

Combining (2.17) and (2.18) (Dalrymple, et al., 1984) came up with a definition of the wave energy dissipation due to vegetation:

$$\epsilon_v = Ba^3 = \frac{2}{3\pi}\rho C_D \frac{D}{k}\frac{\sinh^3 ks + 3\sinh ks}{3\cosh^3 kh}\left(\frac{gk}{\sigma}\right)^3\left(\frac{1}{b^2}\right)a^3 \tag{2.19}$$

In which D is the diameter of cylinders or plants [m], k is the wave number [rad/m], σ is the wave frequency [rad/s], b is the spacing between plants [m] and a is the wave amplitude [m]. Later, many researchers ((Kobayashi, et al., 1993), (Mendez, et al., 2004) and (Suzuki, et al., 2011))) found similar expressions as (2.19) based on the analytical solution of (Dalrymple, et al., 1984).

The transmission through the vegetation is determined with the help of the amount of wave energy dissipation (Dalrymple, et al., 1984). This is defined as follows:

$$K_t = \frac{H_t}{H_0} = \frac{a_t}{a_0} = \frac{1}{1+\alpha x} \tag{2.20}$$

In which H_t is the transmitted wave height after entering the vegetation field [m], H_0 is the incoming wave height before entering the vegetation field and α is defined as:

$$\alpha = \frac{2C_D}{3\pi}\left(\frac{D}{b}\right)\left(\frac{a_0}{b}\right)(\sinh^3 ks + 3\sinh ks)\left[\frac{4k}{\sinh kh\,(\sin 2kh + 2kh)}\right] \tag{2.21}$$

In which s is elevation of the top of the plant relative to the bottom [m].

It can be concluded that the drag force is responsible for most of the wave energy dissipation resulting in damped wave heights. Nowadays this is described by many papers (e.g. (Kobayashi, et al., 1993), (Mendez, et al., 2004), (Suzuki, et al., 2011) and (He, et al., 2019)) as:

$$F = \frac{1}{2}\rho C_D b_v N u|u| \tag{2.22}$$

In which ρ is the fluid density [], C_D is the drag coefficient [-], b_v is the diameter of each stem/branch [m], N is the number of branches per square meter [units/ m^2] and u is the horizontal velocity (perpendicular to the vegetation) due to wave motion.

2.2.3.2 Vegetation factor

In (Suzuki, et al., 2011) the empirical model of (Mendez, et al., 2004) is applied for a full wave spectrum in SWAN. This empirical model is based on (Dalrymple, et al., 1984) and included varying depths and the effects of wave damping due to vegetation and wave breaking for narrow-banded random waves. This empirical model was compared to experimental results with an artificial kelp field (Dubi, et al., 1995) which showed reasonable accuracy.

In (Suzuki, et al., 2011) equations of (Mendez, et al., 2004) are used for a full spectrum model in SWAN and includes vertical layer schematisation for mangrove vegetation (see Figure 2.6).

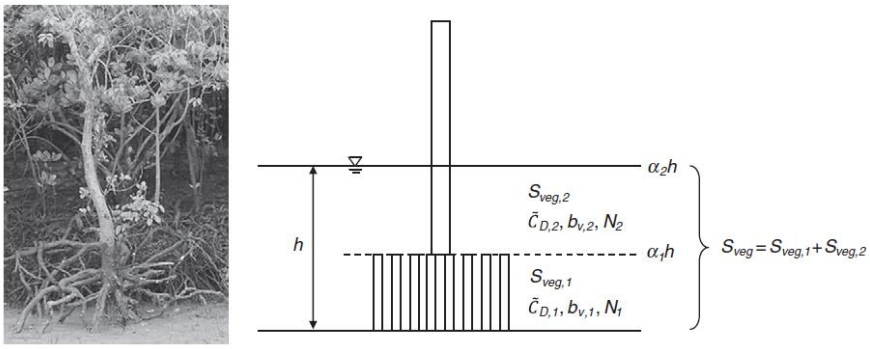

Figure 2.6: Layer schematisation for a mangrove species used in SWAN (Suzuki, et al., 2011)

Also a vegetation factor V_f is introduced, containing all relevant parameters for the vegetation:

$$V_f = b_v N \tilde{C}_D \tag{2.23}$$

With b_v the diameter of each branch/stem [m], N the number of branches/stems per square meter [unit/m^2] and $\tilde{C}_D$ the bulk drag coefficient [-]. This layer schematisation is also used nowadays in SWAN.

The vegetation factor is often used as a calibration factor when precise value of vegetation diameter and density are not available. In (Suzuki, et al., 2011) it can be seen that for larger wave periods layer schematization does not make a difference in determining wave attenuation by vegetation, while for short wave periods clear differences can be seen in use of layer schematization or not. If good vegetation data is available the bulk drag coefficient $\tilde{C}_D$ is often used as calibration parameter even though it is highly dependent on wave characteristics and hydrodynamics. Also processes that are not included in the (Dalrymple, et al., 1984) formulation such as vibration due to vortices and swaying is compensated by calibrating $\tilde{C}_D$.

The diameter of the branches b_v and the number of branches per square meter N can be obtained with measurements. The bulk drag coefficient $\tilde{C}_D$ will be estimated with the help of studies on wave damping vegetation.

2.2.3.3 Drag coefficient

The drag coefficient C_D is difficult to determine and therefore other studies with similar vegetation will be elaborated. Based on findings in studies with similar vegetation and relations to the drag coefficient C_D, an educated estimation of C_D will be made for the vegetation in this research.

First of all in studies with kelp or algae ((Kobayashi, et al., 1993), (Mendez, et al., 1999) and (Mendez, et al., 2004)), relations of C_D were found with the Reynolds number and the Keulegan-Carpenter number. Even though the vegetation in this research is not similar to kelp or algae, the relations provide a better insight into C_D. In (Kobayashi, et al., 1993) the Reynolds number (indicating laminar or turbulent flow) was found to be inversely proportional to the drag coefficient. The Reynolds number is defined as follows:

$$Re = \frac{b u_c}{v} \tag{2.24}$$

In which b is the width of the stem/branch [m], v is the kinematic viscosity [m^2/s] and u_c is the characteristic fluid velocity acting on the stem/brench [m/s]. In (Mendez, et al., 1999) separate expressions of C_D were found for swaying and non-swaying vegetation in flows due to regular waves. The drag coefficient C_D ranged between 0.09-1.55 for no swaying vegetation and between 0.33-6.9 for swaying vegetation.

In (Mendez, et al., 2004) the average bulk drag coefficient $\tilde{C}_D$ of kelp is introduced and found to be dependent on the Keulegan-Carpenter number. The following relations were found:

$$\boldsymbol{K} = \frac{u_c T_p}{b_v} \tag{2.25}$$

$$\boldsymbol{Q} = \boldsymbol{K}/\alpha^{0.76} \tag{2.26}$$

$$\tilde{C}_D = \frac{\exp(-0.0138\mathbf{Q})}{\mathbf{Q}^{0.3}} \quad 7 \leq \boldsymbol{Q} \leq 172 \tag{2.27}$$

In which u_c is the characteristic velocity acting on the plant and defined as the maximum horizontal velocity at the middle of the vegetation field $x = b/2$ and $z = -h + \alpha h$ [m/s], T_p the peak period of the wave [s], b_v the diameter of the branch/stem [m] and α the relative height of the plants [-]. They concluded that higher relative vegetation results in a greater dissipation and a wider vegetation fields result in a greater wave reduction.

In (Liu, et al., 2016) all the influencing factors of the dimensionless drag coefficient C_D was determined by dimensional analysis method. It can be concluded from this paper that F_r has only influence in case of a very low Froude number ($F_r < 0.1$).The Froude number is found to be inversely proportional to C_D. Furthermore a negative lognormal relation between the vegetation density λ and C_D and a linear relation between the relative submergence height h^* and C_D.

Also the drag coefficient C_D and the bulk drag coefficient $\tilde{C}_D$ cannot be interpreted as the same: C_D holds for an individual vegetation stand or object, while $\tilde{C}_D$ is interpreted more as an average value for multiple vegetation stands or objects. However, if all elements are the same they can be interpreted as the same. For all studies in Table 2-2 and Table 2-3 an overview is made of studies with outcomes for C_D and $\tilde{C}_D$. Since all elements are the same C_D and $\tilde{C}_D$ and can be interpreted as the same in these tables. However, both parameters are still separately listed in order to show the original outcomes of the studies. Details of the studies are also included in order to have fair comparisons.

Following the studies in Table 2-2 and Table 2-3 ranges of $\tilde{C}_D$ between 0.5 and 1.2 are expected for vegetation in this study. This will be discussed in chapter 3.

2.2.3.4 Remaining parameters influencing magnitude of damping

In (He, et al., 2019) the wave attenuation by vegetation with the stem, root and canopy has been investigated at small scale. A set of laboratory experiments were conducted with a total of 112 runs with regular waves for five wave heights, four water depths and four vegetation densities. The test was done with plastic simulated *Rhizophora*, a genus of the tropical mangrove tree.

The wave transmission coefficient K_t of vegetation with the stem, root and canopy ranges from 0.21 to 0.83 (He, et al., 2019). It is a function of the combination of vegetation and hydrodynamic parameters. The vegetation parameters are about geometry, distribution density and spatial coverage while hydrodynamic parameters include wave length, wave height and water depth. Interesting to see is the inclusion of the Ursell number in determining the transmission coefficient:

$$Ur = \frac{L^2 H_0}{h^3} \tag{2.28}$$

This provides information about the balance between wave steepness and relative water depth. Another result in (He, et al., 2019) is that the variation in wave height depends on the submergence ratio and vertical vegetation structure. Highest wave attenuation occurs where the still water level is located at the canopy geometrical centroid. Also the canopy is more effective than roots and stems in reducing wave energy for identical testing conditions.

Study	Vegetation/object	Reynolds number/ velocity	Keulegan-Carpenter number	Regular/ Irregular waves/ no waves	Current/ no current	Relative vegetation height[1]	Vegetation density λ[2]	C_D	$\widetilde{C}_D$
(Kothyari, et al., 2009) Experimental study	Single cylinder Array of circular cylinders	2000-10000 2000-4000 1000-7000	- - -	No waves	Current: open channel flow	0.45 0.45 0.45	- 0.0885 0.0022	0.9 1.75-1.9 0.9-1.1	- - -
(Suzuki, et al., 2010) Numerical analysis study	Single cylinder Multiple cylinders	300 3900 8000 6250 6250 6250 6250	- - - - 5 5 5	No waves simulated, but flow is expected to be similar to flow under (regular) wave conditions	No current: flow due to waves	- - - 0.8 0.8 0.8 0.8	- - - - 0.0982 0.1963 0.3927	1.30 0.98 1.05 1.40 - - -	- - - - 1.39 1.40 1.22
(Cheng, 2013) Study on available experimental data	Single isolated cylinder	1900-5500	-	No waves	Current: open channel flow	>1.0	-	0.91-0.99	
(Ozeren, et al., 2014)` Experimental study	(EPDM) foam-rubber cords: flexible vegetation (D=9.4 mm)	>1500	20-35 10-20 5-10	Regular waves	No current, flow due to waves	0.686 0.8 0.96	0.0242	-	0.7-1.0 1.0-2.2 2.2-5.0

Table 2-2: Different studies on the drag coefficient summarised, part I

[1] The relative vegetation height is determined as follows: h_v/h [-] with h_v is the vegetation height [m] and h the water depth [m]

[2] The vegetation density is determined as follows: $\lambda = \frac{1}{A}\left(\frac{n\pi d^2}{4}\right)$ [-] with A is the vegetation field surface area [m^2], n the amount of cylinders [-] and d the diameter of the cylinder [m]

Study	Vegetation/object	Reynolds number	Keulegan-Carpenter number	Regular/ Irregular waves/ no waves	Current/ no current	Relative vegetation height	Vegetation density λ	C_D	$\widetilde{C}_D$
(Maza, et al., 2017) Experimental study	1/12th scale models *Rhizophora* (staggered)	500-3500 (trunk) 300-600 (root)	- -	No waves	Current: flow based on channel-mean velocity at different depths	>1.0 Relative root height: 0.54-0.85	10.4 trees/m^2 10.4 trees/m^2 [3]	1.2 1.2-1.4	- -
(Sanjou, et al., 2017) Experimental study	PVC cylinders: individual and single-lined (perpendicular to flow)	3900 2600-8000 3900 1300, 3900, 8000	∞	No waves	Current: Steady flow conditions	>1.0 >1.0 >1.0 >1.0	1 cyl: 5.11*10^{-3} 3 cyl: 0.0153 5 cyl.: 0.0255 8 cyl.: 0.0408	1.0 1.2 1.2 2.9, 2.1, 1.8	- - - -
(Maza, et al., 2019) Experimental study	1/6th scale models *Rhizophora* (staggered)	500-5500 500-3500	- -	Regular waves Random waves	No current: flow due to waves	>1.0 >1.0	2.06 trees/m^2 2.06 trees/m^2 [3]	0.3-2.4 0.5-1.5	- -
(Kalloe, 2019) Experimental study	Full scale white willows (*Salix alba*)		CD strongly dependent on KC-number	Regular waves	No current	<1.0	0.158 trees/m^2 (estimation) [3]	-	0.48-1.84

Table 2-3: Different studies on the drag coefficient summarised, part II

[3] Since these are no cylinders, but mangrove or willow species the density is given in trees per m^2

3 Vegetation

First of all, leafless vegetation is of interest since most extreme storms occur in winter. On top of that leaves seem to have insignificant contribution to wave damping in the full scale physical experiments of white willow trees conducted in the Delta Flume at Deltares (Wesenbeeck, et al., 2020 (to be published)). These experiments were performed in 2018.

In this chapter a new definition is introduced concerning the frontal area of the vegetation. Then the different vegetation areas within Duursche Waarden are identified and prioritized. Hereafter, methods for estimating the distribution of the different types of vegetation (and hence frontal area) are introduced and applied for Duursche Waarden. Finally, results of hand measurements and ranges for the bulk drag coefficient $\tilde{C}_D$ are discussed.

3.1 Frontal area (per volume)

In SWAN three vegetation parameters can be implemented over the height: b_v, N and $\tilde{C}_D$. The first two, b_v and N, are discussed in this section.

The most import force in wave attenuation due to vegetation is the drag force as discussed in 2.2.3. This force is nowadays described as follows:

$$F = \frac{1}{2}\rho C_D b_v N u|u| \tag{3.1}$$

In which ρ is the fluid density [kg/m^3], C_D the drag coefficient [-], b_v the branch/stem diameter perpendicular to the flow [m], N the number of vegetation stands per horizontal area [units/m^2] and u is the horizontal velocity normal to the object due to wave motion. Multiple parts of the three with different branch diameters can be distinguished with the help of layer schematisation (Suzuki, et al., 2011). This is schematised below (assuming the water level equals the height of the cube):

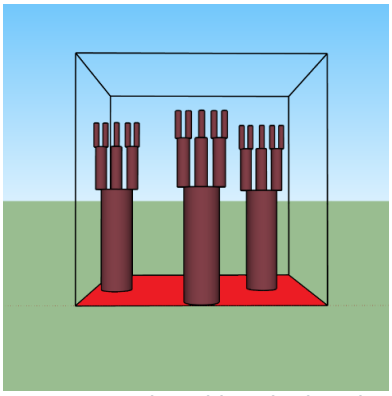

Figure 3.1: Front view old method © Sketchup

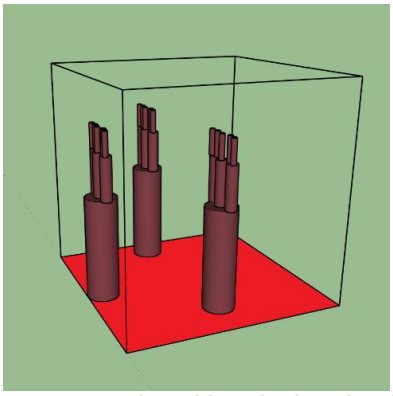

Figure 3.2: 3D view old method © Sketchup

This approximation could be interpreted as quiet rough. The assumption that all the present branches have the same diameter within the horizontal area is simplistic and easy to work with. However, in reality the diameter of branches in vegetation are hardly homogeneous and can differ significantly in the frontal area and throughout volume. Therefore a new definition of the frontal area of the branches perpendicular to the flow is defined:

$$\frac{1}{V}\sum_{i=1}^{n} A_i \tag{3.2}$$

In which $\sum_{i=1}^{n} A_i$ is the summation of the different frontal area parts of the vegetation in flow direction [m^2] and V is the considered volume of water in which the vegetation is present [m^3]. The volume V is defined as the volume of the tree(s): $V = w * l * h$ with w the width, l the length and h the height [m]. This is clarified in Figure 3.3.

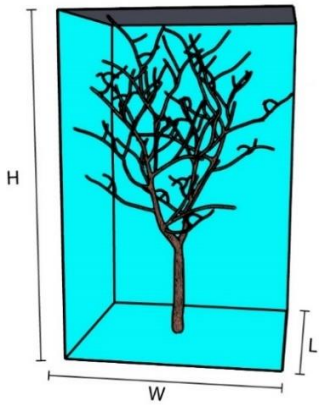

Figure 3.3: Considered volume of the vegetation in flow direction

This gives the same unit as $b_v N$ ([m^{-1}]) and can hence be implemented in SWAN. The assumption that all branches have the same diameter in the frontal area is not used anymore and instead the summation of the different frontal area parts is used to describe the area of the branches perpendicular to the flow.

However, the summed parts of the frontal area do not include 3D effects. Branches might be hidden behind the branches in front: shadowing (Seidel, et al., 2014). This results in underestimation of the present branches and therefore a correction factor should be applied in case of shadowing. This will be treated more elaborately in section 4.2.1.

The new method results in a change of formulation concernign the drag force, but also in the SWAN model (Suzuki et al. 2011):

$$F = \frac{1}{2}\rho C_D \frac{\mathbf{1}}{\boldsymbol{V}} \sum_{\boldsymbol{i=1}}^{\boldsymbol{n}} \boldsymbol{A_i}\, u|u| \tag{3.3}$$

$$H_{rms} = \frac{H_{rms,0}}{1 + \tilde{\beta} x} \tag{3.4}$$

$$\tilde{\beta} = \frac{1}{3\sqrt{\pi}} \tilde{C}_D \frac{\mathbf{1}}{\boldsymbol{V}} \sum_{\boldsymbol{i=1}}^{\boldsymbol{n}} \boldsymbol{A_i}\, H_{rms,0} k \frac{\sinh^3 k\alpha h + 3\sinh k\alpha h}{(\sinh 2kh + 2kh)\sinh kh} \tag{3.5}$$

With H_{rms} the root mean square wave height at location x in the vegetation field [m], $H_{rms,0}$ the root mean square wave height at the start of the vegetation field [m] and $\tilde{\beta}$ the damping coefficient [-].

3.2 Identifying and prioritising vegetation areas

The existing vegetation areas within Duursche Waarden should be identified and prioritised. This gives insight to what vegetation strokes are expected to cause most wave damping.

The different vegetation areas are identified with the help of Google Earth images, drone footage and the tool ‘vegetatielegger’ constructed by Deltares. In Figure 3.4 the tool ‘vegetatielegger’ is shown and this tool distinguishes different types of vegetation, soil, water and rural area. It is clearly shown what areas are assigned to ‘forest’ and hence probably consist of significant (wave damping) vegetation. In Figure 3.6 identified vegetation areas are shown.

Prioritising the vegetation areas will be done based on the governing hydraulic conditions from Hydra-NL (see Appendix Governing parameters dike segments) in which especially the combination of the governing wind direction and fetch is of great importance. Field observations and airoborne Light Detection and Ranging (LiDAR) data (such as Actuele Hoogtebestand Nederland (AHN) 3) are used to estimate the density of the vegetation.

Airborne LiDAR data determines the distance to an object by analysing a laser light return on an object’s surface (Soudarissanane, 2016). A 3D point cloud (a dataset of points) is obtained, consisting of millions of points. This provides elevation information of the tree species.

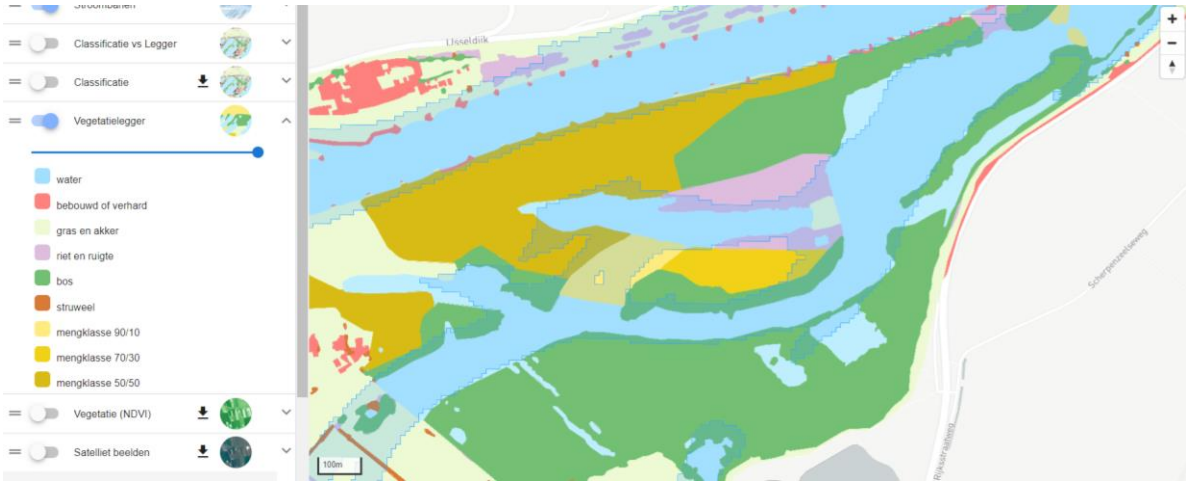

Figure 3.4: 'Vegetatielegger', https://www.openearth.nl/vegetatiemonitor/, © Deltares

Three figures are shown at page 20. Figure 3.5 is of just Duursche Waarden, in Figure 3.6 the identified vegetation areas are identified and in Figure 3.7 all the different dike locations adjacent to the Duursche Waarden are shown, including the combination of the governing wind direction(s) and the corresponding fetch. This is summarised below in Table 3-1:

Dike segment	Governing wind directions
185-189	WNW
190-192	WNW
193-199	WNW & W

Table 3-1: Governing wind direction per dike segment

Prioritising the different vegetation areas will be based on the observed vegetation density and the distance the wind-generated wave will cover through the vegetation in direction with the fetch (Figure 3.5, Figure 3.6 and Figure 3.7). A large distance through the vegetation in combination with a dense vegetation area is assumed to give largest wave attenuation and will therefore be most interesting. A short multi-criteria analysis is done to identify the most interesting vegetation areas concerning wave damping. The two criteria are assessed based on a number of 1 to 5: with 1 indicating a short distance covered by the wave through the vegetation or an open vegetation area and 5 indicating a large distance covered by the wave through the vegetation or a dense vegetation area. Both scores are multiplied to get the total score. This is summarised in Table 3-2:

Vegetation area	Distance through vegetation	Density vegetation	Total score	Priority number
1	2	4	8	3
2	5	3	15	1
3	3	4	12	2
4	4	1	4	6
5	1	1	1	
6	2	1	2	
7	3	2	6	4
8	2	3	6	4
9	1	1	1	

Table 3-2: Multicriteria analysis vegetation areas

Vegetation area 2 is an interesting area to investigate wave attenuation due to vegetation with a total score of 15/25. The reason for this is mainly the large distance through the vegetation that will be covered by the waves. Vegetation area 3 showed some open space, but the observed vegetated areas were dense. Vegetation area 1 showed uniform and moderate dense vegetation even though the distance through the vegetation by the waves will not be that large relatively seen. Even though all vegetation areas will have an effect on wave damping, most wave damping is expected for vegetation areas 1, 2 and 3 and have therefore priority in this research. These vegetation areas will be investigated in detail. Vegetation areas 4,7 and 8 will be investigated more roughly, since they are expected to dampen waves significantly less or only a small part of the dike.

Figure 3.5: Duursche Waarden

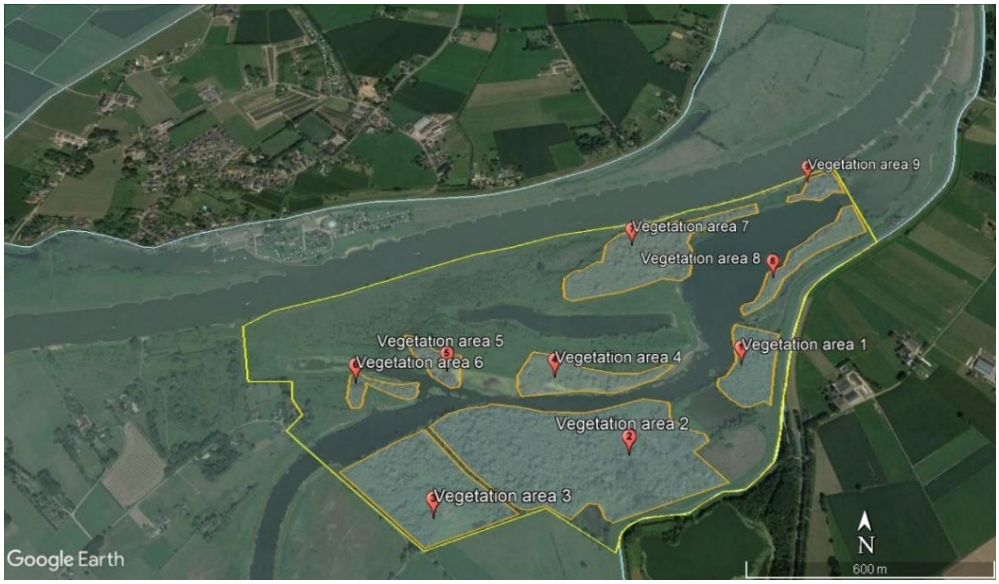

Figure 3.6: Vegetation areas Duursche Waarden

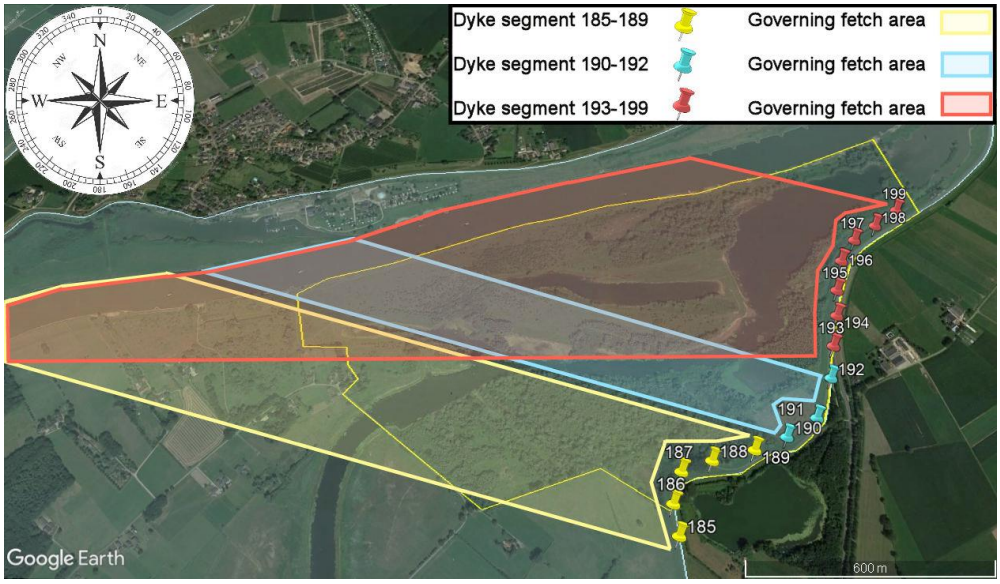

Figure 3.7: Governing fetch per dike segment

3.3 Spatial distribution frontal area

In this section one method is evaluated for determining the spatial distribution of the frontal area. The prioritised vegetation areas have been characterised in terms of uniform or non-uniform areas considering tree species, structure, height and density with the help of field observations, aerial photos (drone footage and Google Earth images), airborne LiDAR data (AHN 3):

- Vegetation area 1: (nearly) uniform, only tree species with similar tree structure, height and density
- Vegetation area 2: non-uniform, multiple different tree species, structure, height and density
- Vegetation area 3: both (nearly) uniform and non-uniform parts

3.3.1 General method

There are three different types of prioritised vegetation areas, but only two type of areas are distinguished: an uniform and non-uniform area. The determination of these two areas is explained first, after which a general expression is given for the introduced method of determining the spatial frontal area distribution.

3.3.1.1 Uniform vegetation area

In an uniform vegetation area the goal is to find an average and representative value for the frontal area per volume over the height. This is done by choosing a representative volume within the vegetation area and could be for example in the centre of the vegetation area. The representative volume should represent the uniform vegetation area in terms of density, height and tree structure and is done by observations and LiDAR data. The estimated frontal area over the height for the considered volume is used for the whole uniform vegetation area.

3.3.1.2 Non-uniform vegetation area

In a non-uniform vegetation area one should determine what the most common tree species in the area are by observations. Then the frontal area per volume over the height is estimated individually for the most common tree species. Different subareas within the non-uniform vegetation area will now be made based on the estimated amount of presence of the most common trees. This could be done manually (time expensive) or by an elevation tool such as AHN 3. Vegetation with different heights can be distinguished with the help of AHN 3 and hence different tree species.

Different subareas can be defined based on the presence of the most common tree species. For instance we have a sparse, medium and dense tree species (in terms of density and hence frontal area). Subareas could then be distinguished during field work and using AHN 3. An example is given in Table 3-3, in which three tree species are considered as most common.

Subarea name	Subarea description	Criteria	Frontal area per volume
Subarea 1	Sparse tree species dominate over medium and dense tree species	- Walkable - Visibility should be quite good - There should be more sparse than medium and dense tree species	Sparse: 3/5 Medium: 1/5 Dense:1/5
Subarea 2	Sparse, medium and dense tree species are equally present	- Hardly walkable - Moderate visibility - About equal presence of sparse, medium and dense tree species	Sparse: 1/3 Medium: 1/3 Dense: 1/3
Subarea 3	Dense tree species dominate over sparse and medium tree species	- Not walkable - Poor visibility - There should be more dense than sparse and medium tree species	Sparse: 1/5 Medium: 1/5 Dense: 3/5

Table 3-3: Categorisation subareas in non-uniform vegetation area

In Table 3-3 a subarea description and criteria are added to specify the different subareas. The frontal area per volume of a certain subarea is presented by fractions of the most common tree species (in this case sparse, medium and dense). These fractions stand for the part of frontal area per volume that is delivered by an individual tree species for the subarea.

3.3.1.3 General expression

A general expression for the spatial distribution of the frontal area (per volume) over the height for uniform and non-uniform areas is developed. This is shown in Equation (3.6):

$$\left(\frac{1}{V}\sum_{i=1}^{n} A_i\,(z)\right)_{area} = a * \left(\frac{1}{V}\sum_{i=1}^{n} A_i\,(z)\right)_1 + b * \left(\frac{1}{V}\sum_{i=1}^{n} A_i\,(z)\right)_2 + c * \left(\frac{1}{V}\sum_{i=1}^{n} A_i\,(z)\right)_3 \quad (3.6)$$

With $\left(\frac{1}{V}\sum_{i=1}^{n} A_i\,(z)\right)_{area}$ the summation of the frontal area per volume over the height of an uniform or non-uniform (sub)area, a the fraction of frontal area per volume delivered by (most common) tree species number 1, $\left(\frac{1}{V}\sum_{i=1}^{n} A_i\,(z)\right)_1$ the summation of the frontal area per volume over the height of (most common tree species) number 1. In case of a non-uniform area with more most common tree species, the same explanation holds for most common tree species 2, 3 and more.

The fractions (a, b, c) are based on the area covered or dominated by the different most common tree species and is determined by (i) manually measuring the area covered by the most common tree species (ii) or making a rough estimation. The first method is recommended for relatively small areas and the latter one for relatively large areas. This can be done with the help of AHN 3. Hence, the magnitude of the fractions are defined as in Equation (3.7):

$$a = \frac{A_1}{A_{total}} = \frac{A_1}{A_1 + A_2 + A_3} \quad (3.7)$$

With A_1, A_2 or A_3 the area covered by most common tree species 1, 2 or 3 [m^2] (in case of three most common tree species). Fractions b and c are determined in the same way, but then with A_2 and A_3 in the numerator. Hence, the following holds for the two different areas:

- Uniform area: $a = 1, b = c = 0$
- Non-uniform area: $a, b, c < 1$

3.3.2 Duursche Waarden

Based on observations three tree species are found to be most common in the non-uniform areas of vegetation area 2 and 3. Furthermore three different uniform areas are identified in vegetation area 1 and 3. The tree species are determined in the vegetation areas with the help of ecologists of WDOD (the waterboard) and (Mayer, et al., 2018). This is summarised in Table 3-4. For specifications of the tree species, see Appendix Tree species.

Vegetation area	Type of area	Tree species	Name in this study
1	Uniform	Mix of white willows (*Salix alba*) and crack willows (*Salix fragilis*)	Uniform Mix of Willows in vegetation area 1: UMW-1
2	Non-uniform Most common tree species 1 Most common tree species 2 Most common tree species 3	Downy oak (*Quercus pubescens*) Pedunculate oak (*Quercus robur*) Osier (*Salix viminalis*)	Individual Downy Oak: IDO Individual Pedunculate Oak: IPO Individual Osier: IO
3	Uniform	Crack willows (*Salix fragilis*)	Uniform Crack Willows: UCW
	Uniform	Mix of frosted willows (*Salix daphnoides*), osier (*Salix viminalis*) and white willows (*Salix alba*)	Uniform Mix of Willows vegetation area 3: UMW-3
	Non-uniform	Same most common tree species as in vegetation area 2	IDO, IPO and IO

Table 3-4: Different tree species in prioritised vegetation areas

As described in section 3.3.1.1 one representative height profile of the frontal area per volume will be used for uniform areas such as in vegetation area 1 and 3. In vegetation area 1 a mix of white willows (*Salix alba*) and crack willows (*Salix fragilis*) form the uniform area.

In vegetation area 3 two different uniform areas are defined by (i) crack willows (*Salix fragilis*) and (ii) a mix of frosted willows (*Salix daphnoides*), osier (*Salix viminalis*) and white willows (*Salix alba*). Hence, uniform considered areas can also consist of multiple tree species if they show similar structure, density and height.

The method as described in section 3.3.1.2 for non-uniform areas will be applied for vegetation area 2 and 3. The most common tree species in vegetation area 2 and 3 are estimated to be the downy oak (*Quercus pubescens*), pedunculate oak (*Quercus robur*) and osier (*Salix viminalis*). Based on observations during field work and elevation information by AHN 3 five different subareas have been described in Table 3-5.

The spatial distribution of the frontal area (per volume) for every subarea is determined with help of Equation (3.6) and in this case it is assumed there is no overlapping vegetation. This assumption is considered to be conservative, because field observations and AHN 3 suggest overlapping. In Appendix Ratio subareas the ratios for different subareas between the most common tree species are illustrated. Finally, this leads to one representative height profile of the frontal area per volume for every subarea.

In Table 3-5 the pedunculate oak is considered as sparse and the downy oak and osier are considered as dense in terms of vegetation density.

Subarea name	Subarea description	Criteria	Frontal area per volume distribution
Subarea 1	No or barely vegetation	- Excellent accessibility - Excellent visibilty - A present tree should be an exception	Downy oak: 0 Osier: 0 Pedunculate oak: 0
Subarea 2	Sparse vegetation dominates	- Easily walkable - Good visibility - Now and then some dense vegetation	Downy oak: 2/20 Osier: 2/20 Pedunculate oak: 16/20
Subarea 3	Relatively large space walking space, more sparse than dense vegetation	- Walkable - Reasonable visibility	Downy oak: 4/20 Osier: 4/20 Pedunculate oak: 12/20
Subarea 4	A balanced mix between dense and sparse vegetation	- Challenging to walk in - Moderate visibility - Clearly balanced mix of vegetation	Downy oak: 5/20 Osier: 5/20 Pedunculate oak: 10/20
Subarea 5	More dense than sparse vegetation	- Barely walkable - Poor visibility - There should be more dense than sparse and medium tree species	Downy oak: 6/20 Osier: 6/20 Pedunculate oak: 8/20

Table 3-5: Criteria subareas Duursche Waarden

3.4 Plan of the vegetation areas

The vegetation of uniform and non-uniform areas is known and now a plan is made to show the distribution of the vegetation and hence the frontal area per volume.

3.4.1 Prioritised vegetation areas

In combination with drone footage, observations during field trips, AHN 3 and Google Earth images a detailed map of every prioritised vegetation area is obtained.

Since vegetation area 1 is uniform (mix of white and crack willows), the same frontal area per volume over the height will be taken for the whole area. This also holds for the two uniform parts in vegetation area 3: (i) crack willows and (ii) a mix of frosted willows, osier and white willows.

Vegetation area 2 and the other parts of vegetation area 3 are non-uniform and therefore subareas have been made based on the presence of the most common tree species: downy oak, osier and pedunculate oak. The AHN 3 images are valuable for estimating the distribution of the subareas as the position of the pedunculate oak (relatively tall tree) and osier and downy oak (both relatively small trees) can be observed pretty good (see Appendix AHN 3 images vegetation areas). A rough estimation of the ratio between those trees lead to the distribution of the subareas. The distribution of the prioritised vegetation areas (and hence frontal area per volume) can be observed in Figure 3.8, Figure 3.9 and Figure 3.10.

Figure 3.8: Plan vegetation area 1

Figure 3.9: Plan vegetation area 2

Figure 3.10: Plan vegetation area 3

3.4.2 Roughly estimated vegetation areas

Vegetation areas 4, 7 and 8 are expected to cause wave damping, but not as much as the prioritised vegetation areas. Therefore the distribution of the frontal area per volume is a rough estimation based on vegetation in the prioritised vegetation areas. The height of the vegetation can be observed with the help of AHN 3 (see Appendix AHN 3 images vegetation areas), while with drone footage more insight is gained in the structure and density of the leafless vegetation.

The greatest part of vegetation area 4 is considered quite uniform and the vegetation shows about the same heights as the uniform area in vegetation area 3 consisting of crack willows. In the smaller part barely vegetation is present and therefore 'subarea 1' is assigned to this part.
Vegetation area 7 seems to be non-uniform and shows the pedunculate oak (tall trees) to be dominant. Therefore 'subarea 2' is assigned to vegetation area 7.
Vegetation area 8 can be divided in two separate parts: uniform and non-uniform. The uniform part shows many similarities with vegetation area 1 and is therefore assumed to have the same vegetation. The non-uniform part shows dense and relatively small vegetation which are the features of 'subarea 5'. Therefore 'subarea 5' is assigned to the non-uniform part.

The distribution of the roughly estimated vegetation areas (and hence frontal area per volume) can be observed in Appendix Roughly estimated vegetation areas.

3.5 Vegetation parameters

First estimations of the frontal area per volume are obtained with the help of hand measurements. Also the ranges for the bulk drag coefficient are determined with the help of section 2.2.

3.5.1 Hand measurements

Hand measurements have been done of some of the tree species in the prioritised vegetation areas to have an idea about the order of magnitude concerning the frontal area per volume (see Appendix Results hand measurements). Due to height limitations only hand measurements could be done until an height of 2 m. The results are shown in Table 3-6:

	Frontal area per volume [m^{-1}]			
Height [m]	**UMW-1, stem**	**IO**	**UCW, stem**	**UMW-3**
0.0-0.5	0.0625	0.330-0.973	0.146	0.165-0.419
0.5-1.0	0.0625	0.330-0.973	0.146	0.165-0.419
1.0-1.5	0.0572	0.330-0.973	0.131	0.143-0.397
1.5-2.0	0.0572	x	0.131	0.143-0.397

Table 3-6: Results hand measurements

3.5.2 Bulk drag coefficient

The dependency of the bulk drag coefficient $\tilde{C}_D$ is extensively treated in section 2.2.3.3. From this section it can be concluded that the $\tilde{C}_D$ is a very uncertain parameter. However, many studies have been done on the drag coefficient. These studies have been summarized in Table 2-2 and Table 2-3. Based on these studies the following categories have been made with a corresponding drag coefficient:

Type of vegetation	**Information**	**Bulk drag coefficient $\tilde{C}_D$**
Rigid stem	Hard to deform, rigid	1.2
Rigid stem + thick branches	Both are approximately equally present	1.1
Thick branches	Bifurcate from the stem, branch diameter greater than 5.0 cm	1.0
Small branches	Bifurcate from 'Thick branches', branch diameter: 0.1-5.0 cm	0.8
Leaves and smaller branches	Very easy to deform	0.0

Table 3-7: Categorisation bulk drag coefficient

The exact applied bulk drag coefficient per layer can be found in Appendix Vegetation parameters for SWAN.

4 TLS measurements

First of all, leafless vegetation is of interest since most extreme storms occur in winter. On top of that leaves seem to have insignificant contribution to wave damping in the full scale physical experiments of white willow trees conducted in the Delta Flume at Deltares (Wesenbeeck, et al., 2020 (to be published)). These experiments were performed in 2018.

In this chapter the details and results are discussed of the Terrestrial Laser Scanner (TLS) measurements. First of all, a data description is given after which possible TLS errors are discussed. Different techniques and studies of estimating the frontal area are discussed. Then frontal area estimation techniques from literature, outcomes of similar vegetation and hand measurements are discussed. Frontal area estimation methods for Duursche Waarden are elaborated for Multiple Scanning Stations (MSS) with the help of this knowledge. Also a frontal area estimation method for a Single Scanning Station (SSS) is introduced. Finally, the outcomes of MSS and SSS frontal area estimation are shown and discussed.

4.1 Data description

TLS is a Light Detection and Ranging (LiDAR) system and determines the distance to an object by analysing a laser light return on an object's surface (Soudarissanane, 2016). Within a matter of minutes, the TLS captures a 3D point cloud (a dataset of points) consisting of millions of (xyz) points with an accuracy of millimetres. This provides both the options to obtain a point cloud of one or multiple tree species in a relative quick and efficient way.

The TLS measurements have been carried out using the Leica P40 (see Appendix Leica P40 for specifications). It is possible to do scans in different resolutions. The higher the resolution, the more time one scan takes. Therefore the scans have been done with a resolution of 3.1 mm at 10 m distance with a duration of 3 minutes and 30 seconds. With this resolution an accuracy in the order of mm is obtained and it allows to do all measurements in one day. Hence, this resolution provides a balance between accuracy and feasible execution of the scans. An overview is given of the TLS measurements (see Appendix Locations TLS measurements for more information) in the prioritised vegetation areas in Figure 4.1, Figure 4.2 and Figure 4.3.

The measurements were done on the 2nd of April, 2020 during leaf-off conditions. The atmospheric conditions were favourable: little windy, bit of sun and little cloudy, no rain and no moisty vegetation. The little wind resulted in little movements at the top of trees. The height at which this movement occurred, was approximately 20 m. Since the vegetation will be studied until 10 m height (see section 4.6), this small error can be neglected. The uniform areas (as described in section 3.3.2) were easily accessible and hence measurements were done in the centre of these areas. The non-uniform parts were moderately accessible and therefore individual tree measurements have been done more towards the edge of these areas. In Appendix Tree species an overview is given of the type of tree species, the amount of TLS measurements per tree species and whether an individual tree species or a small area was captured with the TLS.

Figure 4.1: TLS measurements vegetation area 1

Figure 4.2: TLS measurements vegetation area 2

Figure 4.3:TLS measurements vegetation area 3

4.2 TLS errors

The TLS captures a 3D point cloud with an accuracy of millimetres. However, this method to sample tree structures is not perfect and therefore includes errors. These are discussed in this section.

4.2.1 Shadowing

The term shadowing describes the fact that there are objects located in the shadow of other objects which are standing closer to the scanner (Seidel, et al., 2014). In this particular case this means the phenomena of branches blocking laser pulses so branches/stems behind will not be implemented in the point cloud by the TLS. This results in significant underestimation of the frontal area over the volume and should therefore be corrected with the shadowing correction factor f. The magnitude depends on the density of the considered tree species and whether laser beams are blocked before even reaching the considered tree species (in case of reed or branches of other trees).

In case of dense vegetation the shadowing effect becomes significant (order of 7.5 % for single station scans in dense vegetation according to (Seidel, et al., 2014)) in determining the frontal area and should therefore be corrected. Also in case of a Single Station Scan the frontal area should be corrected for shadowing as no complete point cloud of the vegetation is obtained, since the scan is only from one position. In case of no dense vegetation and multiple scanning stations, the phenomena of shadowing is minimized and it is assumed no shadowing correction factor is needed.

4.2.2 TLS instrument errors

Like every instrument a Terrestrial Laser Scanner (TLS) is not perfect. In Appendix Leica P40 the concept of the way a TLS works is explained. The instrument emits narrow laser beam pulses from a rotating mirror in known direction and measures the backscattered signal reflected by the object surface. This brings a few uncertainties in relation with the reception of the echo signal. These will be mentioned and are shortly evaluated in Appendix Errors following (Soudarissanane, 2016):

1. Beam divergence deviation of the emitted laser beam
2. Error is in relation with the beam deflection unit
3. Axes error
4. Error in pulse arrival time determination

The range noise of the Leica P40 is relatively low: 0.4 mm RMS at 10 m (see Appendix Leica P40). This is a good indicator for the quality delivered by a TLS instrument and therefore the above mentioned errors will be neglected.

4.2.3 Atmospheric conditions

The laser beam needs to travel twice through the atmosphere considering before and after reflection of the object. The main atmospheric factors to take into account are the ambient temperature, humidity, ambient light and the vibrations due to turbulences and pureness of the air (Soudarissanane, 2016). On top of these errors in the point cloud, the measured trees for this study can also be affected in case of wind. The wind will move the tree, especially at the top of the trees where the wind speed is maximum. This will result in small errors of the point cloud at the top of the tree. In case of moisty trees (droplets on branches) the TLS will also measure these droplets as part of the tree and hence the area and volume of the tree will be overestimated.

4.2.4 Leaves

Another error for determining the frontal area (per volume) is the fact that for some tree species there were already some upcoming leaves and buds on the day of the measurements. This study treats only leafless vegetation. However, the TLS instrument does not make a distinction between branches or leaves and hence are included in the point cloud. This is the case for species IDO and IO (see section 3.3.2). A conservative decision is made by multiplying the frontal area per volume by 0.90, since it is estimated about 0 to 10 percent of the point cloud is no woody vegetation but buds or small leaves.

4.2.5 Conclusion

All mentioned errors are summarised in Table 4-1:

Type of error	Additional information	Estimated magnitude of the error
Shadowing	How is dealt with shadowing is explained in section 4.5	Significant
Total TLS errors	See Appendix Errors for more information	Neglected
Atmospheric conditions at the day of TLS measurements	Conditions were favourable, for more information see section 4.1	Neglected
Leaves on trees	x	~ 10 %

Table 4-1: Summary of TLS errors

The magnitude of the errors of TLS measurements are to be neglected. The same holds for errors due to atmospheric conditions, since these conditions were favourable. Shadowing plays a significant role in underestimation of the frontal area per volume for dense vegetation in Single Station Scans and will therefore be corrected.

In case of presence of leaves on trees the frontal area will be corrected. Hence, corrections will be made for shadowing in case of dense vegetation or single station scans and in case of leaves on trees during TLS measurements.

4.3 Estimating frontal area: literature

In this section the methods in estimating the frontal area are evaluated.

4.3.1 Methods

In (Antonarakis, et al., 2009) the frontal area of leafless poplar species in riparian zones are estimated using the branching method. More importantly, two methods have been used with the help of TLS data: complex tree meshing and tree voxelization.
With complex tree meshing, triangle meshes of the individual tree species (measured from three positions) were automatically created from the point cloud data using the Leica Cyclone program. All triangle meshes are added up individually which leads to the full frontal area. Since there is dealt with floods, only one side is in contact with water and therefore the full bark frontal area is halved. This results in the frontal area by complex tree meshing. The estimation of the frontal area with this method lead to deviating values at the canopy. The canopy is the aboveground portion of a plant community formed by plant crowns.
A voxel, or a volumetric pixel, represents a volume element on a regular grid in the third dimension, instead of the second dimension like the pixel, centred on a coordinate grid point. With tree voxelization a 3D regular grid is defined with a minimum set of two points. Then with help of the specific POV-Ray format a voxelized tree is presented with a voxel resolution of 5 cm (due to computational capacity). Hereafter, an image of the voxelized tree (.jpeg format) is imported in MATLAB in which a 10 cm red cube is added. The amount of pixels of the red cube are counted which result in an estimation of the area per pixel. Then the amount of pixels of the tree are counted for four different orientations which lead to the estimation of the frontal area.
The tree voxelization method resulted in slightly greater values for each individual tree.

In (Kalloe, 2019) the frontal area of tree species *Salix alba* was estimated using the alpha shape method. The alpha shape of a given data set is the intersection of all closed discs with radius $1/\alpha$ that contain all the points of the data set (Edelsbrunner, et al., 1983). This leads to a certain surface area of all the points in the data set. The most important parameter α can be positive, negative and equal to zero. In case $\alpha = 0$ the result is a convex hull of the entire plane as no radius restrictions are given. In case $\alpha < 0$ the alpha shape is defined as the intersection of all closed complements of the discs that contain all the points of the data set. In case $\alpha > 0$ the alpha shape is the intersection of all closed discs containing all the points of the data set. However, it has to be guaranteed that there exists at least one disc of the chosen size that contain all points. This means that the smallest positive value for $1/\alpha$ is equal to the smallest enclosing circle. To conclude, α is the parameter to play with in order to get the preferred alpha shape. In Figure 4.4 the alpha shape method is illustrated.

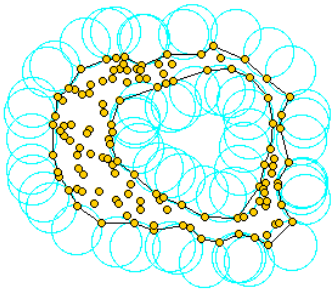

Figure 4.4: Alpha shape method (Da, et al., 2020)

4.3.2 Similar vegetation

In this section different papers will be discussed relevant for this study.

4.3.2.1 Duursche Waarden

First of all, a similar study is done on the hydraulic roughness of Duursche Waarden in (Rahman, et al., 2013). The parameter D_v (vegetation density [m^{-1}]) is studied with the help simulations of airborne laser scanning during leaf-off conditions. The vegetation density is defined as the total frontal area of vegetation in the flow direction per unit volume of water and hence is the same as $\frac{1}{V}\sum_{i=1}^{n} A_i$. However, the approach is different in this study.

Tree models of both dominant trees and understorey vegetation closely imitate various conditions of trees in Duursche Waarden (willow, poplar, oak, ash and small pine) during leaf-off season. In this study the tree models are represented by sets of cylinders with different length, diameter, origin, and direction. A dominant tree is designed to have four canopy layers. Each canopy layer contains six major branches each of which consists of another eight sub-branches. Understorey vegetation contains three canopy layers with a branch structure similar to the dominant tree.

Based on the tree models simulated airborne LiDAR observations are done, generating point clouds. Then predictors of regression models are calculated. Low Point Index (LP), defined as the ratio between the total number of laser hits between h_1 and h_2 (height 1 and 2) and the laser hits on the ground surface, shows best results and therefore this model is used in estimating D_v for trees in forest patches. For isolated trees D_v is estimated based on Diameter at Breast Height (DBH), at which mainly the trunk diameter is used in this case (if measuring the DBH is possible from the point cloud). If this is not the case, the same method for trees in forest patches is used.

Finally, the D_v was mapped for different spatial resolutions (5, 10, 20, 30, 40 and 50 m). All spatial resolutions showed D_v varying from 0.05 to 2.0 m^{-1}. Only some small parts coincide with the considered vegetation areas of this study. These are outlined in blue (see Figure 4.5).

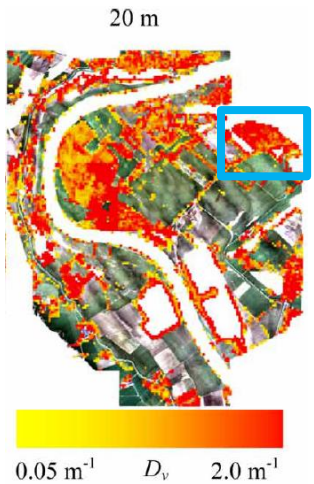

Figure 4.5: Vegetation density of part Duursche Waarden with a spatial resolution of 20 m (Rahman, et al., 2013)

The blue outlined rectangle consist mainly of a vegetations density around 2.0 m^{-1}.

4.3.2.2 Frontal area similar vegetation

In (Kalloe, 2019) the frontal area of willow tree species *Salix alba* is estimated using TLS measurements and hand measurements. Since the TLS measurements were not reliable the results of hand measurements were used. In (Stam, 2018) the wave damping of (partially) submerged young willow branches (not clear which species, probably *Salix alba*) was studied with a field test. The measurement set-up consists of a plot of 7 x 7 meters with young willow branches and pressure transducers perpendicular to the river Noord near Dordrecht, the Netherland. The frontal area per volume over height of one young willow varied from 0.72 to 1.60 m^{-1}. In (Vries, et al., 2009) the wave damping capacity of willow fields (*Salix alba* and *Salix viminalis*) is studied. Estimates show values of 0.90 up to 3.38 m^{-1} on average for the frontal area per volume.

In (Antonarakis, et al., 2009) the frontal area of leafless poplar species in riparian zones are estimated using two methods: complex tree meshing and tree voxelization retrieved from TLS. The frontal area of both methods showed similar outcomes. Since the Duursche Waarden shows similarities with mangrove forests (both on a shallow foreshore with wave damping vegetation), it is interesting to know the order of magnitude of vegetation density for mangrove forests. The vegetation density for mangroves (two types of roots: stilt and pneumatophores) is divided in sparse, medium and dense in (Janssen, 2016). The frontal area per volume of mangroves varies for a sparse density from 0.01 to 0.5 m^{-1} and for high density from 0.68 to 9.60 m^{-1}.

The values are summarised in Table 4-2.

Study	**Tree species**	**Height [m]**	**Frontal area [m^2]**	**Frontal area per volume [m^{-1}]**
(Antonarakis, et al., 2009)	Mature poplar	0.00-5.00 5.00-10.00 10.00-20.00 20.00-25.00	0.00-1.00 increase 1.00-6.00 increase 6.00 constant 1.00-6.00 decrease	- - - -
(Vries, et al., 2009)	Willows (*Salix alba* and *Salix viminalis*)	0.00-0.30 0.30-2.00	- -	0.90 3.38
(Janssen, 2016)	Mangrove species	-	-	Sparse: 0.01-0.50 Dense: 0.68-9.60
(Stam, 2018)	Young willow branches (probably *Salix alba*)	0.0-0.6 0.6-1.2 1.2-1.5	- - -	1.60 1.24 0.72
(Kalloe, 2019)	White willow (*Salix alba*)	0-1.02 1.02-2.02 2.02-3.02 3.02-4.02 4.02-4.89 4.89-5.35	- - - - - -	0.05 0.30 0.28 0.21 0.16 0.10

Table 4-2: Values frontal area (per volume) similar tree species

4.4 Estimating frontal area: Duursche Waarden (MSS)

In this section different methods for estimating the frontal area per volume are discussed. The methods are meant for TLS measurements with Multiple Scanning Stations (MSS). This means two or three scans from different positions of the vegetation area or individual tree species (see Figure 4.6). The different scanning station positions around the considered subarea or individual tree species minimize the effect of shadowing, since multiple point clouds obtained from different scanning position are merged. Shadowing is considered as the largest error in achieving the frontal area (see section 4.2) and with the help of the MSS method this error is believed to be minimized. Hence, the results in this section function as a starting point.

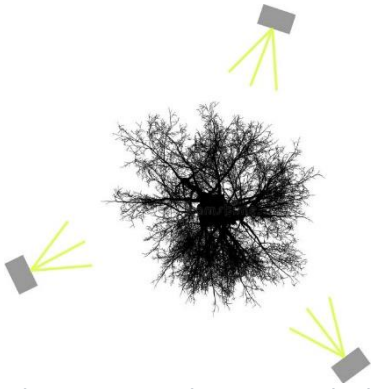

Figure 4.6: Top view MSS method

4.4.1 Type of vegetation area

In section 3.3 two types of vegetation areas are distinguished: uniform and non-uniform. Both type of areas are discussed in estimating the frontal area.

4.4.1.1 Uniform vegetation area

In case of an uniform vegetation area, TLS measurements from different positions of a subarea are made that represent the entire vegetation area. The result is a 3D point cloud or volume of this subarea.
The frontal area per volume can be determined in two different ways:

1. In this method slices are made in depth over the whole volume. The downside of this method is the use of the whole volume containing multiple millions of points. This results in a large computation time.
2. In this method the frontal area of 3 to 5 randomly chosen trees in the considered cubic volume will be determined in order to have an 'average tree'. Then the total amount of trees in the considered volume are counted and multiplied by the average $\sum_i A_i$ of a slice in z-direction. Then per slice this average $\sum_i A_i$ is divided by the volume and hence the frontal area per volume over the height is achieved. This is shown in below equation:

$$A_{avg,i} = \frac{\sum_{j=1}^{n} A_{i,j}}{n} \tag{4.1}$$

$$\left(\frac{A}{V}\right)_{avg,i} = \frac{A_{avg,i} * m}{xyz_i} \tag{4.2}$$

With $A_{avg,i}$ the average frontal area of slice i in z-direction [m^2], $\sum_{j=1}^{n} A_{i,j}$ the sum of the frontal area of slice i [m^2] with j the particular tree of the total amount of trees of which the frontal area is considered [-] and n the total amount of trees considered for the frontal area [-], $\left(\frac{A}{V}\right)_{avg,i}$ the average frontal area per volume of slice i [m^{-1}], m the total amount of trees in the considered volume [-] and xyz_i the considered volume of slice i [m^3].

Method 2 will be used in this study.

4.4.1.2 Non-uniform vegetation area

In case of a non-uniform vegetation area no subarea will be scanned, since the trees species in this subarea will differ too much. Instead, the most common tree species will be measured individually from multiple scanning positions. Only one representative tree per most common tree species will be measured. This results in the frontal area per volume over height per tree species.

$$\left(\frac{A}{V}\right)_i = \frac{\sum_{j=1}^{n} A_{i,j}}{xyz_i} \tag{4.3}$$

In which $\left(\frac{A}{V}\right)_i$ is the frontal area per volume of slice i in z-direction [m^{-1}], $\sum_{j=1}^{n} A_{i,j}$ the sum of the frontal area of slice i in z-direction [m^2], with j one of the areas contributing to total sum of the frontal area [-] and n the total amount of areas that contribute to the frontal area [-] and xyz_i the cubic volume of slice i in z-direction [m^3].

Also now the magnitude of the slices in depth will be in the order of the diameter of the stem or branches. This means the individual tree species will be divided in parts based on the dominance of branches or stem of a certain diameter.

4.4.2 Estimating frontal area

TLS measurements generate a 3D point cloud consisting of millions of points. These points represent a certain volume of, in this case, the prioritised vegetation areas. The frontal area will be estimated with the help of these 3D point clouds. Two methods are considered to determine this parameter:

1. Grid method
2. Alpha shape method

4.4.2.1 Grid method

With the 2D grid method a grid is placed in front of the considered volume from a point of view to be determined by yourself. Then, from the chosen point of view, it is assessed whether a grid cell contains a point from the point cloud or not. If so, the area of the grid cell is added up to the total frontal area. An important aspect in this method is defining the grid cell size. In case a relatively large cell size is assigned, the frontal area will be overestimated. In case of a relatively small cell size the frontal area will be underestimated. This is illustrated in Figure 4.7, Figure 4.8 and Figure 4.9.

In deciding the right grid cell size the resolution of the scanner should be taken into account. Every scan is done with a resolution of 3.1 mm at 10 m. This means that at a distance of 10 m from the scanner the points in the point clouds are 3.1 mm apart from each other. This means that for a closer distance to the scanner the points will be less than 3.1 mm apart from each other and vice versa. Therefore, with every measurement the median resolution (pixel area) of the considered volume is used as grid cell size in case of a single station TLS measurement.

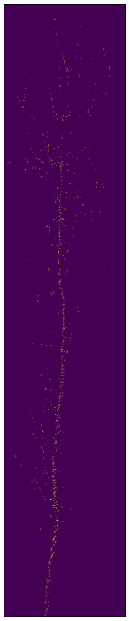

Figure 4.7: Individual tree from vegetation area with too small grid size

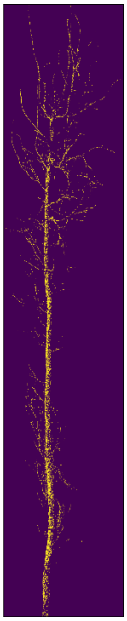

Figure 4.8: Individual tree from vegetation area with median grid size

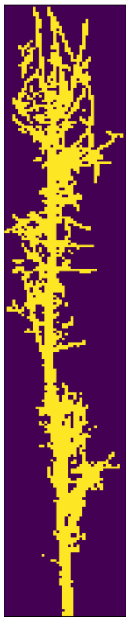

Figure 4.9: Individual tree from vegetation area with too large grid size

With $p_i = (x_i, y_i, z_i)$ the 3D coordinates of a data point and $p_0 = (x_0, y_0, z_0)$ the 3D coordinates of the scanner the total frontal area can be estimated. First the distance of every point to the scanning station (R_i) is determined, then the represented 2D pixel area (a_i) and finally the length of the square grid cell size (L in [m]):

$$R_i = \sqrt{(x_i - x_0)^2 + (y_i - y_0)^2 + (z_i - z_0)^2} \tag{4.4}$$

$$a_i = \left(\frac{3.1}{10} * R_i\right)^2 \tag{4.5}$$

$$L = \sqrt{median\left((a_i) * 10^{-6}\right)} \tag{4.6}$$

The total frontal area ($\sum_n A_i$) is now determined by:

$$\sum_{i=1}^{n} A_i = n * L^2 \tag{4.7}$$

With n [-] the total amount and i [-] one of the total amount of grid cells containing data points in the considered volume. The total frontal area per volume is now defined as:

$$\frac{1}{V}\sum_{i=1}^{n} A_i \tag{4.8}$$

In case scans from multiple stations have been taken, the same as above is done for every station, after which the average of the multiple scanning stations is taken a grid sell size.

4.4.2.2 Alpha shape method

In section 4.3.1 the alpha shape method is extensively treated. The greatest limitation of this method limitation is the minimum radius $1/\alpha$ to close the circle. This is illustrated in Figure 4.10, Figure 4.11 and Figure 4.12 for different α:

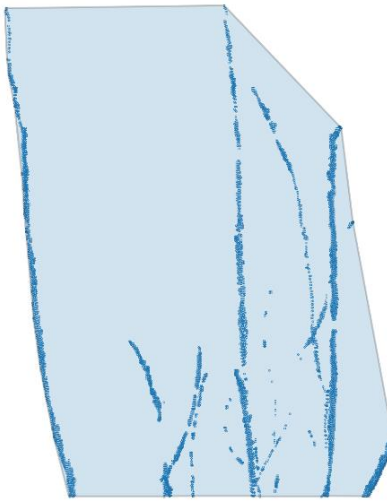

Figure 4.10: Alpha shape method with $\alpha = 1$

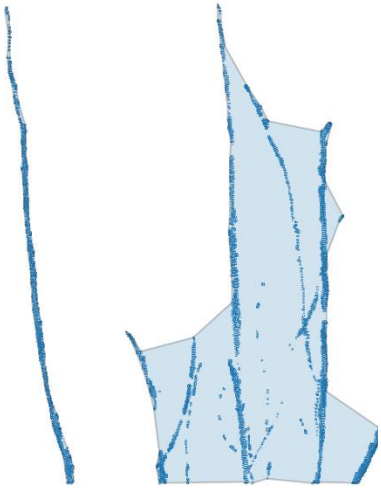

Figure 4.11: Alpha shape method with $\alpha = 10$

Figure 4.12: Alpha shape method with $\alpha = 50$

4.4.2.3 Conclusion

In order find out the advantages of both methods several examples have been tried. In this way better understanding of use is created and the efficiency of both methods is experienced. In Figure 4.13 and Figure 4.14 the empty strokes in stems of both figures are the result of shadowing, since only a TLS measurement from 1 position is used. This will be ignored in discussing both methods.

Figure 4.13: Slice of individual tree vegetation area 1, grid method

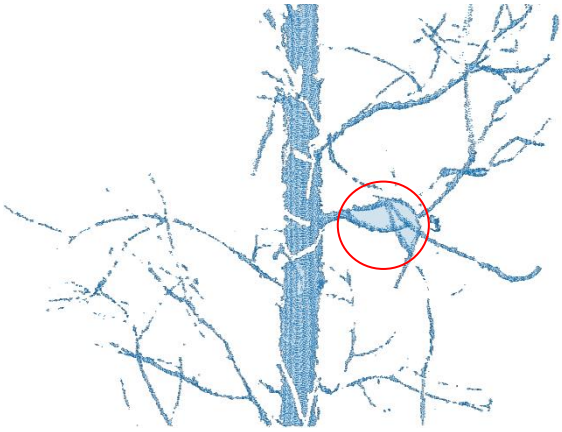

Figure 4.14: Slice of individual tree vegetation area 1, alpha shape method

The grid method is a very straightforward method: a grid is simply hold before the tree and then the filled grid cells are added to the frontal area. However, it is of essence to define the grid cell size correctly in order to not under- or overestimate the frontal area. This grid cell size is easy to adapt. The alpha shape method is slightly more complex: the intersection of all closed discs with radius $1/\alpha$ that contain all the points of the data set. The limitation of this method is outlined red in Figure 4.14. Multiple webs can be observed and the problem is that this cannot be solved. Hence, for the alpha shape method this results in overestimation of the frontal area. However, for simple shapes such as the stem of a tree, the alpha shape method is easy to use.

For uniform areas the frontal area of the stems of the trees will be estimated with the alpha shape method and the branches with the grid method. For non-uniform areas and hence individual tree species only the grid method will be used to estimate the frontal area.

4.4.3 Errors estimating the frontal area

Two methods (alpha shape and grid) have been introduced in section 4.4.2 to obtain the frontal area for uniform and non-uniform areas of tree species. Both methods are two dimensional and consider the point of view on the y-z plane with the x-direction perpendicular to this plane. For the grid method the whole tree slices will be made in x-direction (see Figure 4.15) in order to estimate the frontal area.
The use of slices will lead to errors for the grid method, but the applied orientation of the two dimensional images can lead to errors for both methods. These errors are discussed in this section.

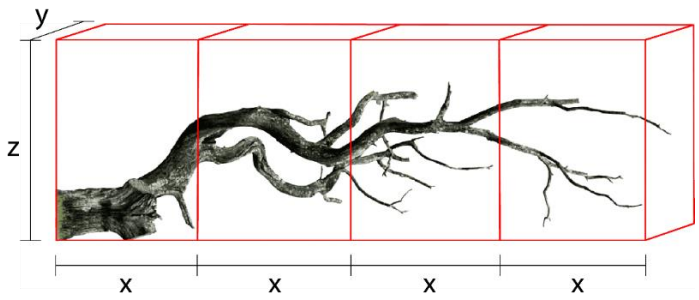

Figure 4.15: Schematisation of slices of a random branch in depth/x-direction

4.4.3.1 Magnitude slices

When the grid method is used (non-uniform areas and branches in uniform areas) slices will be made in x-direction. In order to assess the effect of the magnitude of the slices in x-direction, the frontal area of relatively small branches (order of 1 cm) and relatively large branches (order of 10 cm) will be estimated. This will be done using different magnitudes of slices in x-direction. The magnitude of the slices depend on the magnitude of the diameter of the stem or branches following (Kalloe, 2019). For example, if the stem seems to be dominant over branches, then use slices of the diameter of the stem in x-direction and vice versa. The branches and stems have been measured using the tool 'point picking' in CloudCompare, a program to edit point clouds.

An example of IDO (defined in section 3.3.2) is given in Figure 4.16. For these separate parts the most common diameter will be determined and used as size for the slices in x-direction.

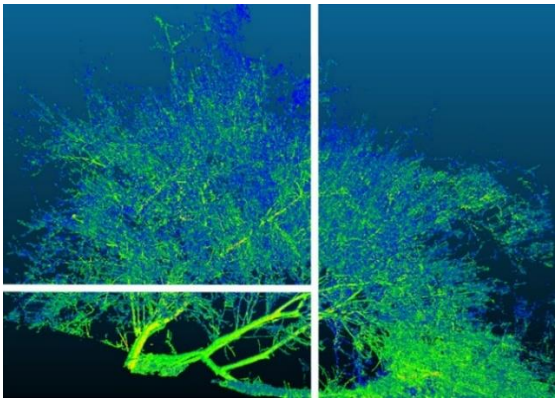

Figure 4.16: Division IDO based on diameter stem/branches

The influence of the magnitude of the slices is assessed by estimating the frontal area of the lower part using slices 8 (half), 16 and 32 (double) cm. The frontal area for the upper part is estimated using slices of 1 (half), 2 and 4 (double) cm. The MSS results are shown in the Figure 4.17 and Figure 4.18.

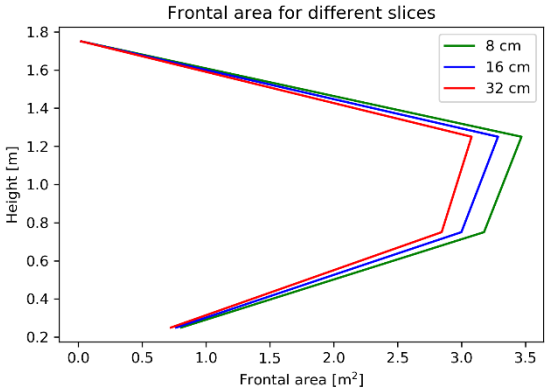

Figure 4.17: Frontal area for different slices: lower part

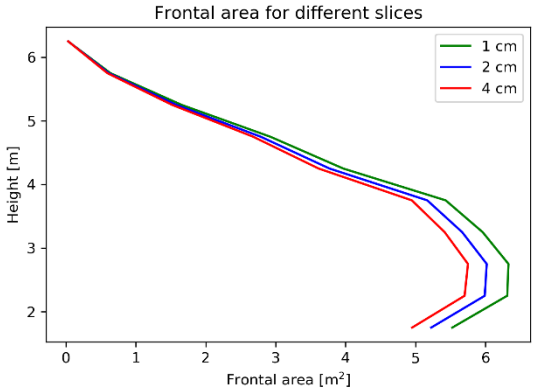

Figure 4.18: Frontal area for different slices: upper part

In both figures it is clear that for a larger value of the frontal area, also a larger difference is observed for different magnitude of slices.

The differences in both figures seem to be the same for the smaller and greater slices compared to the middle magnitude of slices, but this is not exactly the same. For example, the largest difference in Figure 4.17 is at an height of 1.25 m and is 0.18 m^2 for 8 cm and 0.20 m^2 for 32 cm slices. The largest difference in Figure 4.18 is at an height of 2.75 m and is 0.31 m^2 for 1 cm and 0.27 m^2 for 4 cm slices.

Slices with a magnitude greater than half or smaller than double the most common branch diameter will probably result in smaller differences in frontal area. Hence, the effect of the magnitude of slices is minor and taking the most common branch diameter as size of the slices in x-direction seems to be a solid choice.

4.4.3.2 Orientation

Following the theory in section 2.2, the frontal area is determined in the flow direction per unit volume of water. Since the flow direction is not known on beforehand, an average frontal area from multiple orientations is required. However, the large datasets of the point cloud result in large computation times. Therefore only one random orientation is chosen in order to determine the frontal area.

The frontal area from only one orientation is estimated, this could lead to either under- or overestimation of the frontal area. The most extreme situations are those in which the frontal area is based on a slice in Figure 4.19, while the flow direction is such that the frontal area should be as in Figure 4.20 and vice versa. This is illustrated below:

Figure 4.19: Situation 1

Figure 4.20: Situation 2

However, if both cases would be present equally they will cancel each other out.

4.5 Single scanning station (SSS) method

First the theory behind the Single Scanning Station (SSS) method will be explained and afterwards the application of this method for this study is discussed.

4.5.1 Theory

The SSS method takes only the point cloud into consideration from one scan and hence one position orientated towards the vegetation area or individual tree species (see Figure 4.21).

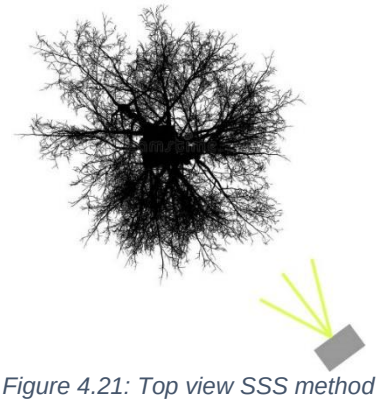

Figure 4.21: Top view SSS method

Shadowing is, as mentioned earlier, the hiding of branches behind other branches and can therefore not be hit by a laser beam of the TLS and hence is not included in the single station point cloud. Therefore it is obvious that when the laser beam hits a branch, the points perpendicular to the station behind the hit branch cannot be hit by the laser beam and hence will not be included in the point cloud. The TLS gathers a 360° point cloud in x,y-direction and nearly in z-direction. This means the perpendicular laser beams result in a 3D radius around the TLS, creating a spherical volume (see Figure 4.22).

When slices in terms of the radius are made, the amount of blocked points can be determined for every slice. This is done by counting the total points of the whole point cloud and subtracting the remaining amount of points by going one step away from a slice that is closer to the scanner. This is illustrated in Figure 4.23, with the red dot being the TLS instrument and the first circle around it being the circle without any points (due to the rotation disability in z-direction).

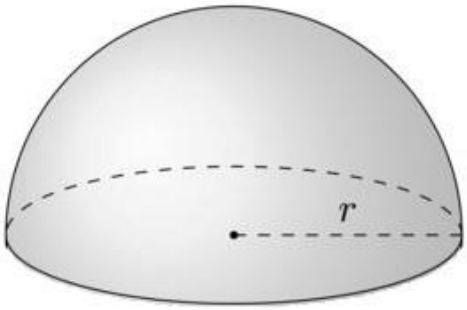

Figure 4.22: Spherical volume

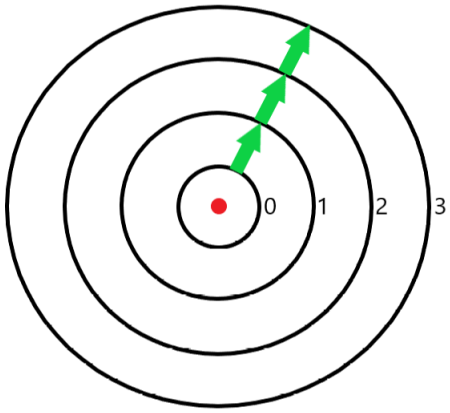

Figure 4.23: Top view 3D radius TLS

When standing at circle 0, all the points of the point cloud are included. All points present in slice 0-1 result in blocking the points in perpendicular line of the slices 1-2 and 2-3. The blocked points are therefore defined as follows:

$$(Blocked\ points)_i = Total\ points - \sum_{j}^{n} amount\ of\ points\ slices \tag{4.9}$$

With i the circle you stand at (standing point), n the total amount of slices and j the amount of slices starting at circle 0 until the standing point.

In order to compensate for the blocked points a shadowing correction factor per standing point is introduced. This will reduce the effect of underestimating the frontal area over the considered volume. This is defined as follows:

$$f_i = \frac{Total\ points}{Total\ points - (Blocked\ points)_i} \geq 1.0 \tag{4.10}$$

With f_i the shadowing factor at circle i. Standing at circle 0 therefore always results in $f_i = 1.0$. With this formulation it is assumed that every blocked point would otherwise result in frontal area of wave damping vegetation.

The TLS measurements using a single station (SSS) obtain point cloud data of vegetation from only one position. Therefore no complete 3D point clouds are obtained, since laser beams of the TLS instrument will be blocked by branches or stems (shadowing). Even though no complete point cloud is obtained, the measurements can still be valuable if the phenomena of shadowing can be corrected for. Based on Equation (4.3) for non-uniform areas, shadowing can be corrected for with the help of Equation (4.11):

$$\frac{1}{V}\sum_{j=1}^{n} A_{i,j} * f_i \tag{4.11}$$

With $\frac{1}{V}\sum_{j=1}^{n} A_{i,j}$ the summation of the frontal area per volume [m^{-1}] at circle (or slice) i in x-direction and f_i the shadowing factor [-] at circle i in x-direction.

4.5.2 Duursche Waarden

In this study the frontal area per volume is obtained using cubic instead of spherical volumes as considered in section 4.4. This demands a different approach in determining the shadowing factor. In case of cubic volumes also cubic slices area made, which is illustrated in Figure 4.24.

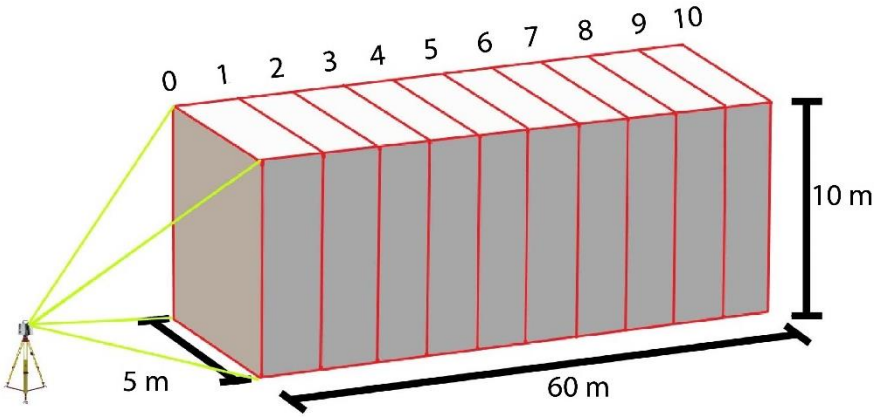

Figure 4.24: TLS in front of considered cubic volume

The total volume from a point cloud is in the order of 5x60x10 m. This volume is based on the width and height of the y-z plane (5x10 m) of the considered tree species perpendicular to the TLS instrument and x depends on the reach of laser beam (60m). In this case the points in the first slice do not necessarily block points in the consecutive slices in case of laser beams hitting the first slice in the corners which means in case of large angles in vertical (z-direction) and horizontal (y-direction) direction. This is the result of the TLS standing relatively close to the considered volume (order 1-5 m) at an height of approximately 1.5 m.

For the cubic volume the same equation can be used as for the spherical volume (Equation (4.11)) in case the laser beams can be assumed parallel in both z- and y-direction. Two laser beams can be assumed parallel in case they have a sufficiently small angle compared to each other (Li, et al., 2017). This is the case if the TLS would stand far enough from the considered volume. This will result in situation illustrated in Figure 4.25.

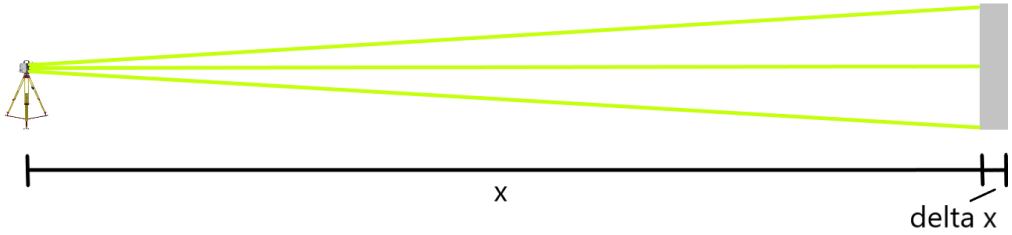

Figure 4.25: Parallel laser beams

If $x + \Delta x$ (with x the distance of the laser to the considered volume and Δx the length of the considered volume) is large enough the angles between the laser beams will be sufficiently small to assume parallel laser beams and hence Equations (4.10) and (4.11) can be used. According to (Li, et al., 2017) the angle is sufficiently small if it is in the order of 1-15°. This means the most upwards and most downwards laser beam within the considered volume should be maximum 15° from each other in order to assume only parallel laser beams within the volume. This is determined as follows:

$$x + \Delta x = \frac{10}{\tan(7.5)} \tag{4.12}$$

Hence, this is the case if $x + \Delta x$ is in the order of 75 m.

This distance is not reached with the TLS measurements. However, the method described in section 4.5.1 for spherical volumes will be applied for the cubic volumes in this study using Equations (4.10) and (4.11). More insight will be gained into whether this approach is valid or not by comparing this method with the MSS method and hand measurements.

4.6 Results

In this section the frontal area per volume of the prioritised vegetation areas (1, 2 and 3) is determined with the help of the point cloud data from the TLS measurements. In case of Multiple Scanning Stations (MSS) this is done with the methods described in sections 4.4.1.1 and 4.4.1.2. In case of a Single Scanning Station (SSS), the frontal area is determined with the help of the shadowing correction factor as described in section 4.5.2.

The minimum ground level found in AHN 3 on which wave damping vegetation is found is 1.6 m NAP. Most extreme condition is in case of water level is 5.70 m NAP with the maximum wave height of approximately 1.00 m. This means the frontal area of the vegetation is only of important in the range 0 to $5.70 + 1.00/2 - 1.6 = 4.60\,m$.

Therefore only the frontal area of tree species over the height will be determined until a maximum of 10 m (to be sure) of slices in z-direction of 0.5 m for all vegetation areas.

4.6.1 Multiple scanning stations (MSS)

In this section only the results of individual tree species or forest patches with multiple scanning stations will be discussed. First the results of two tree species are discussed extensively after which results of the other scans are summarised. The graphs of the other species can be found in Appendix Results TLS .

4.6.1.1 Uniform area

Vegetation area 1 is now used to show the method for uniform areas. As explained in section 3.3.2 this area is considered uniform and consists of a mix of willow species *Salix fragilis* and *Salix alba* (UMW-1). Three TLS measurements close to each other have been done in the centre of vegetation area 1 to obtain a point cloud. The volume of this point cloud is 10x10x10 m (x,y,z). The second method described in section 4.4.1.1 will be used to determine frontal area over the height.

Since the area of the stem dominates over the area of branches, the stem is separated from the branches to determine the frontal area. The branch thickness range from 1 to 6 cm and therefore slices of 3 cm in x-direction are made for the file with only branches. For the stem the alpha shape method is used instead of the grid method as explained in section 4.4.2. Due to the understorey vegetation of circa 1-2 m high in the whole vegetation area, the shadowing phenomena occurs in this region of the stem. This is easily solved with the alpha shape method.

The average frontal area per volume over the height is determined using Equations (4.1) and (4.2) with $m = 17$ (total amount of trees in considered volume) and $n = 3$ (the total amount of trees considered for determining the frontal area). The result of the frontal area over the height of the tree trees is shown in below figures. In Figure 4.29 a graph is made to show whether the branches or stem dominate. This will be useful later in determining the bulk drag coefficient $\tilde{C}_D$.

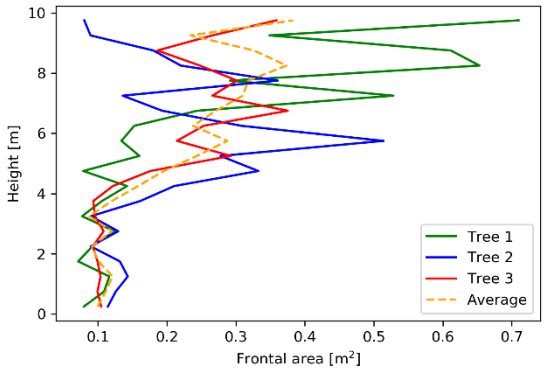

Figure 4.26: Frontal area UMW-1

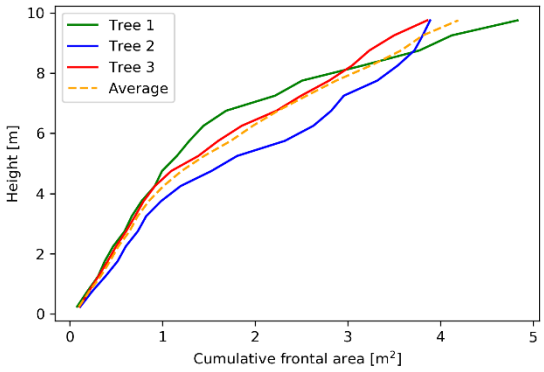

Figure 4.27: Cumulative frontal area UMW-1

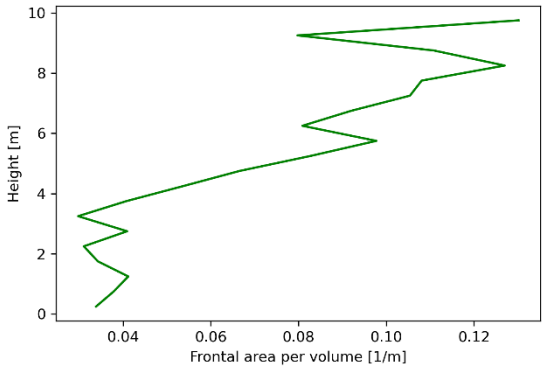

Figure 4.28: Average frontal area per volume UMW-1

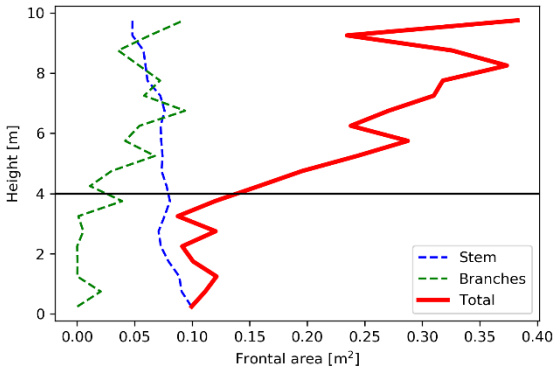

Figure 4.29: Frontal area distribution UMW-1

It can be observed that the frontal area is dominated by the stem until about 4 m and for greater heights both the stem and branches deliver about the same frontal area.

4.6.1.2 Non-uniform area

In a non-uniform area the frontal area of the most common tree species are estimated individually. The oak species *Quercus pubescens* (IDO) is located in vegetation area 2 and 3 and discussed now. These vegetation areas are non-uniform. The three most common trees in these vegetation areas have been measured with the TLS instrument from three different positions. For these three tree species the frontal area per volume over the height is determined with the method described in section 4.4.1.2.

This species consists of one stem of approximately 13 cm thickness bifurcating into branches of 7 cm to approximately 1 mm and is not considered as dense. Due to the large difference in diameter the tree is divided into three parts as explained in section 4.4.3.1. The upper left and right part consist of mainly branches and therefore slices of 1 cm in x-direction have been made. The lower left part consists mainly of stem and therefore slices of 13 cm in x-direction have been used.

Since the considered tree species is located near another tree, a thick branch is located in the considered tree at a height of z = 3-4.5 m. The frontal area of this branch is estimated to be $0.06 * 2.4 = 0.144\ m^2$ and is subtracted over the three slices in z-direction: 0.048 m^2 per slice. Also during the TLS measurements little leaves were present. Since this is no wave damping frontal area a conservative correction factor of 0.90 at all branches is applied. The frontal area per volume over height is determined with the help of Equation (4.3) and the results are shown in Figure 4.30 and Figure 4.31.

Most of the frontal area is observed around 0.5 m. This seems obvious since the stem is almost horizontally positioned and hence a lot of frontal area is concentrated in one or two slices of 0.5 m. At higher parts the frontal area per volume ranges from 0.15 to 0.30 m^{-1}.

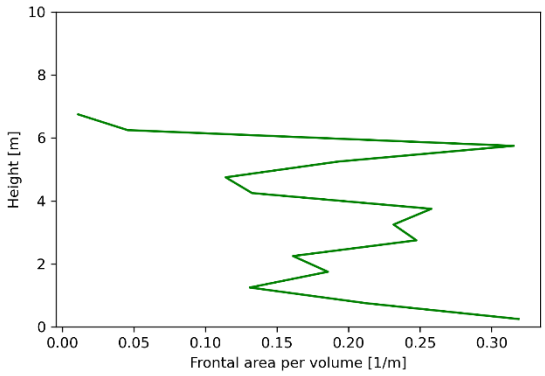

Figure 4.30: Frontal area per volume IDO

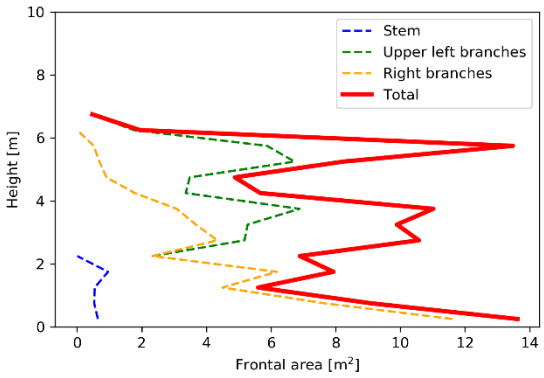

Figure 4.31: Frontal area distribution IDO

4.6.1.3 Other tree species

The other tree species are treated following the same steps as the methods described in sections 4.4.1.1 and 4.4.1.2. The separate parts of branch thickness per tree species are illustrated in Appendix Regions based on branch thickness. In Table 4-3 several aspects for the results of different tree species are summarised.

Tree species[1]	Magnitude slices	Method estimation frontal area	Extra information
Individual Pedunculate Oak (IPO)	Left part: 3 cm Middle part: 47 cm Right part: 9 cm	As described in section 4.4.1.2	x
Individual Osier (IO)	Lower part: 16 cm Upper part: 2 cm	As described in section 4.4.1.2	90% of frontal area due to presence of leaves
Uniform Crack Willows (UCW)	Stem: alpha shape Branches: 3 cm	As described in section 4.4.1.1 - method 2 with $m = 24$ and $n = 3$	x
Uniform Mix of Willows (UMW-3)	Lower part: 12 cm Upper part: 2 cm	As described in section 4.4.1.2	[2]

Table 4-3: Summary of method for obtaining results different tree species

[1] For mor information on the tree species see section 3.3.2 or Appendix Tree species

[2] This area is considered uniform, but due to the high density it was not possible to use method 2 in section 4.4.1.1. Therefore in determining the frontal area, a small isolated subarea was found for the TLS measurements and is considered as an individual tree species by using the method as described in section 4.4.1.2

The frontal area per volume of the separate tree species are illustrated in Appendix Results TLS . In the Figure 4.32 and Figure 4.33 the frontal area (per volume) of the four different tree species is illustrated together.

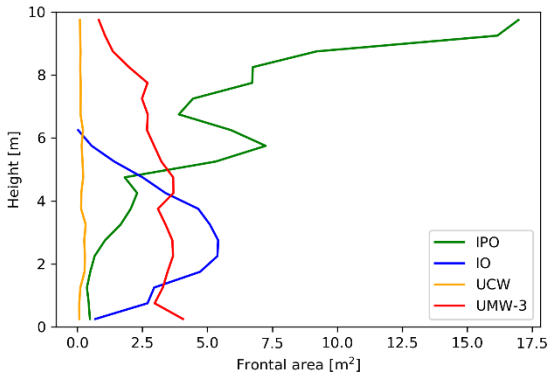

Figure 4.32: Frontal area of 4 different tree species

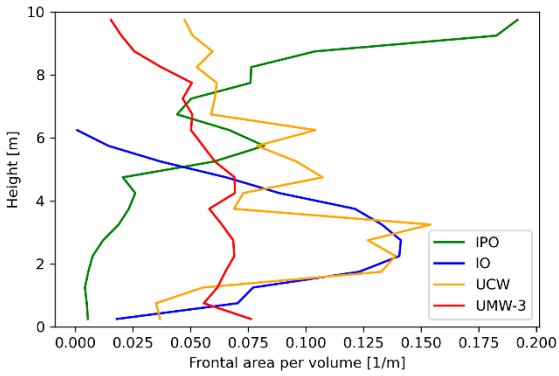

Figure 4.33: Frontal area per volume of 4 different tree species

It can be observed that for the frontal area of IPO is dominating from approximately 5 m height due to the branches that appear from this height. Hence this tree species got quite some frontal area since it is a large it tree, but as a result of its size the frontal area per volume is relatively less (see section 3.1).

The frontal area (per volume) of IO is quite average relative to the other species, while for this relatively dense tree species significantly higher outcomes were expected. The shadowing phenomena within the tree itself probably plays a role for these relatively low outcomes. Due to the high density, even a merged point cloud from three scanning stations cannot contain every branch. The shape of the frontal is similar to a tilted parabola with a peak at circa 2.5 m height and this typically what you would expect for this almost horizontally growing tree species.

The frontal area of an average tree of UCW is significantly low to the other species, while the frontal area per volume is little higher compared to other tree species. This can be explained by the fact this uniform area of tree species is treated as described in section 4.4.1.1 - method 2.
The frontal area is given for an average tree in this uniform area. Due to the high density, many of the (almost) same tree species occur in the considered volume. This results in relatively high values for the frontal area per volume. The zigzag in Figure 4.33 is a result of the absence or presence of branches. The average tree is determined by randomly picking three trees. The frontal area of two of these trees showed similar outcomes over the height, but one deviated from the two. This tree contained more branches and hence got higher values for the frontal area. Therefore the frontal area of the 'average tree' could be overestimated.

The frontal area of UMW-3 is quite constant over the height and shows relatively high values compared to other species. However, the frontal area per volume shows relatively low values. This is against expectations, since this is considered as dense vegetation. The reason is probably the same as for IO and therefore this result is not trusted. In the section 4.6.2 it is investigated whether this assumption is right.

4.6.2 Single scanning station (SSS)

In this section it is checked whether the frontal area per volume of multiple scanning stations is similar to those of one scanning station using a shadowing correction factor (Equation (4.11)) as introduced in section 4.5. This should give more insight in the accuracy of the frontal area per volume using the shadowing correction factor. The same volume as for the multiple scanning stations is considered for each individual tree species. This will be done for individual tree species only (non-uniform areas), since the density in the uniform areas UMW-1 and UCW is low and hence the probability of shadowing is significantly lower. Especially based on field observations, the individual tree species are categorised in 'sparse to moderate' and 'dense' vegetation. Expected order of magnitude of the frontal area per volume for sparse to moderate dense vegetation is 0.01-0.20 m^{-1} and for dense vegetation 0.20 m^{-1} or greater ((Janssen, 2016) , (Stam, 2018), (Vries, et al., 2009) and (Kalloe, 2019)).

4.6.2.1 Sparse to moderate dense vegetation

The individual tree species IDO and IPO are considered to be moderate dense and sparse vegetation. Instead of choosing the magnitude of the slices in x-direction based on the diameter of the stem and branches (and divide the tree into parts), now the average of slices in x-direction is taken. This results in slices of 7 cm in x-direction for scan 2.9 and in slices of 20 cm for scan 2.10. Also now a correction factor of 0.90 is applied for Scan 2.9 to correct for the presence of the leaves. The results are shown in Figure 4.34 until Figure 4.37.

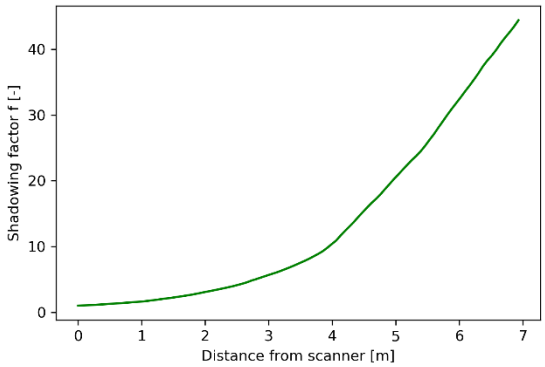

Figure 4.34: Shadowing factor SSS method (tree species IDO) of scan 2.9

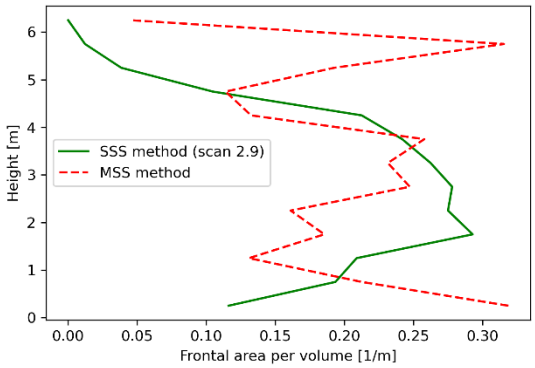

Figure 4.35: SSS vs. MSS method (tree species IDO)

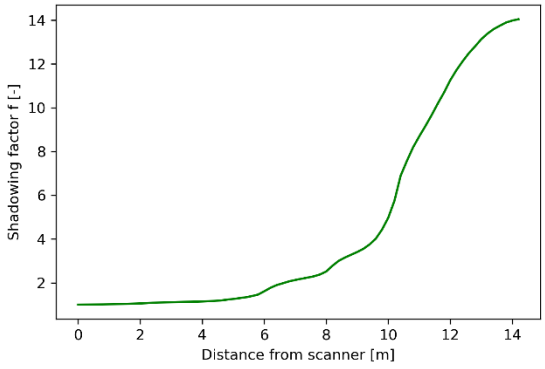

Figure 4.36: Shadowing factor SSS method (tree species IPO) of scan 2.10

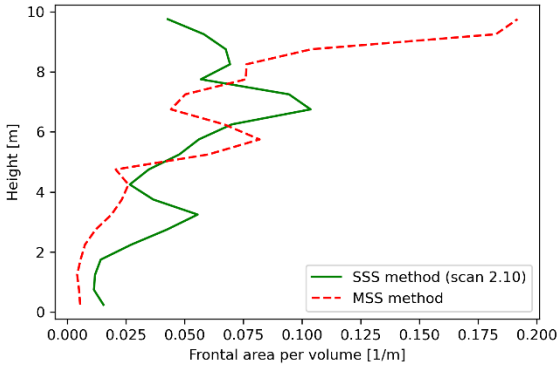

Figure 4.37: SSS vs. MSS method (tree species IPO))

In Figure 4.34 and Figure 4.36 the same trend can be observed for the shadowing factor: first a slight increase after which the increase magnifies. The explanation for this is that at the rapid increase the laser is towards the end of the considered tree and hence only limited amount of voxels are left. The total amount of voxels in the volume is then divided by the left voxels and hence this gives large numbers.

In Figure 4.35 and Figure 4.37 approximately the same values and trend are found. Especially scan 2.10 shows values and the trend that corresponds to the values of three scans, except for 9-10 m. This could be a consequence of the averaged slices in x-direction which could lead to skipping of branches. The same probably holds for scan 2.9, where the lower and upper part are underestimated in comparison to the results of the three scans.

4.6.2.2 Dense vegetation

The individual tree species IO and UMW-3 are considered to be dense vegetation. It is more likely the shadowing phenomena occurs for dense vegetation and therefore the frontal area per volume from the Single Station Scans will be determined using the shadowing correction factor. This will give better insight into the shadowing phenomena. Since the outcomes for dense vegetation are believed to be more uncertain than sparse to moderate dense vegetation, the SSS method is executed for all individual (two or three) scans instead of one scan. This means three scans for IO and two scans for UMW-3. Average slices of 9 cm in x-direction are taken for the single scans of IO and 7 cm for the single scans of UMW-3. The results are shown in Figure 4.38, Figure 4.39, Figure 4.40 and Figure 4.41.

The range of the shadowing factor varies per scan. For IO the range is 0-190 and for UMW-3 0-100. They all show a rapid increase at the location at the end of the volume. It is also clear that the frontal area per volume is underestimated by the Multiple Scanning Stations in which the assumption is made that no shadowing occurs. Apparently shadowing does occur for this dense vegetation.

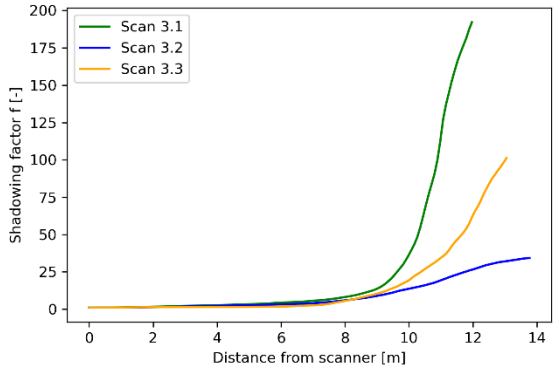

Figure 4.38: Shadowing factor SSS method (tree species IO)

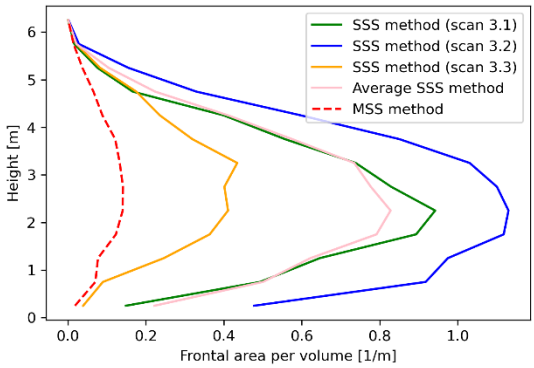

Figure 4.39: SSS vs. MSS method (tree species IO)

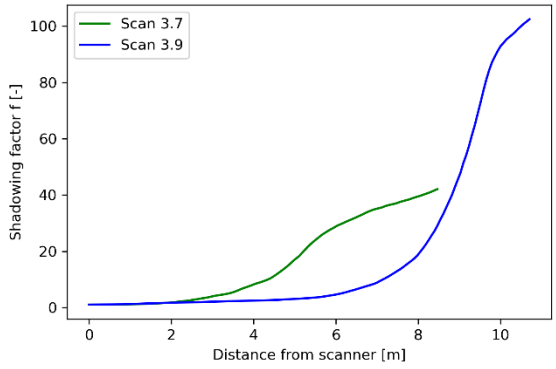

Figure 4.40: Shadowing factor SSS method (tree species UMW-3)

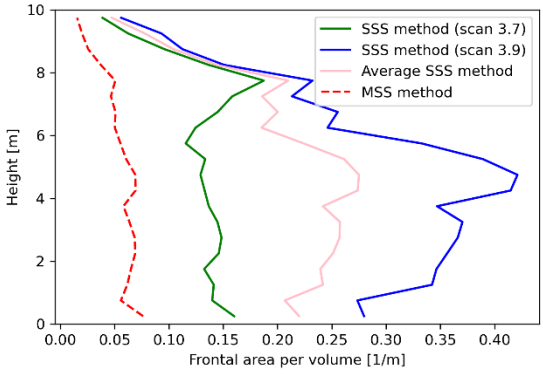

Figure 4.41: SSS vs. MSS method (tree species UMW-3)

In order to have a fair comparison, the orientation of scan 3.3 (SSS method) coincides with the orientation of the MSS method for species IO (see Figure 4.39). The orientation of scan 3.7 (SSS method) coincides with the orientation of the MSS method for species UMW-3 (see Figure 4.41). In Figure 4.39 (species IO) it can be clearly observed that scan 3.3 shows about the same trend as the MSS method, but shows significantly larger values for the frontal area per volume. Even two to three times larges values are observed at an height of 3 m. In Figure 4.41 (species UMW-3) about the same is visible: a similar trend as the MSS method, but significantly larger values for the frontal area per volume by the SSS method.

The other single scanning stations for species IO show the same trend over the height, but show even larger values with peaks at 2.5 m 0.9 and 1.1 m^{-1}. Also for UMW-3, scan 3.9, shows a similar trend but shows even larger values than scan 3.7. The frontal area per volume for scan 3.7 and 3.9 with the SSS method shows a difference of about 0.25 m^{-1} at 5 m height. However, the larger outcomes are still lower than expected, since this vegetation was believed to be most dense. The most obvious reason for this difference between the single scans of IO and UMW-3 is probably that every individual scan has a different orientation towards the individual tree species.

Multiple orientations are included, since the outcomes for dense vegetation is believed to be most uncertain. The average of outcomes for all scans with the SSS method are used.

4.7 Validation TLS outcomes

Results of the frontal area per volume of the different individual species and forest patches for MSS and SSS have been obtained. The starting point are the results of the MSS method, since these results are based on point clouds which are obtained from multiple positions and hence give a more complete point cloud. Only outcomes for the frontal rea per volume until an height of 5 m are discussed now, since this is the maximum height vegetation will be submerged during storm conditions.

However, it is shown in section 4.6.2 that the outcomes of MSS for the dense vegetation differ significantly from the outcomes of SSS for tree species IO and UMW-3. Since it is believed that dense vegetation brings more frontal area than sparse to moderate dense vegetation, the outcomes for MSS of these two species are not trusted.

Also the outcomes of hand measurements (see Appendix Results hand measurements for more information) presented in Figure 4.42 and Figure 4.43 suggest greater values for IO and UMW-3 concerning the frontal area per volume than MSS outcomes. The average outcomes for SSS coincide significantly better with the outcomes of the hand measurements. Therefore the average outcomes of SSS including a shadowing correction factor will be used for IO and UMW-3.

Hand measurements of the stem only for species UMW-1 and UCW in Figure 4.44 and Figure 4.45 suggest underestimation of MSS outcomes. However, it is expected that no significant errors are made by estimating the frontal area per volume of stems from point cloud data from the TLS, due to the simple shape and small probability of shadowing. Also hand measurements were done for significantly smaller volumes (5x5x2 and 3x3x2 m vs. 10x10x5 m) and hence will be less representative than TLS measurements. Therefore the MSS outcomes are used in SWAN computations for species UMW-1 and UCW.

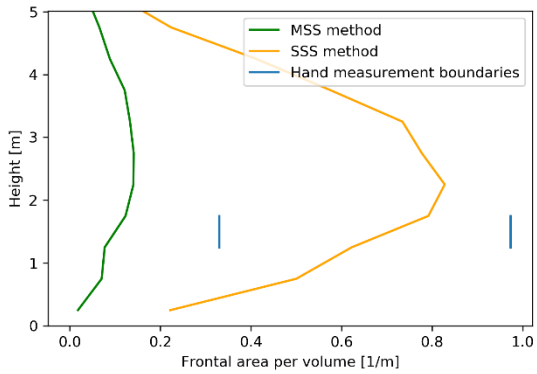

Figure 4.42: MSS vs. SSS method species IO

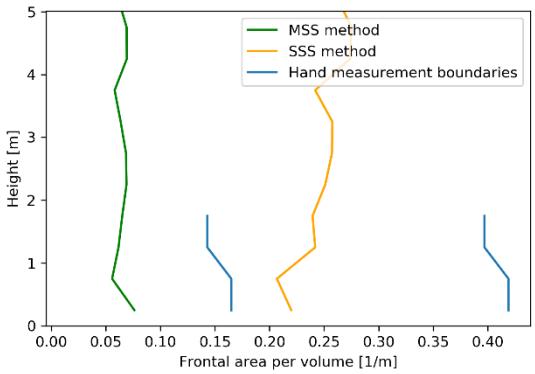

Figure 4.43: MSS vs. SSS method species UMW-3

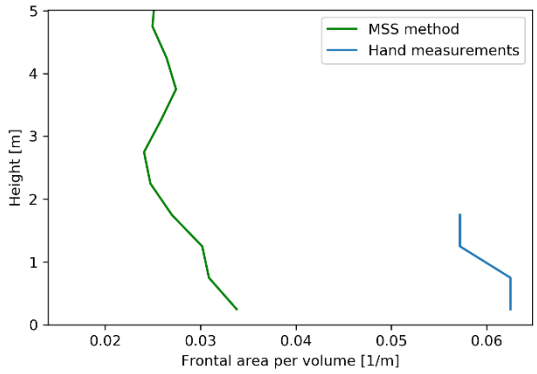

Figure 4.44: MSS method vs. hand measurements species UMW-1

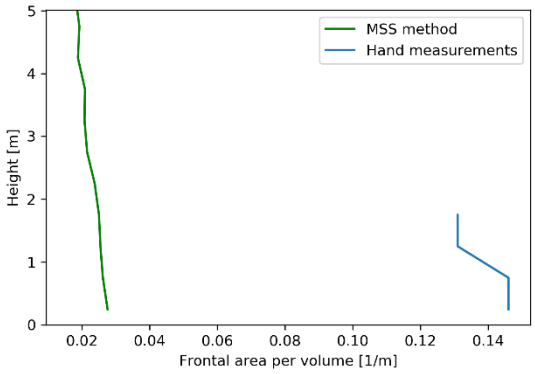

Figure 4.45: MSS method vs. hand measurements species UCW

Hence, both the MSS and SSS method seem to be applicable for sparse to moderate dense vegetation as they give similar results. However, the MSS method is preferred since a more complete point cloud is obtained and hence less uncertainty is included than with the SSS method, This is because the SSS method corrects for the less complete point cloud with a shadowing factor. The SSS method seems to be only applicable for dense vegetation as the method corrects for the excluded branches due to shadowing, which is validated with hand measurements. The outcomes for the frontal area per volume that will be used in SWAN are summarised in Table 4-4. In Figure 4.46 the vegetation parameters for SWAN are visualised, in which IDO, IPO and IO form the subareas as described in section 3.3.2.The values of Figure 4.46 can be found in Appendix Vegetation parameters for SWAN.

Tree species	**Type of outcomes** $\frac{1}{V}\sum_{i=1}^{n} A_i$
Uniform Mix of Willows, vegetation area 1 (UMW-1)	Average of MSS
Individua Downy Oak (IDO)	MSS
Individual Pedunculate Oak (IPO)	MSS
Individual Osier (IO)	Average of SSS
Uniform Crack Willows (UCW)	Average of MSS
Uniform Mix of Willows, vegetation area 3 (UMW-3)	Average of SSS

Table 4-4: Results to be implemented in SWAN

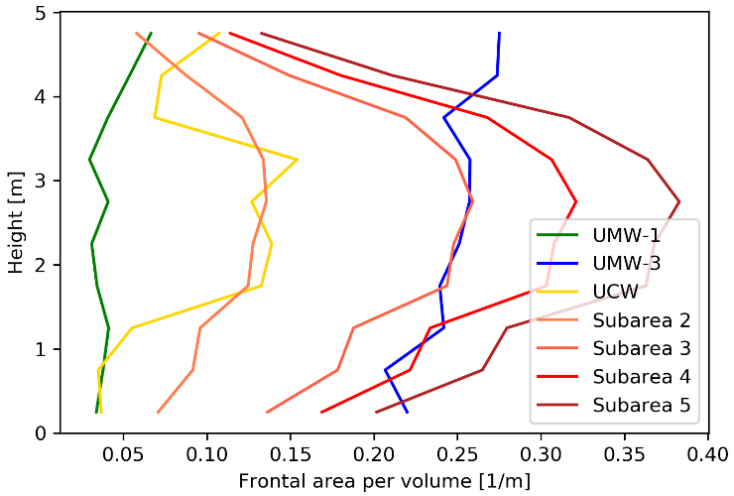

Figure 4.46: Vegetation parameters SWAN

5 Modelling with SWAN

In this chapter SWAN 1D and 2D computations will be performed. First the 1D Hydra-NL (using Bretschneider) computations will be compared with SWAN 1D computations without vegetation. Then SWAN 1D computations including vegetation will give relatively quick insight into the wave damping characteristics and wave heights at Duursche Waarden. Hereafter, SWAN 2D computations with and without vegetation will be performed. Finally a 2D sensitivity analysis is performed. SWAN 41.31 is used for the 1D and 2D computations.

5.1 1D computations

In this section a 1D SWAN model will be set up representing the wave propagation in the Duursche Waarden. This will be done for the output points 185, 190 and 193 in year conditions 2050 and 2100 (results of 2050 and 2100 are linearly interpolated to get the outcome for the desired year 2075) to be used for assessment and design. The outcomes without vegetation are compared to the results using Bretschneider. When the model is validated the effect of vegetation and bottom friction is checked.

5.1.1 General settings

A grid with resolution of 5x5 m including bottom levels have been made of Duursche Waarden and the surrounding area. The bottom levels vary from about -14 to 10 m NAP. For every dike location the two wind directions resulting in highest exceedance frequency of the hydraulic load are considered following Hydra-NL calculations. This results in two different effective fetches per dike location. The bottom level that is used for the 1D computations depends on the length and direction of the effective fetches. A 1D line is drawn on the grid to extract the the bottom levels which results in a computational grid with a resolution of 5.0 to 7.1 m depending on the wind direction. An example is shown in Figure 5.1. Yellow indicates heights of about 10 m NAP and dark blue about -14 m NAP.

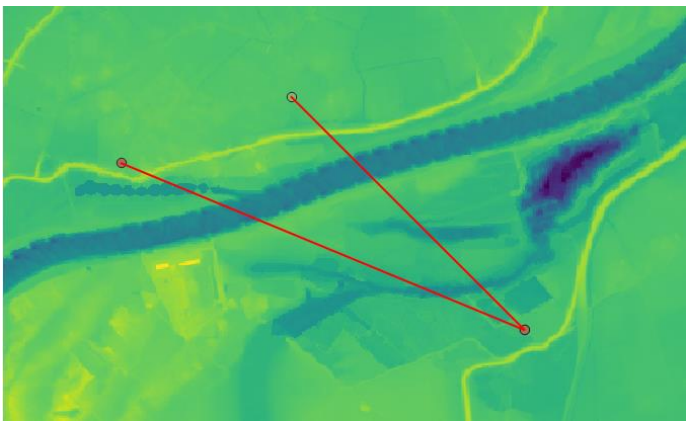

Figure 5.1: Path the wave crosses (dike location 190, wind direction WNW and NW)

In Appendix Settings SWAN 1D a more elaborate explanation is given concerning the used settings in SWAN 1D, including a the 5x5 m grid with colourbar.

5.1.2 Vegetation

In SWAN the vegetation is implemented over the height, starting at the bottom. As explained in section 3.1 the product of branch diameter b_v [m] and the number of stems N [number per m^2] is defined as $\frac{1}{V}\sum_{i=1}^{n} A_i$ [m^{-1}] in this study. Therefore, the product of b_v and N at a certain height in SWAN will be set equal to the outcomes of the frontal area per volume obtained in chapter 0. With the example in Table 5-1 is demonstrated how is dealt with the problem.

Results chapter 0	SWAN input	Results chapter 0	SWAN input		
Height [m]	**Height layer [m]**	**$\frac{1}{V}\sum_{i=1}^{n} A_i$ [m^{-1}]**	**Branch diameter [m]**	**Number of branches [m^{-2}]**	**Bulk drag coefficient [-]**
0.0-0.5	0.5	0.20	0.20	1	1.2
0.5-1.0	0.5	0.15	0.15	1	1.2
1.0-1.5	0.5	0.25	0.25	1	1.1
1.5-2.0	0.5	0.30	0.30	1	1.0
2.0-2.5	0.5	0.18	0.18	1	1.1

Table 5-1: Example input SWAN

The vegetation can be implemented at specific grid cells by defining a file 'Nplants'. In this file the vegetation is implemented in case a '1' is defined at a grid cell. In case there is no vegetation a '0' is defined at a grid cell.

Another problem arises when different areas/types of vegetation need to be implemented in SWAN, since only of only type of vegetation, the vegetation parameters (b_v, N and $\tilde{C}_D$) over the height can be implemented. This problem is dealt with using the average vegetation parameters for every vegetation type. For instance if the wave crosses vegetation areas 'subarea 3' and 'UCW'. Then the vegetation parameters of subarea 3 over the height are implemented in SWAN (could also be UCW) and the average vegetation parameter ratio is used in the 'Nplants' file to implement UCW. This is in this case: $UCW/subarea\ 3 = 0.0943/0.177 = 0.533$. This results in the right average ratio concerning vegetation parameters, but results in a different distribution over the height for UCW. This is shown in Figure 5.2.

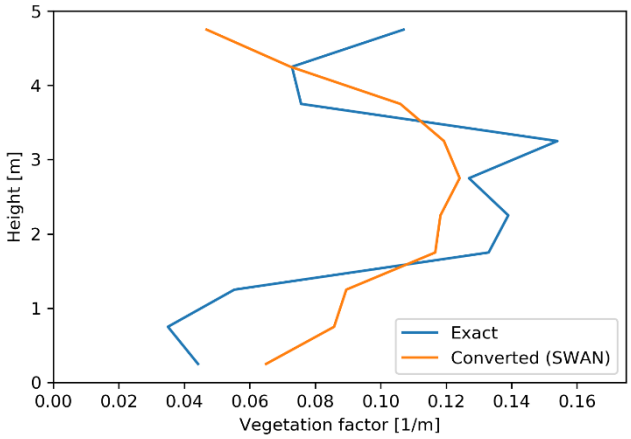

Figure 5.2: Exact vs. converted vegetation factor over the height UCW

Hence, it is of importance what vegetation type is used in SWAN as input vegetation. For every dike location and wind direction the types of vegetation crossed by the wave, the input vegetation, water level and grid cell size are listed in Appendix Input parameters SWAN 1D.

5.1.3 SWAN 1D vs. Hydra-NL (Bretschneider)

With the help of Hydra-NL calculations the wave height has been estimated at three output points (185, 190 and 193) using Bretschneider (see Table 2-1). The model uncertainty of Bretschneider is also included in Hydra-NL outcomes. Now the wave height will be estimated using SWAN. Just as for Bretschneider there exists also model uncertainty for SWAN outcomes. In Table 5-2 model uncertainty of wave parameters (normal distribution) is shown for both models following (Chbab, et al., 2015).

Model	**Wave height**		**Wave period**	
	Mean, μ [-]	Standard deviation, σ [-]	Mean, μ [-]	Standard deviation, σ [-]
Bretschneider	0.96	0.27	1.03	0.13
SWAN	0.94	0.15	0.99	0.07

Table 5-2: Model uncertainty of wave parameters

The difference in both models will be studied by using the same effective fetch, wind speed, wind direction and uniform water depth in SWAN as for Bretschneider's model. Then the exact water depth (and hence no uniform water depth) will be used for the output points. The outcomes of Hydra-NL (Bretschneider including model uncertainty) and SWAN including model uncertainty will be compared. The vegetation is not implemented yet here. The inclusion of model uncertainty is done by assuming the outcomes of the wave parameters are located at the right side compared to the main of the normal distribution (see Figure 5.3).

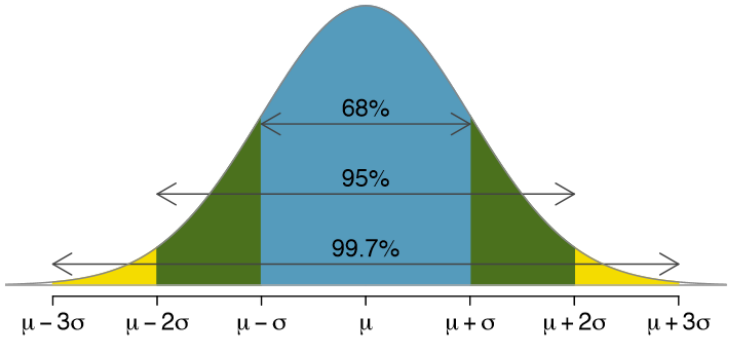

Figure 5.3: Normal distribution (Dataquest, 2018)

This means the outcome of the wave height and wave period including model uncertainty is determined as follows (Chbab, et al., 2015):

$$H_{s,u} = H_s * (1 + (\mu - 1) + \sigma) \quad (5.1)$$

$$T_{p,u} = T_p * (1 + (\mu - 1) + \sigma) \quad (5.2)$$

With H_s the significant wave height without model uncertainty [m], $H_{s,u}$ the significant wave height including model uncertainty [m], T_p the peak period without model uncertainty [s], $T_{p,u}$ the peak period including model uncertainty [s], μ the mean [-] and σ the standard deviation [-]. Hence, including the model uncertainty of SWAN results in a multiplication of 1.09 for H_s and 1.06 for T_p.

Bretschneider's formula is empirical and contains the variables effective fetch, water depth and wind speed for determining the significant wave height. Empirical means the formula is rather based on observations and measurements than theory. However, physical aspects such as the limiting influence of the water depth on the wave height and bottom friction for a certain fetch is all included in Bretschneider's formula. This results in quite good estimations of wind-generated and fetch- and depth-limited waves and is therefore often used as a first indicator. In contrast, the wave model SWAN is completely based on theories of physics, see Appendix SWAN.

5.1.3.1 Uniform depth without friction

The three output points (185, 190 and 193) will be analysed. This will be done for the wind direction resulting in highest exceedance frequency of the hydraulic load level following Hydra-NL (Bretschneider) and a return period of 66666 year as described in section 2.1 and shown in Appendix Governing parameters dike segments. The same conditions will be used in SWAN as for Bretschneider: effective fetch, wind direction, wind speed, a representative uniform depth, water level (5.699 or 5.644 m NAP) and no wave energy losses due to white-capping, bottom friction and vegetation. Quadruplet wave-wave interaction, triad wave-wave interactions and depth-induced breaking are implemented in the SWAN computations as described in Appendix SWAN. The conditions are summarised in Table 5-3.

Output point	Wind direction	Fetch [m]	Water depth [m]	Wind speed [m/s]	
				Year: 2050	Year: 2100
185	WNW	1830	5.699-2.83 = 2.869	23.9	25.7
190	WNW	1760	5.699-0.58 = 5.119	23.1	25.5
193	W	2045	5.644-1.82 = 3.824	22.7	24.7

Table 5-3: Summarised conditions SWAN 1D computation

In order to see the difference in both methods the results of output point 185 will be shown. A uniform water depth of 2.87 m is used (see Table 5-3). The results are shown in Figure 5.4 and Table 5-4.

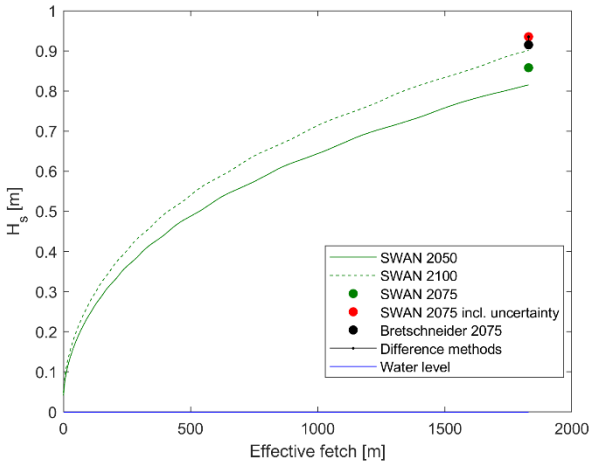

Figure 5.4: Wave generation for output point 185 (no bottom friction and white-capping)

	Hydra-NL (Bretschneider)	SWAN 1D		
Dike location	**$H_{s,u}$ 2075 [m]**	**H_s 2075 [m]**	**$H_{s,u}$ 2075 [m]**	**SWAN/Hydra-NL [%], difference [cm]**
185	0.915	0.858	0.935	102.2, +2.0
190	0.995	0.881	0.960	96.5, -3.5
193	0.960	0.873	0.952	99.2, -0.8

Table 5-4: SWAN 1D vs. Hydra-NL (uniform water depth excluding bottom friction and white-capping)

For almost the exact same conditions about the same values can be observed for the different models in Table 5-4. Lower results for Hydra-NL would be expected since these already include bottom friction and white-capping.

5.1.3.2 Uniform depth with friction

In this case energy losses due to white-capping and bottom friction are incorporated and hence vegetation not yet. All other conditions and settings are still the same as in section 5.1.3.1. The results are shown in Figure 5.5 and Table 5-5:

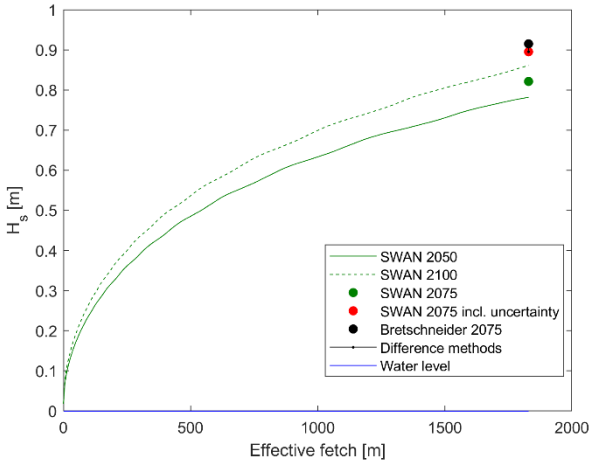

Figure 5.5: Wave generation for output point 185, wind direction WNW (no bottom friction and white-capping)

	Hydra-NL (Bretschneider)	SWAN 1D		
Dike location	**$H_{s,u}$ 2075 [m]**	**H_s 2075 [m]**	**$H_{s,u}$ 2075 [m]**	**SWAN/Hydra-NL [%], difference [cm]**
185	0.915	0.821	0.895	97.8, -2.0
190	0.995	0.874	0.953	95.8, -4.2
193	0.960	0.851	0.928	96.7, -3.2

Table 5-5: SWAN 1D vs. Hydra-NL (uniform water depth including bottom friction and white-capping)

Now for exact the same conditions, including bottom friction and white-capping, slightly lower results (2 to 4 cm) for SWAN can be observed in Table 5-5.

As white-capping will give about the same reduction for every dike location, the bottom friction for dike location 185 is significantly higher than for the other two. This is due the lower water depth (2.869 m vs. 3.824 and 5.119 m) and hence the waves will start 'feeling the bottom' earlier, resulting in higher bottom friction and hence more wave energy dissipation.

5.1.3.3 Exact water depth

No uniform depth is used now, but instead the exact water depth is used as described in section 0. All other conditions and settings remain the same as in sections 5.1.3.1 and 5.1.3.2. Computational grid is regular with a step size varying from 5.0 to 7.1 m. The results are shown in Figure 5.6, Figure 5.7 and Table 5-6.

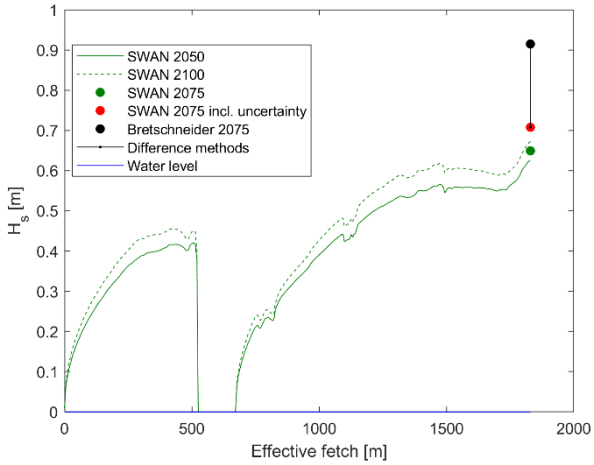

Figure 5.6: Wave generation for output point 185, wind direction WNW (including friction and white-capping)

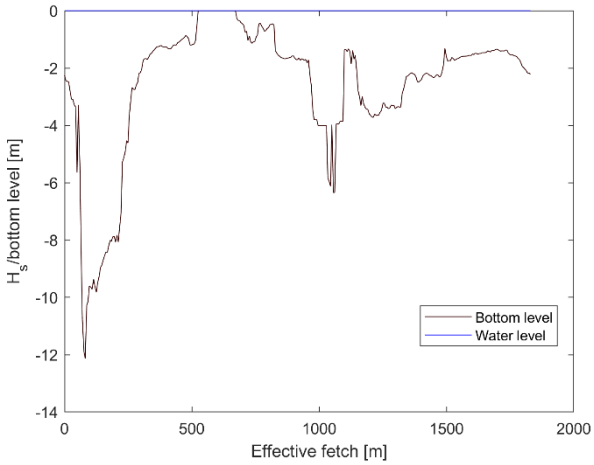

Figure 5.7: Exact water depth for output point 185

	Hydra-NL (Bretschneider)	SWAN 1D		
Dike location	**$H_{s,u}$ 2075 [m]**	**H_s 2075 [m]**	**$H_{s,u}$ 2075 [m]**	**SWAN/Hydra-NL [%], difference [cm]**
185	0.915	0.649	0.707	77.3, -20.8
190	0.995	0.783	0.853	85.7, -14.2
193	0.960	0.729	0.795	82.8, -16.5

Table 5-6: SWAN 1D vs. Hydra-NL (exact water depth including bottom friction and white-capping)

Now the exact water depth is used instead of an uniform water depth great differences in $H_{s,u}$ are noticeable of 14 to 21 cm. For all three dike locations the wave is broken at least once due to very low water depth or even dry land in these storm conditions. When the wave is broken in quite a late stage (e.g. dike location 185 at 700 m out of an effective fetch of 1830 m in Figure 5.6) this means the wave has only limited amount of distance to be generated by the wind. Therefore these huge reductions are noticeable. It can be concluded that calculations with the uniform water depth do not properly reflect or approach calculations using the exact water depth for these dike locations.

Hence, it should be kept in mind that SWAN results give about 2-4 cm lower outcomes than Hydra-NL and by using the exact water depth even more wave reduction can occur due to wave breaking.

5.1.4 1D computations

In section 4.1.2 the Bretschneider method assumed a uniform water depth. This turned out to be in some cases a bad approximation due to the highly varying exact bottom depth which could lead to breaking waves and hence a huge reduction in $H_{s,u}$. At every dike location the two wind directions resulting in highest exceedance frequency of the hydraulic load (following Hydra-NL/Bretschneider calculations using an uniform depth) are taken for estimating the wave heights. Because the exact water depth is used now, the order of the wind directions resulting in highest exceedance frequency of the hydraulic load can change (due to the possible occurrence of breaking waves). Therefore calculations for the two most important wind directions of every dike location will be done.

This will be done with or without vegetation and for statistical data of 2050 or 2100. The wind direction, wind speed and water level resulting in highest exceedance frequency of the hydraulic load of:

- 185 is used for dike locations 186 until 189:
  Table A-1: 185-NW-2050, 185-NW-2100, 185-WNW-2050 and 185-WNW-2100
- 190 is used for dike locations 191 and 192
  Table A-2: 190-NW-2050, 190-NW-2100, 190-WNW-2050 and 190-WNW-2100
- 193 is used for dike locations 194 until 199
  Table A-3: 193-W-2050, 193-W-2100, 193-WNW-2050 and 193-WNW-2100

This is done, because these dike locations have similar characteristics. The effective fetch is rounded to tens of metres. Furthermore every SWAN 1D computation is named as follows: *dike location number*-*wind direction*-*year*.

5.1.4.1 Results

The vegetation is implemented as described in section 5.1.2 with the vegetation parameters found in section 4.7, listed in Appendix Input parameters SWAN 1D. In order to show some of the effects of the vegetation on the significant wave height, several dike locations are picked out to show certain phenomena. The results are shown at page 53. The wave propagation with and without vegetation is plotted to see the difference. The start and end of the vegetation is shown, but this does not necessarily mean that vegetation is present in the whole interval. All the other plots and results of the wave propagation through vegetation can be found in Appendix SWAN 1D plots (without model uncertainty) and SWAN 1D results (including model uncertainty).

From now on the outcomes of H_s from SWAN are presented including the model uncertainty as described in section 5.1.3. The outcomes of H_s are located at the toe of the dike and are not corrected for difference in wave angle compared to the normal of the dike ($(1 - 0.0022\beta) * H_s$ with β the difference in angle [°] following (Schiereck, et al., 2016)).

In Figure 5.8, Figure 5.9, Figure 5.10 and Figure 5.11 the wave propagation is shown (without including model uncertainty). It is clear that the wave propagation for every dike location and wind direction is unique in terms of effective fetch, wave breaking, water depth and vegetation field. In Figure 5.8, H_s is damped by vegetation and stays more or less constant, while in Figure 5.9 the significant wave height decreases significantly due to vegetation. The peak in the vegetation field of Figure 5.9 is due to the absence of vegetation in this small interval. However, both cases result in wave damping at the toe of the dike.

In Figure 5.9 about 300 m of vegetation is encountered of the highly dissipating ‘subarea 5’ vegetation. In Figure 5.11 no vegetation is encountered at all by the waves and hence only a limited amount of energy is dissipated through white-capping and bottom friction. Figure 5.10 shows that a vegetation field interval of almost 100 m of the low dissipating vegetation type UMW-1 results in only 5 cm of reduction in H_s and hence has very limited influence on H_s.

Besides wave attenuation due to vegetation, also bottom friction or wave breaking could result in a reduction of the significant wave height. Wave breaking occurs in three out of the four above figures, but in Figure 5.11 an increased bottom friction is visible at 600-800 m as a result of an increase in the ratio wave height/water depth. In Figure 5.12 (including model uncertainty) an overview is made of H_s and the wave attenuation due to vegetation per dike location.

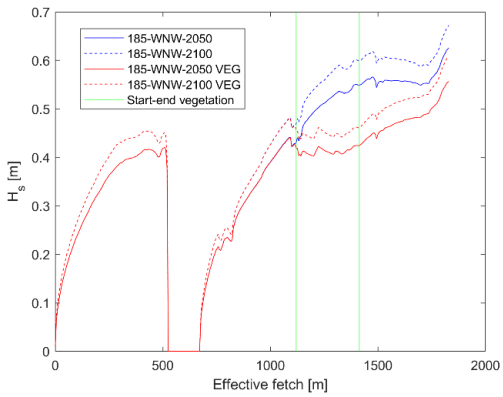

Figure 5.8: SWAN 1D wave propagation 185-WNW

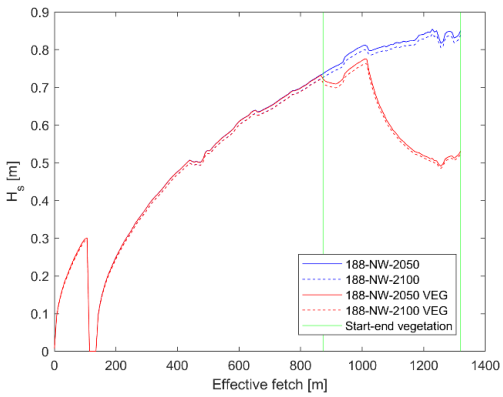

Figure 5.9: SWAN 1D wave propagation 188-NW

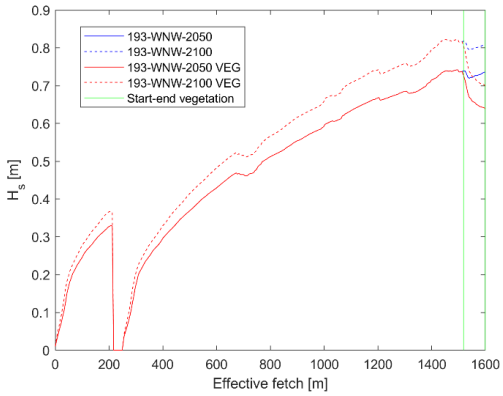

Figure 5.10: SWAN 1D wave propagation 193-WNW

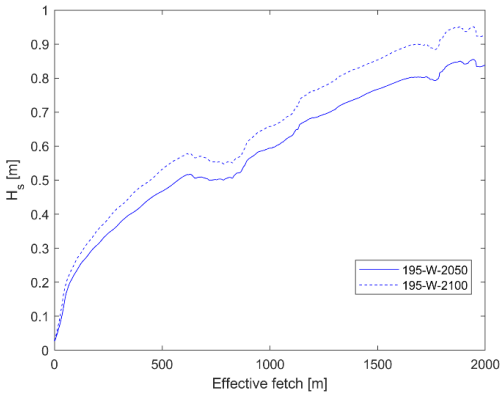

Figure 5.11: SWAN 1D wave propagation 195-W

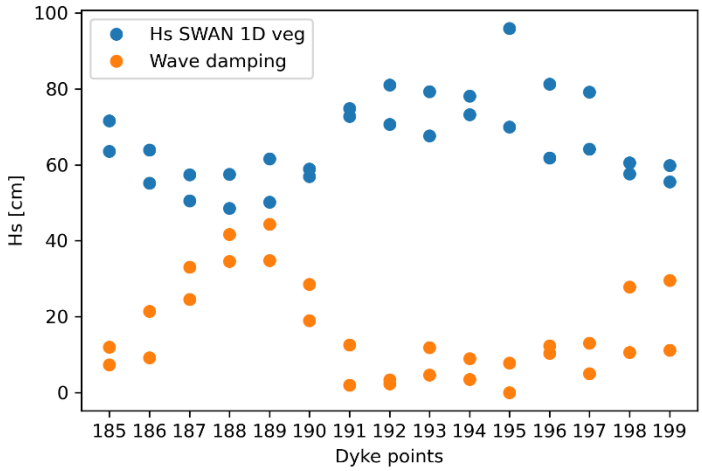

Figure 5.12: Hs SWAN 1D veg and wave damping due to vegetation

First of all per dike location, two different hydraulic conditions (two different wind directions) are considered and therefore two dots per dike location are visible. The magnitude of wave attenuation to vegetation varies from 0 to about 44 cm (Figure 5.9) for all dike locations. It is clearly observed that the region 186-190 has a lot of wave damping (up to 44 cm) and 192-197 only a limited amount (up to 13 cm). Many metres of vegetation is met by the wave heading towards dike locations 186-190, while only a limited amount of metres of vegetation is met by the waves heading towards 192-197. Also the type of vegetation plays a role as dike locations 186-190 encounter the highly energy dissipating vegetation area 'subarea 5' and dike locations 192-197 meet the low energy dissipating vegetation areas 'UMW-1' and 'UCW'. This results in the greatest values of H_s for dike locations 192-197.

The necessity of studying every single dike location adjacent to Duursche Waarden is proven by the great contrast in wave attenuation by vegetation between Figure 5.9 and Figure 5.11, but also in Figure 5.12.

For this study it is of importance to pick out and evaluate the dike locations and corresponding wind directions that result in the highest significant wave height at the toe of the dike. These are called the critical dike locations and are given in Table 5-7.

Dike location, HC[1]	Actual H_s [m]	Range H_s [m]
195, 193-W	0.959	0.95-1.00
192, 190-WNW 196, 193-W	0.810 0.813	0.80-0.85
193, 190-WNW 194, 193-W 197, 193-W	0.793 0.781 0.791	0.75-0.80

Table 5-7: Critical dike locations SWAN 1D computations (including vegetation)

5.2 2D computations

In order to get more insight into the behaviour of the waves in this particular area, SWAN 2D calculations without currents will be done. The hydraulic conditions are based on the hydraulic conditions from calculations with Hydra-NL (Bretschneider) for the three output points 185, 190 and 193. These are the same as used in SWAN 1D computations:

- 185 is used for dike locations 186 until 189:
  Table A-1: 185-NW-2050, 185-NW-2100, 185-WNW-2050 and 185-WNW-2100
- 190 is used for dike locations 191 and 192
  Table A-2: 190-NW-2050, 190-NW-2100, 190-WNW-2050 and 190-WNW-2100
- 193 is used for dike locations 194 until 199
  Table A-3: 193-W-2050, 193-W-2100, 193-WNW-2050 and 193-WNW-2100

For every output point the hydraulic conditions of the two governing wind directions are taken (see Appendix Governing parameters dike segments).

5.2.1 Settings

The settings for the SWAN 2D calculations are similar to the SWAN 1D settings (see Appendix Settings SWAN 1D). Except for now, boundary conditions in terms of H_s and T_p are implemented at the West side of the considered grid. The reason for this is that the water level in storm conditions results in submergence of the Western land. With wind directions of W, WNW and NW this results in wind-generated waves at the Western boundary of the considered grid. This is illustrated below (considered grid outlined in black):

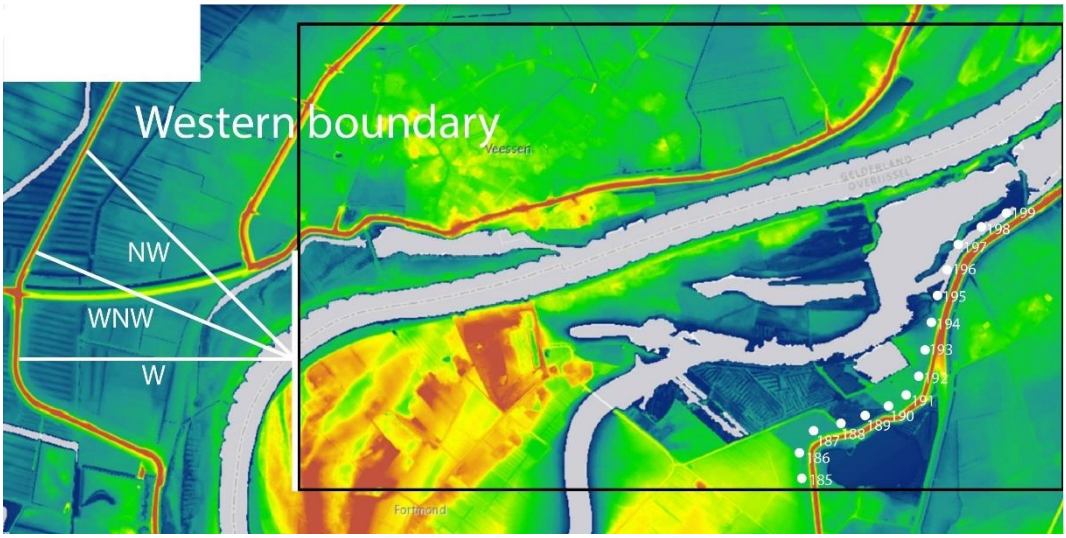

Figure 5.13: Western boundary with background elevation © AHN 3 viewer

For all the three wind directions the fetch is approximately 1000 m. In SWAN 2D computations it is observed this will result probably in a significant wave height of about 0.5 m and a peak period of about 2.0 s. This H_s and T_p are set constant as Western boundary condition for all SWAN 2D computations.

[1] HC = hydraulic conditions

5.2.2 No vegetation

First of all SWAN 2D computations without vegetation have been done. The results of H_s and T_p concerning the dike locations can be found in Appendix SWAN 2D resultsand the plots for H_s can be found in Appendix SWAN 2D plots of H_s. In order to have a better understanding of the wave propagation in this area, in Figure 5.14, containing the significant wave height and the mean wave direction, is shown.

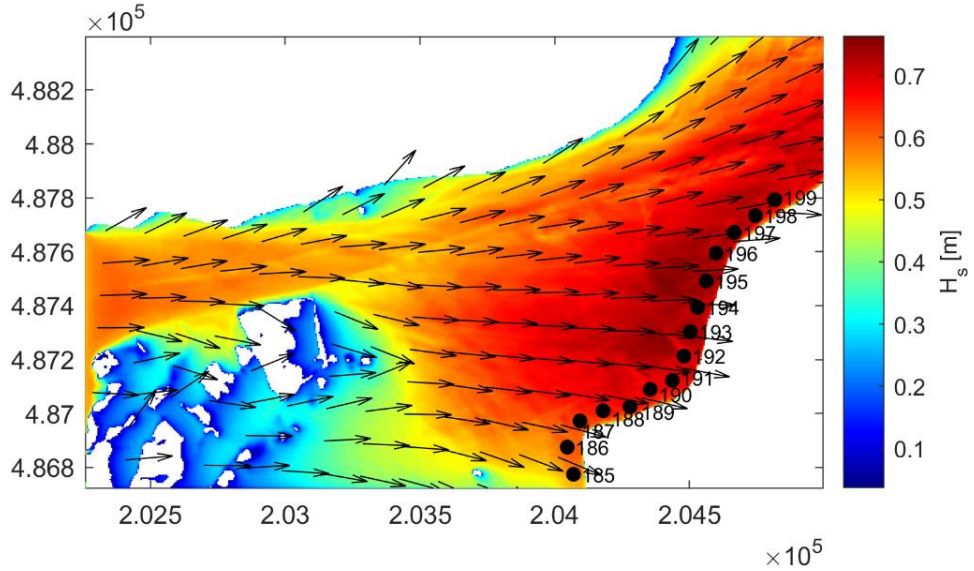

Figure 5.14: Significant wave height for hydraulic condition 193-W-2100, without vegetation

Especially for wind directions of W and WNW the highly elevated area at the under left of Figure 5.14 forms an obstacle for wind-generated waves towards the considered dike locations (located at the lower to middle right part of the figure). Hence, most of the wave energy is transferred from the relatively small passage at the Western boundary.

It can be concluded from the SWAN 2D results that H_s is significantly lower compared to outcomes of SWAN 1D computations (difference of up to 25 cm). One of the first reasons that comes up is the directional spreading in SWAN 2D computations. In SWAN 1D computations directional spreading is also taken into account and shows similar values as SWAN 2D computations. In both SWAN 1D and 2D computations the wave energy is spread over 30-40 degrees relative to its main direction. However, since a 2D grid takes into account the directional spreading for the whole 2D grid more energy will be lost towards the dike locations than in case of a 1D computation, where directional spreading only occurs along a 1D line. For the 2D computations this is shown in Figure 5.15.

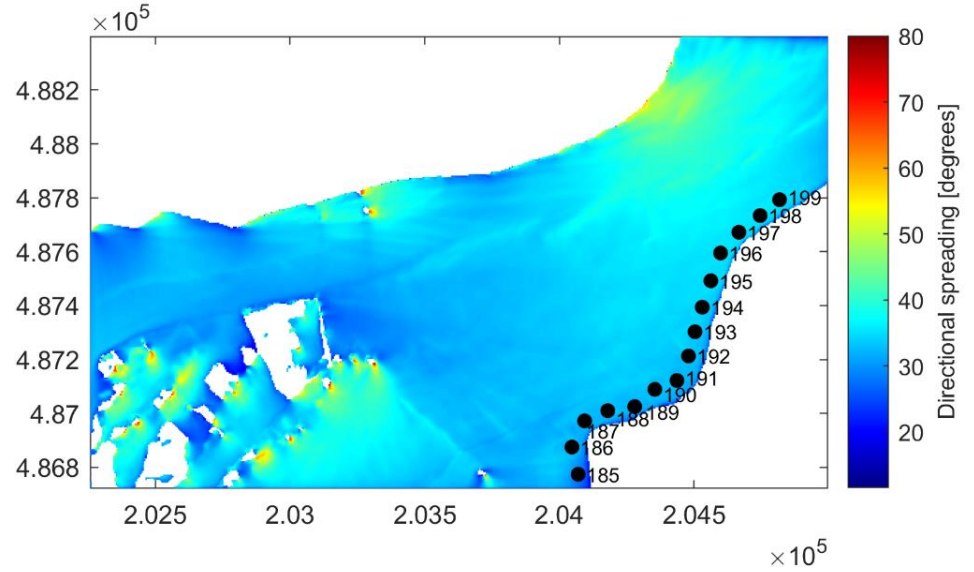

Figure 5.15: Directional spreading 185-NW-2100

Refraction is a phenomenon that is related to depth variations. When waves approach underwater contours at an angle, it is evident that the sections of the crest in the deeper parts travel faster than those in shallower parts. This causes change in direction of the wave and this bending effect is called refraction (Bosboom, et al., 2015).

This could cause an increase of H_s in case refraction causes concentration of wave energy, but in most cases it cause a decrease of H_s as refraction results in divergence of wave energy. This will be shown with the help of the peak wave direction. The peak wave direction is the direction of the peak period waves. Peak period waves are defined as the waves associated with most energetic waves in the wave spectrum.

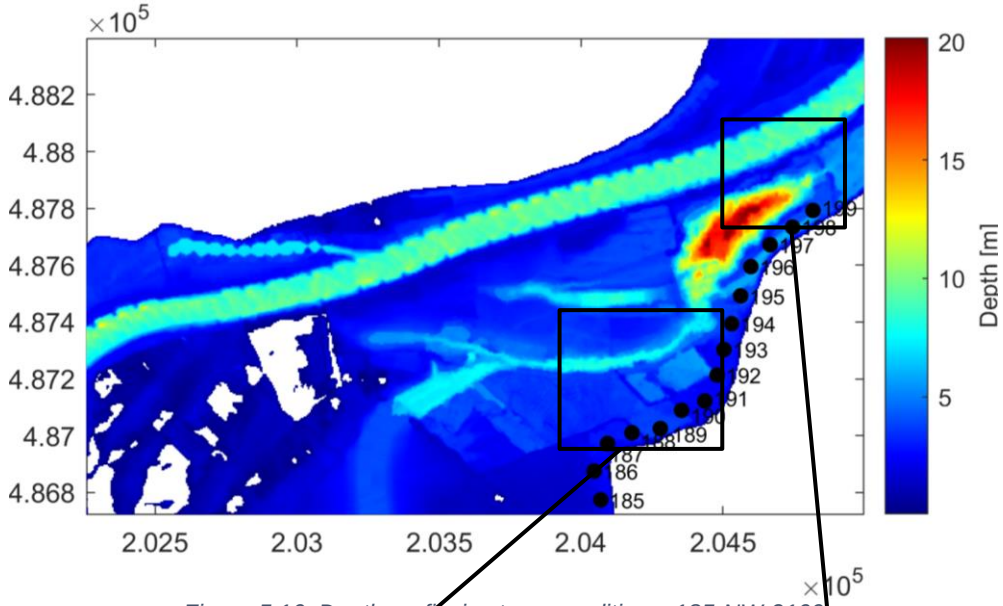

Figure 5.16: Depth profile in storm conditions, 185-NW-2100

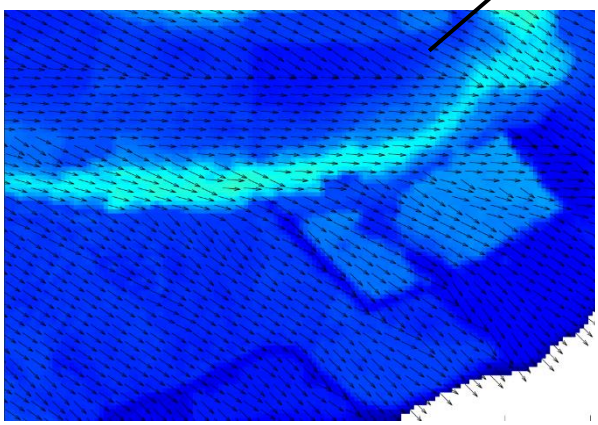

Figure 5.17: Peak wave direction zoomed in (i)

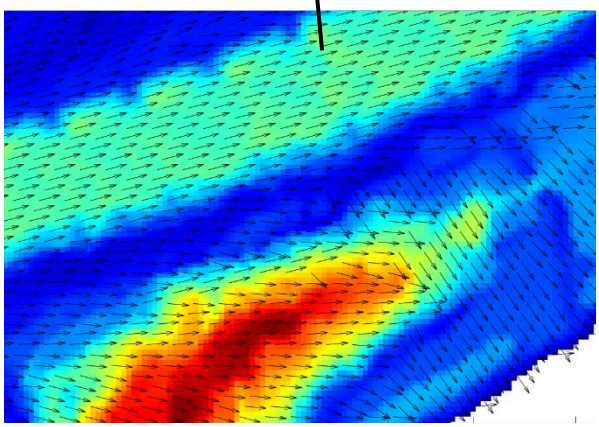

Figure 5.18: Peak wave direction zoomed in (ii)

In the Figure 5.17 and Figure 5.18 it is visible that depth-variation close to dike locations results in refraction. In most of the cases this causes divergence of wave energy and hence a reduction in H_s, just as in Figure 5.18, but also convergence of wave energy is visible in Figure 5.17.

5.2.3 Vegetation

Now vegetation is added to the 2D computations. Vegetation parameters over the height of subarea 4 are implemented in SWAN 2D. This type of vegetation is chosen, because most of the vegetation areas (subarea 2 until 5) have the same distribution of frontal area per volume over the height. In the same way as in section 5.1.2 is dealt with the fact only one vegetation type over the height can be implemented in SWAN. The characteristics of the different vegetation types can be found in Appendix Vegetation parameters for SWAN. In Figure 5.19 'Nplants' is shown, which represents the different types of vegetation (with subarea 4 = 1.0).

The same trend for all different hydraulic conditions is observed concerning energy dissipation due to vegetation. This is shown in the following Figure 5.20. The white outlined areas, see Figure 5.20, show most of the wave energy dissipation per m^2 at the edge of the vegetation areas 'subarea 4 and 5'. First of all this is due to highly dissipative vegetation parameters and secondly the most dissipation occurs at the edges since the most wave energy is present here and hence more wave energy can be dissipated by the vegetation.

However, the wave attenuation due to vegetation is of interest. For all different hydraulic conditions more or less the same trend can be observed, visible in Figure 5.21.

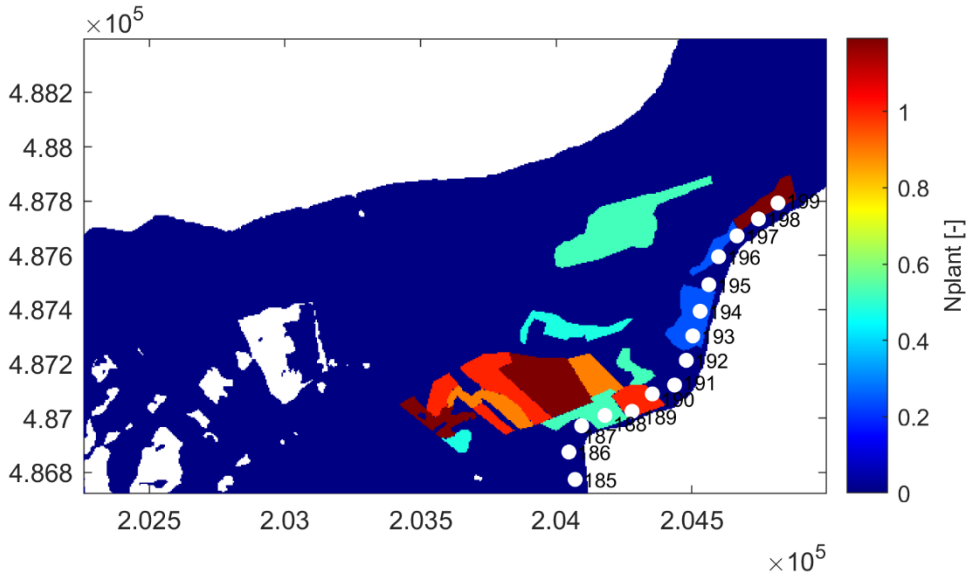

Figure 5.19: Input vegetation SWAN 2D computations

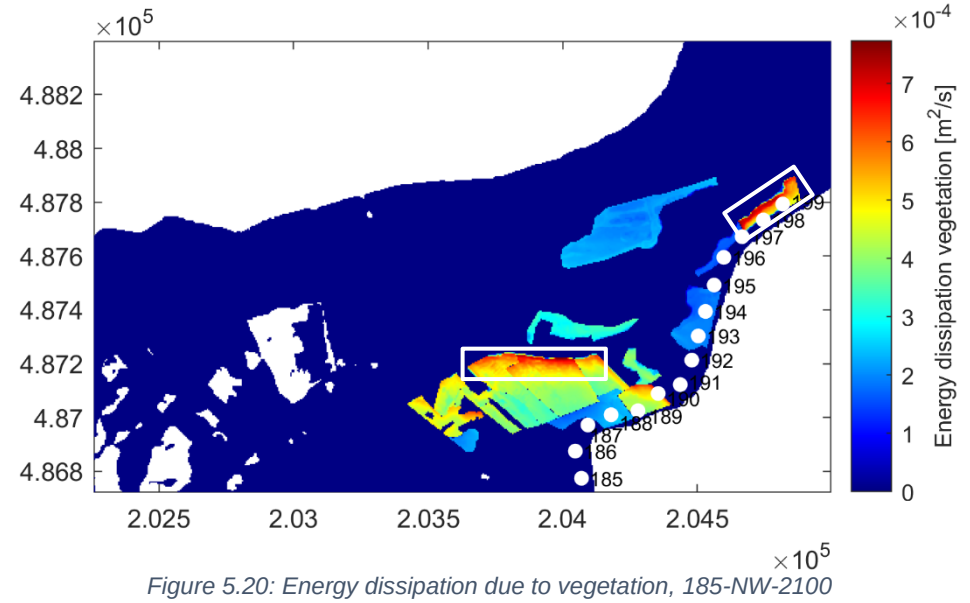

Figure 5.20: Energy dissipation due to vegetation, 185-NW-2100

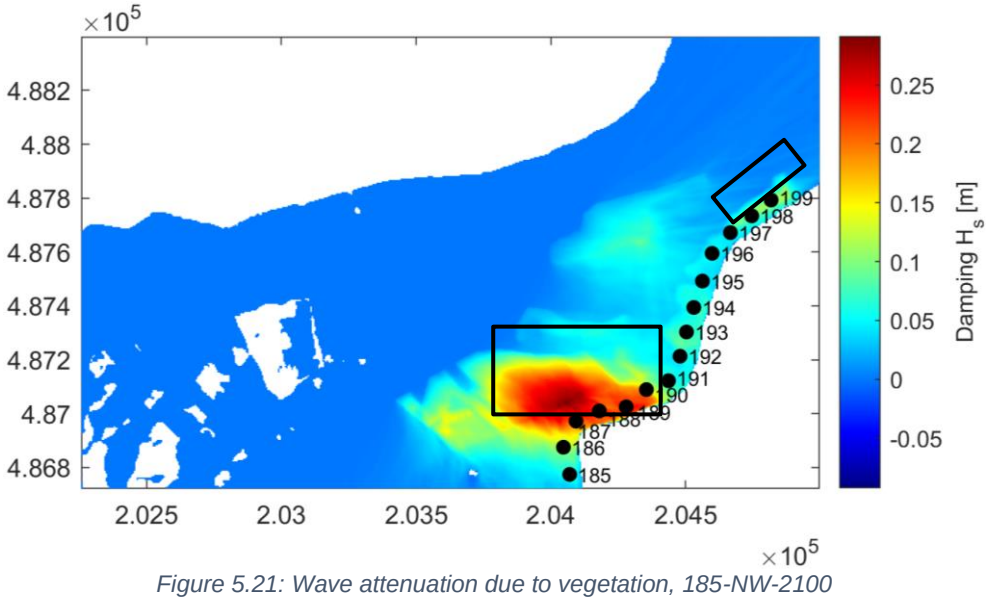

Figure 5.21: Wave attenuation due to vegetation, 185-NW-2100

In the most extreme hydraulic conditions (185-NW-2100, wind speed of about 28 m/s) it can be observed in Figure 5.21 that wave damping of more than 25 cm occurs in the lower black outlined rectangle (vegetation area 2). Vegetation area 2 consists of a large area of wave damping vegetation and hence the total wave energy dissipation is enormous. It is visible in upper black outline rectangle (Figure 5.21) that the significantly smaller area with the same vegetation parameter results also in significantly smaller wave attenuation. Hence, the magnitude of the vegetation area is of importance.

In Appendix SWAN 2D results for 2075 it is visible that the wave damping varies from approximately 4 (dike locations 192, 195 and 197) to 24 cm (189). For the SWAN 1D computations this varies from 0 (195) to 44 cm (189). On average less wave damping due to vegetation occurs for SWAN 2D computations than for 1D computations. The reason for this is probably that the 2D computations without vegetation already result in lower wave heights than for 1D computations. This means the vegetation is entered with less wave energy in 2D computations and hence less wave energy will be dissipated, resulting in less wave damping due to vegetation. However, the final results for H_s that include vegetation (with the same hydraulic conditions for 1D and 2D) are for most dike locations similar for the 1D and 2D computations (see Appendix Difference H_s SWAN 1D and 2D).

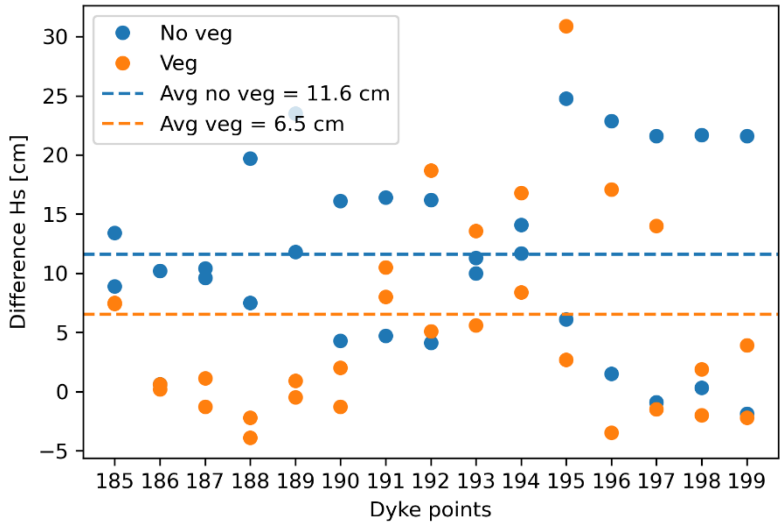

Figure 5.22: Difference Hs SWAN 1D-SWAN 2D

Also a few enormous differences can be observed in outcomes for H_s (SWAN 1D - SWAN 2D) in Figure 5.22 for dike locations 192 until 197. The best example is dike location 195 with the wind direction West (hydraulic condition 193-W). In 1D computations no vegetation is encountered and hence no wave attenuation due to vegetation resulted in a significant wave height of about 96 cm, while in 2D computations wave attenuation due to vegetation of about 6 cm occurred (see Figure 5.21 for the trend of wave damping at dike location 195). Since the 2D computations without vegetation showed already a reduction of 25 cm, the total difference with 1D computations is 31 cm. This difference shows that the 2D interaction of wave energy in 2D computations play a significant role in this studied area.

However, it is remarkable that the hydraulic conditions corresponding to 185-NW are governing for almost all dike locations in SWAN 2D computations. This is probably due the significantly higher wind speed, 27.9-28.2 m/s, while other hydraulic conditions are in the range 22.7-25.8 m/s. The results of H_s and T_p of all the dike locations with hydraulic conditions of 185-NW can be found in Appendix SWAN 2D results 185-NW all dike locations.

In Figure 5.23 the 2D results (including vegetation) of H_s with the same hydraulic conditions for every dike location as in 1D computations versus the 2D results of H_s with the hydraulic condition 185-NW for all dike locations is shown. In Figure 5.23 it is visible that the red stars and dots (hydraulic conditions 185-NW) are greater than the green stars and dots (original hydraulic conditions: same as used in 1D computations) for every dike location, except for dike locations 185-189, since these already have the hydraulic conditions of 185-NW in the original SWAN 2D computations. This figure also shows that dike locations 191-197 are the most vulnerable dike locations as these show the highest significant wave height for computations including vegetation. The significant wave height of critical dike locations in 2D computations (including vegetation) is shown in Table 5-8.

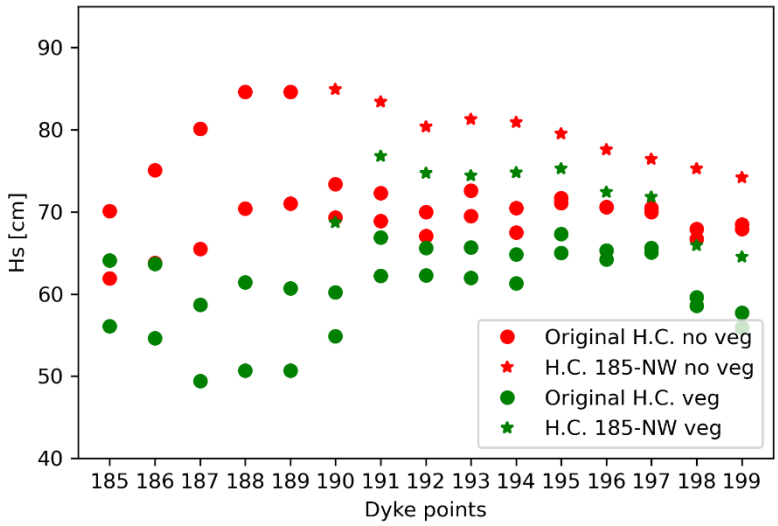

Figure 5.23: Results Hs SWAN 2D original H.C. vs. H.C. 185-NW

Dike location, HC[1]	Actual H_s [m]	Range H_s [m]
191, 185-NW	0.768	0.75-0.80
195, 185-NW	0.753	
192, 185-NW	0.747	0.70-0.75
193, 185-NW	0.744	
194, 185-NW	0.748	
196, 185-NW	0.724	
197, 185-NW	0.718	

Table 5-8: Critical dike locations SWAN 2D computations (including vegetation)

5.3 2D sensitivity analysis

The results of H_s for 1D computations including vegetation are only slightly higher than 2D computations, except for dike location 195: 96 (1D) vs. 71 cm (2D, H.C. 185-NW). Even though 1D results of H_s are hence governing, the spatial variability in water depth and fetch of the studied area is believed to be better described by 2D computations. Therefore the 2D computations are believed to more closely represent the reality and hence the sensitivity analysis will be done with SWAN 2D computations.

5.3.1 Parameters

The sensitivity analysis will be done for vegetation parameters, water level and wind speed. In a vegetation area with the magnitude of Duursche Waarden, vegetation parameters will always have some uncertainty. By using greater or smaller values of the vegetation parameters insight will be gained on the effect of H_s. Also, statistical data of the water level and wind speed for storm conditions in 2050 and 2100 is going to be evaluated. These are predictions (with climate change predictions included, see section 2.1) and hence uncertainty is included. Therefore smaller and greater values of the water level (and hence water depth) and wind speed will be used to see the effect on H_s.

Considering the consequences of climate change, there is an increase for the design discharge of the Rhine from 16,000 to 18,000 m^3/s (Deltacommissie, 2008). This results in in the downstream river branch IJssel a water level increase of 0.20 to 0.60 m (Sokolewicz, et al., 2011). It should be kept in mind that for the hydraulic conditions, originating from Hydra-NL, there is already 0.25 m added to the water level for climate change.
Storm conditions can be heavier than expected for the future as a consequence of climate change. This would mean greater wind speeds and hence higher significant wave heights. According to (Royal Netherlands Meteorological Institute, 2015) average wind speeds will only slightly change as a consequence of climate change. Since the wind speed is an important parameter, it will still be checked what difference it makes in case somewhat smaller or greater values are used.

Hand measurements (see Appendix Results hand measurements) provide even a better check for the outcomes of the TLS measurements that are used for SWAN and can hence provide a range to vary with vegetation parameters in this sensitivity analysis. In section 4.7 the values of hand measurement results are illustrated of species UMW-1, UCW, IO and UMW-3 are given. These values are going to be used for the sensitivity analysis.

[1] HC = hydraulic conditions

In the sensitivity analysis concerning vegetation, a worst case scenario (lower vegetation parameters) and a best case scenario (greater vegetation parameter values) will be done. The subareas (defined in section 3.3.2) consist of the species IDO, IPO and IO, but only hand measurements could be done for IO. Since IDO is quite similar to the tree IO the same range of uncertainty extracted from the hand measurements will be used in the sensitivity analysis. Since IPO consists mainly of a stem up to 5 meters, the values for this species will remain unchanged in the sensitivity analysis.

The bulk drag coefficient $\tilde{C}_D$ is highly uncertain and will therefore be considered too. In the worst case scenario the bulk drag coefficient will be 0.2 lower, while in the best case scenario the original values for $\tilde{C}_D$ are used.

With the help of above mentioned studies and hand measurements the order of uncertainty can be implemented in the sensitivity analysis. The following will be done in the sensitivity analysis:

- Water level: -0.50 m, -0.25 m, original water level, +0.25 m, +0.50 m
- Wind speed: -2.0 m/s, original wind speed, +2.0 m/s
- Vegetation:

Species	$\frac{1}{V}\sum_{i=1}^{n} A_i$: worst case scenario, % of values TLS	$\frac{1}{V}\sum_{i=1}^{n} A_i$: best case scenario, % of values TLS
UMW-1	75	207
UCW	75	405
IO	42	123
IDO	42	123
UMW-3	60	166

Table 5-9: Percentages vegetation parameters sensitivity analysis

For the lower limit of UMW-1 and UCW 75% is used to study the effect of lower vegetation parameters, even though hand measurements suggest the TLS results are already an underestimation. The values of IDO and IO will affect subareas 2 until 5. The exact vegetation parameters over the height can be found in Appendix Vegetation parameters sensitivity analysis.

5.3.2 Results

Playing with the water level certainly affects the magnitude of H_s. In Figure 5.24 it can be observed that higher water levels result in greater values of H_s and vice versa. Lower water levels cause the waves to feel the bottom earlier resulting in higher bottom friction and hence more wave energy dissipation. On the other hand higher water levels cause less wave energy dissipation resulting in greater values of H_s. Except for dike location 185 and 186, the same trend can be observed for every dike location: about 2-5 cm reduction in case of 0.50 m water lever decrease and vice versa. In Figure 5.25 different wind speeds are applied. This suggests a linear relation with H_s and the wind speed as for every dike location the same difference in H_s can be observed. It is also visible that dike locations 190-199 are more vulnerable for different wind speeds as larger differences (5-7 cm) can be observed between the minimum and maximum H_s per dike location. This is probably due to the fact that dike locations 185-189 (with differences of 4-5 cm) are more sheltered by high elevated land and dike locations 190-199 are not.

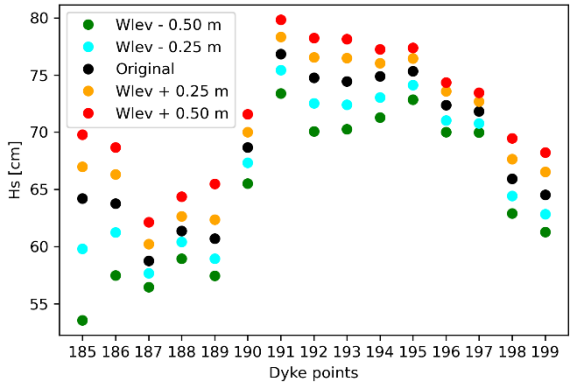

Figure 5.24: Sensitivity analysis - water level

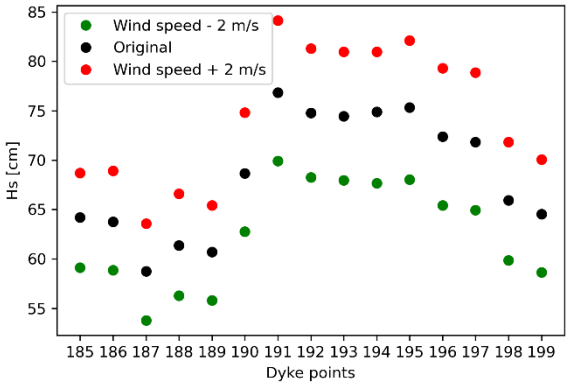

Figure 5.25: Sensitivity analysis - wind speed

For the vegetation parameters a worst case (WCS) and best case scenario (BCS) is defined in section 5.3.1. Figure 5.26 shows clearly a difference in sensitivity concerning H_s. Dike locations 187-190 have significantly greater values for H_s in WCS. These dike locations are 'protected' by large areas of moderate high dissipative vegetation and hence are more vulnerable for a reduction of vegetation parameters. Differences up to 15 cm can be observed, compared with the original parameters. Dike locations 191-197 are clearly less sensitive to changes in vegetation parameters as only small difference are observed (2-3 cm).

These dike locations are protected by significanlty smaller and less dissipative vegetation areas. Dike locations 185, 186, 198 and 199 have differences of H_s in between.

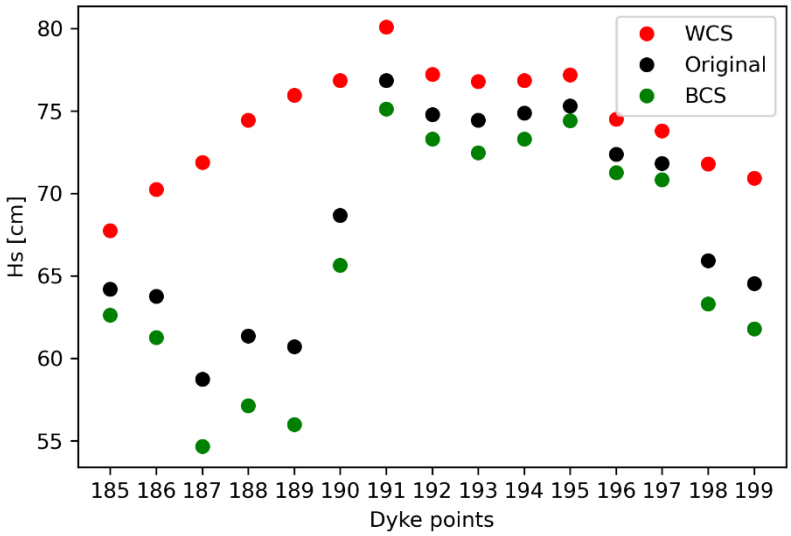

Figure 5.26: Sensitivity analysis - vegetation

6 Discussion and recommendations

This chapter presents discussions regarding relevant vegetation properties and SWAN outcomes. Also recommendations for the future will be done.

An overview of the different tree species that were distinguished for the prioritised vegetation areas (see section 3.3.2) is presented in Table 6-1.

Present in vegetation area	Name tree species	Scientific name tree species	Name in this study
1	Mix of crack and white willows	*Salix fragilis* and *Salix alba*	Uniform Mix of Willows: UMW-1
2 and 3	Downy oak	*Quercus pubescens*	Individual Downy Oak: IDO
2 and 3	Pedunculate oak	*Quercus robur*	Individual Pedunculate Oak: IPO
2 and 3	Osier	*Salix viminalis*	Individual Osier: IO
3	Crack willows	*Salix fragilis*	Uniform Crack Willows: UCW
3	Mix of frosted willows, osiers and white willows	*Salix daphnoides*, *Salix viminalis*, *Salix alba*	Uniform Mix of Willows: UMW-3

Table 6-1: Names tree species of the prioritised vegetation areas

6.1 Discussion

In this section mapping the vegetation, Single Scanning Station (SSS method), outcomes of TLS and hand measurements, vegetation parameters in literature and the outcomes of wave damping and height are discussed.

6.1.1 Vegetation

The prioritised vegetation areas were determined, based on a Multi Criteria Analysis (MCA). The MCA consisted of two criteria: distance covered through the vegetation area and the expected density of the vegetation. Roughly estimated vegetation areas (4, 7 and 8) are based on findings in the prioritised vegetation areas and Actuele Hoogtebestand Nederland (AHN) 3 data by looking to the heights of the vegetation. These vegetation areas are actually quite important for the wave attenuation of dike locations 190-199, but yet they are roughly estimated. Therefore, another criteria should be added in the MCA for prioritising the vegetation areas.

Tree species IDO, IPO and IO (that form the defined subareas) are believed to be the most common tree species in the non-uniform parts based on field observations and AHN 3 data. Since only a small part was accessible during field observations, only a limited part of the non-uniform areas is observed which could lead to the wrong most common species end hence wrong values of the frontal area per volume. On the other hand, it is checked by AHN 3 data that at least vegetation with the same heights as species IDO, IPO and IO are distributed over the non-uniform area. Also, the assumption of no overlapping vegetation in the subareas is conservative as AHN 3 and field observations suggest overlapping vegetation in some parts of the vegetation areas.

Also in this study the different tree species could be distinguished by height with the help of airborne Light Detection and Ranging (LiDAR) data like AHN 3 which is useful for the distribution over the non-uniform vegetation areas of the most common tree species. However, there will also be cases in which there is no clear difference in height between the most common tree species. In this case tracking of different tree species by hand during field work is an alternative. This is only achievable for smaller or similar sized areas as Duursche Waarden (~ 1.1 km^2). In order to make this less time expensive, certain subareas can be distinguished as with non-uniform areas (see section 3.3.1.2) with dominant and less dominant tree species.

6.1.2 SSS method

In the Single Scanning Station (SSS) method a shadowing correction factor f is used. The shadowing factor is based on the theory that a laser beam blocked by a branch cannot hit any branches behind the blockage. The theory actually assumes that if the laser beam would not be blocked, branches behind the blockage would be included in the point cloud and would result in frontal area. The shadowing factor increases for increasing distance from the Terrestrial Laser Scanner (TLS) instrument, but the higher this shadowing factor becomes the more uncertain the assumption becomes that all blocked laser beams would otherwise result in frontal area of a branch behind. Therefore it seems reasonable to apply a maximum shadowing correction factor. This is done based on a maximum slope of the shadowing factor and hence excludes the rapid increase of the shadowing factor.

The SSS method is applied for the tree species: IDO, IPO, IO and UMW-3 (see section 4.6.2). Values of f up to 200 are observed for these species. This is due to the little amount of laser beams getting through, see Appendix SSS method: amount of laser beams getting through. All scans show about the same trend which is shown in Figure 6.1 for a single scan of IO.

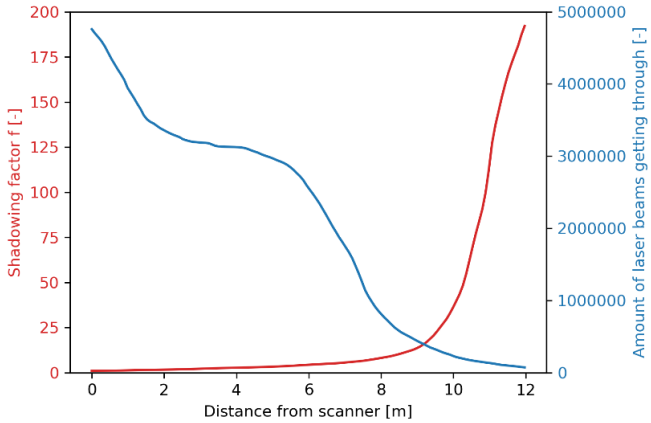

Figure 6.1: Shadowing factor and amount of laser beams getting through for scan 3.1 of tree species IO

The turning point from a gradually to rapidly increasing shadowing factor is observed to be at a derivative (or slope) of around 5.0 m^{-1} for all tree species. This derivative is described as $\Delta f / \Delta d$, with Δf the difference in shadowing factor between two consecutive points [-] and Δd the difference in distance from the scanner between two consecutive points [m]. A maximum shadowing factor f is set at a slope of 5.0 m^{-1}. This results in maximum shadowing factors varying from 5.79 to 11.39 instead of about 14 to 200 for the originally used shadowing factors. An example is given in Figure 6.2 of scan 3.2 of species IO. This can be found for all tree species in Appendix SSS method: maximum f.

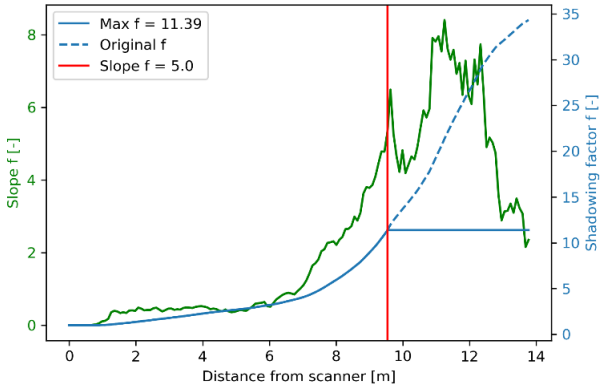

Figure 6.2: Maximum shadowing factor of scan 3.2 from species IO

The frontal area per volume following the SSS method with a limited shadowing factor for the four tree species is estimated. This is done with the help of Equation (4.11). The SSS method with a limiting shadowing factor results for the sparse tree species IPO in a very similar outcome as the SSS method without limiting shadowing factor and MSS method (see Figure 6.4). As sparse vegetation includes barely shadowing this result is following expectation. For tree species IDO in Figure 6.3 significant differences can be observed between the SSS method with limited and original shadowing factor. However, on average the outcomes of the MSS method shows results in between. The significant differences between the methods actually demand for hand measurements as validation, but since this tree species showed about the same results for the MSS and SSS method in section 4.6.2.1 there are no hand measurements done.

Separate graphs of the scans instead of average values for the frontal area per volume of species IO and UMW-3 can be found in Appendix SSS methods: frontal area per volume. Scans 3.3 and 3.7 of species IO and UMW-3 in Figure 6.5 and Figure 6.6 have the same orientation as the MSS method (see section 4.6.2.2) and can therefore be compared fairly with the outcomes of the MSS method. First of all it is visible in Figure 6.5 and Figure 6.6 that scans 3.3 and 3.7 using the SSS method with a limited f show smaller values than the SSS method with original f. Also the outcomes of the limited f are greater than the MSS method, but the differences are significantly less than using the original f.

As concluded in section 4.7 the MSS method for species IO and UMW-3 probably underestimates the frontal area per volume compared to the hand measurements (see Figure 6.5 and Figure 6.6). Dense vegetation (IO and UMW-3) includes more shadowing than sparse to moderate vegetation (IDO and IPO).

Hence, significant differences in results of the SSS method with original f and limiting f are expected. This is also clearly visible in Figure 6.5 and Figure 6.6. In Figure 6.5 it can be observed that both the average SSS methods with original f and limited f are positioned within the range of the hand measurements. In Figure 6.6 it can be observed that the average SSS method with original f fits the outcomes of the hand measurements better than the SSS method with limited f. Hence, these outcomes suggest the SSS method with original f performs better than the SSS method with limited f.

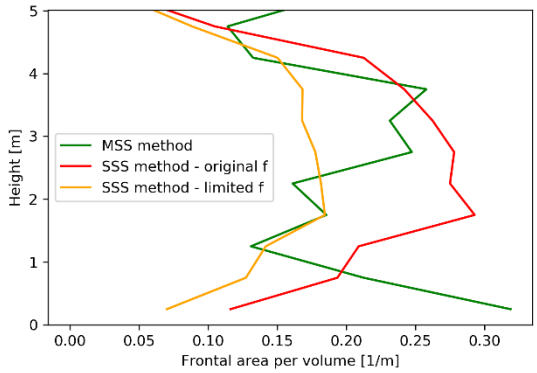

Figure 6.3: Scan 2.9 of species IDO with MSS and SSS method

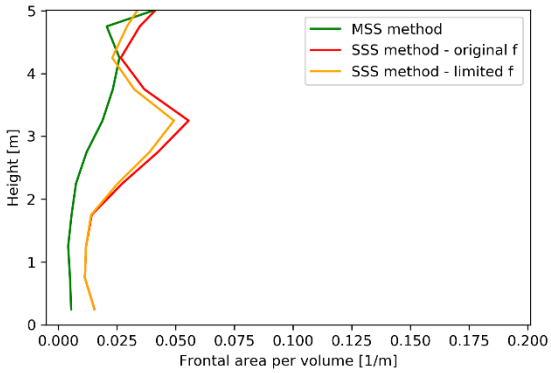

Figure 6.4: Scan 2.10 of species IPO with MSS and SSS method

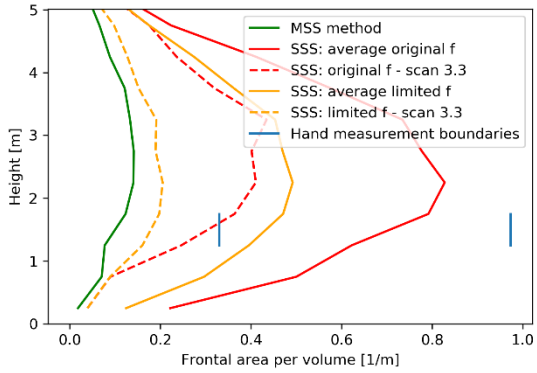

Figure 6.5: Average of scan 3.1, 3.2 and 3.3 of SSS method vs. MSS method and hand measurements of species IO

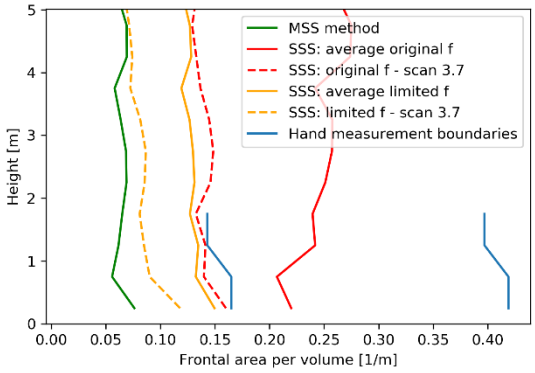

Figure 6.6: Average of scan 3.7 and 3.9 of SSS method vs. MSS method and hand measurements of species UMW-3

6.1.3 TLS and hand measurements

One of the possible errors with doing TLS measurements could be the presence of leaves during the scans (see section 4.2.4), since this study only treats leafless vegetation. During the TLS measurement small buds and upcoming leaves were present for species IDO and IO. Based on field observations, the part of frontal area by these buds and small leaves was estimated to be between 0 and 10 percent. A decision was made to subtract 10 percent of the total frontal area of both species. Hence, the estimated part of frontal area delivered by the small leaves and buds is actually quite uncertain since this estimation is based on field observations by the human eye. However, it is believed a conservative decision is taken by subtracting 10 percent of the frontal area.

The results of the Multiple Scanning Station (MSS) method for the frontal area per volume for only the stem of vegetation in uniform areas (UMW-1 and UCW) differ significantly with hand measurements. However, since the MSS method considers a larger and more representative volume than the hand measurements (10x10x5 m vs. 5x5x2 and 3x3x2 m) and it is assumed no significant errors are made due to the simple shape using the alpha shape method, MSS results are believed to be more reliable.

The MSS method outcomes of the frontal area per volume are used in numerical wave model SWAN for individual species IDO and IPO. These species are considered sparse to moderate dense vegetation (on average 0.01-0.20 m^{-1}) and hence no significant uncertainties were expected. The SSS method with original f confirmed this expectation for both species since similar results were obtained as the MSS method. However, the SSS method with limited f showed significantly different outcomes for species IDO. No validation could be done since no hand measurements were done for this species and hence this entails uncertainties.

Hand measurements were done for dense species IO and UMW-3 (on average 0.20-0.50 m^{-1}), but due to the high density hand measurements were difficult to execute. The number of branches were counted, but due to the high numbers of branches errors can be made easily. Also the range of the perimeter of branches was estimated since it is time expensive to measure the perimeter of every branch. On top of that there could only take place hand measurements until an height of 2 meter. Hence, outcomes of the hand measurements are used to validate outcomes of the TLS measurements while there also exists uncertainty due to difficulties in execution.

The MSS method in general and the SSS method for sparse to moderate dense vegetation (IDO and IPO) consider only one random orientation of the vegetation species in contrast to the SSS method of dense vegetation (IO and UMW-3). The orientation in direction of the waves is of importance for the frontal area. Only one orientation was chosen for the MSS method and SSS method for sparse to moderate dense vegetation due to the large point cloud files and hence large computation times. Also no significant differences of outcomes for different orientations were expected due to the sparsity of the vegetation. On the other hand, multiple orientations will lead to a more complete outcome of the frontal area distribution over height. As observed for the SSS method of dense vegetation the different orientations can cause significant difference in the frontal area distribution over height.

In a relatively quick way (order of minutes) large and pretty accurate point cloud data is obtained with the help of TLS measurements. Also it can be used for both sparse and dense vegetation. On the other hand, the accurate point cloud data entails large files and results in large computation times. Also, the error imposed to the magnitude of used slices, leaves on vegetation and shadowing result in uncertainty. Hand measurements can be done relatively quick and accurate. Also the presence of leaves on the vegetation can be easily excluded, since the amount and diameter of branches are counted and measured. On the other hand, hand measurements can only be done until an height of 2 meter. Also hand measurements are difficult to execute for dense vegetation, since many branches need to be measured and counted. The overview is easily lost and it is time expensive.

In chapter 3 and 4 a general approach is presented for mapping the vegetation and obtaining vegetation parameters of (riparian) forests of smaller or a similar size as Duursche Waarden (1.1 km^2). However, if the studied vegetation area is of greater orders of magnitude with many different tree species, the TLS and hand measurements could be time expensive.

6.1.4 Vegetation parameters in literature

As mentioned in section 4.3.2.1 a similar study has been done on the vegetation density in Duursche Waarden (Rahman, et al., 2013). In this study dominant trees and understorey vegetation are imitated with cylinders. Then simulated airborne LiDAR observations are done, generating point clouds. From these point clouds the vegetation density D_v [m^{-1}] was determined. This is exactly the same parameter as the frontal area per volume, $\frac{1}{V}\sum_{i=1}^{n} A_i$, used in this study. Only a small part of the vegetation area coincides with vegetation areas studied in this study (outlined in blue, Figure 4.5), but shows values in the order of 1.5-2.0 m^{-1}. This suggests that the frontal area per volume obtained in this study (in the order of 0.05-0.40 m^{-1}) is too low. The assumption of no overlapping of trees in this study as described in section 3.3.2 is a significant difference, since (Rahman, et al., 2013) does assume overlapping and includes understory vegetation. However, TLS and hand measurements in this study estimate the frontal area from the orientation of the waves, while (Rahman, et al., 2013) estimate the frontal area from above. Also the results are believed to be more accurate, since the measurements are done closer to the vegetation compared to airborne LiDAR data. Therefore, the outcomes of the frontal area per volume for vegetation in Duursche Waarden in this study are believed to be estimated better.

In (Antonarakis, et al., 2009) poplar species were studied, which show similarities with species IDO. The frontal area distribution over the height is estimated for the whole tree and shows values in the same order of magnitude. For example, both the poplar species and IDO (MSS method) show frontal area in the order of about 6 m^2 at the middle part of the tree.

In (Kalloe, 2019) the frontal area per volume of willow tree species *Salix alba* is estimated using hand measurements. Values of the frontal area per volume varying from 0.05 to 0.30 m^{-1} were found. This is about the same order for willow species found in this study (IO, UCW, UMW-1 and UMW-3): 0.05-0.40 m^{-1}.
In (Stam, 2018) the wave damping of (partially) submerged young willows (not clear which species, probably *Salix alba*) was studied with a field test. The measurement set-up consists of a plot of 7 x 7 meters with young willow branches and pressure transducers perpendicular to the river Noord near Dordrecht, the Netherland. The frontal area per volume over height of one young willow varied from 0.72 to 1.60 m^{-1}. Hence, these values are significantly higher than values of willow species (IO, UCW, UMW-1 and UMW-3) used in this study (0.05-0.40 m^{-1}). This is following expectations since in this study often stems dominate the frontal area which results in low values for the frontal area per volume. In (Stam, 2018) willow branches are used and hence this results in relatively high values for the frontal area per volume.
In (Vries, et al., 2009) the wave damping capacity of willow fields (*Salix alba* and *Salix viminalis*) is studied. Estimates show values of 0.90 up to 3.90 m^{-1} for the frontal area per volume. An individual *Salix viminalis* (IO) is studied for Duursche Waarden in which values of 0.20 to 0.90 m^{-1} is found. This is significantly lower than the values found in (Vries, et al., 2009).

The difference is probably due to the high density of the willow field in (Vries, et al., 2009) where individual species overlap. In this study just an individual species is considered without other overlapping species. Hence, the values of IO are believed to be in the right order of magnitude.

6.1.5 Numerical models

All SWAN 1D and 2D computations have been done using the governing hydraulic conditions from Hydra-NL and include model uncertainty. SWAN 1D computations showed 2 to 4 cm lower outcomes than Hydra-NL (using Bretschneider including model uncertainty) for exact the same conditions. This difference is considered small, but should be kept in mind while comparing the results of SWAN 2D and Hydra-NL. Also SWAN 1D computations with the exact water depth showed 14 to 21 cm lower outcomes mainly due to wave breaking. Therefore using a uniform depth as in Bretschneider is not representative. SWAN 2D computations without vegetation show significant lower outcomes than 1D computations without vegetation: on average about 12 cm. This difference is explained by refraction and directional spreading resulting from the spatial variability in water depth and fetch of the studied area. Therefore the studied area is believed to be better described by 2D computations.

In (Stam, 2018) mean wave damping values of 4.1% of the incoming wave height per meter for wave heights higher than 20 cm were found. The vegetation field is 7 m and the frontal area per volume of the young willow branches (not clear which species, probably *Salix alba*) varies from 0.72 to 1.60 m^{-1}. In (Vries, et al., 2009) the wave damping capacity of willows (*Salix alba* and *Salix viminalis*) is studied. It is estimated that a vegetation field of 100 m of willows with frontal area per volume varying between 0.70 and 1.00 m^{-1}, 75% wave reduction can be realized for an incoming wave height of 1.2 m.

Since the Duursche Waarden shows similarities with mangrove forests, both on a shallow foreshore with wave damping characteristics, it is interesting to know the order of magnitude of vegetation density for mangrove forests. In (Janssen, 2016) different studies on wave damping by mangroves are considered in a literature study which shows wave damping rates (wave damping per meter in the vegetation field) between 0.0005 and 0.06 m^{-1} for incoming wave heights between 0.04 and 0.40 m. Also wave damping by mangrove species *Rhizophora* and *Avicennia*, with a frontal area varying from is studied by collecting relevant data and validating models in estimating the wave damping. The ranges of the wave attenuation varies between 0.004 m^{-1} and 0.02 m^{-1} for an incoming wave height of 1.5 m.

In this study, for 2D computations one hydraulic condition is proven to be governing for all dike locations (see Figure 5.23): 185-NW. For this hydraulic conditions, 2D computations estimate the wave damping to vary between 16 to 24 cm at dike locations 187-190 as they are sheltered by the large vegetation areas 1 and 2 consisting of low and high energy dissipative vegetation. Critical dike locations 191-197 have a wave damping estimated to vary between 4 to 7 cm as they are sheltered by small areas of low energy dissipative vegetation. On average the length of the vegetation field in North-West direction, just as the governing hydraulic condition, is 390 m for dike locations 187-190 and 140 m for dike locations 191-197 (see Appendix Input parameters SWAN 1D). The incoming wave height is about 0.60 to 0.80 m. This means at dike locations 187-190 an estimated wave damping of 0.00041 to 0.00062 m^{-1} and at dike locations 191-197 0.00029 to 0.00050 m^{-1}.

This case study on Duursche Waarden shows most similarities with the studies in (Stam, 2018) and (Vries, et al., 2009) as all three study vegetation in rivers and consider willow species. If the same range of incoming wave height (0.60-0.80 m) as in this study would be used in (Stam, 2018), the wave attenuation would be 0.025 to 0.033 m^{-1}. The wave attenuation in (Vries, et al., 2009) is 0.0090 m^{-1}. Both studies have about the same order of vegetation parameters, but in (Stam, 2018) greater wave damping capacities are shown. This is probably due to the short vegetation field length of 7 m compared to a length of 100 m in (Vries, et al., 2009): when the wave enters a vegetation field much more energy is to be dissipated compared to the wave travelling at the end of the vegetation field (see Figure 5.21). Hence, the wave attenuation rate decrease over the vegetation field and therefore a longer vegetation field will result in lower wave attenuation rates. Therefore the outcomes in (Stam, 2018) are considered too optimistic for comparing with the wave damping in Duursche Waarden
In (Vries, et al., 2009) significantly higher values are shown than at Duursche Waarden. This is probably due to the fact they have greater values of the frontal area per volume and have a shorter vegetation field. Also the vegetation in (Vries, et al., 2009) was planted and hence the vegetation density could be manipulated in contrast to the existing riparian forest Duursche Waarden. Even though significant differences in frontal area per volume are present, no differences in the order of ten was expected for the wave attenuation rate. Outcomes of this study seem therefore relatively conservative.

On average mangrove forests show greater wave damping capacities than Duursche Waarden. This probably due to the greater values of the frontal area per volume (sparse vegetation: 0.01 to 0.5 m^{-1} and dense vegetation: 0.68 to 9.60 m^{-1} (Janssen, 2016)). Also the length of the vegetation field is shorter on average leading to higher wave damping rates.

In (Penning, et al., 2017) an overview is made of promising wave damping foreshores in the Netherlands. Rough estimations show possible wave damping up to 10 cm at Duursche Waarden (see Appendix Quickscan), which is in about the same order as in this study.

In order to find out whether dike reinforcements are needed for dikes adjacent to Duursche Waarden, an indicative calculation is done for failure mechanism 'erosion of the outer slope due to wave attack on grass' (GEBU). This is done with the program 'Basis Module Gras Buitentalud' prescribed by WBI (Wettelijk Beoordelingsinstrumentarium) 2017, the legal Dutch guidelines for assessment of primary flood defences. In Appendix GEBU calculations detailed info on the calculations are shown for 'an average' dike location at Duursche Waarden. A safety factor of 1.0 would mean no reinforcement is needed for the dikes adjacent to Duursche Waarden.

Only one maximum wave height for all dike locations is considered since the design of dikes is preferably one design for a significant dike length. For example, a different design every 100 m is not efficient in the execution phase. The maximum significant wave height for dikes adjacent to Duursche Waarden of Hydra-NL is 100 cm and for SWAN 2D 77 cm with a water level of 5.70 m NAP. Both outcomes lead to a safety factor below 1.0 and hence these indicative calculations suggest that dike reinforcements are still needed at Duursche Waarden.

6.2 Recommendations

6.2.1 General

It is recommended to add another criteria in the MCA for prioritising the vegetation areas in order to prevent that important vegetation areas are roughly estimated. This extra criteria should be 'estimated importance in wave height reduction of flood defence'.

If there are no height differences the ratio of presence for most common tree species can be determined by tracking the different tree species by hand during field work. This is only achievable for smaller or similar sized areas as Duursche Waarden (~ 1.1 km^2) and will still by relatively time consuming. Therefore, it is recommended to find an alternative method for determining the ratio of presence of the most common tree species without looking to height differences.

In case leafless vegetation is studied and leaves are present during TLS or hand measurements it is recommended to measure the area of the leaves and count the number of leaves instead of estimating it with the human eye. This will result in a founded estimation of the part of frontal area delivered by the leaves and will create less uncertainty in the final outcomes of the frontal area.

In this study only 3 trees were picked out of the 10x10 m area to determine the frontal area per volume of an average tree in an uniform area. Next time five trees should be picked out in order to get a more representative value for the frontal area per volume.

In section 6.1.2 the limited shadowing factor f is determined, based on a maximum derivative $\Delta f/\Delta d$ of 5.0. This value is based on where the turning point was observed from a gradually increasing f into a rapidly increasing f. It is recommended to study what the right value of $\Delta f/\Delta d$ is or what an alternative method would be in order to determine the maximum f. This will improve the SSS method.

The MSS method in general and the SSS method for sparse to moderate dense vegetation (IDO and IPO) consider only one random orientation of the vegetation species in contrast to the SSS method of dense vegetation (IO and UMW-3). The orientation in direction of the waves is of importance for the frontal area. The orientation parallel to the governing wind direction in storm conditions seems to be the most obvious choice. However, the spatial variability in water depth could cause change in direction. On top of that also storms with a different wind direction could occur. Therefore multiple scanning positions is also recommended for sparse to moderate dense vegetation for similar future studies to obtain a more complete frontal area distribution over the height.

In this study the hydraulic conditions are based on what in Hydra-NL caused the most exceedance frequency of the hydraulic load using a uniform water depth. Since it is proven that the uniform water depth does not represent reality sufficiently (see SWAN 1D and 2D computations), other hydraulic conditions are more likely to result in the most exceedance frequency of the hydraulic load. Hence the governing hydraulic conditions should be determined using the exact water depth.

It is recommended to use airborne LiDAR data like AHN 3 for vegetation areas of greater magnitude than Duursche Waarden. This LiDAR data will generate lower accuracy point clouds than TLS measurements, but since also a significant larger area is studied this is reasonable. A similar general approach as in chapter 3 and 4 is followed:

1. Identify vegetation areas with the help of airborne LiDAR data (AHN 3) and aerial photos (Google Earth images or drone footage)
2. Choose two/three representative subareas within the vegetation area
3. Extract point cloud (of leafless woody vegetation) from the airborne LiDAR data for every subarea
4. Estimate frontal area distribution over the height per subarea
5. Compare data with hand measurements and assess whether the results are representative

6. Choose a representative frontal area per volume distribution of the considered vegetation area

6.2.2 Duursche Waarden

It is recommended for the roughly estimated vegetation areas (4, 7 and 8) to do more detailed research concerning present tree species and whether or not the vegetation is similar to the vegetation in the prioritised vegetation areas.

In (Smale, 2019) currents were taken into account in SWAN 2D computations for the IJsseldelta of which Duursche Waarden is part. This study showed that including currents results in a reduction of 0.1-0.2 m for H_s. Therefore it is recommended to include currents in future SWAN 2D computations for Duursche Waarden. Since Duursche Waarden is located in a floodplain no significant magnitude of currents is expected during normal conditions. However, in extreme storm conditions the increase of discharge could lead to significant current in the floodplain. At least significant currents are present in the river part. If these currents are in direction of the wind direction, this could result in 'shortening of the fetch' and hence lower H_s. If the currents are in opposite direction of the wind direction, this could 'increase the fetch' and increase H_s. On the other hand this will also lead to more wave energy dissipation due to the wind and change in direction.

7 Conclusions

In this study the wave attenuation of woody vegetation was studied for a riparian forest, Duursche Waarden, located in a floodplain along the Dutch river IJssel. First of all, the different vegetation areas within Duursche Waarden were identified and prioritised on expected wave damping. This resulted in a clear distribution over the vegetation areas of the leafless frontal area per volume and bulk drag coefficient, the most important vegetation parameters for wave damping due to vegetation. These vegetation parameters were estimated for the prioritised vegetation areas with the help of Terrestrial Laser Scanning (TLS) and hand measurements. Finally, the wave damping due to vegetation without currents was estimated using 1D and 2D computations with the numerical program SWAN.

An overview of the different tree species that were distinguished for the prioritised vegetation areas (see section 3.3.2) is presented in Table 7-1.

Present in vegetation area	Name tree species	Scientific name tree species	Name in this study
1	Mix of crack and white willows	*Salix fragilis* and *Salix alba*	Uniform Mix of Willows: UMW-1
2 and 3	Downy oak	*Quercus pubescens*	Individual Downy Oak: IDO
2 and 3	Pedunculate oak	*Quercus robur*	Individual Pedunculate Oak: IPO
2 and 3	Osier	*Salix viminalis*	Individual Osier: IO
3	Crack willows	*Salix fragilis*	Uniform Crack Willows: UCW
3	Mix of frosted willows, osiers and white willows	*Salix daphnoides*, *Salix viminalis*, *Salix alba*	Uniform Mix of Willows: UMW-3

Table 7-1: Names tree species of the prioritised vegetation areas

7.1 Mapping the vegetation

The different vegetation areas were mapped within Duursche Waarden by identifying the different vegetation areas with the help of aerial photos (drone footage and Google Earth images) and field observations. As a result of a Multi Criteria Analysis, based on the distance covered through the vegetation and expected wave damping vegetation parameters, vegetation areas with most expected wave damping were studied in detail: the prioritised vegetation areas. The other vegetation areas were roughly estimated based on outcomes for the prioritised vegetation areas. Uniform and non-uniform vegetation areas in terms of tree species, structure, density and height were distinguished with the help of field observations, aerial photos and airborne Light Detection and Ranging (LiDAR) data (Actuele Hoogtebestand Nederland (AHN) 3).

One general equation is developed to determine the distribution frontal area per volume for both uniform and non-uniform areas (see Equation (3.6)). Uniform areas (UMW-1, UMW-3 and UCW) have one frontal area per volume distribution over the height for the whole area. The most common tree species are determined for non-uniform areas in which no overlapping vegetation is assumed. Subareas are made out of the most common tree species (IO, IDO and IPO) including criteria for every subarea. The ratio of presence of the most common tree species in subareas is used to distinguish the different subareas and to determine the uniform frontal area per volume distribution over the height of such a subarea. The ratio of presence is determined with the help of airborne LiDAR data such as AHN 3 as the most common tree species can be distinguished based on height.

7.2 Vegetation parameters

The frontal area per volume for uniform and non-uniform areas is obtained by TLS measurements with the Multiple Scanning Stations (MSS) and Single Scanning Station (SSS) method. The MSS method uses a merged point cloud of two to three scanning stations. The introduced SSS method uses the point cloud of one scanning station and corrects for the error shadowing by applying the ‘original’ shadowing correction factor. In section 6.1.2 a maximum shadowing factor was applied for the SSS method when the slope, the shadowing factor over the distance, of 5.0 m^{-1} was reached. This value of the slope is the observed turning point from a gradually to rapidly increasing shadowing factor. A rapidly increasing shadowing factor induces more uncertainty as the assumption that all blocked laser beams would otherwise result in frontal area becomes less likely. The frontal area per volume is estimated using the alpha shape method for only the stems in uniform areas and the grid method in all other cases.

In this study the MSS method is used for an uniform vegetation area. A representative subarea within the uniform vegetation area is measured with the TLS. From this representative subarea the frontal area per volume over the height of an ‘average tree’ is found.

The frontal area per volume for non-uniform areas is obtained by the MSS or SSS method. The frontal area per volume over the height of most common tree species is then estimated individually (see Equation (4.3) for MSS and Equation (4.11) for SSS). The values of the frontal area per volume for the different vegetation areas that were applied in computations of the numerical wave model SWAN, varied from about 0.05 to 0.40 m^{-1} on average as observed in Figure 7.1. Values of studies on similar vegetation ((Stam, 2018), (Antonarakis, et al., 2009), (Kalloe, 2019) and (Vries, et al., 2009)) suggest rather conservative than optimistic outcomes in this study. The bulk drag coefficient over the height is estimated using Table 3-7 based on a literature study in section 2.2.3.3.

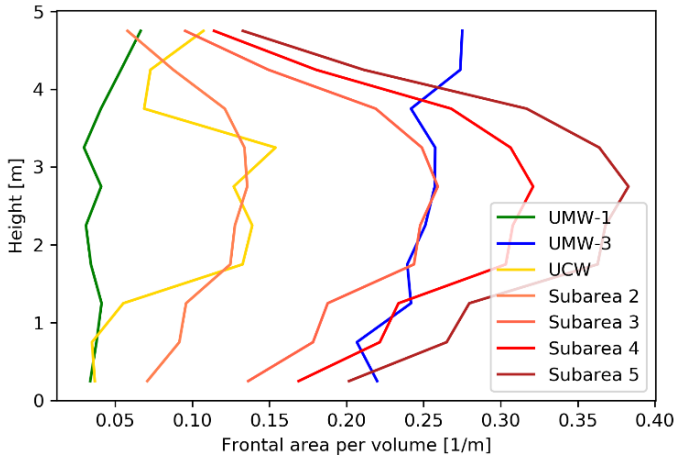

Figure 7.1: Frontal area per volume over height for different vegetation types in Duursche Waarden

Hand measurements are believed to be more reliable than TLS measurements to estimate the frontal area for individual sparse to moderate woody vegetation (on average 0.01-0.20 m^{-1}) since the number and diameter of branches can be counted and measured easily, the exclusion of leaves is easy and no errors occur due to the chosen magnitude of slices and shadowing. The estimation of the frontal area per volume for uniform areas consisting of sparse vegetation can be done best with the MSS method for uniform woody vegetation areas, since with this method in a relatively quick way a representative volume is considered and no significant errors are expected. The estimation of frontal area for dense woody vegetation (on average greater than 0.20 m^{-1}) is the most uncertain and therefore no preference is indicated for one of the two measurement types. Therefore both hand and TLS measurements should be done. In case of TLS measurements, for dense woody vegetation, the SSS method with original shadowing factor is believed to perform best.

7.3 Wave damping

A comparison between the numerical wave model SWAN and Hydra-NL (using Bretschneider) using an uniform depth shows negligible differences in outcomes of the significant wave height. SWAN 1D computations with the exact water depth showed 14 to 21 cm lower outcomes mainly due to wave breaking and therefore using the a uniform depth as in Bretschneider is not representative. Also the studied area is believed to be better described by SWAN 2D computations due to refraction and directional spreading resulting from the spatial variability in water depth and fetch.

One hydraulic condition is proven to be governing for all dike locations: 185-NW (see Appendix Governing parameters dike segments). In Figure 7.2 2D computations are shown for these hydraulic conditions. These computations lead to a maximum wave height of 77 cm at dike location 191. The wave damping is estimated to be 16 to 24 cm at dike locations 187-190 as they are sheltered by the large vegetation areas 2 and 3 (about 0.26 km^2) consisting of low and high energy dissipative vegetation. Dike locations at which the significant wave height is the greatest are called critical dike locations. Critical dike locations 191-197 are most vulnerable as they are sheltered by small areas of low energy dissipative vegetation. The wave damping for these dike locations is estimated to vary between 4 to 7 cm.

The same order of magnitude was found in (Penning, et al., 2017), in which an overview is made of promising wave damping foreshores in the Netherlands. Rough estimations show possible wave damping up to 10 cm at Duursche Waarden (see Appendix Quickscan). Also studies on similar vegetation ((Vries, et al., 2009), (Stam, 2018) and (Janssen, 2016)) show significant greater values for the wave damping rate, suggesting rather conservative than optimistic outcomes in this study. The wave damping rate is the wave damping per meter in the vegetation field.

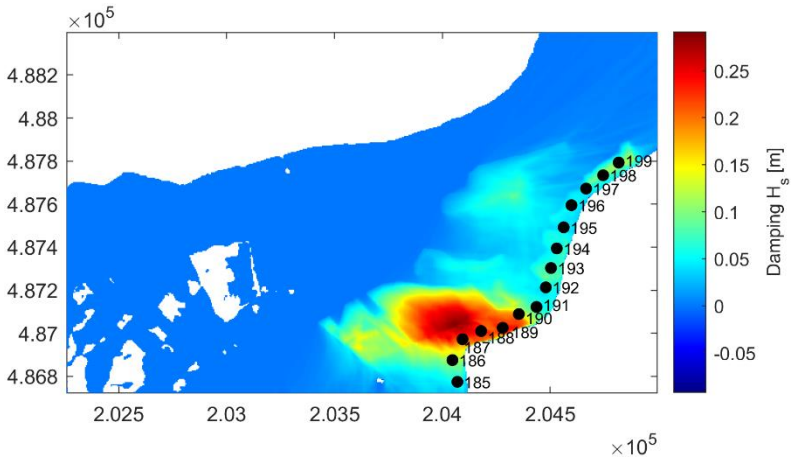

Figure 7.2: Wave damping for the governing hydraulic condition

Sensitivity analysis shows that dike locations close to large vegetation areas are vulnerable for lower vegetation parameters, while the critical dike locations are insensitive. The increase in water level shows negligible results for the increase in significant wave height. The wind speed increase shows a more significant increase of the significant wave height, but since an increase in wind speed is unlikely to happen in the future this uncertainty will be ignored. Therefore the failure mechanism 'erosion of the outer slope' with a return period of 66666 year results in an estimated maximum wave height of 77 cm for dike locations adjacent to Duursche Waarden. Hence, this is a reduction of about 23 cm compared to the results of Hydra-NL. Indicative calculations suggest that dike reinforcements are still needed at Duursche Waarden.

7.4 Monitoring plan

In order to include existing woody vegetation into the design of dikes, the riparian forest (Duursche Waarden) should also be monitored to keep track of the quality and amount of presence of the vegetation. Diseases, insects, beavers, storms, vandalism, ice and fire could a affect the quality of the vegetation and hence the amount of frontal area following (Stam, 2018). Two categories, that are important for the wave damping features of vegetation in a riparian forest, can be distinguished: (i) the amount and (ii) quality of woody vegetation.

The amount of woody vegetation for any (riparian) forest can be monitored best by satellite data due to the size of such areas. Data should be analysed during leaf-off season. Airborne LiDAR data (AHN 3) and aerial photos (Google Earth images and drone footage) over time give insight in the size development of the vegetation area. Hence, with these programmes and data sources it is possible to keep track of the amount of woody vegetation.

The quality of the woody vegetation is assessed by either the health and frontal area of the vegetation. Dead trees, ill trees or broken branches will have reduced wave damping effect in comparison with healthy trees. Since recognising this demands expertise, the health status of vegetation should be checked by tree experts or ecologists of the waterboard. This should be done by field observations over the whole area. In this way insight is gained into the health status of vegetation in the whole area.

The amount of frontal area for wave damping vegetation assumed in this study is both affected by the amount and health status of woody vegetation. Besides monitoring these two aspects, also hand measurements of the exact same sparse to moderate vegetation could be done (for the locations see Appendix Locations TLS measurements and Coordinates scans). A TLS instrument can be used for dense vegetation in case this is available, otherwise hand measurements suffice too for maintenance. A comparison between the frontal area can then be made over the years and hence the safety of the dike design can be assessed.

The amount of woody vegetation can be tracked every year by airborne LiDAR data. The field work needed to assess the quality of the woody vegetation and to do hand measurements could be applied every three years.

7.5 General approach

In this study the focus was mainly on how to map the vegetation and to obtain vegetation parameters of this vegetation in Duursche Waarden (~ 1.1 km^2). Lessons have been learned to create a general approach for smaller or similar sized woody vegetation areas. The general approach is schematised in Figure 7.3, including the tools needed during every step or extra information. An explanation is given on the next page for most boxes in Figure 7.3. The bold text represents one box.

- **Prioritise vegetation areas**: execute a Multi Criteria Analysis based on three criteria:
    1. The observed and expected vegetation density,
    2. The distance the wind-generated wave will cover through the vegetation in direction with the governing fetch and
    3. Estimated importance in wave height reduction of flood defence.
- **Roughly estimated vegetation areas**: use field observations, aerial photos and LiDAR to estimate similarities with the prioritised vegetation areas. Copy and apply frontal area per volume distribution of prioritised vegetation area (uniform or non-uniform) with most similarities.
- **Uniform or non-uniform?**: determine whether the vegetation areas are uniform or non-uniform areas based on tree species, structure, density and height
- **Uniform areas**: use one distribution of the frontal area per volume.
    - **Expected: sparse to moderate dense vegetation** (0.01-0.20 m^{-1}): do TLS measurements (MSS method) of a representative smaller area (~ 10 x 10 m) within the uniform area. This is done as follows:
        1. Find the frontal area per volume of an average tree using alpha shape for the stem and grid method for the branches.
        2. Multiply average tree with number of trees within smaller area and divide by the total volume.
    - **Expected: dense vegetation** (greater than 0.20 m^{-1}): do hand and TLS measurements (SSS method) of a representative, but significant smaller area (~ 3 x 3 m) in the uniform area:
        1. Find 'original' shadowing correction factor
        2. Estimate the frontal area per volume with the help shadowing factor using the grid method

      → Compare TLS and hand measurements.
- **Non-uniform areas**: find most common tree species and their ratio of presence, make subareas within the non-uniform area based on ratio of presence and other criteria. Every subarea has its own frontal area per volume distribution.
    - **Expected: sparse to moderate dense vegetation** (0.01-0.20 m^{-1}): do hand measurements of individual most common tree species
    - **Expected: dense vegetation** (greater than 0.20 m^{-1}): do hand and TLS measurements (SSS method) of a representative, but way smaller area (~ 3 x 3 m) in the uniform area:
        1. Find 'original' shadowing correction factor
        2. Estimate the frontal area per volume with the help shadowing factor using the grid method

      → Compare TLS and hand measurements.

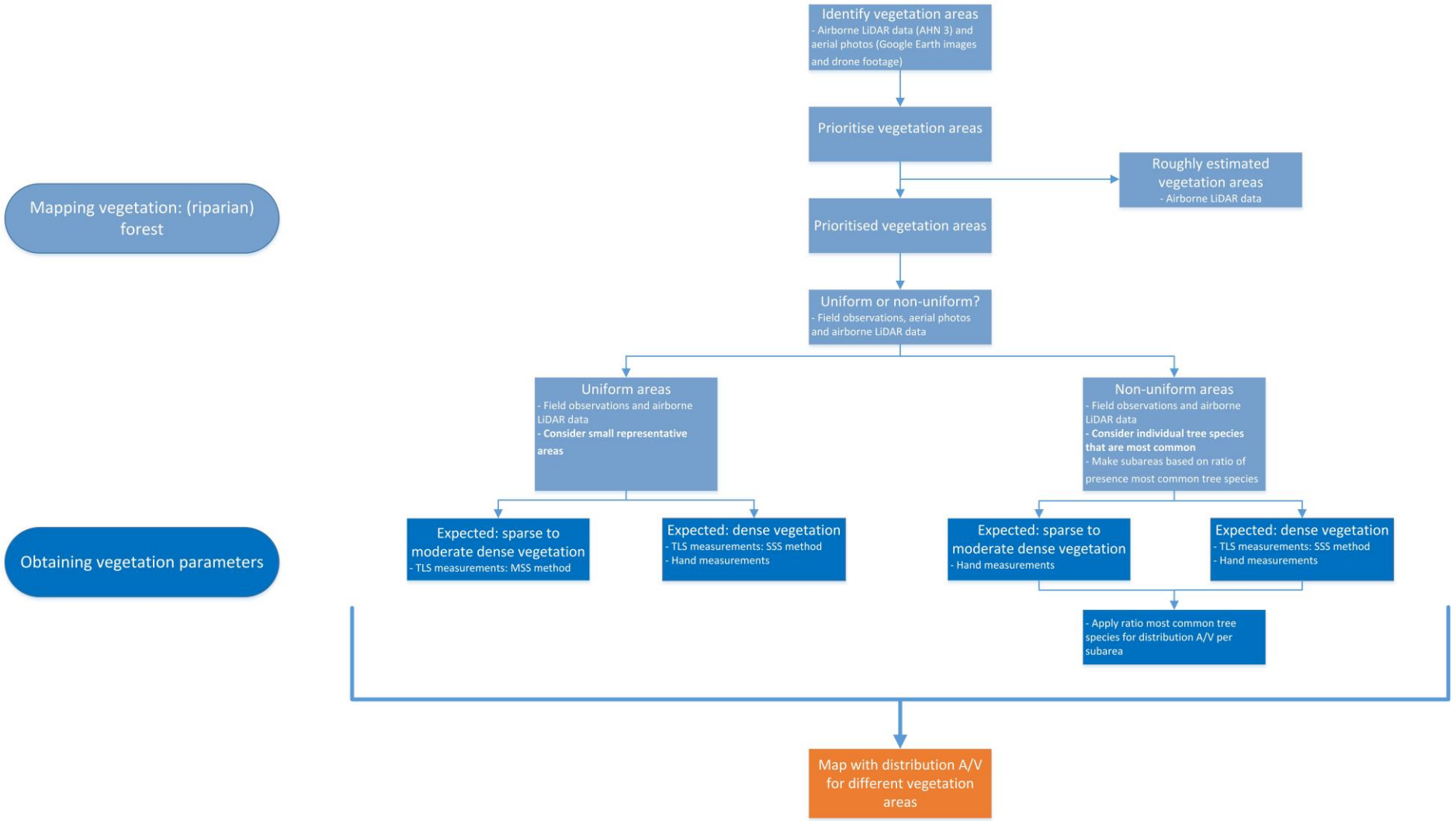

Figure 7.3: General approach

Bibliography

Alliantie van waterschappen en Rijkswaterstaat. Info about the Dutch Flood Protection Programme. *Website of the Dutch Flood Protection Programme.* [Online] https://www.hoogwaterbeschermingsprogramma.nl/programma/programmering/default.aspx.

Antonarakis, A.S., et al. 2009. *Leafless roughness of complex tree morphology using terrestrial lidar.* sl : Water resources research, 2009. 0043-1397/09/2008WR007666.

Bosboom, J. en Stive, M.J.F. 2015. *Coastal Dynamics I.* Delft : VSSD, 2015. ISBN 978-90-6562-3720.

Chbab, H. en Groeneweg, J. 2015. Modelonzekerheid belastingen WTI-2017. *Publicatiedatabank IenW.* [Online] Ministerie van Infrastructuur en Waterstaat, July 2015. [Citaat van: 6 October 2020.] http://publicaties.minienm.nl/documenten/modelonderzekerheid-belastingen.

Cheng, N.S. 2013. *Calculation of Drag Coefficient for Arrays of Emergent Circular Cylinders with Pseudofluid Model.* sl : Journal of Hydraulic Engineering, ASCE, Vol. 139, Issue 6 (June 2013), 2013. https://doi.org/10.1061/(ASCE)HY.1943-7900.0000722.

Da, T.K.F., Loriot, S. en Yvinec, M. 2020. CGAL 5.1 - 3D Alpha Shapes. *CGAL.* [Online] 6 September 2020. [Citaat van: 1 October 2020.] https://doc.cgal.org/latest/Alpha_shapes_3/index.html#title3..

Dalrymple, R. A., Kirby, J. T. en Hwang, P.A. 1984. *Wave diffraction due to areas of energy dissipation.* sl : Waterway, Port, Coastal and Ocean Engineering, Vol. 110, No. 1, February, 1984. , 1984. ©ASCE, ISSN 0733-950X/84/0001-0067/$01.00. Paper No. 18601..

Dataquest. 2018. Tutorial: Basic Statistics in Python — Probability. *Dataquest.* [Online] Dataquest, 18 July 2018. [Citaat van: 6 October 2020.] https://www.dataquest.io/blog/basic-statistics-in-python-probability/.

Deltacommissie. 2008. Working together with water. *Deltacommissie.* [Online] 2008. [Citaat van: 10 August 2020.] http://www.deltacommissie.com/doc/deltareport_full.pdf.

Dubi, A. en Torum, A. 1995. *Wave damping by kelp vegetation.* sl : Proceedings of the Twenty-Fourth Coastal Engineering Conference, 1995. https://doi.org/10.1061/9780784400890.012.

Ecoshape. The Building with Nature philosophy . *Ecoshape.* [Online] [Citaat van: 11 May 2020.] https://www.ecoshape.org/en/the-building-with-nature-philosophy/.

Edelsbrunner, H., Kirkpatrick, D.G. en Seidel, R. 1983. *On the Shape of a Set of Points in the Plane.* sl : IEEE Transactions on Information Theory, VOL. IT-D, NO. 4, JULY 1983, 1983. 0018-9448/83/0700-0551$01.00 01983 IEEE.

He, F., Chen, J. en Jiang, C. 2019. *Surface wave attenuation by vegetation with the stem, root and canopy.* sl : Elsevier, Coastal Engineering, 2019. Volume 152, October 2019, 103509.

Holthuijsen, L.H. 2007. *Waves in Oceanic and Coastal Waters.* sl : Camebridge University Press, 2007. ISBN 978-0-521-12995-4.

Janssen, M.P.J. 2016. Flood hazard reduction by mangroves - MSc thesis. *Repository TU Delft.* [Online] 6 October 2016. [Citaat van: 6 June 2020.] https://repository.tudelft.nl/islandora/object/uuid%3Ab3cfe9b0-c8d3-4eb6-aad2-977d879430b5.

Kalloe, S. 2019. Wave attenuation through woody riparian vegetation, a comparison between terrestrial laser scanning and manual measuring techniques. *Repository TU Delft.* [Online] 13 May 2019. [Citaat van: 20 March 2020.] https://repository.tudelft.nl/islandora/object/uuid%3A6e9c1f7a-4ef9-48ef-bb97-796a9b74fe6b.

Kobayashi, N., Raichle, A. W. en Asano, T. 1993. *Wave attenuation by vegetation.* sl : Journal of Waterway, Port, Coastal, and Ocean Engineering Vol. 119, No. 1, January/February, 1993. , 1993. ISSN 0733-950X/93/0001-0030/$1.00 + $.15 per page..

Kothyari, U.C., Hayashi, K. en Hashimoto, H. 2009. *Drag coefficient of unsubmerged rigid vegetation stems in open channel.* sl : Journal of Hydraulic Research, 47:6, 691-699, 2009. https://doi.org/10.3826/jhr.2009.3283.

Leica Geosystems. 2016. *Leica ScanStation P40/P30 User Manual.* 2016.

Li, Y., et al. 2017. *Retrieving the gap fraction, element clumping index, and leaf area index of individual trees using single-scan data from a terrestrial laser scanner.* sl : ElsevierI, SPRS Journal of Photogrammetry and Remote Sensing 130:308-316, 2017. https://doi.org/10.1016/j.isprsjprs.2017.06.006.

Liu, G., et al. 2018. *Estimating Individual Tree Height and Diameter at Breast Height (DBH) from Terrestrial Laser Scanning (TLS) Data at Plot Level.* sl : Forests 2018, 9, 398; doi:10.3390/f9070398, 2018. https://doi.org/10.3390/f9070398.

Liu, X.G. en Zeng, Y. H. 2016. *Drag coefficient for rigid vegetation in subcritical open channel.* sl : Elsevier, Procedia Engineering Volume 154, 2016, Pages 1124-1131, 2016. doi: 10.1016/j.proeng.2016.07.522.

Mayer, J. en Schwegler, H.W. 2018. *ANWB Bomengids.* sl : Kosmos, 2018. ISBN 9789021569048.

Maza, M., et al. 2017. *Velocity and Drag Evolution From the Leading Edge of a Model Mangrove Forest.* sl : AGU Publications Journal of Geographysical Research: Oceans, 2017. 10.1002/2017JC012945.

Maza, M., Lara, J. L. en Losada, I. J. 2019. *Experimental analysis of wave attenuation and drag forces in a realistic fringe Rhizophora mangrove forest.* sl : Elsevier, Advances in Water Resources Volume 131, September 2019, 103376, 2019. https://doi.org/10.1016/j.advwatres.2019.07.006.

Mendez, F. J. en Losada, I. J. 2004. *An empirical model to estimate the propagation of random breaking and nonbreaking waves over vegetation fields.* sl : Elsevier Coastal Engineering 51 (2004) 103 – 118, 2004. doi:10.1016/j.coastaleng.2003.11.003.

—. 1999. *Hydrodynamics induced by wind waves in a vegetation field.* sl : JOURNAL OF GEOPHYSICAL RESEARCH, VOL. 104,N O. C8, PAGES 18,383-18,39, 1999. Paper number 1999JC900119..

Morison, J. R., et al. 1950. *The force exerted by surface waves on piles.* sl : PETROlEUM TRANSACTIONS, AIME Vol. 189, 1950, 1950. T.P.2846.
Natura 2000. Natura 2000. *Natura 2000.* [Online] https://www.natura2000.nl/.
Oude, R. de. 2010. Modelling wave attenuation by vegetation with SWAN-VEG (MSc thesis). *University of Twente.* [Online] January 2010. [Citaat van: 6 May 2020.] https://essay.utwente.nl/59406/1/scriptie_R_de_Oude.pdf.
Overheid. Waterwet. *Wettenbank Overheid.* [Online] Overheid.[Citaat van: 4 Maart 2020.] https://wetten.overheid.nl/BWBR0025458/2020-01-01#BijlageII.
Ozeren, Y., Wren, D.G. en Wu, W. 2014. *Experimental Investigation of Wave Attenuation through Model and Live Vegetation.* sl : Journal of Waterway, Port, Coastal, and Ocean Engineering Vol. 140, Issue 5 (September 2014), 2014. https://doi.org/10.1061/(ASCE)WW.1943-5460.0000251.
Penning, E. en Levelt, O. 2017. Publicaties. *Deltares.* [Online] 2017. [Citaat van: 15 October 2020.] https://www.deltares.nl/nl/publicaties/13/?search=Quickscan%20effect%20vegetatie%20in%20voorlanden%20op%20golfbelasting&target=all.
Rahman, M.Z.A., et al. 2013. *A generic approach in estimating vegetation density for hydrodynamic roughness parameterization using high density airborne laser scanning data.* sl : Journal of Hydroinformatics Volume 15, Issue 2, 2013. https://doi.org/10.2166/hydro.2012.188.
Rijksoverheid. Golfgroei - Bijlage E Golfberekeningen volgens eenvoudige benadering. *Helpdesk Water Rijksoverheid.* [Online] [Citaat van: 20 April 2020.] https://www.helpdeskwater.nl/onderwerpen/waterveiligheid/primaire/technische-leidraden/zoeken-technische/@192798/golfgroei-bijlage/.
Rijkswaterstaat. 2019. Info about Delta Programma. *Website of the Government of the Netherlands.* [Online] 2019. https://english.deltacommissaris.nl/documents/publications/2018/09/18/dp2019-en-printversie.
Rijkswaterstaat, Deltares en VNK2. 2013. Achtergrondrapport ontwerpinstrumentarium 2014. [Online] 23 December 2013. [Citaat van: 10 April 2020.] https://www.helpdeskwater.nl/publish/pages/142606/achtergrondrapport_oi2014_v1_0.pdf.
Royal Netherlands Meteorological Institute. 2015. KNMI'14 Climate Scenarios for the Netherlands - Revised edition 2015. [Online] 2015. [Citaat van: 11 July 2020.] http://www.klimaatscenarios.nl/brochures/images/Brochure_KNMI14_EN_2015.pdf.
Sanjou, M., Okamoto, T. en Nezu, I. 2017. *Experimental study on fluid energy reduction through a flood protection forest.* sl : Journal of Flood Risk Management, CIWEM, 2017. https://doi.org/10.1111/jfr3.12339.
Schiereck, G. J. en Verhagen, H.J. 2016. *Introduction to Bed, bank and shore protection, 2nd edition, revised 2016.* sl : Delft Academic Press, 2016. ISBN 97890-6562-4031.
Seidel, D. en Ammer, C. 2014. *Efficient measurements of basal area in short rotation gorests based on tls under special consideration of shadowing.* sl : iForest - Biogeosciences and Forestry Volume 7, Issue 4, Pages 227-232 , 2014. https://doi.org/10.3832/ifor1084-007.
Smale, A.J. 2019. *Invloed stroming op Hydraulische Ontwerprandvoorwaarden, unpublished (confidential) report upon request Waterschap Drents Overijsselse Delta.* Zwolle : Deltares, 2019.
Sokolewicz, M., Louters, T. en Otten, A. 2011. *Modern integrated river flood management for climate change in the Netherlands: the IJssel Delta project.* sl : International Association for Hydro-Environment Engineering and Research, 2011. https://doi.org/10.1080/15715124.2011.607824.
Soudarissanane, S.S. 2016. The Geometry of Terrestrial Laser Scanning: Identification of errors, modeling and mitigation of scanning geometry (doctoral thesis). *Repository TU Delft.* [Online] 5 January 2016. [Citaat van: 4 March 2020.] https://repository.tudelft.nl/islandora/object/uuid%3Ab7ae0bd3-23b8-4a8a-9b7d-5e494ebb54e5?collection=research. ISBN 978-94-6233-203-4.
Stam, M.M. 2018. Reliability of willows for wave load reduction on river dikes (MSc thesis). *Repository TU Delft.* [Online] 26 April 2018. [Citaat van: 10 March 2020.] https://repository.tudelft.nl/islandora/object/uuid%3A005a4184-2c08-4faa-8044-8230c0873b4c?collection=education.
Suzuki, T. en Arikawa, T. 2010. *Numerical analysis of bulk drag coefficient in dense vegetation by immersed boundary method.* sl : Coastal Engineering Proceedings, 1(32), waves.48., 2010. https://doi.org/10.9753/icce.v32.waves.48.
Suzuki, T., et al. 2011. *Wave dissipation by vegetation with layer schematization in SWAN.* sl : Elsevier, Coastal Engineering Volume 59, Issue 1, January 2012, Pages 64-71, 2011. https://doi.org/10.1016/j.coastaleng.2011.07.006.
TU Delft. 2020. User Manual SWAN Cycle III version 41.31A. *SWAN.* [Online] 29 May 2020. [Citaat van: 5 July 2020.] http://swanmodel.sourceforge.net/download/zip/swanuse.pdf.
Vries, M. de en Dekker, F. 2009. Ontwerp groene golfremmende dijk Fort Steurgat bij Werkendam. *Ontwerp groene golfremmende dijk Fort Steurgat bij Werkendam.* [Online] 2009. [Citaat van: 24 October 2020.] https://www.deltares.nl/app/uploads/2015/07/Golfremmende-dijk-Noordwaard-rapport.pdf.
Vuik, V. 2019. Building safety with nature. *Repository TU Delft.* [Online] 27 March 2019. [Citaat van: 9 March 2020.] https://repository.tudelft.nl/islandora/object/uuid%3A9339474c-3c48-437f-8aa5-4b908368c17e?collection=research.
Wageningen University & Research. 2007. Duursche Waarden. *WUR.* [Online] Wageningen University & Research, 11 December 2007. [Citaat van: 4 March 2020.] https://www.wur.nl/nl/show/Duursche-Waarden.htm.
Waterschap Drents Overijsselse Delta. 2019. Information meeting about dyke reinforcements (Powerpoint), confidential file. Zwolle : WDOD, 2019. Vol. 2019.

Wesenbeeck, B. Van en Kalloe, S. 2020 (to be published). *Full scale physical experiments of white willow trees conducted in the Delta Flume at Deltares .* Delft : Unknown, 2020 (to be published).

Appendices

A. Hydra-NL

Calculation GEBU Duursche Waarden

The failure probability is determined with the following equation:

$$P_{eis,dsn} = \frac{P_{max}\omega_B\lambda_1\lambda_2}{N} \quad \text{(A.1)}$$

In which P_{max} is the maximum allowable failure probability for flooding of the trajectory Zwolle-Olst (1/3000 per year), ω_B failure probability space for the failure mechanism erosion outer talud (0.10), λ_1 the part of the failure probability space meant for grass revetments (0.5), λ_2 the part of the failure probability space meant for failure of grass revetments by grass erosion (0.9) and N the length effect for the failure mechanism height (1). This results in 1/66666 per year for the output point adjacent to Duursche Waarden.

Uncertainties

Uncertainties concerning water level, wave height and wave period:

- Expected uncertainty water level = 0.00 m with a standard deviation of 0.20 m
- Expected uncertainty wave height = *0.96 x calculated wave height* with a standard deviation of 0.27
- Expected uncertainty spectral/peak wave period = *1.03 x calculated spectral/peak wave period* with a standard deviation of 0.13

Effective fetch

The effective fetch is the weighted average of all projections $l(\alpha)$ on the water surface in front of the flood defence relative to the wind direction. This is expressed as follows (Rijksoverheid):

$$F_e = \frac{\int_{-\alpha_m}^{+\alpha_m} w(\alpha)l(\alpha)d\alpha}{\int_{-\alpha_m}^{+\alpha_m} w(\alpha)d\alpha} \quad \text{(A.2)}$$

In which $w(\alpha) = \cos(\alpha)$ is a weight function and the mostly used value of α is 42°. In this project a value of $\alpha = 90°$ is used. In the following picture the theory of the effective fetch is schematised (Rijksoverheid):

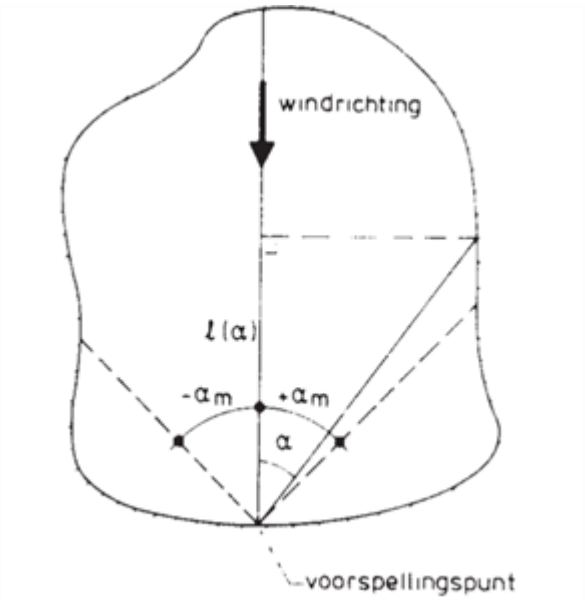

Figure A-1: All projections with angle α on the water surface relative to the wind direction

Governing parameters dike segments

For every dike segment the several wind directions with the corresponding wind speed and exceedance frequency is given for a return period of 66666 year:

Wind direction [°N]		Wind speed [m/s]		Exceedance frequency [%]	
	Year	2050	2100	2050	2100
ZW		27.6	25.4	2.6	1.8
WZW		24.8	22.0	16.6	16.8
W		27.6	24.0	11.6	11.8
WNW		23.9	25.7	47.1	50.9
NW		28.2	27.9	19.8	17.2
NNW		33.8	40.3	1.4	0.4
N		36.9	38.5	0.0	0.0

Table A-1: Output point 185 representing dike segment 185-189 (WL 5,699)

Wind direction [°N]		Wind speed [m/s]		Exceedance frequency [%]	
	Year	2050	2100	2050	2100
W (270 degrees)		33.6	40.7	1.5	0.4
WNW		23.1	25.5	43.8	40.6
NW		25.2	25.1	29.7	31.6
NNW		24.1	23.9	19.2	21.2
N		23.0	24.8	4.5	5.2

Table A-2: Output point 190 representing dike segment 190-192 (WL 5,699)

Wind direction [°N]		Wind speed [m/s]		Exceedance frequency [%]	
	Year	2050	2100	2050	2100
ZW		32.3	33.3	0.0	0.0
WZW		22.9	25.7	4.1	2.2
W		22.7	24.7	42.6	47.2
WNW		23.9	25.8	44.6	45.5
NW		30.0	33.3	6.9	4.0
NNW		42.1	42.4	0.8	0.2
N		41.6	43.2	0.0	0.0

Table A-3: Output point 193 representing dike segment 193-199 (WL 5,644)

* The exceedance frequency of the hydraulic load level for the corresponding wind direction per winter half year expressed in percentage.

* Normally you would expect higher wind speeds in 2100 than for 2050, but this is not the case. Hydra-NL uses a different ratio of stochastic variables which leads to lower wind speeds in 2100. Even though a lower wind speed is assumed, instead Hydra-NL uses a higher model uncertainty for waves or an higher river discharge. The lower wind speeds could also be a result of numerical inaccuracy.

Names of the hydraulic conditions:

- Table A-1: 185-NW-2050, 185-NW-2100, 185-WNW-2050 and 185-WNW-2100
- Table A-2: 190-NW-2050, 190-NW-2100, 190-WNW-2050 and 190-WNW-2100
- Table A-3: 193-W-2050, 193-W-2100, 193-WNW-2050 and 193-WNW-2100

Dike segment	Output point	Governing wind direction	Dike orientation [°N]	Effective fetch [m]	Bottom level [m +NAP]	Water level [m +NAP]	Water depth [m]
185-189	185	NW WNW	270	1522.65 1829.97	1.50 2.83	5.70	4.20 2.87
190-192	190	NW WNW	340	1327.41 1760.29	0.95 0.58	5.70	4.75 5.12
193-199	193	W WNW	280	2045.17 1604.84	1.82 0.97	5.64	3.82 4.67

Table A-4: Effective fetch and water depth per dike segment

Calculation steps

The calculation in Hydra-NL is performed as follows:

1. To start with the parameters described concerning the geometry are fixed.
2. The failure probability is implemented. In this case it is 1/66666 per year.
3. This is an Hydraulic Load Level ('Hydraulisch Belasting Niveau', (HBN)). This means a maximum allowable overtopping discharge is chosen in most cases. This is a GEBU calculation at which for the given water level, the maximum wave impact will be determined.
   This depends on the stochastic variables such as river discharge, water level IJssel Lake, wind speed, open/closed Rampspol etc. River discharge, wind speed and water level IJssel Lake are already integrated. This is different than fully probabilistic calculations.
4. Additionally, Hydra-NL uses four variable stochastics concerning model uncertainties as described in Appendix Uncertainties.
5. With the help of all these data Hydra-NL determines (i) the Hydraulic Load Level (in this case the required crest height of the dike in order to withstand the extreme wave characteristics and water level conditions). In case the Hydraulic Load Level is known, Hydra-NL determines (ii) the overtopping discharge. In case both are known, Hydra-NL determines (iii) the return time that is valid for the entered Hydraulic Load Level and overtopping discharge.

GEBU calculations

The calculations have been performed with 'Basis Module Gras Buitentalud' prescribed by WBI (Wettelijk Beoordelingsinstrumentarium) 2017. These calculations assume a closed grass sod on an 'average' dike location at Duursche Wuurden and a (peak) storm duration of twelve hours. Hence, the wave attack on the outer slope of grass holds for 12 hours in these calculations. The results of the performed calculations are shown below. The safety factors are outlined in red.

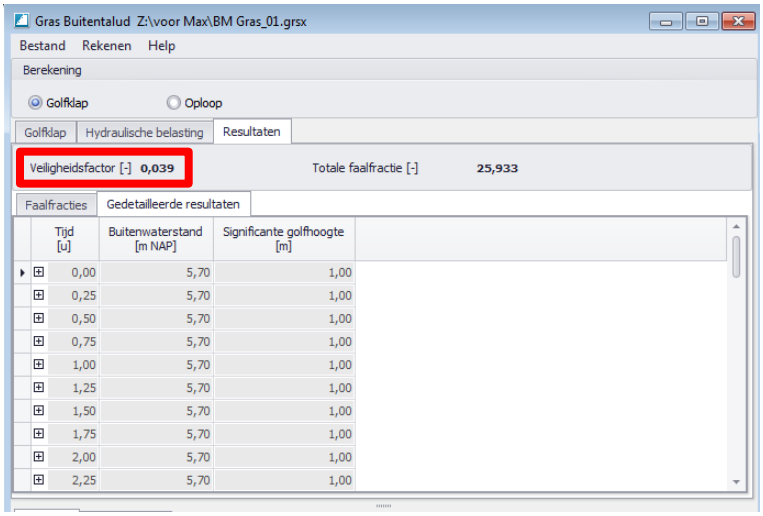

Figure A-2: Hs of 100 cm (Hydra-NL), WL 5.70 m NAP

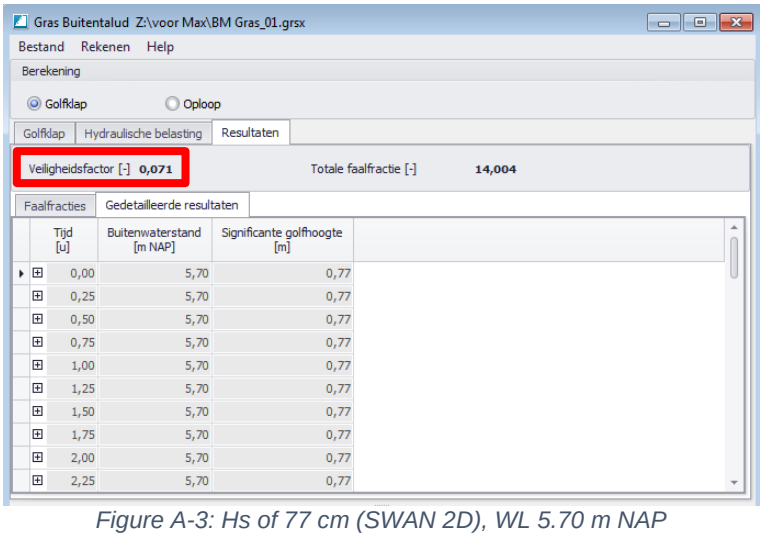

Figure A-3: Hs of 77 cm (SWAN 2D), WL 5.70 m NAP

B. Vegetation Duursche Waarden

Tree species

Tree species	Type of area, name	Amount of TLS scans and names
Vegetation area 1 (uniform)		
- Mix of white willows (*Salix alba*) and crack willows (*Salix fragilis*) - Length of 15-20 m - Mature (maximum length is 15-20 m for this species)	Uniform area, UMW-1	- Scan 1.3, 1.4 and 1.5 - Scan of a small area
Vegetation area 2 (non-uniform)		
- Downy oak (*Quercus pubescens*) - Length of 5-10 m - Mature (maximum length is 10 m) - Positioned horizontally instead of vertically	Non-uniform area, IDO	- Scan 2.7, 2.8 and 2.9 - Scan of an individual tree
- Pedunculate oak (*Quercus robur*) - Length of approximately 30-40 m - Mature (maximum length is 40 m)	Non-uniform area, IPO	- Scan 2.10, 2.11 and 2.12 - Scan of an individual tree
- Osier (*Salix viminalis*) - Length of approximately 10 m - Mature (maximum length is 10 m for this species) - Positioned horizontally instead of vertically	Non-uniform area, IO	- Scan 3.1, 3.2 and 3.3 - Scan of an individual tree
Vegetation area 3 (both uniform and non-uniform)		
- Crack willows (*Salix fragilis*) - Length of approximately 15 m - Mature (maximum length is 15 m for this species)	Uniform area, UCW	- Scan 3.4, 3.5 and 3.6 - Scan of a small area
- Mix of frosted willows (*Salix daphnoides*), Osier (*Salix viminalis*) and white willows (*Salix alba*) - Length 5 to 10 m - Young mature (maximum length is 10-20 m)	Uniform area, UMW-3	- Scan 3.7 and 3.9 Scan of a small area
Consist of same individual tree species as in vegetation area 2	Non-uniform area IDO, IPO, IO	Same scans as IDO, IPO and IO

Table B-1: Different tree species in prioritised vegetation areas

Images species

These images are made during field trips at 22nd of June and 3rd of September 2020.

UMW-1:

*Figure B-1: White willow (*Salix alba*)*

*Figure B-2: Crack willow (*Salix fragilis*)*

IDO:

*Figure B-3: Downy oak (*Quercus pubescens*)*

IPO:

*Figure B-4: Pedunculate oak (*Quercus robur*)*

IO:

*Figure B-5: Osier (*Salix viminalis*)*

UCW:

Figure B-6: Crack willow (Salix fragilis)

UMW-3:

Figure B-7: Frosted willows (Salix daphnoides)

Figure B-8: Osier (Salix viminalis)

Figure B-9: White willow (Salix alba)

AHN 3 images vegetation areas

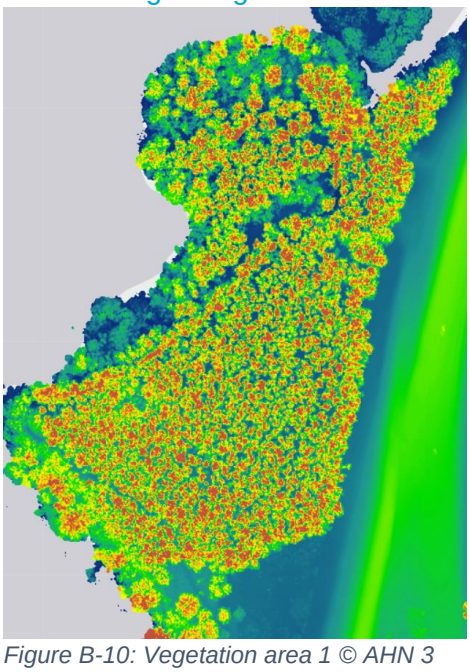

Figure B-10: Vegetation area 1 © AHN 3

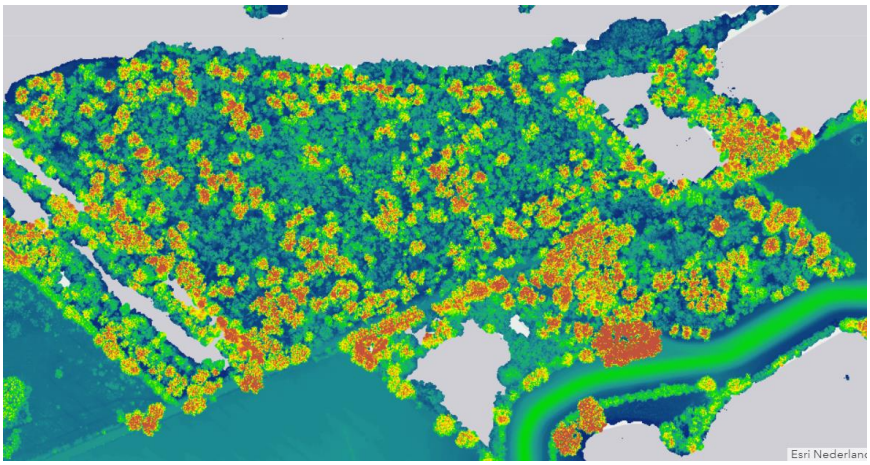

Figure B-11: Vegetation area 2 © AHN 3

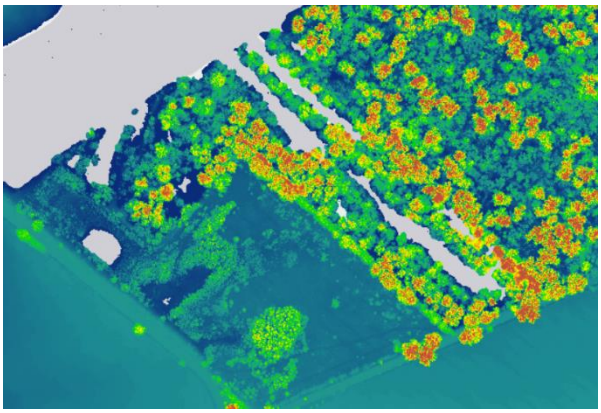

Figure B-12: Vegetation area 3 © AHN 3

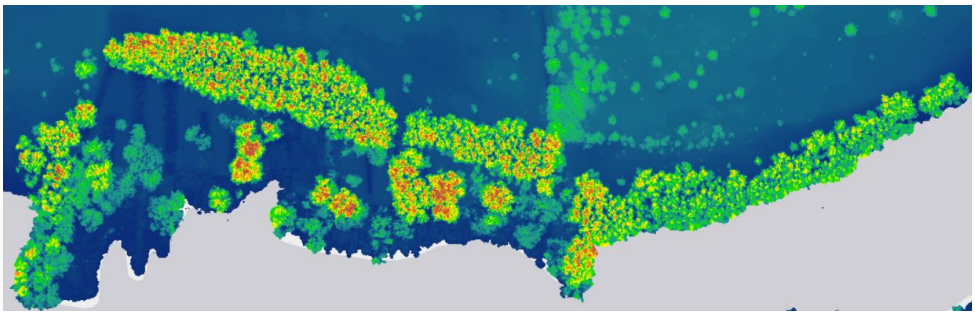

Figure B-13: Vegetation area 4 © AHN 3

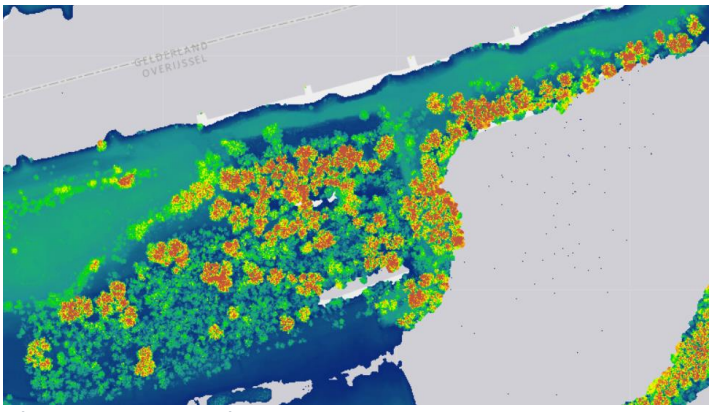

Figure B-14: Vegetation area 7 © AHN 3

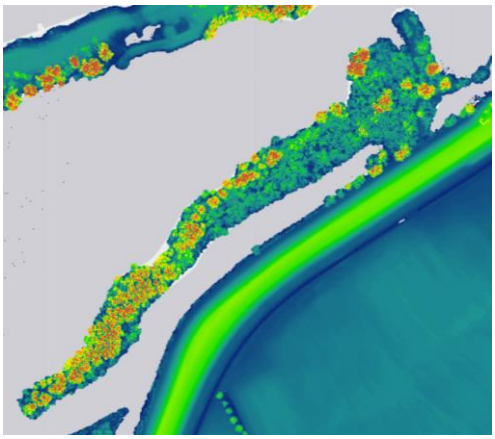

Figure B-15: Vegetation area 8 © AHN 3

Ratio subareas

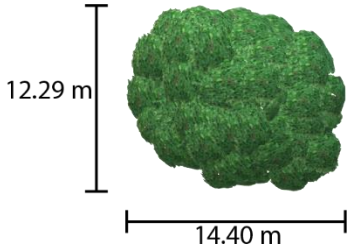

Figure B-16: Top view Pedunculate Oak with an height of 30-40 m

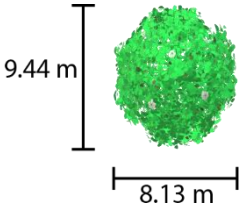

Figure B-17: Top view Downy Oak with an height of 6.0-6.5 m

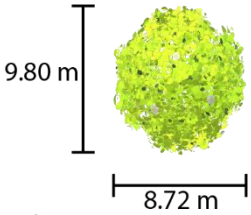

Figure B-18: Top view Osier with an height of 6.5-7.0 m

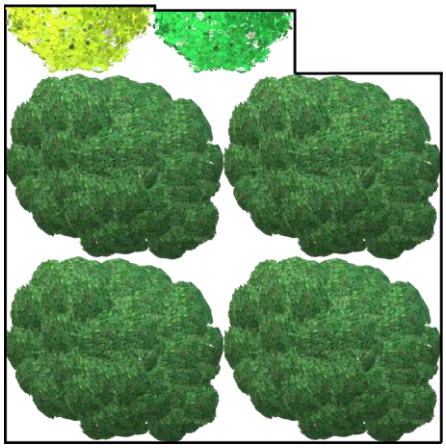

Figure B-19: Distribution and ratio subarea 2

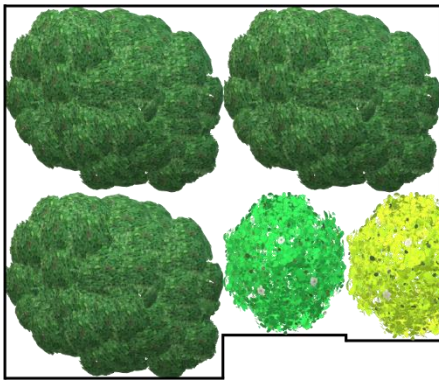

Figure B-20:Distribution and ratio subarea 3

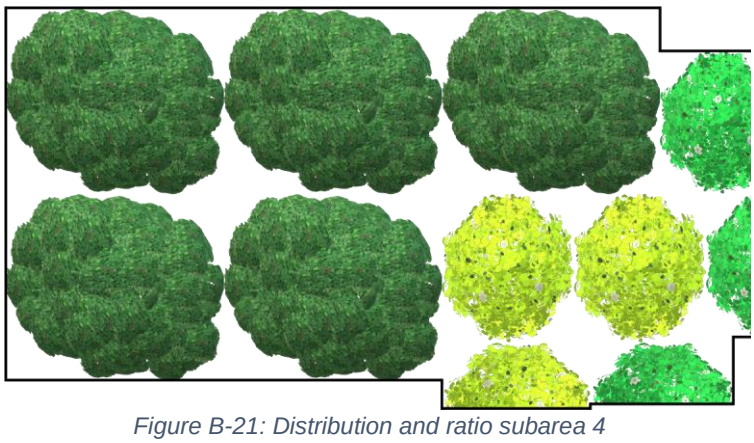

Figure B-21: Distribution and ratio subarea 4

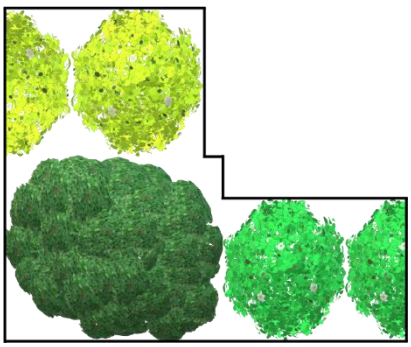

Figure B-22: Distribution and ratio subarea 5

Roughly estimated vegetation areas

Figure B-23: Rough plan vegetation area 4

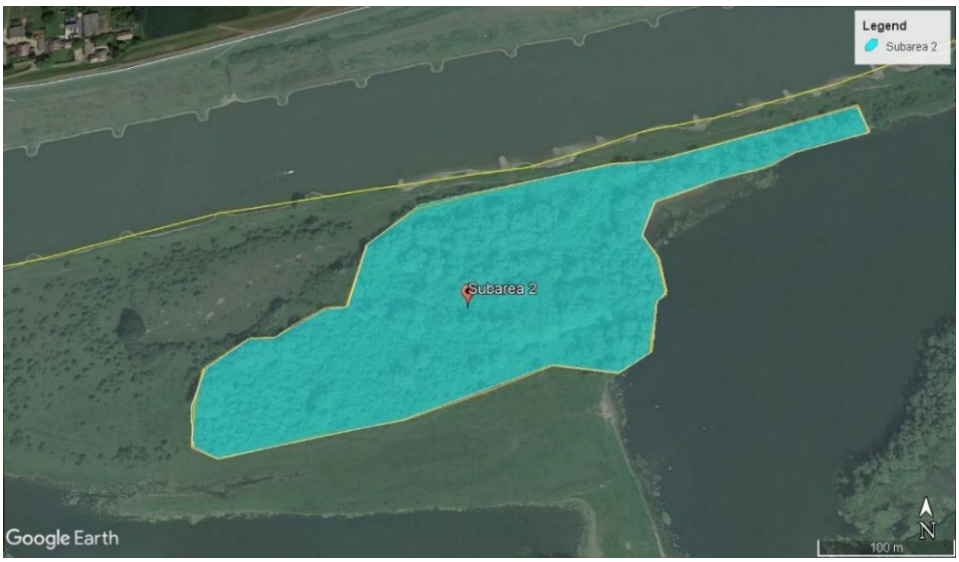

Figure B-24: Rough plan vegetation area 7

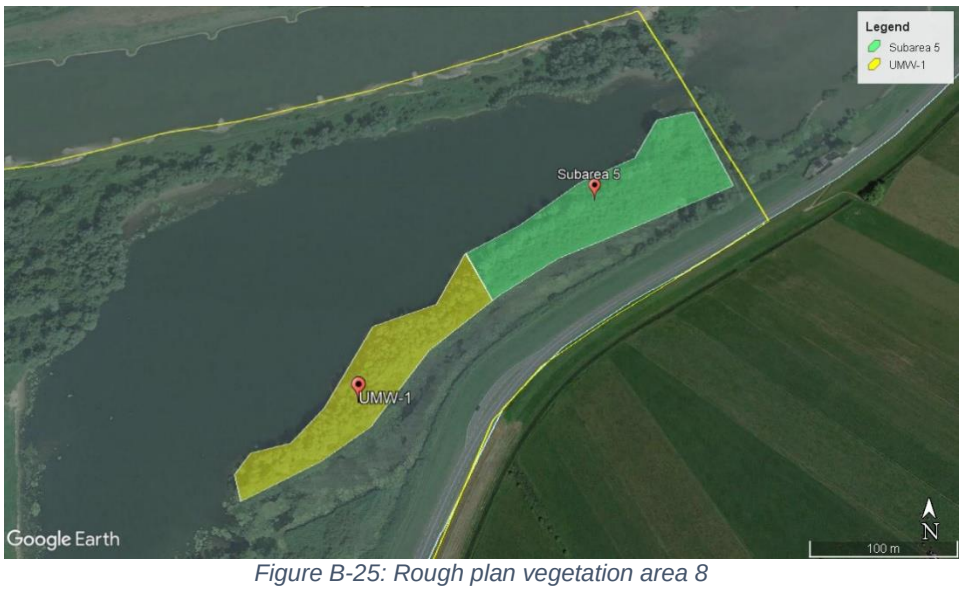

Figure B-25: Rough plan vegetation area 8

C. TLS

Leica P40

The Leica P40 is a 3D Terrestrial Laser Scanner (TLS) and provides a 3D point cloud of the surroundings by determining the position of visible surface using the reflection of light. The Leica P40 is a time-of-flight scanner which emits narrow laser beam pulses in known direction and measure the backscattered signal reflected by the object surface. This is shown in the following figure:

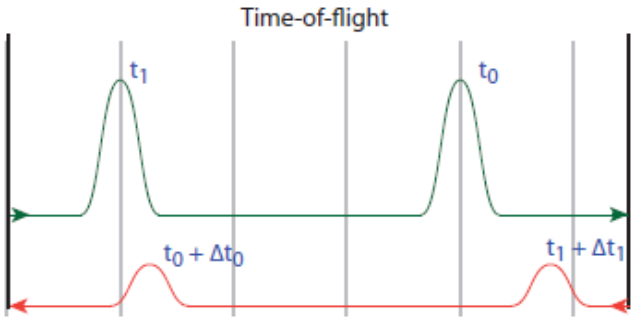

Figure C-1: Laser beam pulses (Soudarissanane, 2016)

The laser incorporated in the Leica P40 produces a beam which emerges from the rotating mirror. The instrument has also a rotating scan-head. Both cover 360° x 290° field of view.

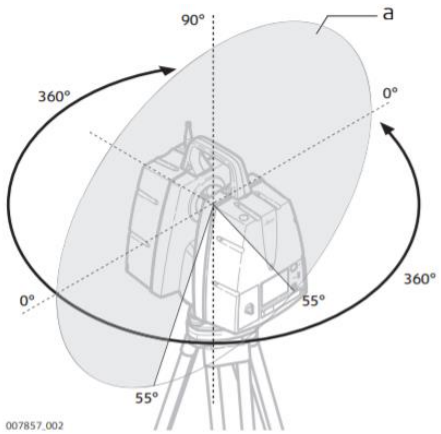

Figure C-2: Rotating Leica P40 (Leica Geosystems, 2016)

The Leica P40 has a 3D position accuracy of 3 mm at 50 mm and 6 mm at 100 mm. Different resolutions can be obtained varying from 50 to 0.8 mm at 10 m. Also two sensitivity levels are categorised: normal and high. The scan duration of different resolutions and sensitivity levels are given:

Resolution [mm @ 10 m]	Estimated scan duration [HH:MM:SS] for a full dome scan @ sensitivity level	
	Normal	High
50	00:00:20	00:00:20
25	00:00:33	00:00:33
12.5	00:00:58	00:00:58
6.3	00:01:49	00:03:25
3.1	00:03:30	00:13:30
1.6	00:13:33	00:54:06
0.8	00:54:06	03:36:21

Figure C-3: Resolution options Leica P40 (Leica Geosystems, 2016)

The resolution is expressed in millimetre between cloud points at a distance of 10 m. This distance between cloud point increase with increased distance of the scanner and vice versa.

The performance indicators of Leica P40:

Indicators	Descriptions
Range Accuracy	1.2 mm + 10 ppm
3D position Accuracy	3 mm @ 50 m 6 mm @ 100 m
Wavelength	1550nm (invisible); 658 nm (visible)
Scan Rate	Up to 1,000,000 points per second
Field-of-View	360° (Horizontal); 290° (Vertical)
Range and Reflectivity	Minimum range: 0.4 m Maximum range at reflectivity: 120 m (8%), 180 m (18%), 270 m (34%)
Range Noise	0.4 mm RMS at 10 m 0.5 mm RMS at 50 m

Figure C-4: Performance indicators Leica P40 (Liu, et al., 2018)

Errors

The first is beam divergence deviation of the emitted laser beam. This results in the possibility of a small deviation from the centre axis in the desired direction and hence a small error in the coordinate.
The second error is in relation with the beam deflection unit and depends on the type of laser scanner in use. Depending on the rotating mirror (single- or multi-facet) both systems have their own errors sources such as surface roughness and mirror deformation. However, these error sources both lead to lower beam deflection angular precision and hence in an error of the vertical angle position of a point in the final point cloud.

The third error is the axes error. Three axes are included: horizontal axis (rotation axis of the mirror), vertical axis (rotation axis of the head of the scanner) and the collimation axis (axis that passes through the centre of the mirror both for emission and reception). These axes are never perfectly aligned and stable and therefore result in uncertainties.
On top of the reception errors a time-of-flight scanner, which the Leica P40 is, brings an uncertainty in the pulse arrival time determination. This is created because of the effect of non-linearities and noise in the received pulse.

Locations TLS measurements

On the day 02-04-2020 the TLS measurements have been carried out with the Leica P40. All measurements have been done with resolution 3.1 mm (at a distance of 10 m). For every vegetation area the naam of the scan, the GPS coordinates, the accuracy of the GPS coordinates and the type of scan are shown below. The app ‘Mijn GPS Coördinaten’ has been used to determine the GPS coordinates and accuracy.

Scan name	GPS coordinates	Accuracy of GPS coordinates	Type of scan
1.1	52.372364 06.114902	6 m	2D area
1.2	52.371205 06.114265	6 m	2D area
	3D area in the middle of the little forest, 3 targets used		
1.3	52.371850 06.114435	6 m	1/3 3D
1.4	52.371903 06.114287	6 m	2/3 3D
1.5	52.371837 06.114237	6 m	3/3 3D

Table C-1: TLS measurements vegetation area 1

Scan name	GPS coordinates	Accuracy of GPS coordinates	Type of scan
2.1	52.369711 06.110677	6 m	2D area
2.2	52.369646 06.111900	6 m	2D area
2.3	52.369366 06.112286	4 m	2D area
2D area put together, 2 targets used (on the dike)			
2.4	52.368937 06.111999	4 m	1/2 2D area
2.5	52.368508 06.110864	8 m	2/2 2D area
2.6	52.368702 06.109721	8 m	2D area
3D individual shrub/tree, 3 targets used			
2.7	52.369128 06.108822	8 m	1/3 3D
2.8	52.369052 06.108848	16 m	2/3 3D
2.9	52.369270 06.108592	6 m	3/3 3D
3D big tree, 3 targets used			
2.10	52.369211 06.109277	8 m	1/3 3D
2.11	52.369283 06.109226	8 m	2/3 3D
2.12	52.369260 06.109253	6 m	3/3 3D
2.13	52.369087 06.108911	12 m	2D area
2.14	52.368964 06.107800	4 m	2D area
2.15	52.368743 06.106808	6 m	2D area
2.16	52.368576 06.104924	6 m	2D area

Table C-2: TLS measurements vegetation area 2

Scan name	GPS coordinates	Accuracy of GPS coordinates	Type of scan
3D tree/shrub, 3 targets used			
3.1	52.367968 06.103072	6 m	1/3 3D
3.2	52.368023 06.103175	6 m	2/3 3D
3.3	52.367991 06.103356	8 m	3/3 3D
3D thinner tree area than at veg. area 1, 3 targets used			
3.4	52.367970 06.101575	6 m	1/3 3D
3.5	52.368110 06.101539	8 m	2/3 3D
3.6	52.368043 06.101539	8 m	3/3 3D
3D area thinnest tree (only 2 scans were possible due to high density), 2 targets used			
3.7	52.368715 06.101986	8 m	1/2 3D
3.8 (3.9 in TLS)	52.368776 06.102080	8 m	2/2 3D
3.10	52.368236 06.099757	6 m	2D area
3.11	52.368935 06.098409	8 m	2D area

Table C-3: TLS measurements vegetation area 3

Coordinates scans

Vegetation area 1
Area 1: Scan 1.3: position x = -1.31, y = -17.10, z=-1.94--1.82=-0.12 Scan 1.4: position x = 0, y = 0, z=0 (grond z=-1.82) Scan 1.5: position x = 10.30 y = -10.38, z=-1.85--1.82=-0.03
Vegetation area 2
Species x1: Scan 2.7, position x = 0, y = 0, z=0 (grond z=-1.72 Scan 2.8, position x = -0.33, y = -5.25, z= -2.40--1.72=-0.68 Scan 2.9, position x = -6.07, y = -4.20, z= -2.80--1.72=-1.08
Species x2: Scan 2.10, position x = 0, y = 0, z=0 (grond z=-1.73) Scan 2.11, position x = -6.39, y = 6.71,z = -1.75--1.73 = -0.02 Scan 2.12, position x = -8.44, y = 2.40, z=-1.68--1.73=0.05
Species x3: Scan 3.1, position x = 0, y = 0, z = 0 (grond z=-1.83) Scan 3.2, position x = -5.66, y = -11.83, z=-1.94--1.83=-0.11 Scan 3.3, position x = -17.08, y = -2.49, z = -1.87--1.83=-0.04
Vegetation area 3
Area 2: Scan 3.4, position x = 0, y = 0, z = 0 (grond z=-1.49) Scan 3.5, position x = 3.08, y = 11.68, z = -1.70--1.49=-0.21 Scan 3.6, position x = -6.80, y = 9.77, z =-1.80--1.49=-0.31
Area 3: Scan 3.7, position x = 0, y = 0, z = 0 (grond z=-1.48) Scan 3.9, position x = -10.15, y = 6.09, z = -1.65--1.48 = -0.17

Table C-4: Coordinates scans

Regions based on branch thickness

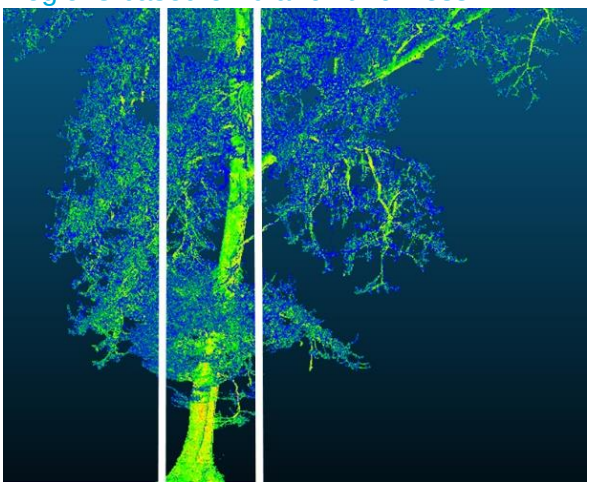

Figure C-5: IPO

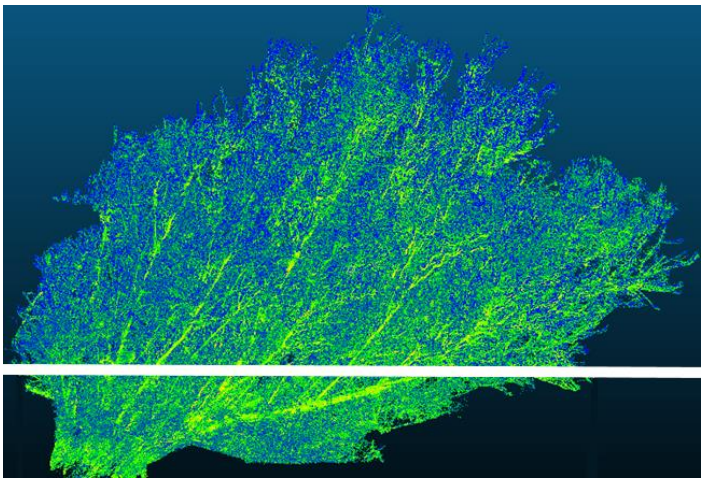

Figure C-6: IO

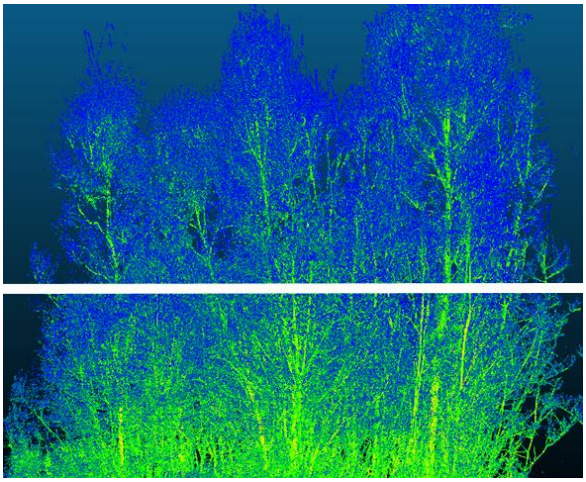

Figure C-7: UMW-3

Results TLS (MSS): Frontal area

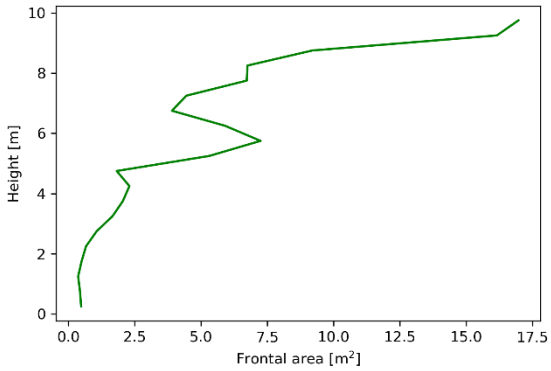

Figure C-8: IPO

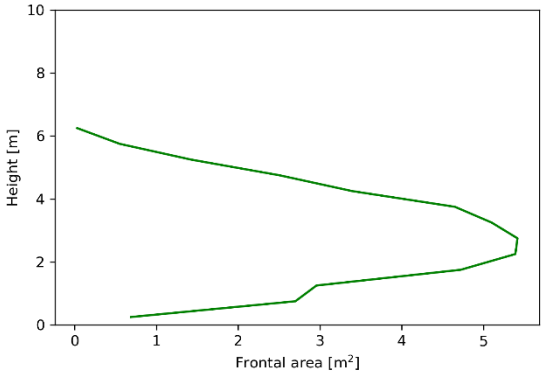

Figure C-9: IO

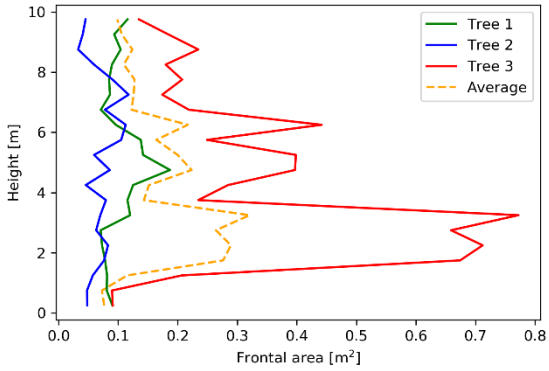

Figure C-10: UCW

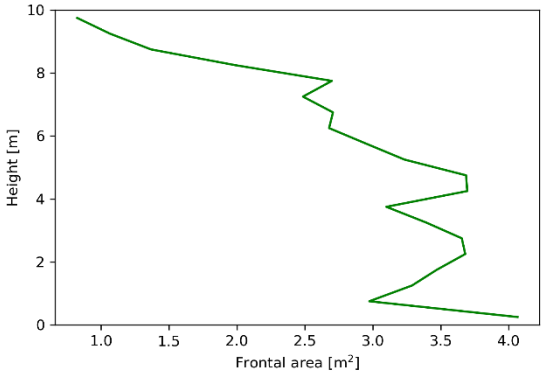

Figure C-11: UMW-3

Results TLS (MSS): cumulative frontal area

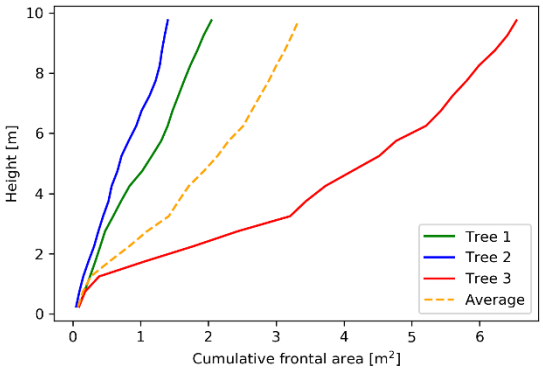

Figure C-12: UCW

Results TLS (MSS): frontal area per volume

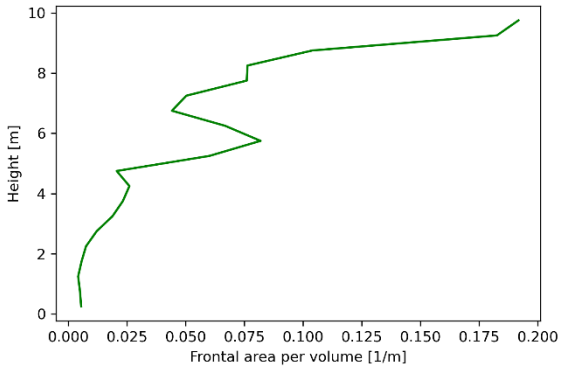

Figure C-13: IPO

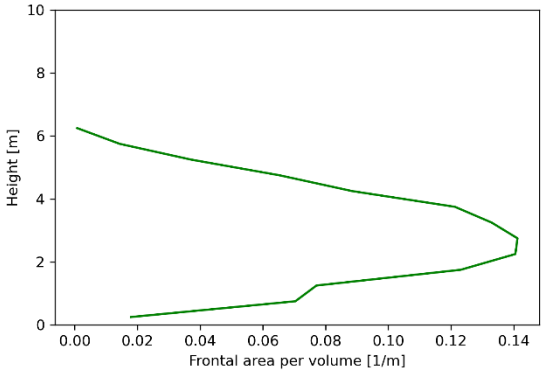

Figure C-14: IO

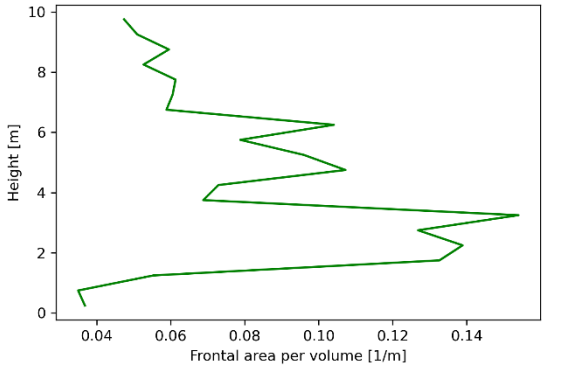

Figure C-15: Average tree UCW

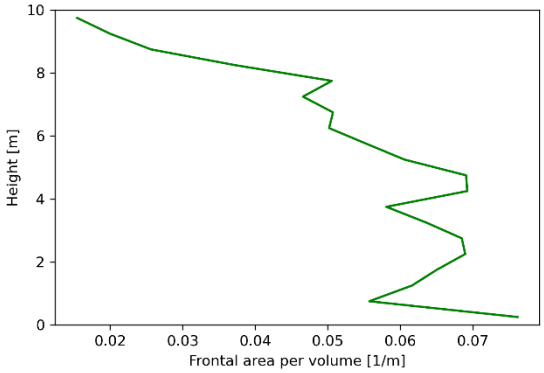

Figure C-16: UMW-3

Results TLS (MSS): distribution stem and branches

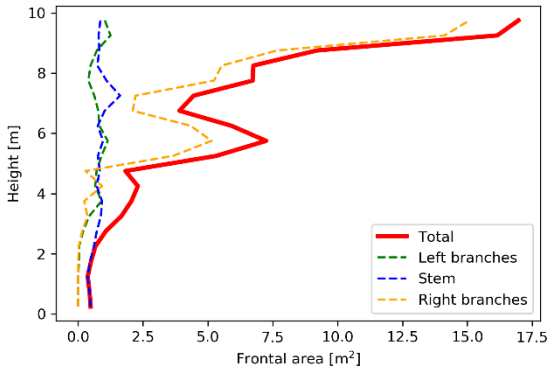

Figure C-17: IPO

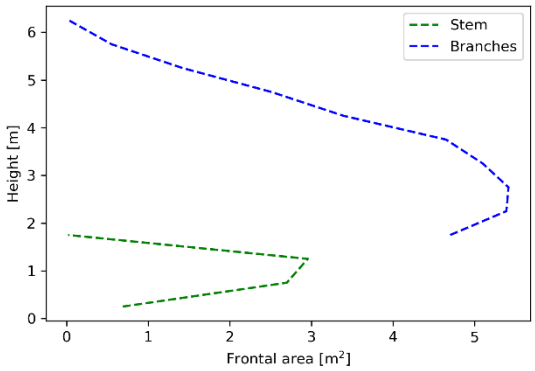

Figure C-18: IO

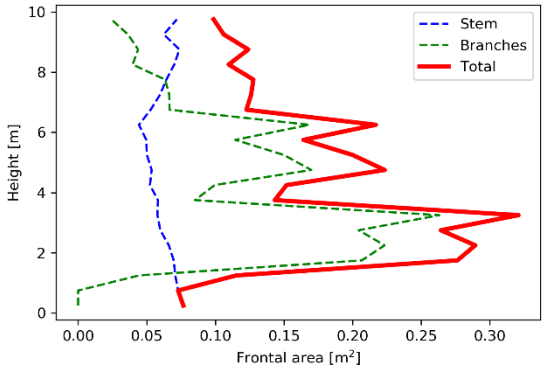

Figure C-19: Average tree UCW

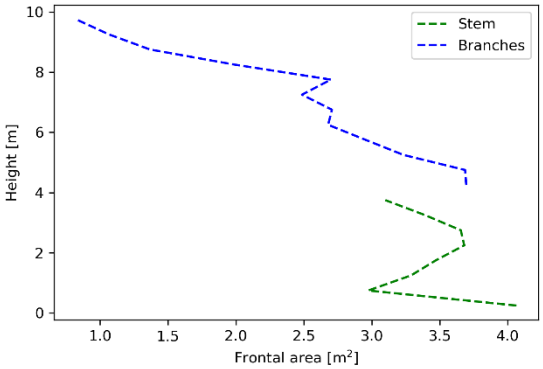

Figure C-20: UMW-3

SSS method: amount of laser beams getting through

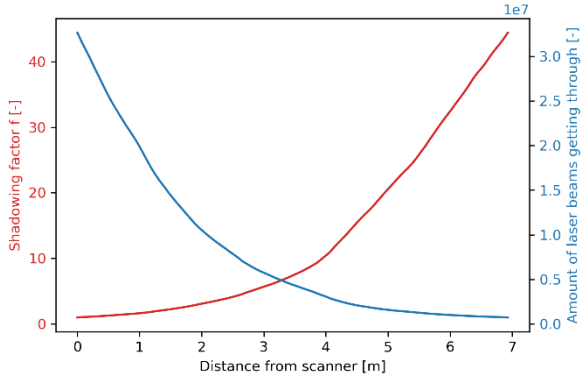

Figure C-21: Scan 2.9, tree species IDO

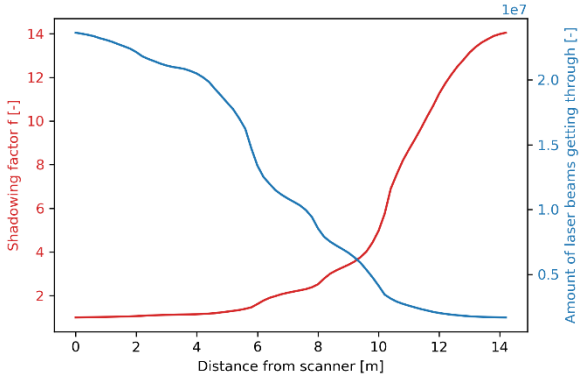

Figure C-22: Scan 2.10, tree species IPO

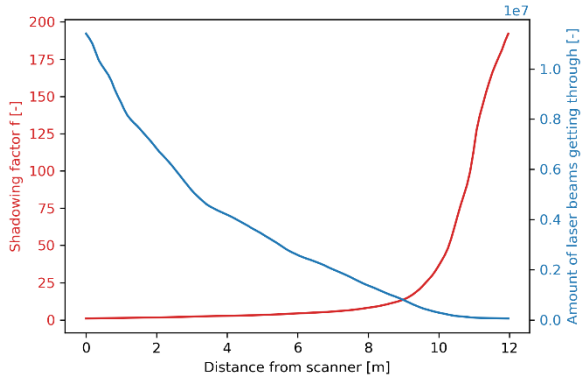

Figure C-23: Scan 3.1, tree species IO

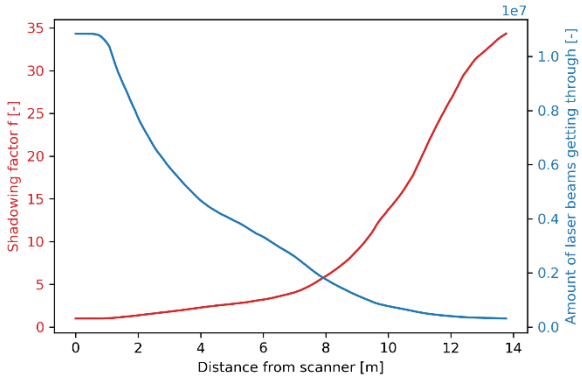

Figure C-24: Scan 3.2, tree species IO

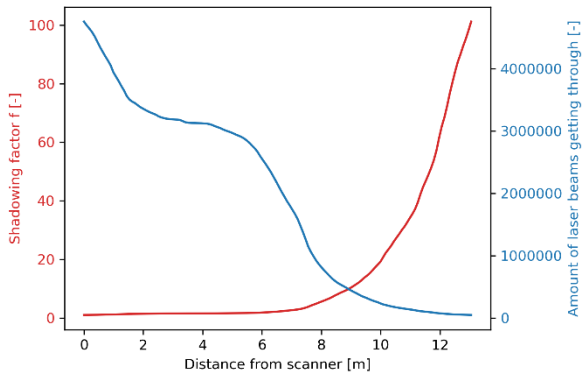

Figure C-25: Scan 3.3, tree species IO

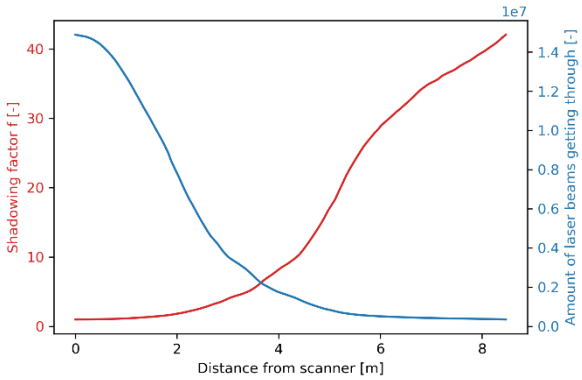

Figure C-26: Scan 3.7, tree species UMW-3

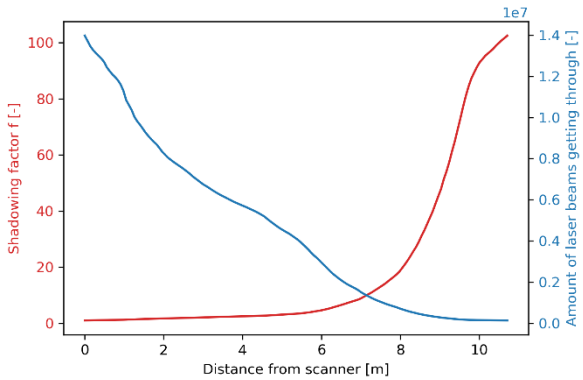

Figure C-27: Scan 3.9, tree species UMW-3

SSS method: maximum f

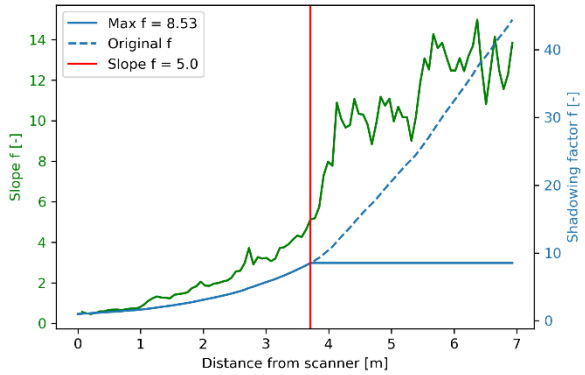

Figure C-28: Scan 2.9, tree species IDO

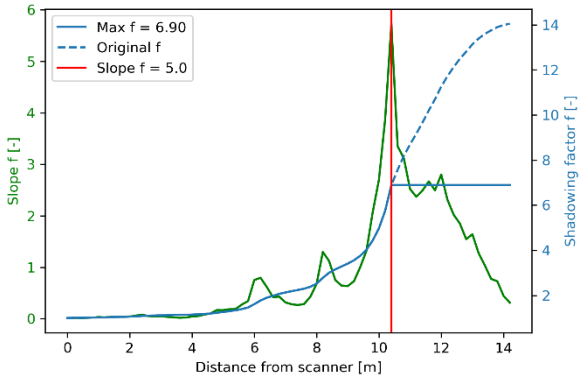

Figure C-29: Scan 2.10, tree species IPO

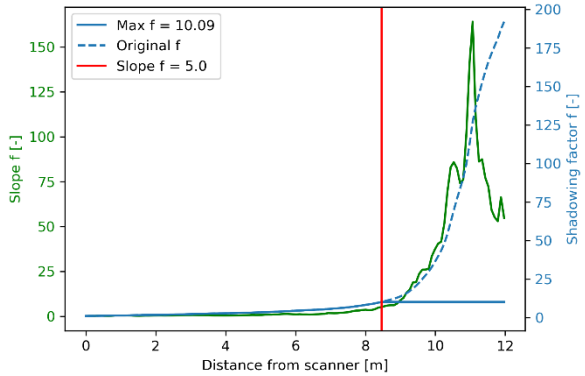

Figure C-30: Scan 3.1, tree species IO

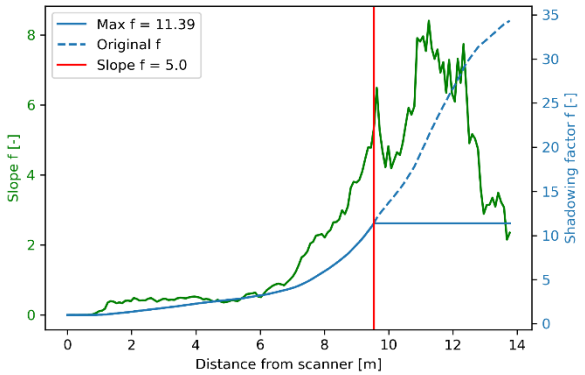

Figure C-31: Scan 3.2, tree species IO

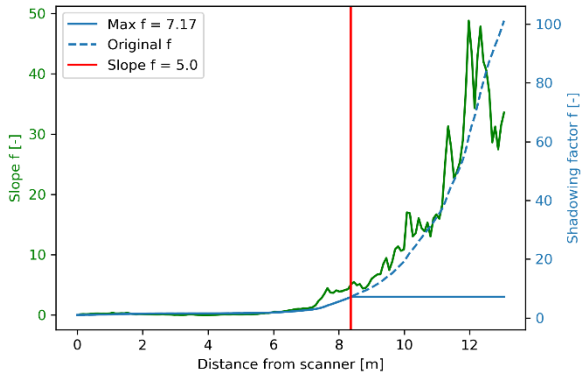

Figure C-32: Scan 3.3, tree species IO

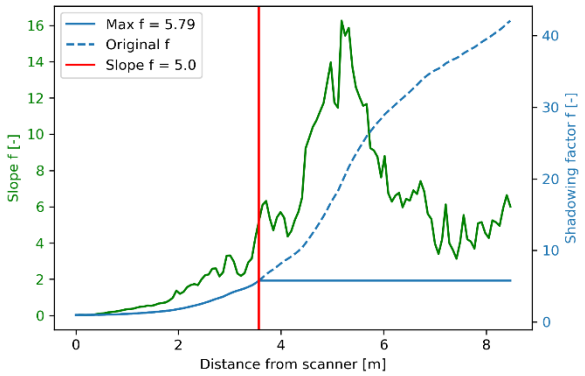

Figure C-33: Scan 3.7, tree species UMW-3

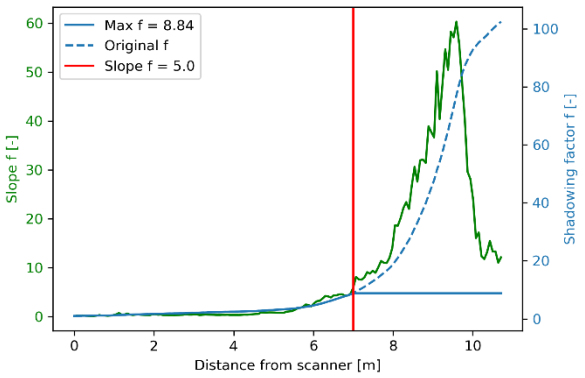

Figure C-34: Scan 3.9, tree species UMW-3

SSS methods: frontal area per volume

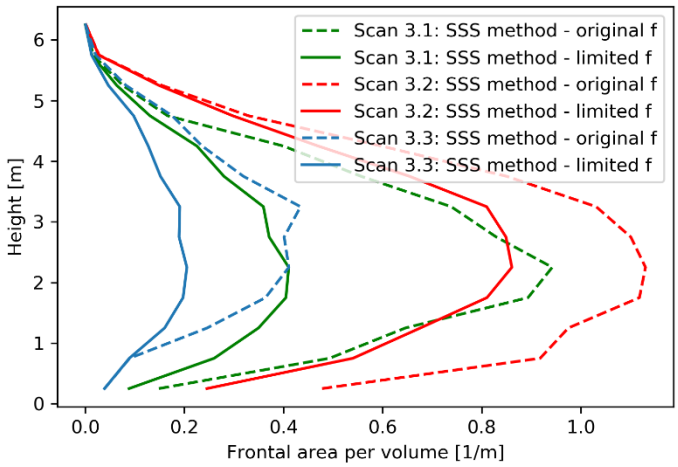

Figure C-35: Tree species IO

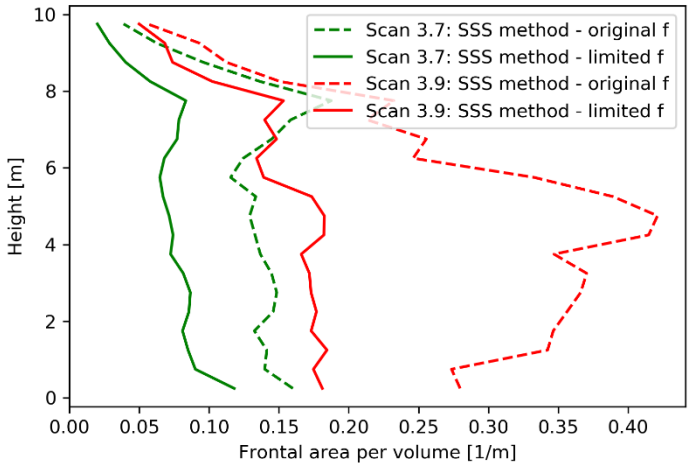

Figure C-36: Tree species UMW-3

D. Results hand measurements

The hand measurements were done at the 3th of September, 2020. For the calculations of the frontal area per volume it is assumed that the diameter of the branch or stem is constant until the height it is measured. The branches and stems are (nearly) vertically directed.

UMW-1

Area 5x5 m, measurement stem

Tree	Perimeter, diameter at 1 m height [cm]	Perimeter, diameter at 2 m height [cm]
1	56, 17.83	51,16.23
2	64, 20.37	56, 17.83
3	47, 14.96	40, 12.73
4	28, 8.91	26, 8.28
5	78, 24.83	76, 24.19
6	37, 11.78	34, 10.82
7	42, 13.37	38, 12.10
8	50, 15.92	46, 14.64
9	89, 28.33	82, 26.10
Total diameter:	156.30	142.92

Table D-1: Hand measurements UMW-1

Total volume that is considered: = $5\text{x}5\text{x}2\ \text{m} = 50\ \text{m}^3$. This means per 0.5 m height a volume of 12.5 m^3 is considered. The frontal area per volume is determined as follows:

$$\frac{1}{V}\sum_{i=1}^{n} A_i = \frac{h * \sum D}{V} = \frac{0.5 * \sum D}{12.5} \qquad \text{(D.1)}$$

With $\sum D$ [m] the summed diameters at the given height. This gives the following frontal area per volume:

Height [m]	$\frac{1}{V}\sum_{i=1}^{n} A_i$ [m^{-1}]
0.5-1.0	$\frac{0.5 * (156.30 * 10^{-2})}{12.5} = 0.0625$
1.5-2.0	$\frac{0.5 * (142.92 * 10^{-2})}{12.5} = 0.0572$

Table D-2: Ranges frontal area per volume UMW-1

UCW

Area 3x3 m, kraakwilg blz. 102, measurement stem.

Tree	Perimeter, diameter at 1 m height [cm]	Perimeter, diameter at 2 m height [cm]
1	20, 6.37	19, 6.05
2	28, 8.91	25, 7.96
3	27, 8.59	25, 7.96
4	38, 12.10	33, 10.50
5	27, 8.59	24, 7.64
6	65, 20.69	60, 19.10
7	44, 14.01	38, 12.10
8	53, 16.87	50, 15.92
9	11, 3.50	10, 3.18
10	11, 3.50	8, 2.55
11	37, 11.78	33, 10.50
12	21, 6.68	18, 5.73
13	31, 9.87	26, 8.28
Total diameter:	131.46	117.47

Table D-3: Hand measurements UCW

The frontal area per volume is determined the same way as above (Equation D.1), except for the volume per 0.5 m height is now 4.5 m^3 (3x3x0.5 m).

Height [m]	$\frac{1}{V}\sum_{i=1}^{n} A_i$ [m^{-1}]
0.5-1.0	$\frac{0.5 * (131.46 * 10^{-2})}{4.5} = 0.146$
1.5-2.0	$\frac{0.5 * (117.47 * 10^{-2})}{4.5} = 0.131$

Table D-4: Ranges frontal area per volume UCW

UMW-3

Area 3x3 m, measurement stem with perimeter greater than 5 cm:

Stem	Perimeter, diameter at 1 m height [cm]	Perimeter, diameter at 2 m height [cm]
1	77, 24.51	67, 21.33
2	22, 7.00	18, 5.73
3	17, 5.41	14, 4.46
4	11, 3.50	10, 3.18
5	18, 5.73	15, 4.77
6	29, 9.23	23, 7.32
7	12, 3.82	10, 3.18
8	21, 6.68	19, 6.05
9	20, 6.37	19, 6.05
10	12, 3.82	10, 3.18
11	9, 2.86	7, 2.23
12	20, 6.37	17, 5.41
13	18, 5.73	13, 4.14
14	13, 4.14	12, 3.82
15	22, 7.00	19, 6.05
16	19, 6.05	15, 4.77
17	16, 5.09	10, 3.18
18	12, 3.82	10, 3.18
19	8, 2.55	7, 2.23
20	9, 2.86	8, 2.55
Total diameter:	122.54	102.76

Table D-5: Hand measurements UMW-3

At 1 m height circa 160 branches with perimeter of 5 mm - 5 cm. This means a diameter of 0.16 cm - 1.59 cm. It is assumed that the same amount of branches appear it 2 m height.

The frontal area per volume is determined the same way as above (Equation D.1), except now small branches with a diameter of 0.16 to 1.59 cm are added.

Height [m]	$\frac{1}{V}\sum_{i=1}^{n} A_i$, D small branches = 0.16 cm [m^{-1}]	$\frac{1}{V}\sum_{i=1}^{n} A_i$, D small branches = 0.88 cm [m^{-1}]	$\frac{1}{V}\sum_{i=1}^{n} A_i$, D small branches = 1.59 cm [m^{-1}]
0.5-1.0	$\frac{0.5 * ((122.54 + 160 * 0.16) * 10^{-2})}{4.5} = 0.165$	$\frac{0.5 * ((122.54 + 160 * 0.88) * 10^{-2})}{4.5} = 0.0.293$	$\frac{0.5 * ((122.54 + 160 * 1.59) * 10^{-2})}{4.5} = 0.419$
1.5-2.0	$\frac{0.5 * ((102.76 + 160 * 0.16) * 10^{-2})}{4.5} = 0.143$	$\frac{0.5 * ((102.76 + 160 * 0.88) * 10^{-2})}{4.5} = 0.271$	$\frac{0.5 * ((102.76 + 160 * 1.59) * 10^{-2})}{4.5} = 0.397$

Table D-6: Ranges frontal area per volume UMW-3

IO

Area 1x1 m, only measurements at one height have been done due to circumstances of high understorey vegetation.

Stem	Perimeter, diameter at 1.5 m height [cm]
1	10, 3.18
2	16, 5.09
3	5, 1.59
4	9, 2.86
5	4, 1.27
6	10, 3.18
7	12, 3.82
8	15, 4.77
Total diameter:	25.76

Table D-7: Hand measurements IO

Circa 45 branches with perimeter of 5 mm - 5 cm at an height of 1.5 m. This means a diameter of 0.16 cm - 1.59 cm. The frontal area per volume is determined the same way as above (Equation D.1), except now the volume is 0.5 m^3 (1x1x0.5 m).

Height [m]	$\frac{1}{V}\sum_{i=1}^{n} A_i$, D small branches = 0.16 cm [m^{-1}]	$\frac{1}{V}\sum_{i=1}^{n} A_i$, D small branches = 0.88 cm [m^{-1}]	$\frac{1}{V}\sum_{i=1}^{n} A_i$, D small branches = 1.59 cm [m^{-1}]
1.5-2.0	$\frac{0.5 * ((25.76 + 45 * 0.16) * 10^{-2})}{0.5} = 0.330$	$\frac{0.5 * ((25.76 + 45 * 0.88) * 10^{-2})}{0.5} = 0.654$	$\frac{0.5 * ((25.76 + 45 * 1.59) * 10^{-2})}{0.5} = 0.973$

Table D-8: Range frontal area per volume IO

E. SWAN

Vegetation parameters for SWAN

UMW-1			
Height [m]	$\frac{1}{V}\sum_{i=1}^{n} A_i \ [m^{-1}]$	$\widetilde{C}_D$ [−]	**Vegetation factor:** $\frac{1}{V}\sum_{i=1}^{n} A_i * \widetilde{C}_D [m^{-1}]$
0.00-0.50	0.0338	1.2	0.0406
0.50-1.00	0.0379	1.2	0.0455
1.00-1.50	0.0412	1.2	0.0494
1.50-2.00	0.0343	1.2	0.0412
2.00-2.50	0.0311	1.2	0.0373
2.50-3.00	0.0409	1.2	0.0491
3.00-3.50	0.0298	1.2	0.0358
3.50-4.00	0.0408	1.1	0.0449
4.00-4.50	0.0537	1.2	0.0644
4.50-5.00	0.0665	1.1	0.0732
Average vegetation factor: 0.0481			

Table E-1: Vegetation parameters of UMW-1

Subarea 1			
Height [m]	$\frac{1}{V}\sum_{i=1}^{n} A_i \ [m^{-1}]$	$\widetilde{C}_D$ [−]	**Vegetation factor:** $\frac{1}{V}\sum_{i=1}^{n} A_i * \widetilde{C}_D \ [m^{-1}]$
0.00-0.50	0	-	0
0.50-1.00	0	-	0
1.00-1.50	0	-	0
1.50-2.00	0	-	0
2.00-2.50	0	-	0
2.50-3.00	0	-	0
3.00-3.50	0	-	0
3.50-4.00	0	-	0
4.00-4.50	0	-	0
4.50-5.00	0	-	0
Average vegetation factor: 0			

Table E-2: Vegetation parameters of subarea 1

Subarea 2			
Height [m]	$\frac{1}{V}\sum_{i=1}^{n} A_i \ [m^{-1}]$	$\widetilde{C}_D$ [−]	**Vegetation factor:** $\frac{1}{V}\sum_{i=1}^{n} A_i * \widetilde{C}_D [m^{-1}]$
0.00-0.50	0.0584	1.2	0.0701
0.50-1.00	0.0752	1.2	0.0902
1.00-1.50	0.0787	1.2	0.0944
1.50-2.00	0.102	1.2	0.122
2.00-2.50	0.105	1.2	0.126
2.50-3.00	0.112	1.2	0.134
3.00-3.50	0.112	1.2	0.134
3.50-4.00	0.102	1.2	0.122
4.00-4.50	0.0752	1.2	0.0902
4.50-5.00	0.0502	1.2	0.0602
Average vegetation factor: 0.104			

Table E-3: Vegetation parameters of subarea 2

Subarea 3			
Height [m]	$\frac{1}{V}\sum_{i=1}^{n} A_i \ [m^{-1}]$	$\widetilde{C}_D \ [-]$	**Vegetation factor:** $\frac{1}{V}\sum_{i=1}^{n} A_i * \widetilde{C}_D [m^{-1}]$
0.00-0.50	0.111	1.1	0.122
0.50-1.00	0.146	1.1	0.161
1.00-1.50	0.153	1.1	0.168
1.50-2.00	0.199	1.1	0.219
2.00-2.50	0.202	1.1	0.222
2.50-3.00	0.212	1.1	0.233
3.00-3.50	0.204	1.1	0.224
3.50-4.00	0.181	1.1	0.199
4.00-4.50	0.124	1.1	0.136
4.50-5.00	0.0799	1.1	0.0879
Average vegetation factor: 0.177			

Table E-4: Vegetation parameters of subarea 3

Subarea 4			
Height [m]	$\frac{1}{V}\sum_{i=1}^{n} A_i \ [m^{-1}]$	$\widetilde{C}_D \ [-]$	**Vegetation factor:** $\frac{1}{V}\sum_{i=1}^{n} A_i * \widetilde{C}_D [m^{-1}]$
0.00-0.50	0.138	1.0	0.138
0.50-1.00	0.181	1.0	0.181
1.00-1.50	0.190	1.0	0.190
1.50-2.00	0.247	1.0	0.247
2.00-2.50	0.251	1.0	0.251
2.50-3.00	0.262	1.0	0.262
3.00-3.50	0.251	1.0	0.251
3.50-4.00	0.220	1.0	0.220
4.00-4.50	0.149	1.0	0.149
4.50-5.00	0.0947	1.0	0.0947
Average vegetation factor: 0.198			

Table E-5: Vegetation parameters of subarea 4

Subarea 5			
Height [m]	$\frac{1}{V}\sum_{i=1}^{n} A_i \ [m^{-1}]$	$\widetilde{C}_D \ [-]$	**Vegetation factor:** $\frac{1}{V}\sum_{i=1}^{n} A_i * \widetilde{C}_D [m^{-1}]$
0.00-0.50	0.164	1.0	0.164
0.50-1.00	0.216	1.0	0.216
1.00-1.50	0.228	1.0	0.228
1.50-2.00	0.295	1.0	0.295
2.00-2.50	0.300	1.0	0.300
2.50-3.00	0.312	1.0	0.312
3.00-3.50	0.297	1.0	0.297
3.50-4.00	0.259	1.0	0.259
4.00-4.50	0.174	1.0	0.174
4.50-5.00	0.110	1.0	0.110
Average vegetation factor: 0.236			

Table E-6: Vegetation parameters of subarea 5

UCW			
Height [m]	$\frac{1}{V}\sum_{i=1}^{n} A_i \ [m^{-1}]$	$\widetilde{C}_D \ [-]$	**Vegetation factor:** $\frac{1}{V}\sum_{i=1}^{n} A_i * \widetilde{C}_D [m^{-1}]$
0.00-0.50	0.0368	1.2	0.0442
0.50-1.00	0.0350	1.0	0.0350
1.00-1.50	0.0553	1.0	0.0553
1.50-2.00	0.133	1.0	0.133
2.00-2.50	0.139	1.0	0.139
2.50-3.00	0.127	1.0	0.127
3.00-3.50	0.154	1.0	0.154
3.50-4.00	0.0688	1.1	0.0757
4.00-4.50	0.0729	1.0	0.0729
4.50-5.00	0.107	1.0	0.107
Average vegetation factor: 0.0943			

Table E-7: Vegetation parameters of UCW

UMW-3			
Height [m]	$\frac{1}{V}\sum_{i=1}^{n} A_i \ [m^{-1}]$	$\widetilde{C}_D \ [-]$	**Vegetation factor:** $\frac{1}{V}\sum_{i=1}^{n} A_i * \widetilde{C}_D [m^{-1}]$
0.00-0.50	0.220	1.0	0.220
0.50-1.00	0.207	1.0	0.207
1.00-1.50	0.242	1.0	0.242
1.50-2.00	0.239	1.0	0.239
2.00-2.50	0.251	1.0	0.251
2.50-3.00	0.257	1.0	0.257
3.00-3.50	0.258	1.0	0.258
3.50-4.00	0.242	1.0	0.242
4.00-4.50	0.274	0.8	0.219
4.50-5.00	0.275	0.8	0.220
Average vegetation factor: 0.236			

Table E-8: Vegetation parameters of UMW-3

SWAN

SWAN is third-generated wave model (assumes for wind sea a JONSWAP spectrum *a priori*), developed at the Delft University of Technology. It computes random, short-crested wind-generated waves in coastal regions and inland water. SWAN accounts for wave-current interactions and is therefore rather based on the action balance equation than the energy balance equation. The action balance equation is defined as:

$$\frac{\partial N(\sigma,\theta;x,y,t)}{\partial t}+\frac{\partial c_{g,x}N(\sigma,\theta;x,y,t)}{\partial x}+\frac{\partial c_{g,y}N(\sigma,\theta;x,y,t)}{\partial y}+\frac{\partial c_{g,\theta}N(\sigma,\theta;x,y,t)}{\partial \theta}+\frac{\partial c_{g,\sigma}N(\sigma,\theta;x,y,t)}{\partial \sigma}=\frac{S(\sigma,\theta;x,y,t)}{\sigma} \quad \text{(E.1)}$$

This equation reduces to the energy balance equation in the absence of an ambient current:

$$\frac{\partial E(\omega,\theta;x,y,t)}{\partial t}+\frac{\partial c_{g,x}E(\omega,\theta;x,y,t)}{\partial x}+\frac{\partial c_{g,y}E(\omega,\theta;x,y,t)}{\partial y}+\frac{\partial c_{g,\theta}E(\omega,\theta;x,y,t)}{\partial \theta}=S(\omega,\theta;x,y,t) \quad \text{(E.2)}$$

In which $N(\sigma,\theta)$ is the action density spectrum and $E(\omega,\theta)$ the energy density spectrum. The first term in Equation E.1 and E.2 represents the local change of action/energy density in time, the second and third terms represent propagation of action/energy in geographic space, the fourth term represents depth-induced and current-induced refraction, the fifth term (only in Equation E.1) represents shifting of the relative frequency due to variations in depth and currents and the last term at the right-hand side is the source term in terms of energy.

SWAN includes generation by wind, nonlinear wave-wave interactions, dissipation and wave-induced set-up. The input of energy by wind is based on a friction velocity u_* which can be determined with the help of the governing wind speed at 10 m elevation U_{10}, a wind drag coefficient C_D and a given wave spectrum $E(\sigma,\theta)$.

Nonlinear wave-wave interaction implies quadruplet wave-wave interactions and triad wave-wave interactions. Quadruplet wave-wave interactions fulfil the resonance criterion when the frequency, wave number and direction of one pair of wave components coincide with those of another pair of wave components. This holds for both deep and shallow water. Triad wave-wave interactions implies the same as for quadruplet wave-wave interactions, but here the resonance criterion is fulfilled if the frequency, wave number and direction of one pair of wave components coincides with a single wave component. This is only relevant in shallow water since such a combination of wave components cannot be created with the dispersion relationship of LWT for deep water. In case of resonance, energy is transferred amongst the four free components and hence will be a source of energy. In case of no resonance, energy is dissipated due to wave-wave interaction.

The processes causing dissipation considered in SWAN are white-capping, bottom friction, depth-induced (surf-)breaking, reflection, transmission and absorption. Transmission due to vegetation is of interest for this research.

First of all white-capping is a form of dissipation of wave breaking in deep water. It involves nonlinear hydrodynamics and therefore it contains a lot of empirical coefficients in the determination of the magnitude of white-capping. However, the overall wave steepness is an important factor for obtaining the amount of dissipated energy. Averaged over a large number of waves it is rather weak.
The dissipated energy by bottom friction in SWAN is highly dependent on the bottom friction coefficient C_{bfr} and $u_{rms,bottom}$. The bottom friction is determined with the help of the model of Madsen which estimates the most non-dimensional friction factor f_w with the help of the formulation of Jonsson. This factor depends on the following factors:

- The bed roughness k_s (Nikuradse roughness) or r of the wall. The bed roughness represents the size of the roughness elements, for example the grains.
- The particle excursion close to bed $\hat{\xi}_0 = \hat{u}_0/\omega$. These are the time integrals of the oscillatory horizontal and vertical flow velocities respectively close to bed (Bosboom, et al., 2015).

The depth-induced (surf-)breaking is modelled with the dissipation of a bore applied to breaking waves in a random field in shallow water. A maximum wave height is set:

$$H_{max} = \gamma D$$

In which D is the total water depth including the wave-induced set-up [m] and γ the breaker parameter with a default value of $\gamma = 0.73$ [-].
The transmission due to vegetation in SWAN is based on (Dalrymple et al., 1984) their formula. The vegetation, modelled as rigid cylinders, can be divided over a number of vertical segments and so the possibility to vary the vegetation vertically is included.

The different variables in SWAN are lister below:

- [height]: the plant height per vertical segment [m]
- [diamtr]: the diameter of each plant stand per vertical segment [m]
- [nstems]: the number of plant stands per square meter for each segment [unit/m^2]
- [drag]: the drag coefficient per vertical segment [-]

(TU Delft, 2020), (Schiereck, et al., 2016)

Settings SWAN 1D

The outcomes of SWAN computations depend on the settings that have been used. The settings should be such that it represents the prescribed storm conditions. The used settings are explained in this section.

General settings:

- Density of the water, rho ρ_w is set to 1000 kg/m^3.
- The mode is stationary and one dimensional (1D).
- Computational grid is regular with a step size varying from 5.0 to 7.1 m. Eastern direction is positive.
- Spectral directions over the whole circle are used with frequencies from 0.1 to 2.5 Hz following (Smale, 2019), which is typical for wind generated waves with short periods (Oude, 2010).

Depth, water level and boundary conditions:

The input grid of the bottom level should match the computation grid. A raster including depths (in m NAP) of Duursche Waarden has been made using ground level data of AHN 3 (5x5 m resolution, using Airborne Laser Scanning in the period 2014-2019), bottom depths of the flow section of the IJssel (data from 2019) by WDOD and bottom depths of the small channels within the floodplain by Rijkswaterstaat (data from 2014, obtained by sonar soundings and a GPS measuring stick). With the help of the program QGIS, the data has been interpolated using the nearest neighbour method and this resulted in a raster of 5x5 m resolution:

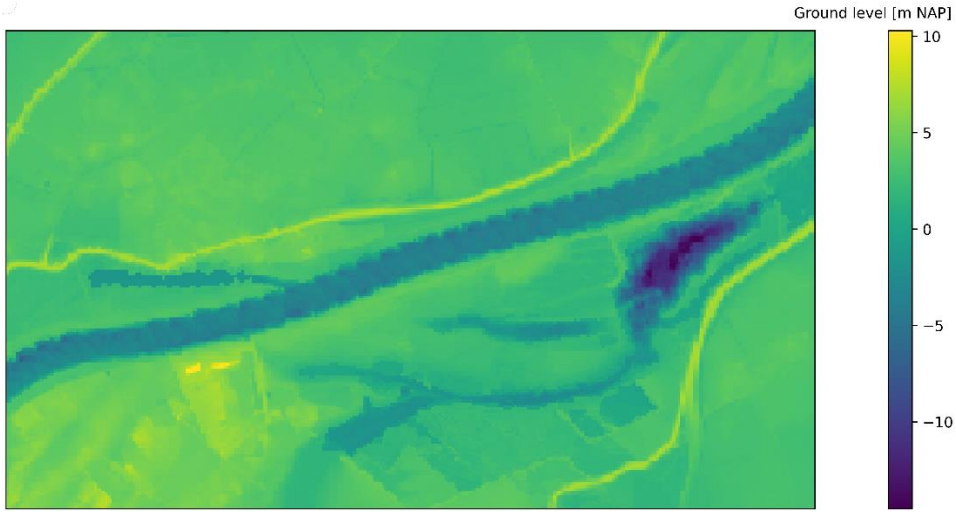

Figure E-1: Raster Duursche Waarden, 5x5 m resolution

The bottom depth depends on the wind direction and hence which path the wave crosses. An example is shown below:

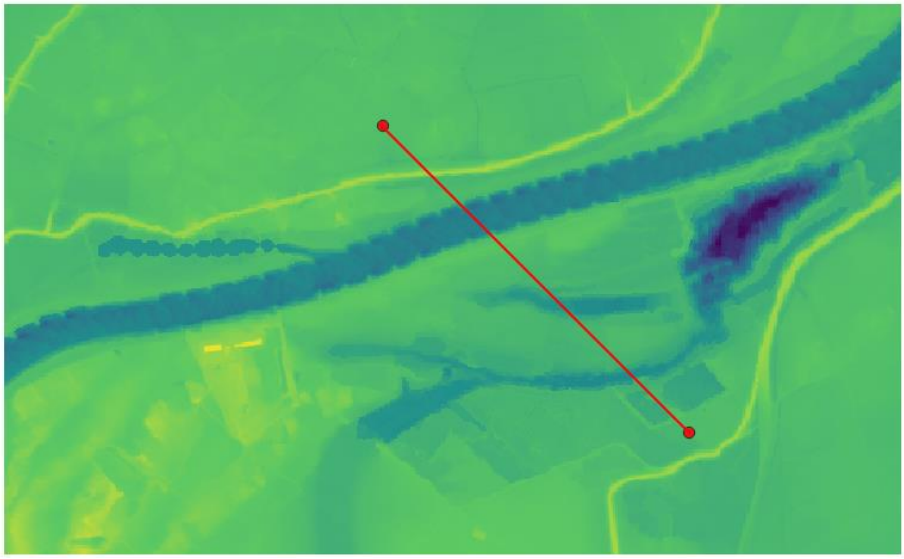

Figure E-2: Path the wave crosses (dike location 190, wind direction NW)

- The water level is set constant over the whole grid: 5.699 (dike locations 185-192) or 5.644 (dike locations 193-199) m NAP depending on the dike location
- The shape of the spectra at the boundary of the computational grid is set to JONSWAP, with default settings of gamma=3.3. A boundary condition is defined with a starting significant wave height (0.0 m), peak period (0.01s), peak wave direction (270 degrees and hence from Western direction, since direction of grid is positive in eastward direction) and a coefficient of the directional spreading ($\cos^m(\theta)$) with a default setting of m = 2.

Physics:

- A constant wind speed and direction is assumed. Both depend on which dike location is studied.
- Physics conform WBI 2017, but since SWAN 40.72ABCDE was used not all settings could be copied:
    - Third generation mode is used. This is the most advanced mode in SWAN. First and second generation mode are deprecated. Westhuysen is used in this mode: nonlinear saturation-based whitecapping combined with wind input of Yan (1987).
    - For Whitecapping the default settings have been taken of Komen et al. (1984). Whitecapping results in dissipation of energy due to wave breaking in deep water and is highly nonlinear.
    - For quadruplet wave-wave interactions the default settings have been taken. Quadruplet wave-wave interactions are the interactions between two pairs of wave components and result in redistribution of energy in the spectrum. No energy is added or withdrawn from the spectrum as a whole. It transfers a significant fraction of the wind input from the mid-range frequencies to the lower frequencies and a small fraction to the higher frequencies (Holthuijsen, 2007). LIMITER URSELL: With this command the user can de-activate permanently the quadruplets when the actual Ursell number exceeds 10 (default settings).
    - Depth-influenced wave-breaking is implemented with alpha=1.00 (proportionality coefficient of the rate of dissipation) and gamma=0.78 (the ratio of maximum individual wave height over depth or breaker index). The default gamma equals 0.73, but following (Bosboom, et al., 2015) the breaker index for shallow foreshores is between 0.78-0.88. LIMITER qb=1: threshold for fraction of breaking waves.
    - Bottom friction defined by JONSWAP = 0.038 m^2/s^3 is assumed just as in (Smale, 2019). This is a typical used value for sandy bottoms.
    - Triad wave-wave interactions: default settings. These are basically the same as Quadruplet interactions, except now there are three wave-number vectors instead of four.

Numerics:

The numerics is such chosen that SWAN stops the process if the absolute change in H_s from one iteration to the next is less than 0.005 or the relative change in H_s from one iteration to the next is less than 0.01 and the curvature of the iteration curve of H_s normalized with H_s is less than 0.005. Both conditions need to be fulfilled in more than fraction 99.99% of all wet grid points (for SWAN 2D 99.00 % is used). On top a maximum number of iterations for stationary computations is set to 50 and proportionality constant is set to 0.01. These are all default settings.

The distance covered through vegetation by the wave and type of vegetation is manually measured in Google Earth:

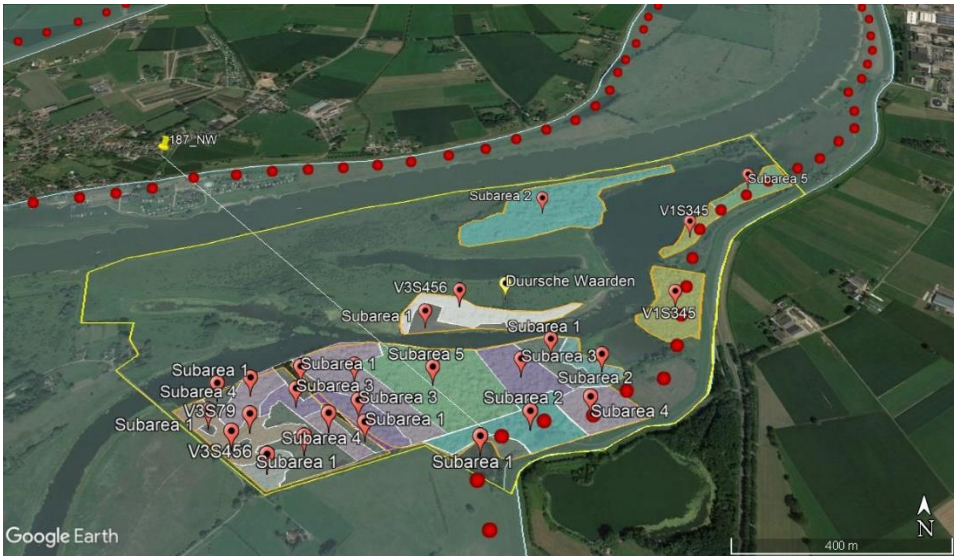

Figure E-3: Distance covered through the vegetation by the wave (dike location 187, wind direction NW)

Input parameters SWAN 1D

D.L. [1]	Wind direction, input vegetation	Wind speed [m/s]	Effective fetch [m]	Grid size [m]	W.L.[2] [m NAP]	Year	Type of vegetation at L =	Implemented in grid SWAN [m], grid cells
185	WNW	23.9	1830	5.4142	5.699	2050	-	-
	WNW	25.7				2100	-	-
	WNW	23.9				2050	1120-1200 m: UMW-3 1200-1227 m: Subarea 1 1227-1293 m: UMW-3 1293-1309 m: Subarea 1 1309-1333 m: UMW-3 1333-1367 m: Subarea 1 1367-1413 m: UCW 1413-1487 m: Subarea 1	1120.7-1202.0, 207-222 1202.0-1229.0, 222-227 1229.0-1294.0, 227-239 1294.0-1310.2, 239-242 1310.2-1331.9, 242-246 1331.9-1364.4, 246-252 1364.4-1413.1, 252-261 1413.1-1488.9. 261-275
	WNW **Input veg. = UMW-3**	25.7				2100		
	NW	28.2	1520	7.1028		2050	-	
	NW	27.9				2100	-	
	NW	28.2				2050	940-1090 m: Subarea 4 1090-1270 m: Subarea 3	937.6-1086.7, 132-153 1086.7-1271.4, 153-179
	NW **Input veg. = Subarea 4**	27.9				2100		
186	WNW	23.9	1770	5.4128	5.699	2050	-	
	WNW	25.7				2100	-	
	WNW	23.9				2050	1175-1211 m: Subarea 1 1211-1279 m: Subarea 4 1279-1305 m: Subarea 3 1305-1400 m: Subarea 1 1400-1521 m: Subarea 4 1521-1561 m: Subarea 1	1174.6-1212.5, 217-224 1212.5-1277.4, 224-236 1277.4-1304.5, 236-241 1304.5-1401.9, 241-259 1401.9-1521.0, 259-281 1521.0-1558.9, 281-288
	WNW **Input veg. = Subarea 4**	25.7				2100		
	NW	28.2	1430	7.0792		2050	-	
	NW	27.9				2100	-	
	NW	28.2				2050	943-1283 m: Subarea 4 1283-1301 m: Subarea 2	941.5-1281.3, 133-181 1281.3-1302.6, 181-184
	NW **Input veg. = Subarea 4**	27.9				2100		

Table E-9: Input SWAN 1D 185-186

[1] D.L. = Dike location
[2] W.L. = Water level

D.L.	Wind direction, input vegetation	Wind speed [m/s]	Effective fetch [m]	Grid size [m]	W.L. [m NAP]	Year	Type of vegetation at L =	Implemented in grid SWAN [m], grid cells
187	WNW	23.9	1700	5.4140	5.699	2050	-	
	WNW	25.7				2100	-	
	WNW	23.9				2050	1175-1252 m: Subarea 1 1252-1534 m: Subarea 4 1534-1606 m: Subarea 5 1606 -1657 m: Subarea 2 1657-1700 m: Subarea 1	1174.8-1250.6, 217-231 1250.6-1532.2, 231-283 1532.2-1608.0, 283-297 1608.0-1656.7, 297-306 1656.7-1700.0, 306-314
	WNW **Input veg. = Subarea 5**	25.7				2100		
	NW	28.2	1340	7.0899		2050	-	
	NW	27.9				2100	-	
	NW	28.2				2050	962-1269 m: Subarea 5 1269-1307 m: Subarea 2 1307-1340 m: Subarea 1	964.2-1269.1, 136-179 1269.1-1304.5, 179-184 1304.5-1340.0, 184-189
	NW **Input veg. = Subarea 5**	27.9				2100		
188	WNW	23.9	1710	5.4286	5.699	2050	-	
	WNW	25.7				2100	-	
	WNW	23.9				2050	1180-1287 m: Subarea 4 1287-1626 m: Subarea 5 1626-1710 m: Subarea 2	1178.0-1286.6, 217-237 1286.6-1628.6, 237-300 1628.6-1710.0, 300-315
	WNW **Input veg. = Subarea 5**	25.7				2100		
	NW	28.2	1320	7.0968		2050	-	
	NW	27.9				2100	-	
	NW	28.2				2050	876-912 m: UCW 912-956 m: Subarea 1 1019-1253 m: Subarea 5 1253-1320 m: Subarea 2	872.9-915.5, 123-129 915.5-958.1, 129-135 1021.9-1256.1, 144-177 1256.1-1320.0 177-186
	NW **Input veg. = Subarea 5**	27.9				2100		

Table E-10: Input SWAN 1D 187-188

D.L.	Wind direction, input vegetation	Wind speed [m/s]	Effective fetch [m]	Grid size [m]	W.L. [m NAP]	Year	Type of vegetation at L =	Implemented in grid SWAN [m], grid cells
189	WNW	23.9	1750	5.4180	5.699	2050	-	
	WNW	25.7				2100	-	
	WNW	23.9				2050	1190-1263 m: Subarea 4 1263-1568 m: Subarea 5 1568-1599 m: Subarea 3 1599-1688 m: Subarea 2 1688-1750 m: Subarea 4	1192.0-1262.4, 220-233 1262.4-1565.8, 233-289 1565.8-1598.3, 289-295 1598.3-1690.4, 295-312 1690.4-1750.0 312-323
	WNW **Input veg. = Subarea 4**	25.7				2100		
	NW	28.2	1350	7.1053		2050	-	
	NW	27.9				2100	-	
	NW	28.2				2050	828-888 m: UCW 888-897 m: Subarea 1 897-977 m: UCW 977-986 m: Subarea 1 1065-1236 m: Subarea 3 1236-1259 m: Subarea 2 1259-1350 m: Subarea 4	831.3-888.2, 117-125 888.2-895.3, 125-126 895.3-980.5, 126-138 980.5-987.6, 138-139 1065.8-1236.3, 150-174 1236.3-1257.6, 174-177 1257.6-1350.0. 177-190
	NW **Input veg. = Subarea 4**	27.9				2100		

Table E-11: Input SWAN 1D 189

D.L.	Wind direction, input vegetation	Wind speed [m/s]	Effective fetch [m]	Grid size [m]	W.L. [m NAP]	Year	Type of vegetation at L =	Implemented in grid SWAN [m], grid cells
190	WNW	23.1	1760	5.4154	5.699	2050	-	
	WNW	25.5				2100	-	
	WNW	23.1				2050	1231-1289 m: UCW 1425-1604 m: Subarea 3 1604-1668 m: Subarea 1 1668-1687 m: Subarea 2 1687-1760 m: Subarea 4	1229.3-1288.9, 227-238 1424.3-1603.0, 263-296 1603.0-1667.9, 296-308 1667.9-1689.6, 308-312 1689.6-1760.0, 312-325
	WNW **Input veg. = Subarea 4**	25.5				2100		
	NW	25.2	1330	7.0745		2050	-	
	NW	25.1				2100	-	
	NW	25.2				2050	976-1042 m: UCW 1042-1047 m: Subarea 1 1093-1146 m: Subarea 1 1146-1285 m: Subarea 2 1285-1330 m: Subarea 4	976.3-1040.0, 138-147 1040.0-1047.0 147-148 1089.5-1146.1, 154-162 1146.1-1287.6, 162-182 1287.6-1330.0, 182-188
	NW **Input veg. = Subarea 4**	25.1				2100		

Table E-12: Input SWAN 1D 190

D.L.	Wind direction, input vegetation	Wind speed [m/s]	Effective fetch [m]	Grid size [m]	W.L. [m NAP]	Year	Type of vegetation at L =	Implemented in grid SWAN [m], grid cells
191	WNW	23.1	1720	5.4259	5.699	2050	-	
	WNW	25.5				2100	-	
	WNW	23.1				2050	1118-1142 m: UCW 1142-1197 m: Subarea 1 1197-1288 m: UCW 1288-1303 m: Subarea 1 1401-1486 m: Subarea 1 1486-1638 m: Subarea 2	1117.7-1139.4, 206-210 1139.4-1199.1, 210-221 1199.1-1285.9, 221-237 1285.9-1302.2, 237-240 1399.9-1486.7, 258-274 1486.7-1638.6 274-302
	WNW **Input veg. = UCW**	25.5				2100		
	NW	25.2	1290	7.0879		2050	-	
	NW	25.1				2100	-	
	NW	25.2				2050	662-675 m: Subarea 2 974-1008 m: UCW	659.2-673.4, 93-95 971.0-1006.5, 137-142
	NW **Input veg. = UCW**	25.1				2100		
192	WNW	23.1	1670	5.4221	5.699	2050	-	
	WNW	25.5				2100	-	
	WNW	23.1				2050	1344-1397 m: UCW	1344.7-1398.9, 248-258
	WNW **Input veg. = UCW**	25.5				2100		
	NW	25.2	1220	7.0931		2050	-	
	NW	25.1				2100	-	
	NW	25.2				2050	600-708 m: Subarea 2	602.9-709.3, 85-100
	NW **Input veg. = Subarea 2**	25.1				2100		

Table E-13: Input SWAN 1D 191-192

D.L.	Wind direction, input vegetation	Wind speed [m/s]	Effective fetch [m]	Grid size [m]	W.L. [m NAP]	Year	Type of vegetation at L =	Implemented in grid SWAN [m], grid cells
193	W	22.7	2050	5.0122	5.644	2050	-	
	W	24.7				2100	-	
	W	22.7				2050	1412-1438 m: UCW 1438-1497 m: Subarea 1 1497-1740 m: UCW 1950-2050 m: UMW-1	1413.4-1438.5, 282-287 1438.5-1498.6, 287-299 1498.6-1739.2, 299-347 1949.7-2050.0 389-409
	W **Input veg. = UCW**	24.7				2100		
	WNW	23.9	1600	5.4238		2050	-	
	WNW	25.8				2100	-	
	WNW	23.9				2050	1516-1600 m: UMW-1	1518.7-1600.0, 280-295
	WNW **Input veg. = UMW-1**	25.8				2100		
194	W	22.7	2030	5.0123	5.644	2050	-	
	W	24.7				2100	-	
	W	22.7				2050	1958-2030 m: UMW-1	1959.8-2030.0, 391-405
	W **Input veg. = UMW-1**	24.7				2100		
	WNW	23.9	1470	5.4244		2050	-	
	WNW	25.8				2100	-	
	WNW	23.9				2050	888-1008 m: Subarea 2 1391-1470 m: UMW-1	889.6-1008.9, 164-186 1388.6-1470.0, 256-271
	WNW **Input veg. = Subarea 2**	25.8				2100		
195	W	22.7	2000	5.0125	5.644	2050	-	
	W	24.7				2100	-	
	W	22.7				2050	-	-
	W **No veg.**	24.7				2100	-	-
	WNW	23.9	1400	5.4264		2050	-	
	WNW	25.8				2100	-	
	WNW	23.9				2050	903-1064 m: Subarea 2 1325-1330 m: UMW-1	900.8-1063.6, 166-196 1324.0-1329.5, 244-245
	WNW **Input veg. = Subarea 2**	25.8				2100		

Table E-14: Input SWAN 1D 193-195

D.L.	Wind direction, input vegetation	Wind speed [m/s]	Effective fetch [m]	Grid size [m]	W.L. [m NAP]	Year	Type of vegetation at L =	Implemented in grid SWAN [m], grid cells
196	W	22.7	1900	5.0132	5.644	2050	-	
	W	24.7				2100	-	
	W	22.7				2050	1291-1492 m: Subarea 2 1851-1900 m: UMW-1	1293.4-1493.9, 258-298 1849.9-1900.0, 369-379
	W **Input veg. = Subarea 2**	24.7				2100		
	WNW	23.9	1270	5.4273		2050	-	
	WNW	25.8				2100	-	
	WNW	23.9				2050	796-1020 m: Subarea 2 1226-1270 m: UMW-1	797.8-1020.3, 147-188 1226.6-1270.0, 226-234
	WNW **Input veg. = Subarea 2**	25.8				2100		
197	W	22.7	1880	5.0000	5.644	2050	-	
	W	24.7				2100	-	
	W	22.7				2050	1291-1574 m: Subarea 2 1826-1880 m: UMW-1	1290.0-1575.0, 258-315 1825.0-1880.0, 365-376
	W **Input veg. = Subarea 2**	24.7				2100		
	WNW	23.9	1220	5.4222		2050	-	
	WNW	25.8				2100	-	
	WNW	23.9				2050	838-916 m: Subarea 2 1181-1220: UMW-1	840.4-916.4, 155-169 1182.0-1220.0, 218-225
	WNW **Input veg. = Subarea 2**	25.8				2100		
198	W	22.7	1850	5.0000	5.644	2050	-	
	W	24.7				2100	-	
	W	22.7				2050	1220-1469 m: Subarea 2 1760-1850 m: Subarea 5	1220.0-1470.0, 244-294 1760.0-1850.0. 352-370
	W **Input veg. = Subarea 2**	24.7				2100		
	WNW	23.9	1190	5.4338		2050	-	
	WNW	25.8				2100	-	
	WNW	23.9				2050	876-926 m: Subarea 2 1133-1190 m: Subarea 5	874.8-923.7, 161-170 1135.7-1190.0, 209-219
	WNW **Input veg. = Subarea 2**	25.8				2100		

Table E-15: Input SWAN 1D 196-198

D.L.	Wind direction, input vegetation	Wind speed [m/s]	Effective fetch [m]	Grid size [m]	W.L. [m NAP]	Year	Type of vegetation at L =	Implemented in grid SWAN [m], grid cells
199	W	22.7	1870	5.0000	5.644	2050	-	
	W	24.7				2100	-	
	W	22.7				2050	1272-1447 m: Subarea 2 1787-1870 m: Subarea 5	1270.0-1445.0, 254-289 1785.0-1870.0, 357-374
	W **Input veg. = Subarea 2**	24.7				2100		
	WNW	23.9	1190	5.4338		2050	-	
	WNW	25.8				2100	-	
	WNW	23.9				2050	1132-1190: Subarea 5	1130.2-1190.0, 208-219
	WNW **Input veg. = Subarea 5**	25.8				2100		

Table E-16: Input SWAN 1D 199

SWAN 1D plots

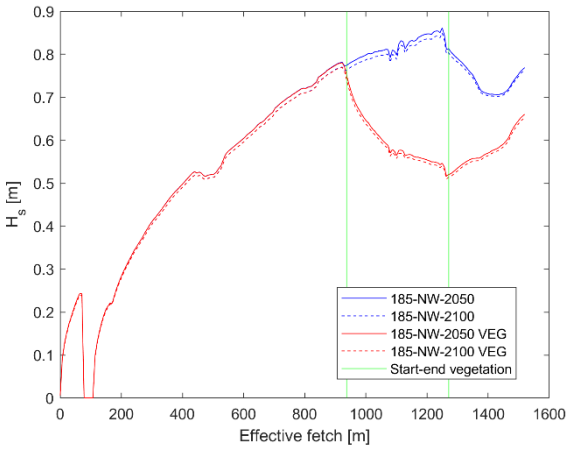

Figure E-4: SWAN 1D wave propagation 185-NW

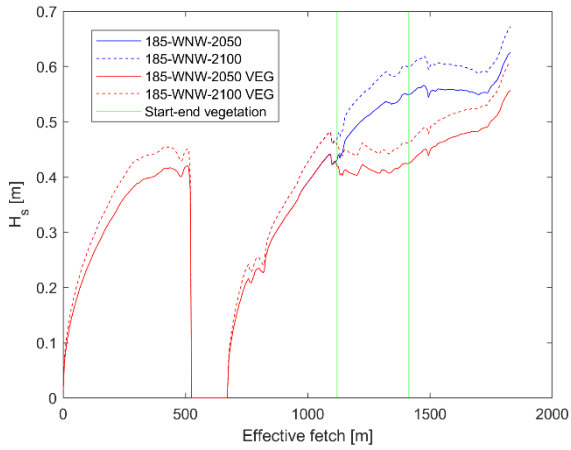

Figure E-5: SWAN 1D wave propagation 185-WNW

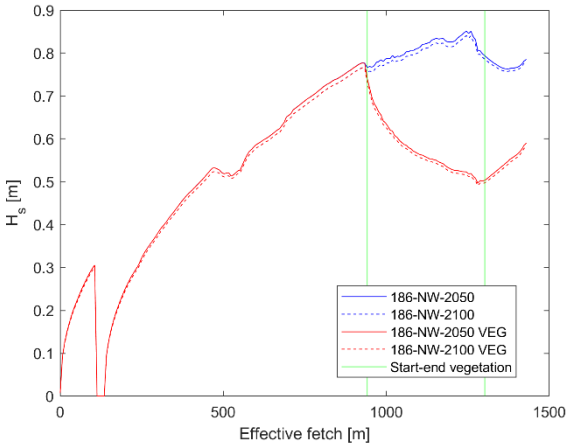

Figure E-6: SWAN 1D wave propagation 186-NW

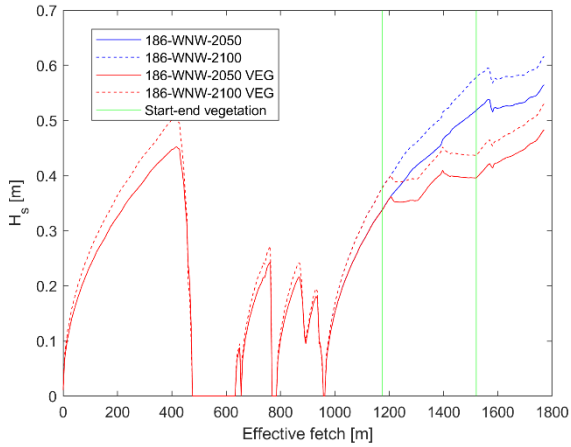

Figure E-7: SWAN 1D wave propagation 186-WNW

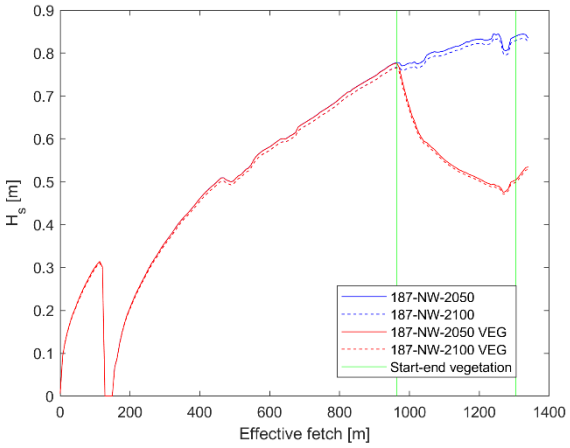

Figure E-8: SWAN 1D wave propagation 187-NW

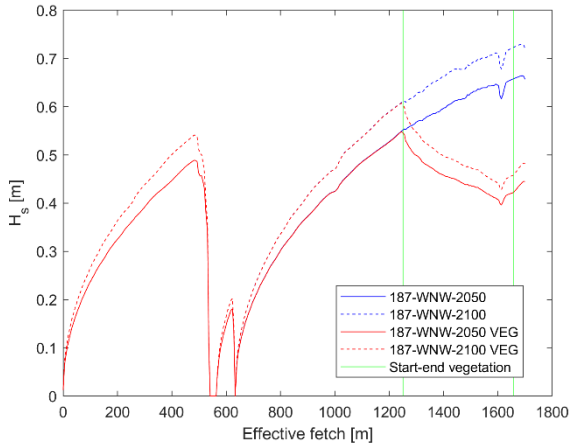

Figure E-9: SWAN 1D wave propagation 187-WNW

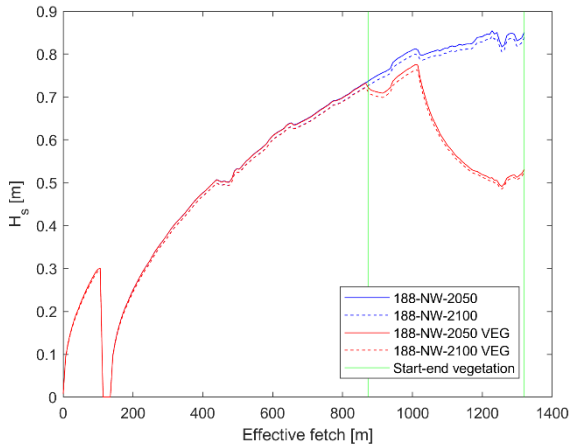

Figure E-10: SWAN 1D wave propagation 188-NW

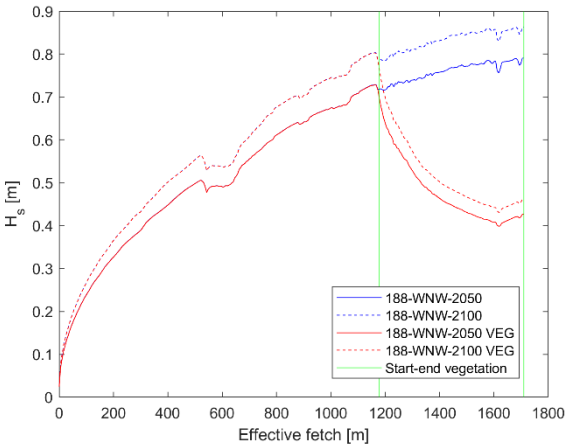

Figure E-11: SWAN 1D wave propagation 188-WNW

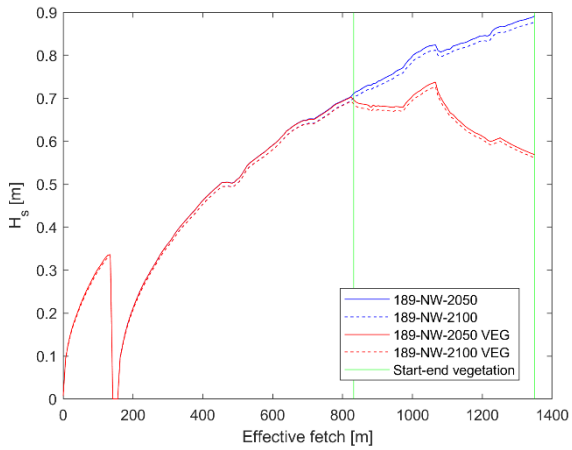

Figure E-12: SWAN 1D wave propagation 189-NW

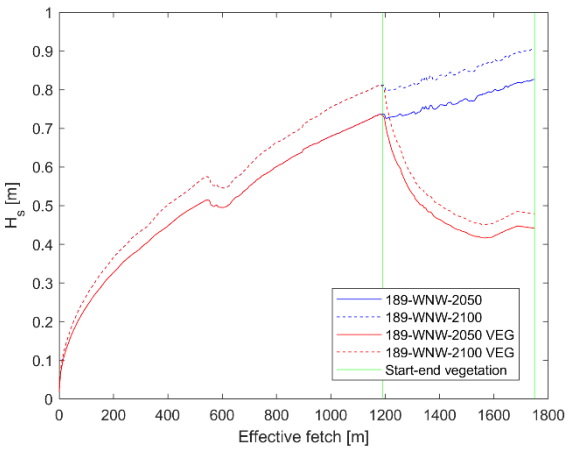

Figure E-13: SWAN 1D wave propagation 189-WNW

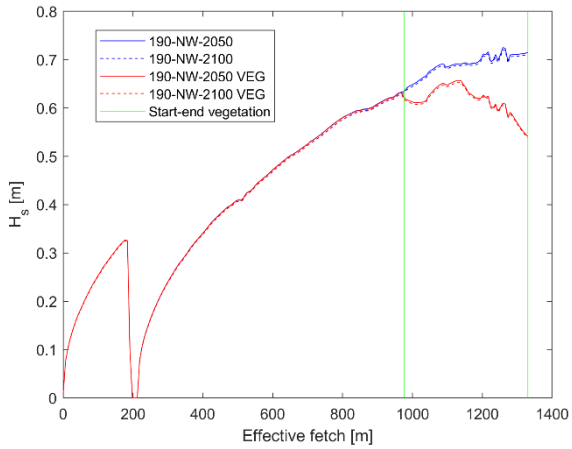

Figure E-14: SWAN 1D wave propagation 190-NW

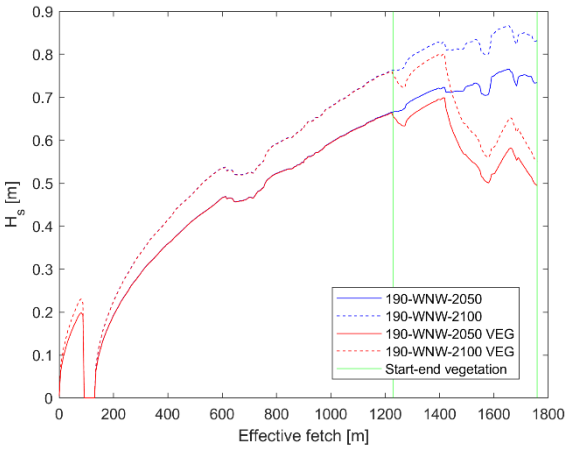

Figure E-15: SWAN 1D wave propagation 190-WNW

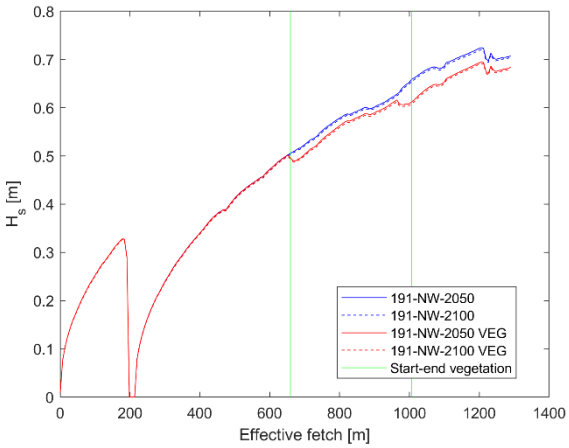

Figure E-16: SWAN 1D wave propagation 191-NW

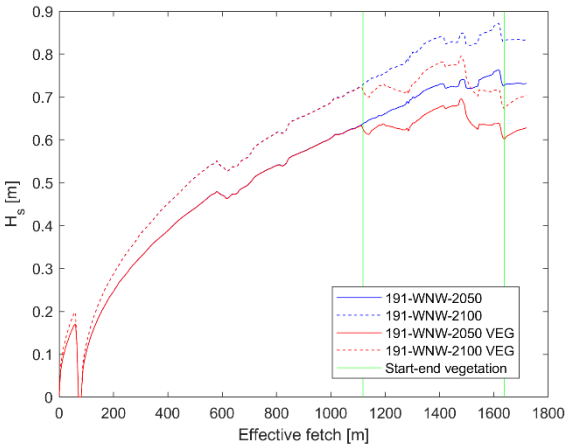

Figure E-17: SWAN 1D wave propagation 191-WNW

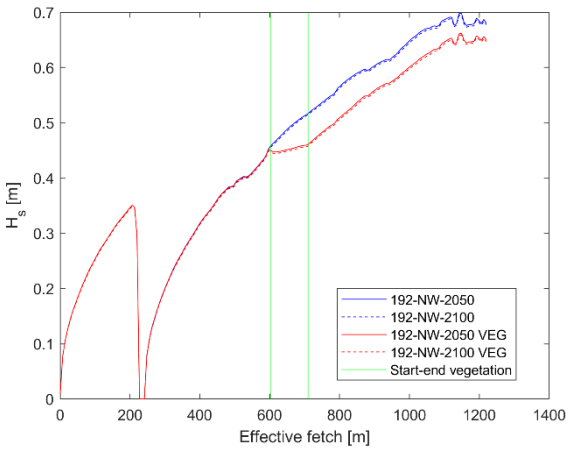

Figure E-18: SWAN 1D wave propagation 192-NW

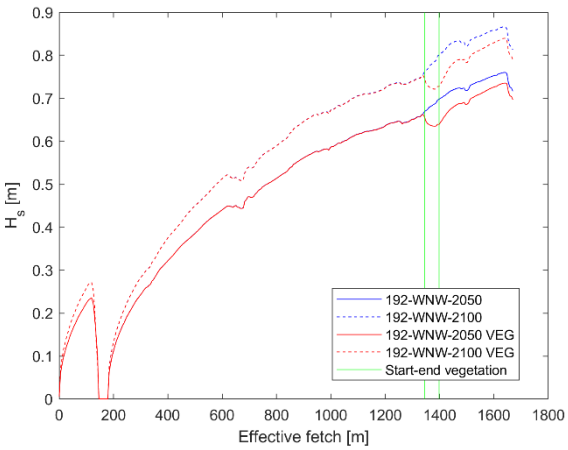

Figure E-19: SWAN 1D wave propagation 192-WNW

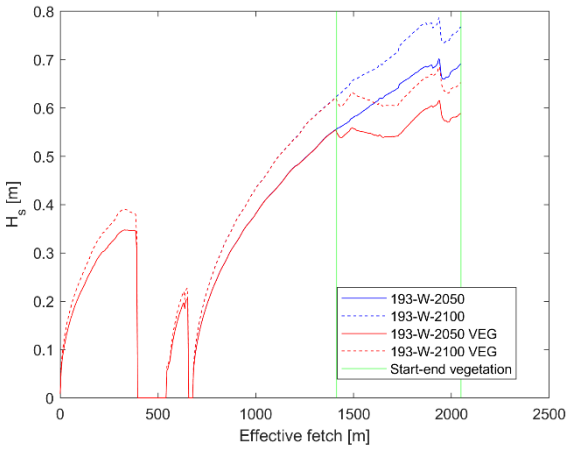

Figure E-20: SWAN 1D wave propagation 193-W

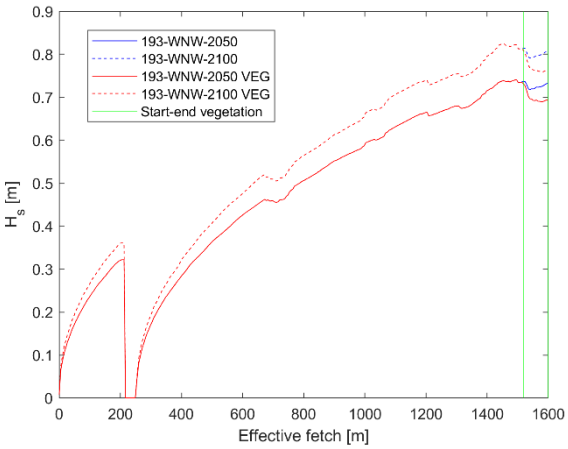

Figure E-21: SWAN 1D wave propagation 193-WNW

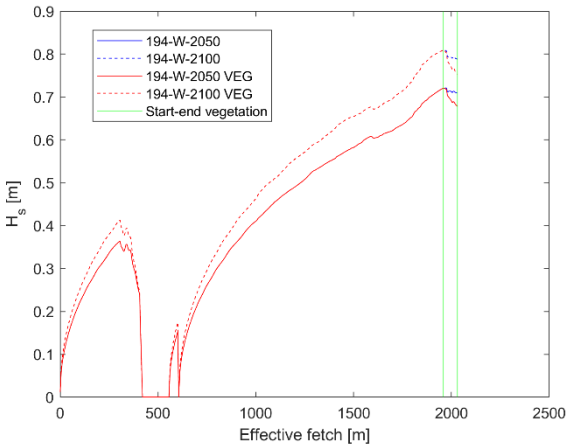

Figure E-22: SWAN 1D wave propagation 194-W

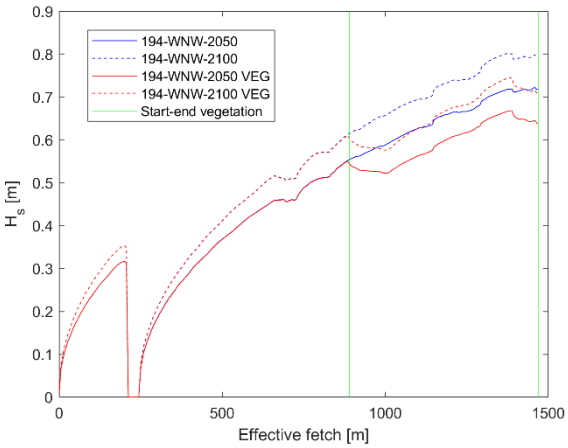

Figure E-23: SWAN 1D wave propagation 194-WNW

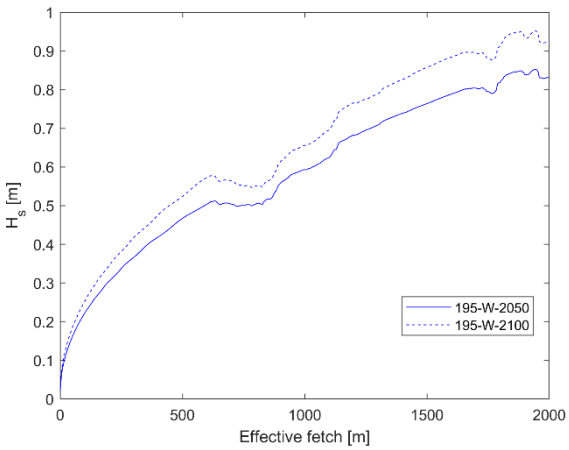

Figure E-24: SWAN 1D wave propagation 195-W

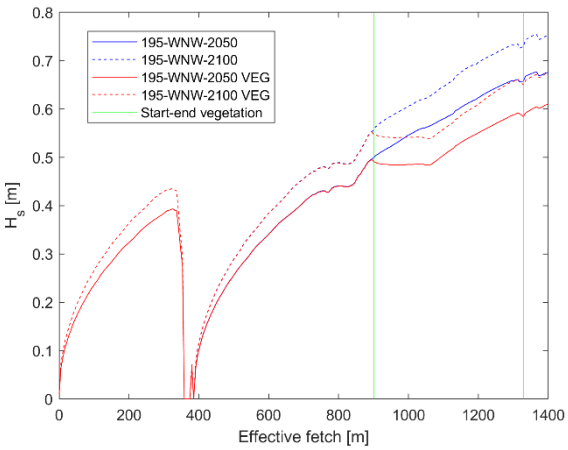

Figure E-25: SWAN 1D wave propagation 195-WNW

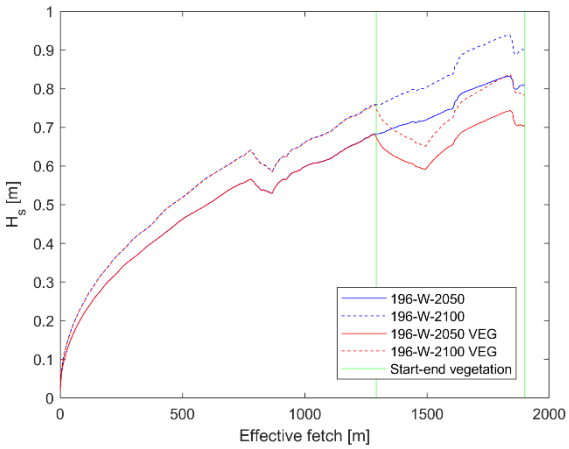

Figure E-26: SWAN 1D wave propagation 196-W

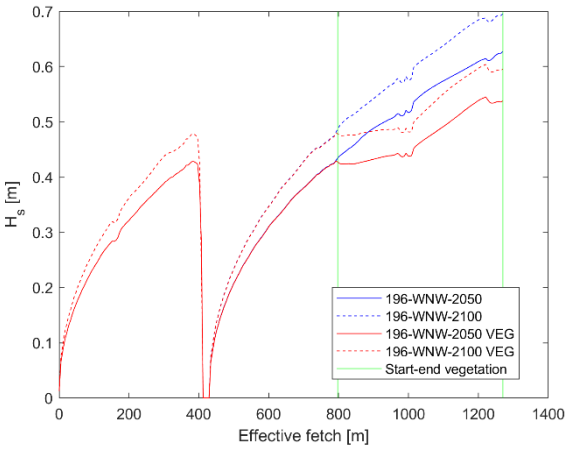

Figure E-27: SWAN 1D wave propagation 196-WNW

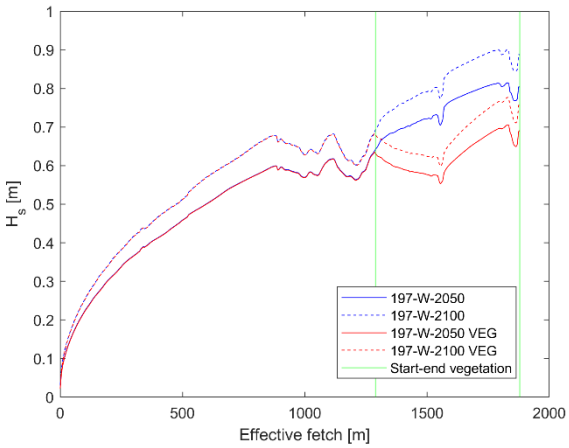

Figure E-28: SWAN 1D wave propagation 197-W

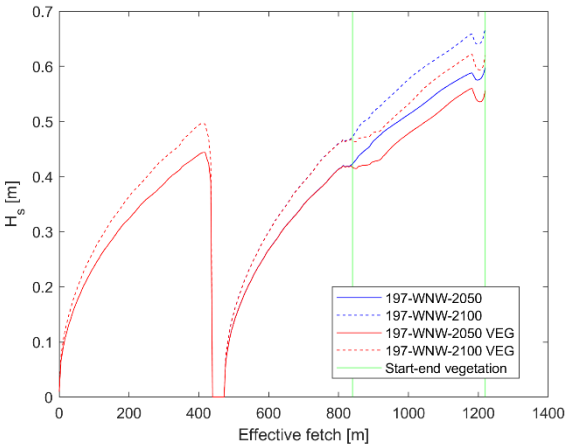

Figure E-29: SWAN 1D wave propagation 197-WNW

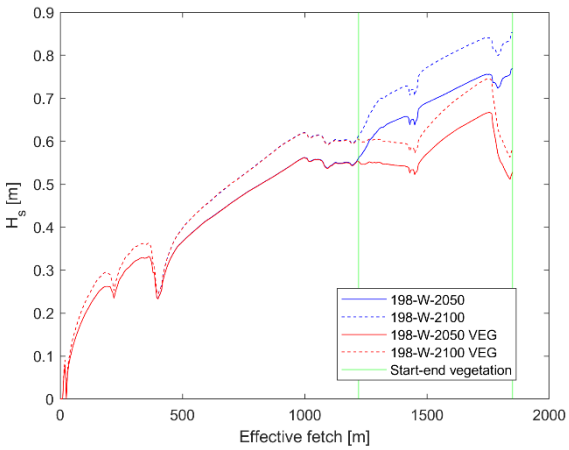

Figure E-30: SWAN 1D wave propagation 198-W

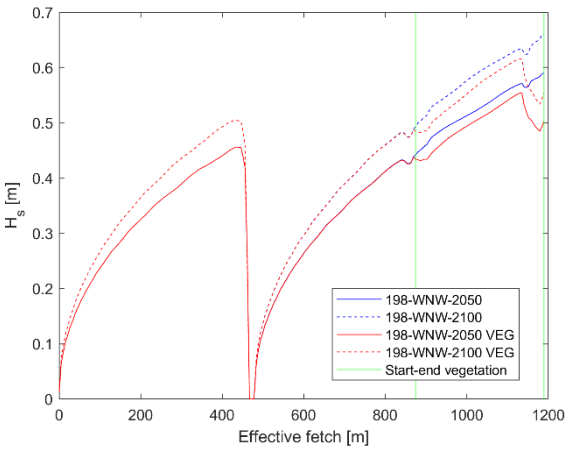

Figure E-31: SWAN 1D wave propagation 198-WNW

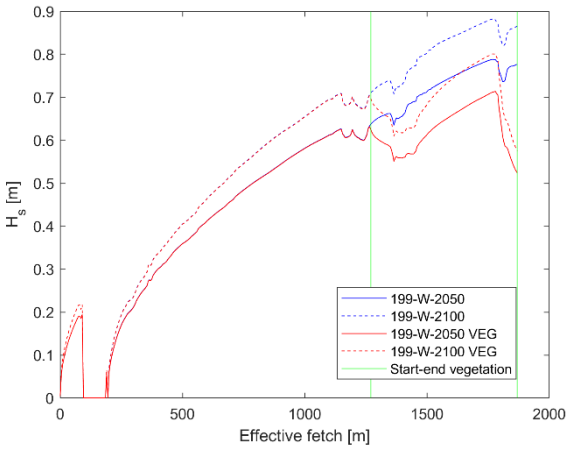

Figure E-32: SWAN 1D wave propagation 199-W

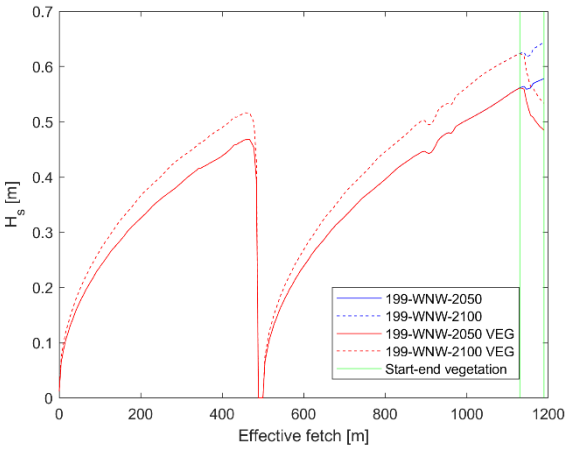

Figure E-33: SWAN 1D wave propagation 199-WNW

SWAN 1D results

Dike location	HC[1]	Input	Significant wave height, H_s [m] including model uncertainty			Reduction Hs [cm]	Relative peak period, T_p [s] including model uncertainty		
			2050	2100	2075	2075	2050	2100	2075
185	185-NW	No veg	0.838	0.833	0.835		2.870	2.843	2.857
		Veg	0.719	0.712	0.716	12.0	2.598	2.576	2.587
	185-WNW	No veg	0.682	0.734	0.708		2.511	2.561	2.536
		Veg	0.607	0.663	0.635	7.3	2.300	2.387	2.344
186	185-NW	No veg	0.857	0.850	0.853		2.841	2.820	2.830
		Veg	0.643	0.635	0.639	21.4	2.516	2.506	2.511
	185-WNW	No veg	0.616	0.673	0.644		2.314	2.395	2.354
		Veg	0.526	0.578	0.552	9.2	2.108	2.224	2.166
187	185-NW	No veg	0.910	0.900	0.905		2.812	2.801	2.806
		Veg	0.571	0.577	0.574	33.1	2.337	2.325	2.331
	185-WNW	No veg	0.716	0.786	0.751		2.521	2.639	2.580
		Veg	0.485	0.525	0.505	24.6	2.161	2.239	2.200
188	185-NW	No veg	0.928	0.915	0.921		2.812	2.799	2.806
		Veg	0.579	0.571	0.575	34.6	2.526	2.511	2.519
	185-WNW	No veg	0.862	0.941	0.901		2.849	2.996	2.922
		Veg	0.465	0.504	0.485	41.7	2.019	2.061	2.040
189	185-NW	No veg	0.971	0.957	0.964		2.839	2.821	2.830
		Veg	0.620	0.613	0.616	34.8	2.480	2.474	2.477
	185-WNW	No veg	0.901	0.989	0.945		2.923	3.026	2.975
		Veg	0.482	0.522	0.502	44.3	2.065	2.114	2.089
190	190-NW	No veg	0.779	0.775	0.777		2.605	2.600	2.603
		Veg	0.590	0.588	0.589	18.9	2.489	2.487	2.488
	190-WNW	No veg	0.801	0.907	0.854		2.780	2.975	2.878
		Veg	0.538	0.600	0.569	28.5	2.569	2.744	2.657
191	190-NW	No veg	0.771	0.768	0.770		2.578	2.575	2.576
		Veg	0.756	0.742	0.749	2.0	2.544	2.539	2.541
	190-WNW	No veg	0.798	0.909	0.853		2.773	2.961	2.867
		Veg	0.686	0.768	0.727	12.6	2.645	2.766	2.705
192	190-NW	No veg	0.742	0.739	0.741		2.528	2.523	2.525
		Veg	0.710	0.705	0.707	3.3	2.489	2.486	2.487
	190-WNW	No veg	0.780	0.886	0.833		2.748	2.876	2.812
		Veg	0.760	0.861	0.810	2.3	2.717	2.811	2.764

Table E-17: SWAN 1D results 185-192

[1] HC = hydraulic conditions

Dike location	HC	Input	Significant wave height, H_s [m] including model uncertainty			Reduction Hs [cm]	Relative peak period, T_p [s] including model uncertainty		
			2050	2100	2075	2075	2050	2100	2075
193	193-W	No veg	0.753	0.836	0.795		2.666	2.766	2.716
		Veg	0.641	0.711	0.676	11.9	2.483	2.561	2.522
	193-WNW	No veg	0.798	0.881	0.839		2.720	2.787	2.753
		Veg	0.755	0.831	0.793	4.6	2.720	2.787	2.753
194	193-W	No veg	0.773	0.859	0.816		2.701	2.777	2.739
		Veg	0.740	0.822	0.781	3.5	2.706	2.776	2.741
	193-WNW	No veg	0.782	0.863	0.822		2.632	2.758	2.695
		Veg	0.695	0.770	0.732	9.0	2.516	2.664	2.590
195	193-W	No veg	0.908	1.009	0.959		2.988	3.067	3.027
		Veg	-	-	0.959	0.0	-	-	-
	193-WNW	No veg	0.737	0.819	0.778		2.512	2.602	2.557
		Veg	0.665	0.735	0.700	7.8	2.437	2.502	2.469
196	193-W	No veg	0.884	0.986	0.935		2.899	3.038	2.969
		Veg	0.768	0.857	0.813	12.3	2.744	2.866	2.805
	193-WNW	No veg	0.683	0.759	0.721		2.374	2.498	2.436
		Veg	0.586	0.650	0.618	10.3	2.264	2.318	2.291
197	193-W	No veg	0.875	0.967	0.921		2.841	3.009	2.925
		Veg	0.753	0.828	0.791	13.0	2.714	2.768	2.741
	193-WNW	No veg	0.652	0.730	0.691		2.297	2.444	2.371
		Veg	0.606	0.676	0.641	5.0	2.273	2.348	2.310
198	193-W	No veg	0.838	0.930	0.884		2.767	2.846	2.806
		Veg	0.576	0.635	0.605	27.8	2.558	2.724	2.641
	193-WNW	No veg	0.643	0.720	0.682		2.283	2.378	2.330
		Veg	0.548	0.604	0.576	10.6	2.246	2.297	2.272
199	193-W	No veg	0.847	0.943	0.895		2.788	2.978	2.883
		Veg	0.570	0.627	0.598	29.6	2.705	2.783	2.744
	193-WNW	No veg	0.630	0.702	0.666		2.269	2.338	2.304
		Veg	0.529	0.582	0.555	11.1	2.262	2.310	2.286

Table E-18: SWAN 1D results 192-199

SWAN 2D plots of H_s

185 NW 2050:

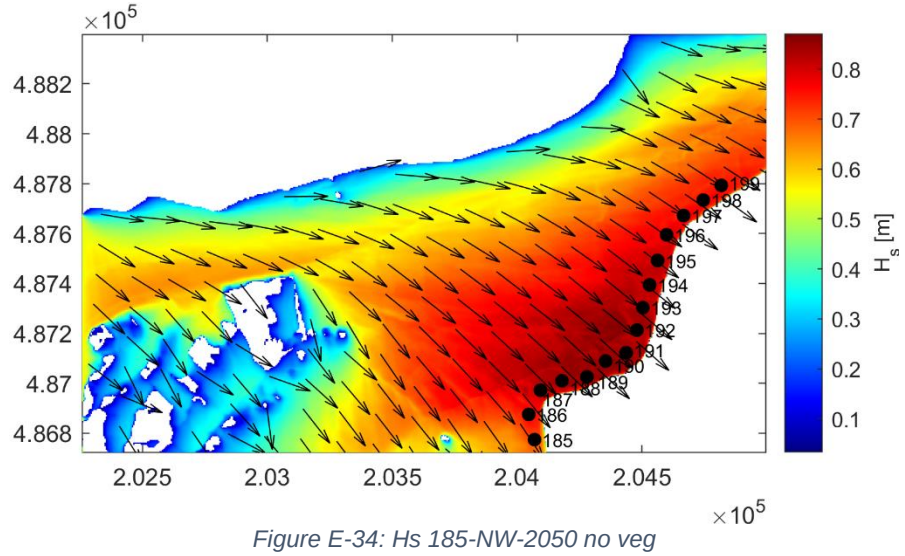

Figure E-34: Hs 185-NW-2050 no veg

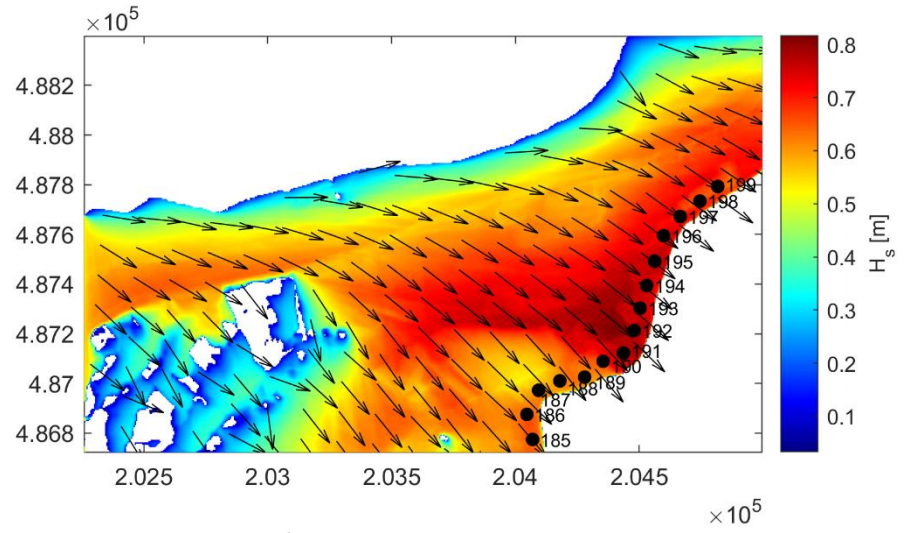

Figure E-35: Hs 185-NW-2050 veg

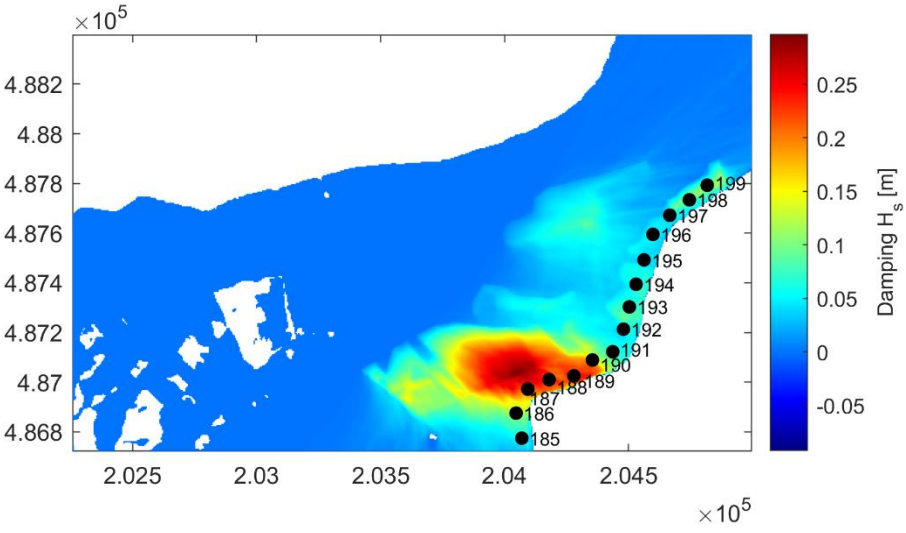

Figure E-36: Wave damping due to vegetation 185-NW-2050

185 NW 2100

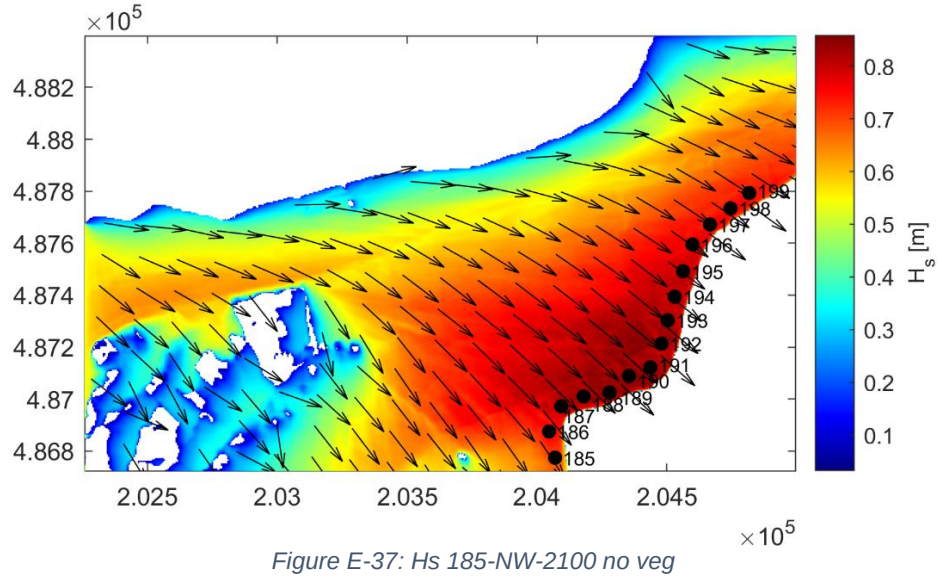

Figure E-37: Hs 185-NW-2100 no veg

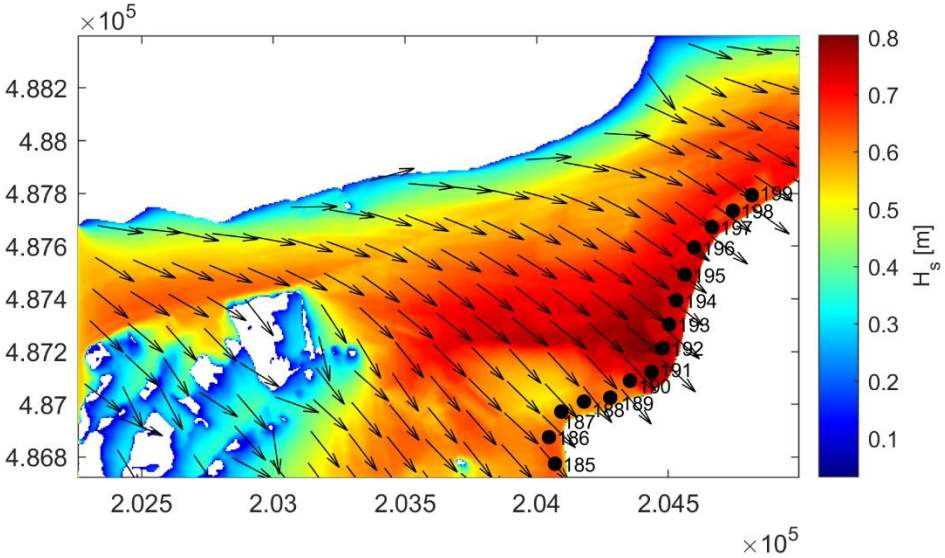

Figure E-38: Hs 185-NW-2100 veg

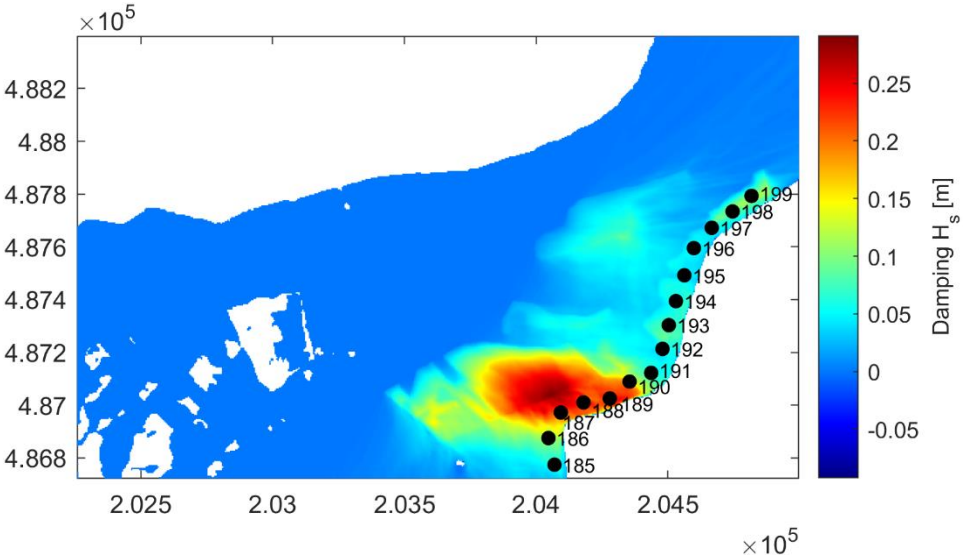

Figure E-39: Wave damping due to vegetation 185-NW-2100

185 WNW 2050:

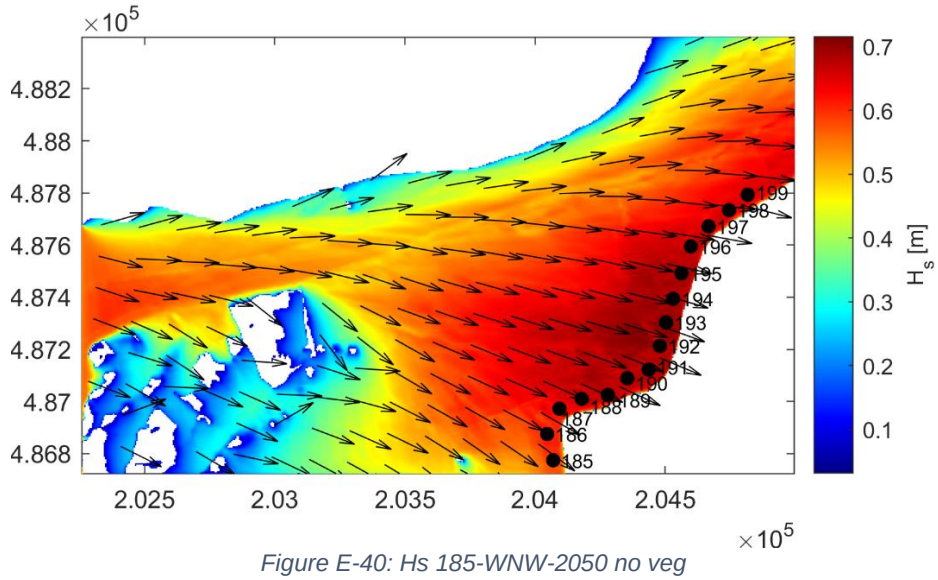

Figure E-40: Hs 185-WNW-2050 no veg

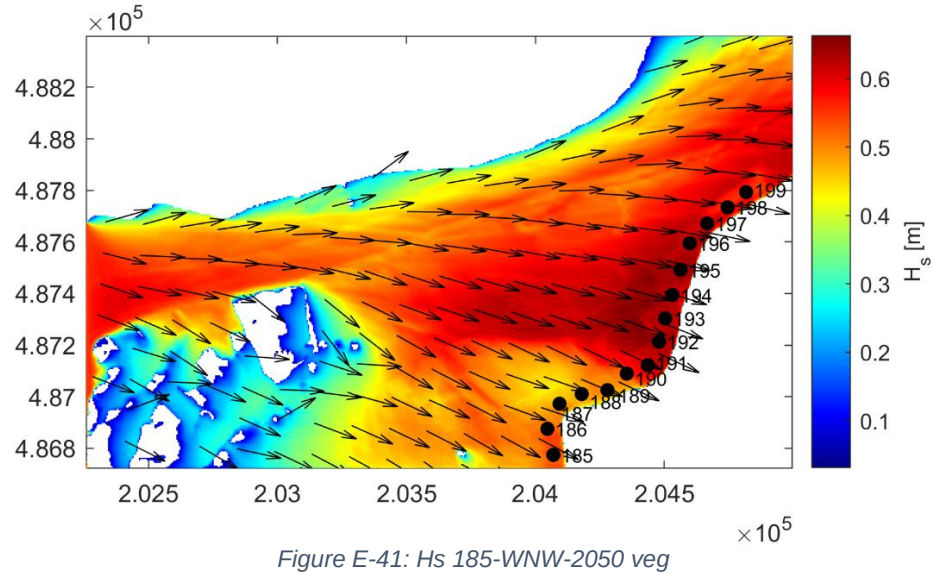

Figure E-41: Hs 185-WNW-2050 veg

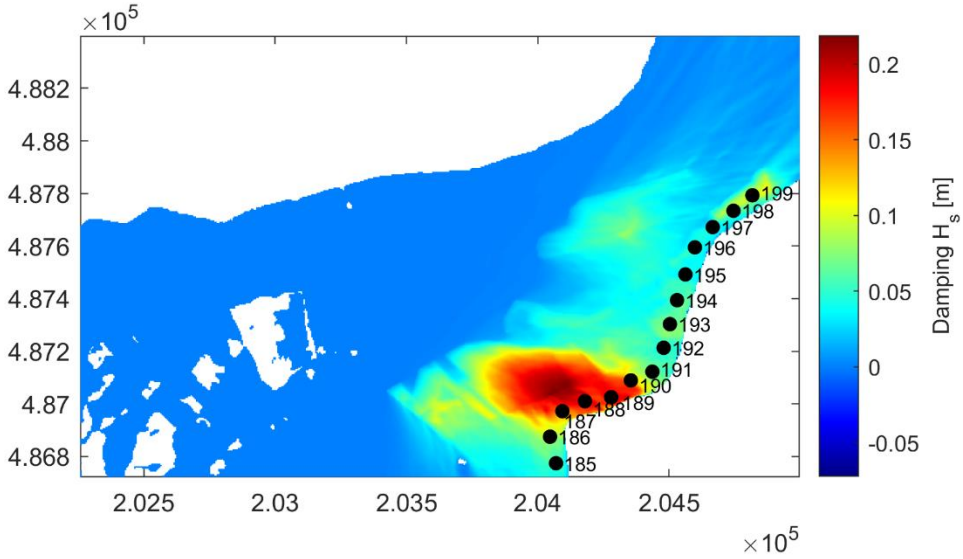

Figure E-42: Wave damping due to vegetation 185-WNW-2050

185 WNW 2100:

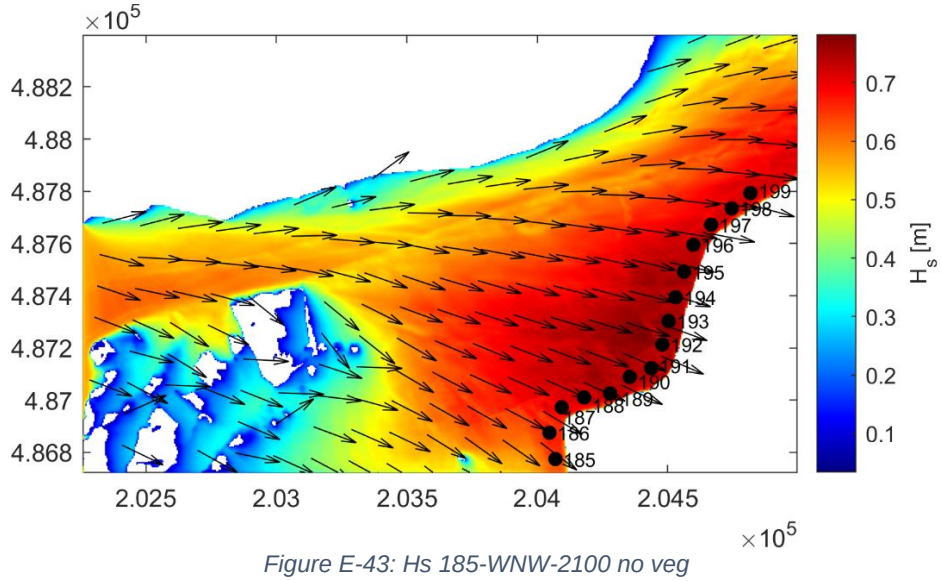

Figure E-43: Hs 185-WNW-2100 no veg

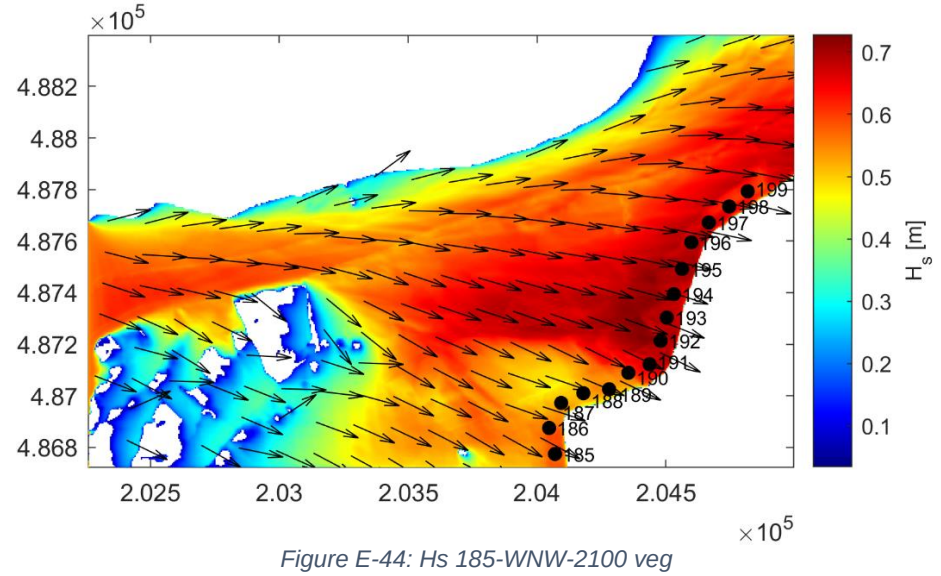

Figure E-44: Hs 185-WNW-2100 veg

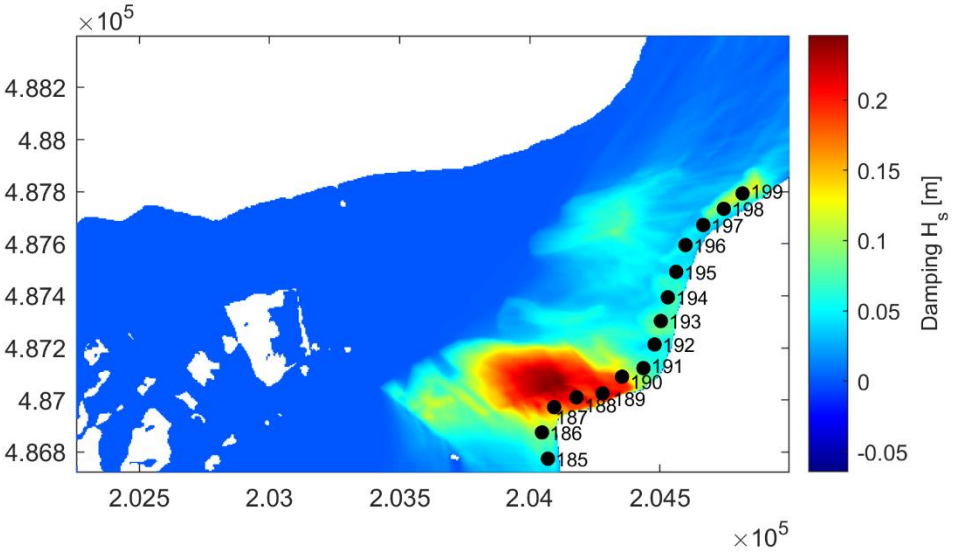

Figure E-45: Wave damping due to vegetation 185-WNW-2100

190 NW 2050:

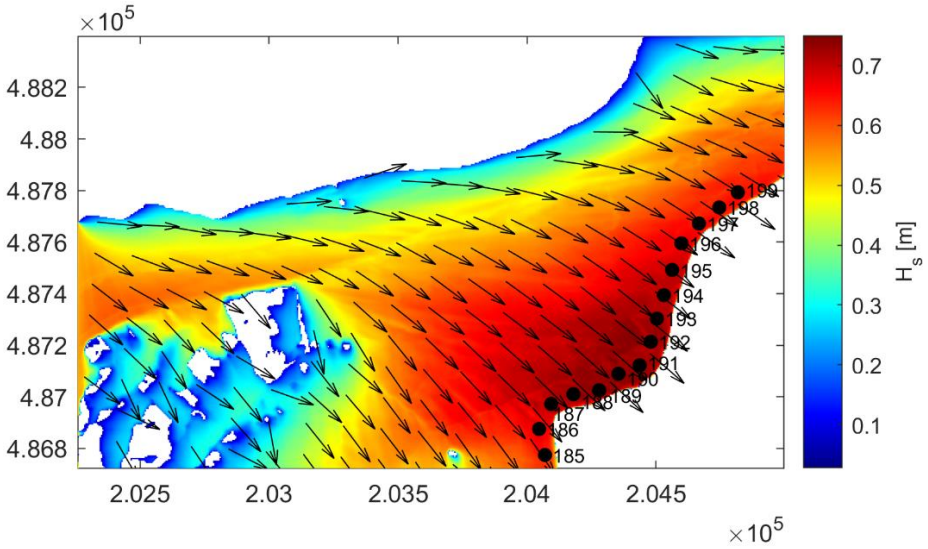

Figure E-46: Hs 190-NW-2050 no veg

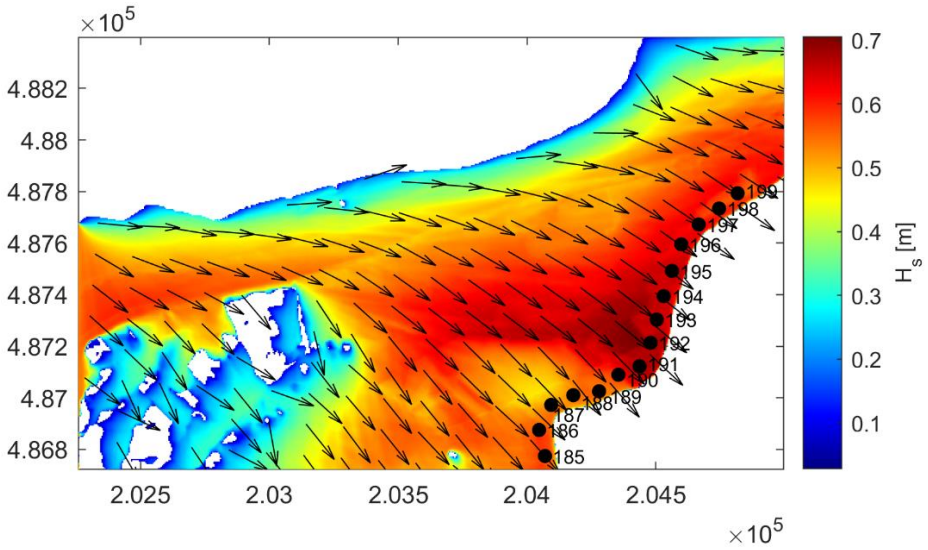

Figure E-47: Hs 190-NW-2050 veg

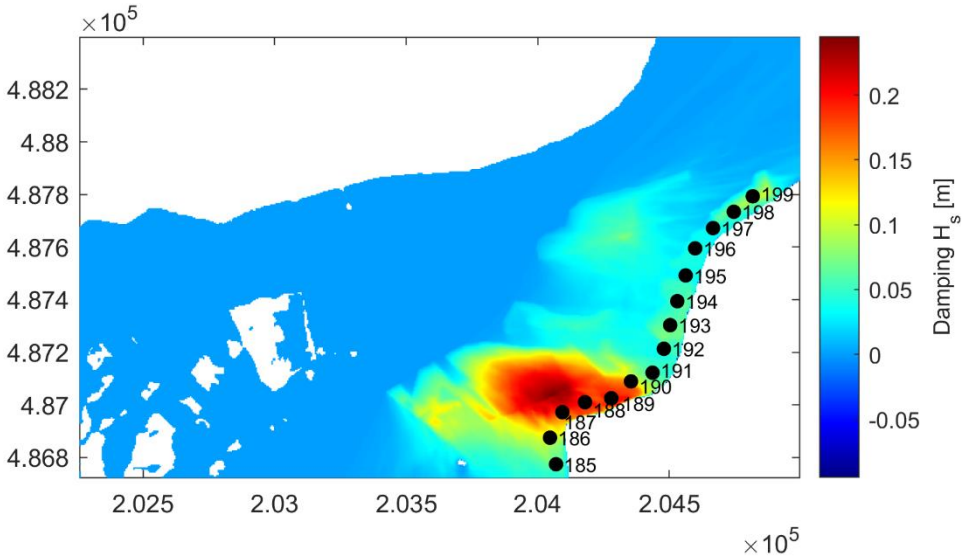

Figure E-48: Wave damping due to vegetation 190-NW-2050

190 NW 2100:

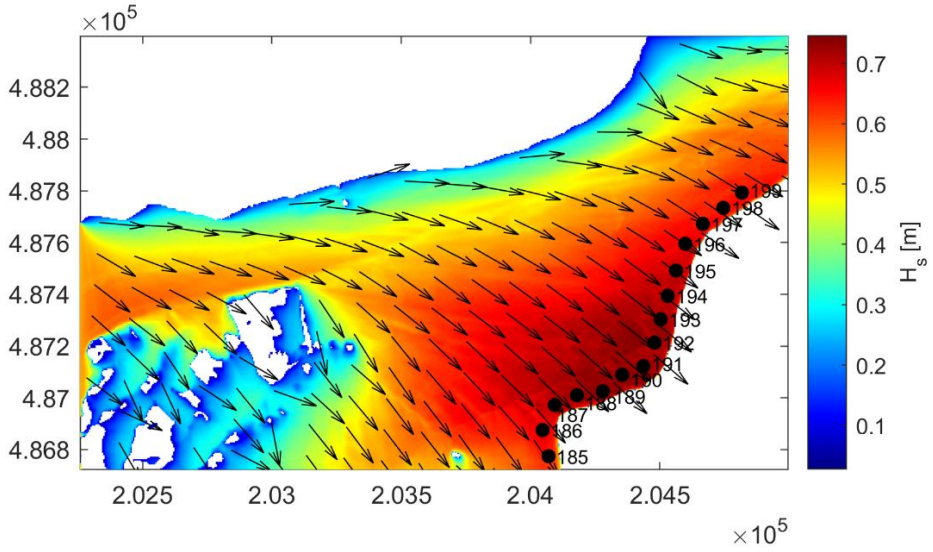

Figure E-49: Hs 190-NW-2100 no veg

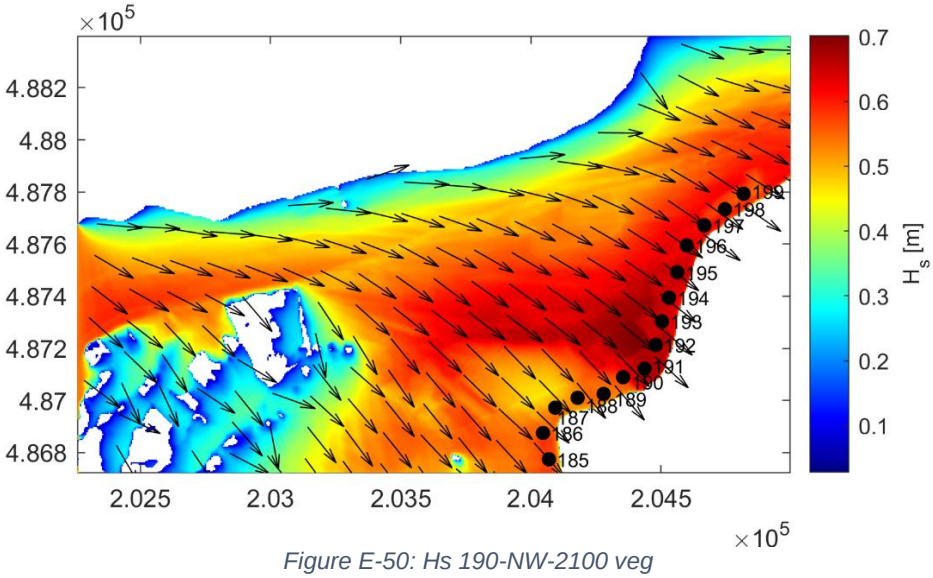

Figure E-50: Hs 190-NW-2100 veg

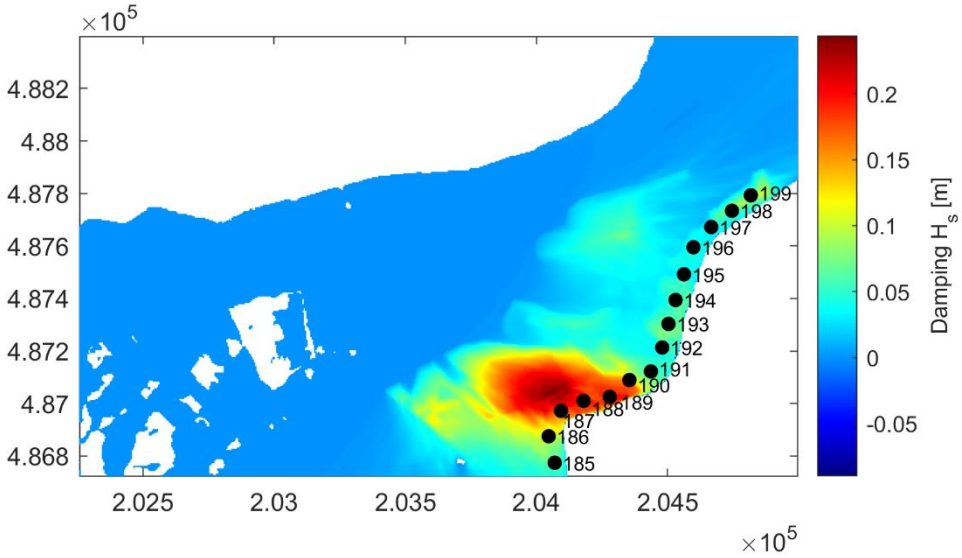

Figure E-51: Wave damping due to vegetation 190-NW-2100

190 WNW 2050:

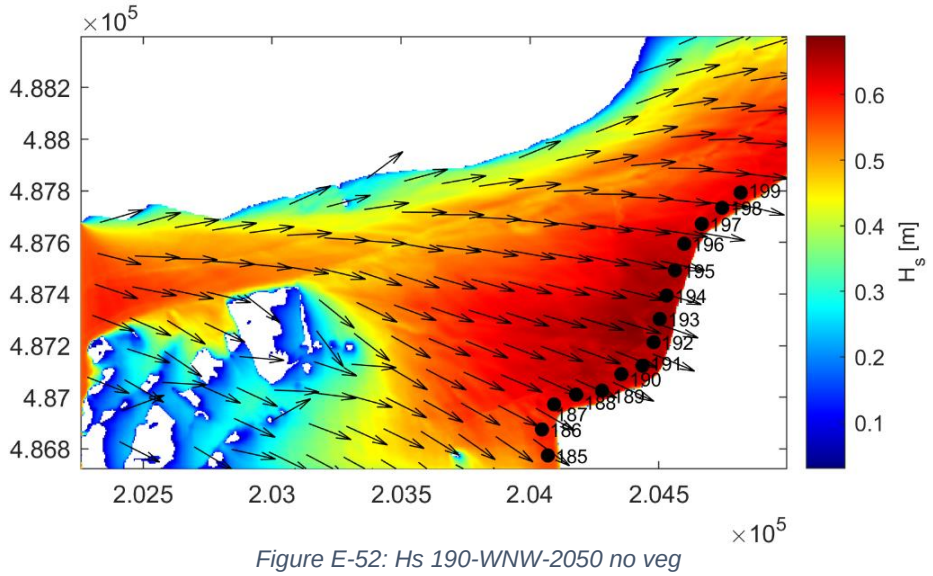

Figure E-52: Hs 190-WNW-2050 no veg

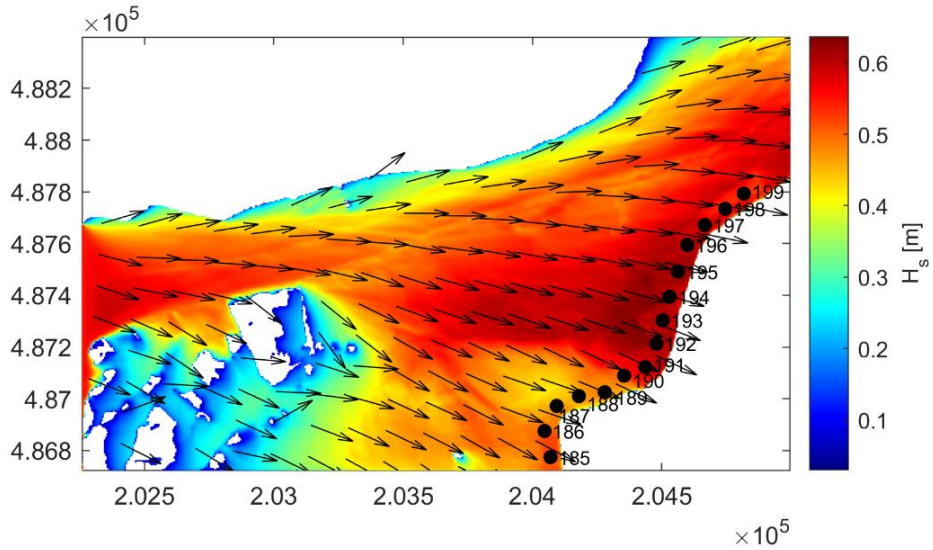

Figure E-53: Hs 190-WNW-2050 veg

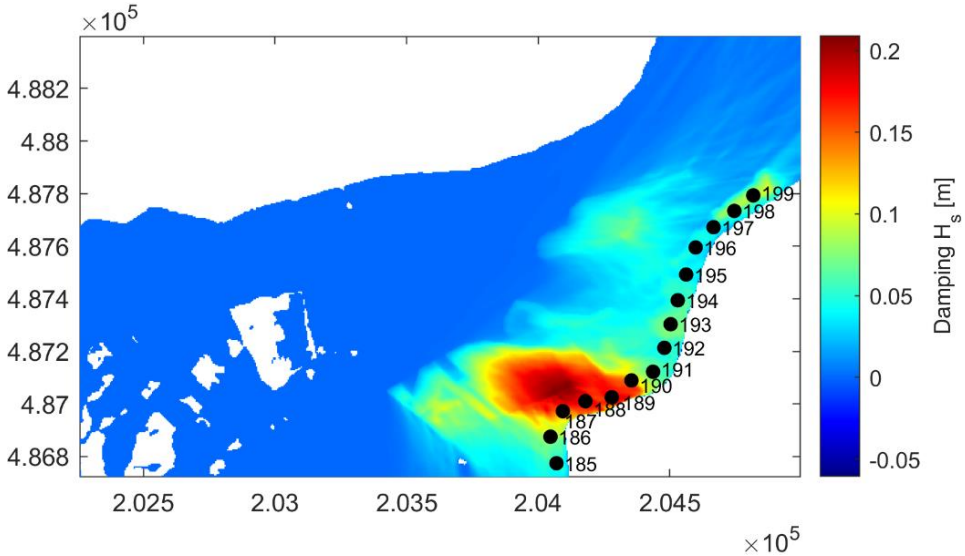

Figure E-54: Wave damping due to vegetation 190-WNW-2050

190 WNW 2100:

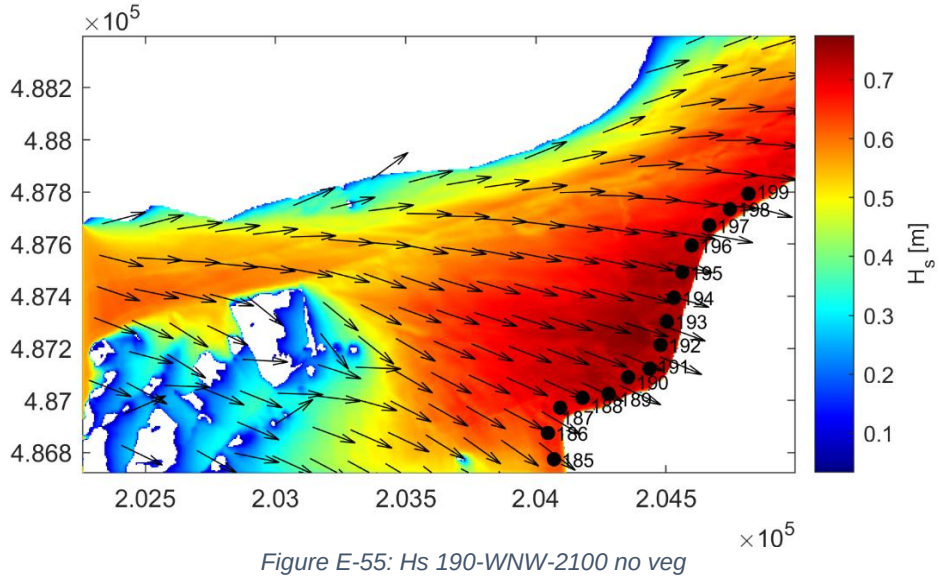

Figure E-55: Hs 190-WNW-2100 no veg

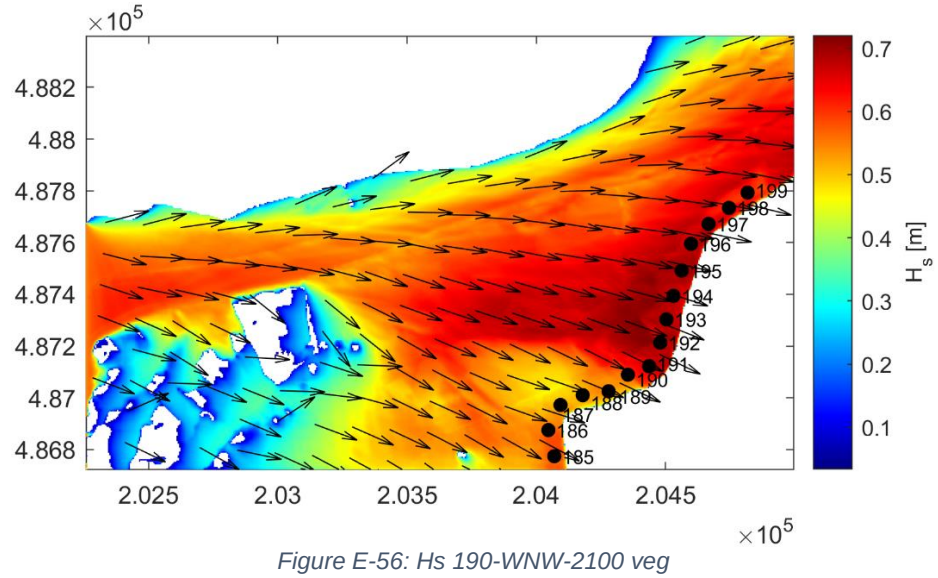

Figure E-56: Hs 190-WNW-2100 veg

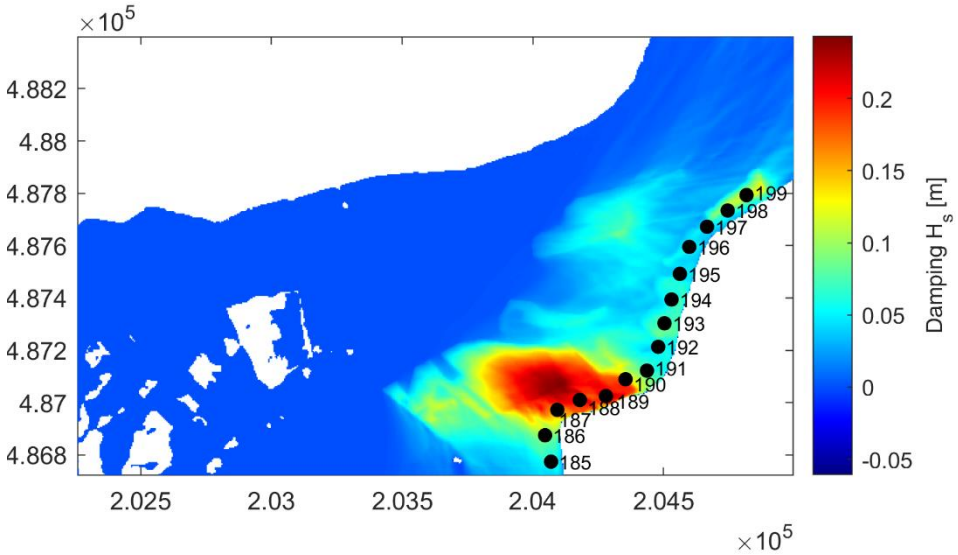

Figure E-57: Wave damping due to vegetation 190-WNW-2100

193 W 2050:

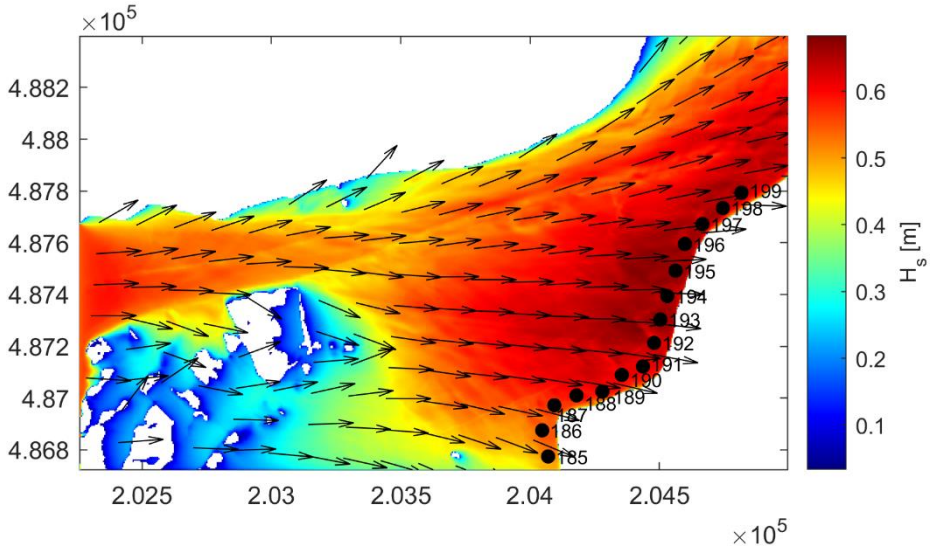

Figure E-58: Hs 193-W-2050 no veg

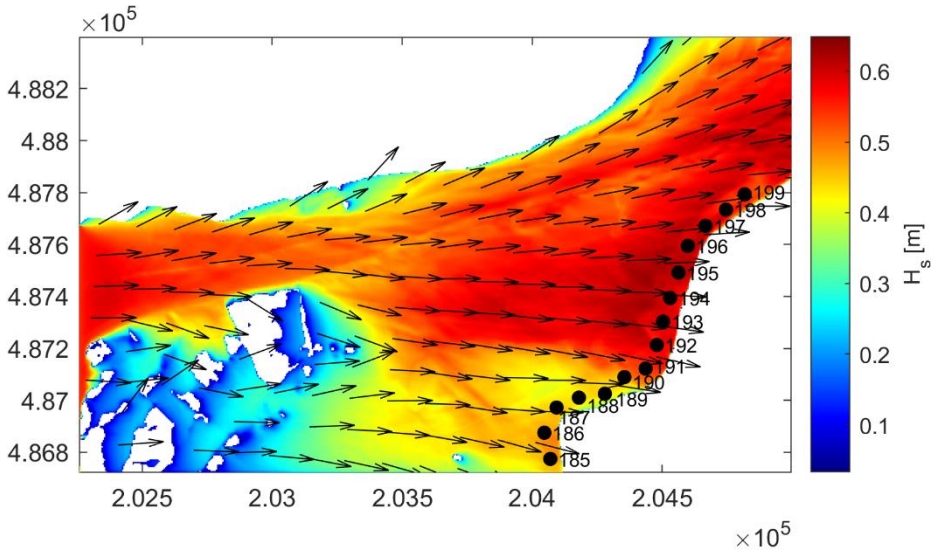

Figure E-59: Hs 193-W-2050 veg

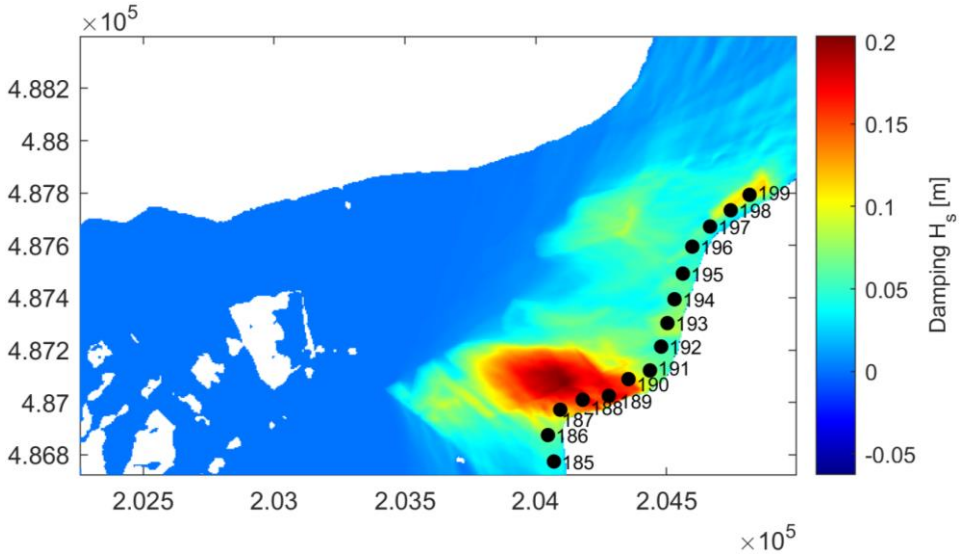

Figure E-60: Wave damping due to vegetation 193-W-2050

193 W 2100:

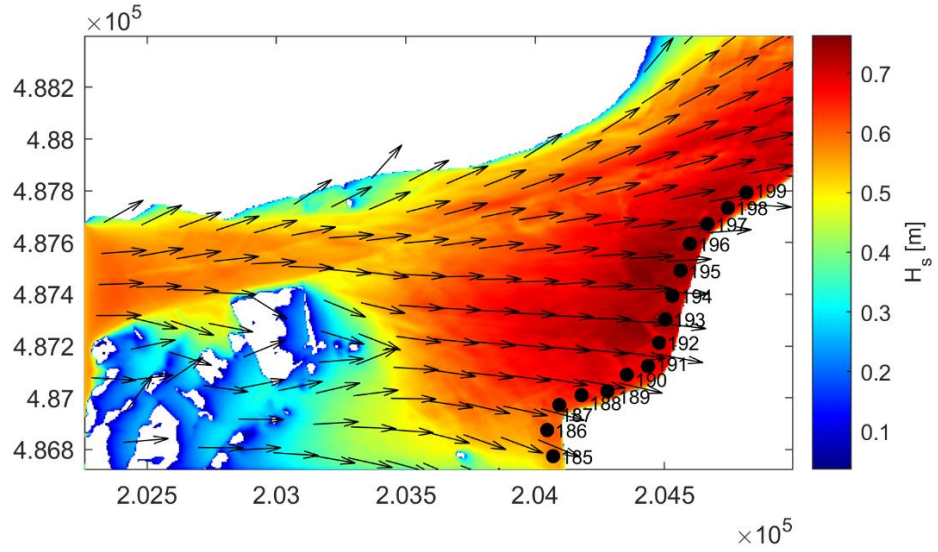

Figure E-61: Hs 193-W-2100 no veg

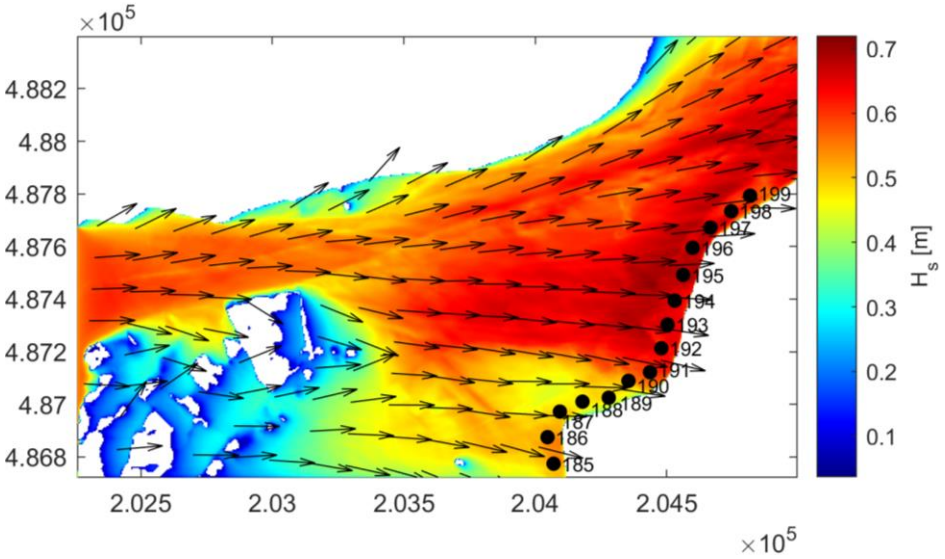

Figure E-62: Hs 193-W-2100 veg

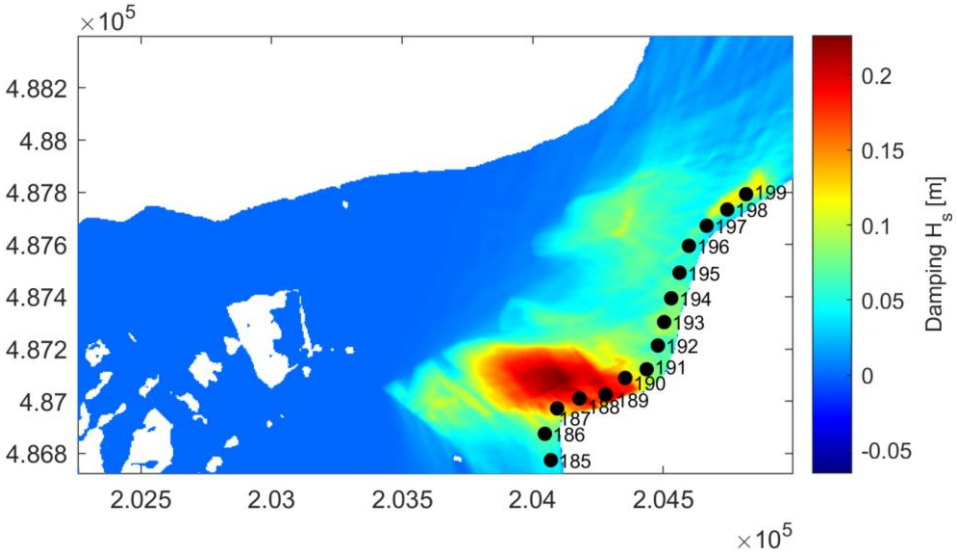

Figure E-63: Wave damping due to vegetation 193-W-2100

193 WNW 2050:

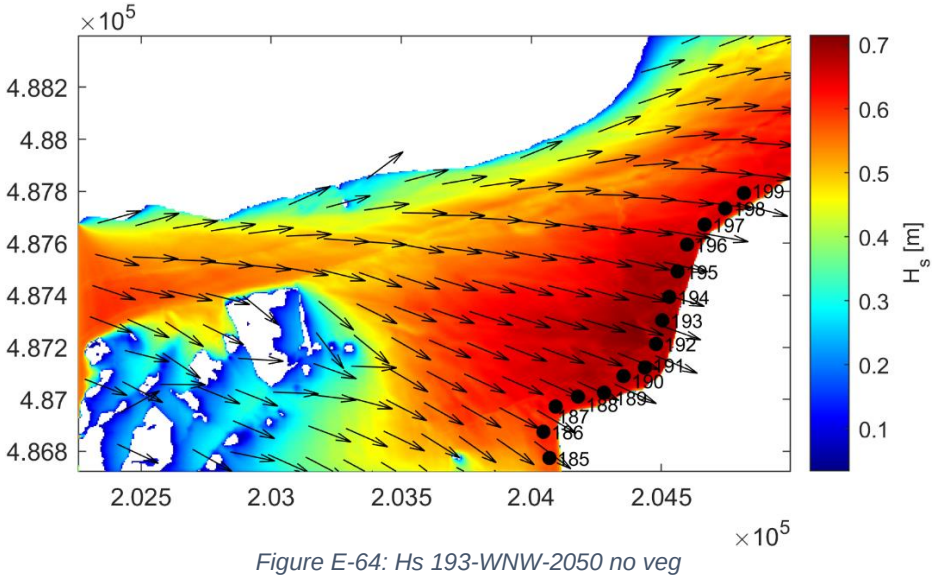

Figure E-64: Hs 193-WNW-2050 no veg

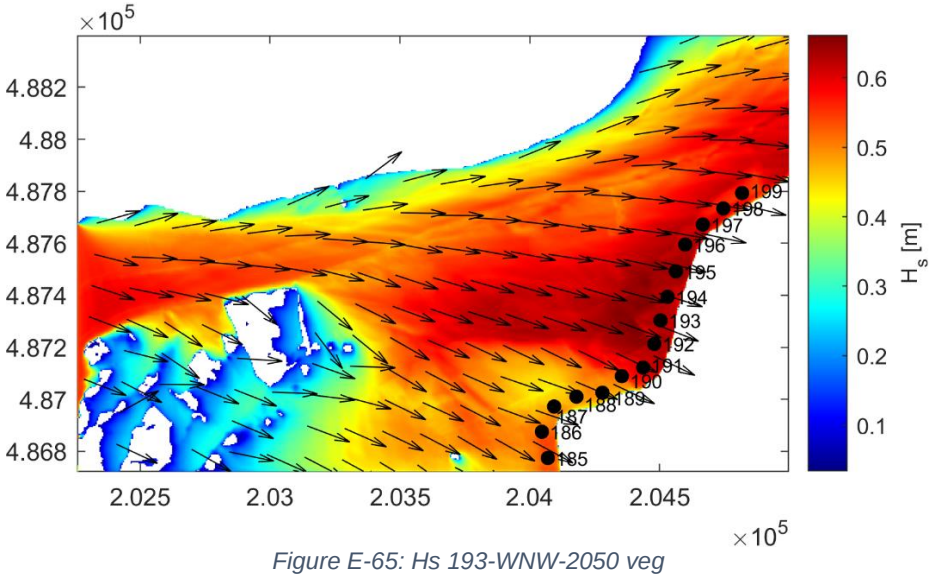

Figure E-65: Hs 193-WNW-2050 veg

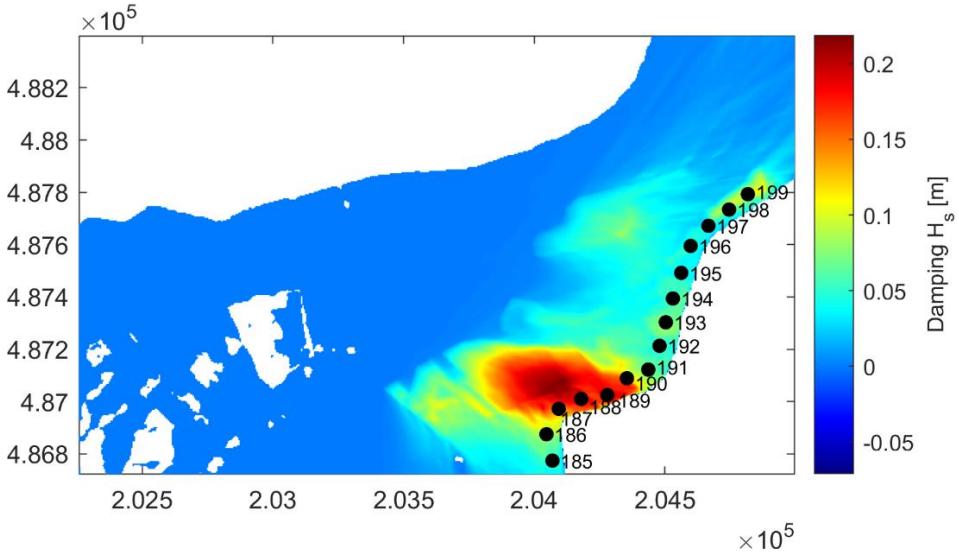

Figure E-66: Wave damping due to vegetation 193-WNW-2050

193 WNW 2100:

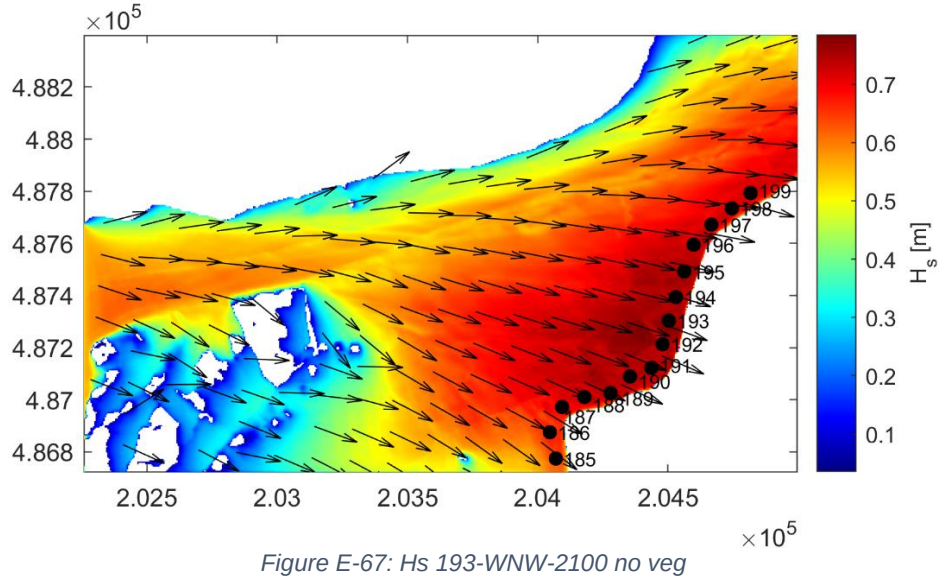

Figure E-67: Hs 193-WNW-2100 no veg

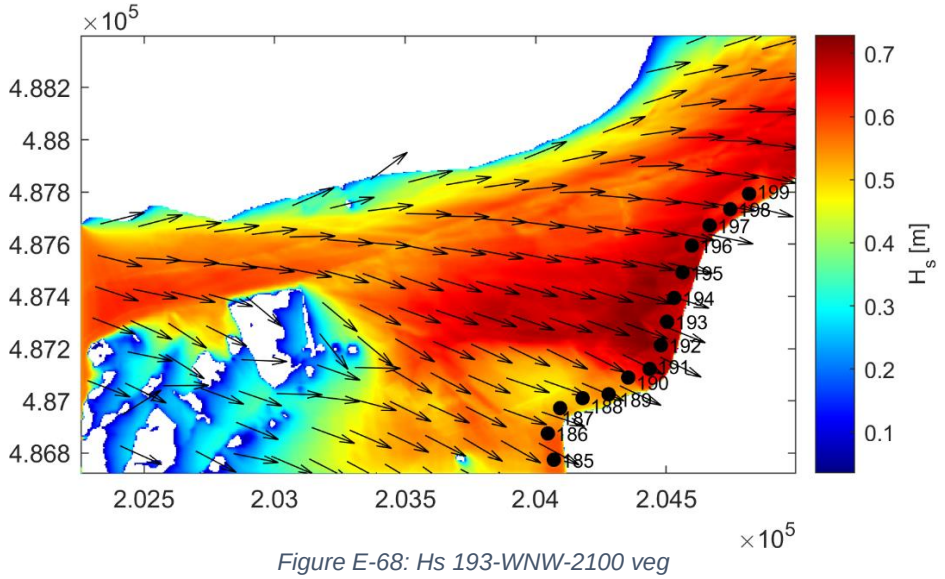

Figure E-68: Hs 193-WNW-2100 veg

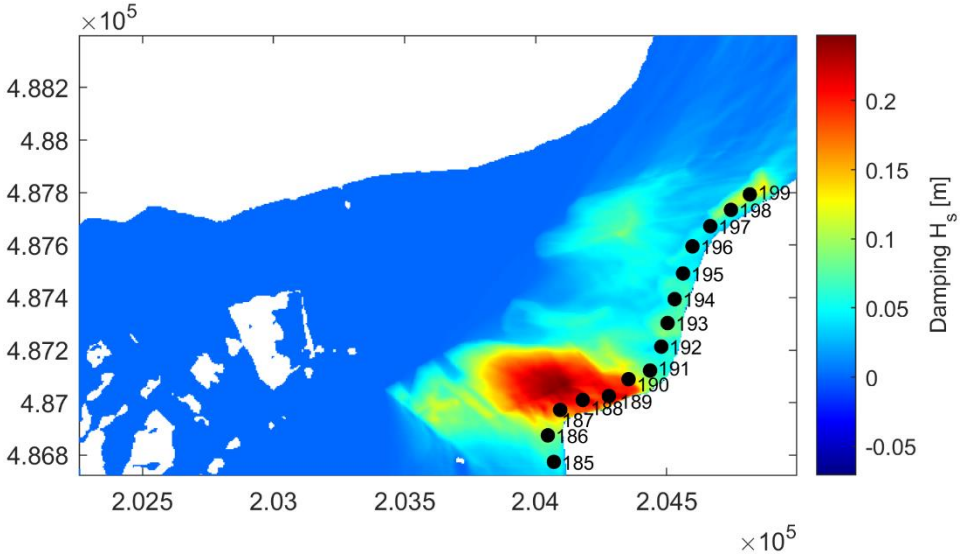

Figure E-69: Wave damping due to vegetation 193-WNW-2100

SWAN 2D results

Dike location	HC[1]	Input	Significant wave height, H_s [m] including model uncertainty			Reduction Hs [cm]	Relative peak period, T_p [s] including model uncertainty		
			2050	2100	2075	2075	2050	2100	2075
185	185-NW	No veg	0.704	0.698	0.701	5.9	2.719	2.721	2.720
		Veg	0.645	0.638	0.641		2.486	2.478	2.482
	185-WNW	No veg	0.593	0.644	0.619	5.7	2.600	2.688	2.644
		Veg	0.537	0.585	0.561		2.461	2.518	2.489
186	185-NW	No veg	0.755	0.747	0.751	11.4	2.646	2.654	2.650
		Veg	0.641	0.633	0.637		2.273	2.262	2.267
	185-WNW	No veg	0.610	0.666	0.638	9.2	2.530	2.600	2.565
		Veg	0.523	0.569	0.546		2.310	2.441	2.375
187	185-NW	No veg	0.807	0.796	0.801	21.4	2.780	2.753	2.767
		Veg	0.591	0.583	0.587		2.083	2.079	2.081
	185-WNW	No veg	0.626	0.683	0.655	16.1	2.544	2.657	2.601
		Veg	0.474	0.513	0.494		2.088	2.173	2.131
188	185-NW	No veg	0.851	0.840	0.846	23.2	2.895	2.872	2.883
		Veg	0.617	0.610	0.614		2.132	2.121	2.126
	185-WNW	No veg	0.671	0.736	0.704	19.6	2.736	2.795	2.766
		Veg	0.486	0.529	0.507		2.032	2.160	2.096
189	185-NW	No veg	0.851	0.840	0.846	23.9	2.933	2.898	2.916
		Veg	0.610	0.604	0.607		2.118	2.113	2.115
	185-WNW	No veg	0.677	0.742	0.710	20.3	2.759	2.885	2.822
		Veg	0.485	0.529	0.507		2.062	2.167	2.114
190	190-NW	No veg	0.736	0.732	0.734	13.2	2.726	2.724	2.725
		Veg	0.603	0.601	0.602		2.475	2.470	2.472
	190-WNW	No veg	0.650	0.737	0.693	14.4	2.660	2.732	2.696
		Veg	0.517	0.582	0.549		2.109	2.292	2.201
191	190-NW	No veg	0.725	0.722	0.723	5.5	2.706	2.705	2.706
		Veg	0.670	0.667	0.669		2.614	2.611	2.612
	190-WNW	No veg	0.647	0.731	0.689	6.7	2.617	2.723	2.670
		Veg	0.584	0.661	0.622		2.704	2.741	2.723
192	190-NW	No veg	0.702	0.699	0.700	4.5	2.514	2.507	2.511
		Veg	0.657	0.654	0.656		2.541	2.540	2.540
	190-WNW	No veg	0.632	0.711	0.671	4.9	2.496	2.563	2.530
		Veg	0.585	0.661	0.623		2.733	2.326	2.529

Table E-19: SWAN 2D results 185-192

[1] H.C. = Hydraulic condition

Dike location	HC	Input	Significant wave height, H_s [m] including model uncertainty			Reduction Hs [cm]	Relative peak period, T_p [s] including model uncertainty		
			2050	2100	2075	2075	2050	2100	2075
193	193-W	No veg	0.662	0.729	0.695	7.6	2.710	2.770	2.740
		Veg	0.588	0.652	0.620		2.682	2.755	2.718
	193-WNW	No veg	0.694	0.758	0.726	6.9	2.620	2.719	2.670
		Veg	0.627	0.688	0.657		2.663	2.731	2.697
194	193-W	No veg	0.641	0.710	0.675	6.3	2.705	2.754	2.730
		Veg	0.584	0.641	0.613		2.565	2.705	2.635
	193-WNW	No veg	0.675	0.736	0.705	5.7	2.596	2.697	2.646
		Veg	0.620	0.676	0.648		2.585	2.666	2.626
195	193-W	No veg	0.677	0.746	0.711	6.1	2.730	2.766	2.748
		Veg	0.616	0.685	0.650		2.616	2.735	2.675
	193-WNW	No veg	0.683	0.751	0.717	4.5	2.608	2.709	2.658
		Veg	0.642	0.703	0.673		2.558	2.622	2.590
196	193-W	No veg	0.670	0.742	0.706	6.4	2.738	2.777	2.758
		Veg	0.610	0.674	0.642		2.596	2.715	2.655
	193-WNW	No veg	0.673	0.740	0.706	5.3	2.551	2.652	2.602
		Veg	0.623	0.683	0.653		2.504	2.546	2.525
197	193-W	No veg	0.668	0.742	0.705	5.4	2.732	2.766	2.749
		Veg	0.616	0.687	0.651		2.601	2.723	2.662
	193-WNW	No veg	0.664	0.736	0.700	4.4	2.525	2.605	2.565
		Veg	0.623	0.688	0.656		2.498	2.539	2.519
198	193-W	No veg	0.635	0.699	0.667	8.1	2.707	2.742	2.725
		Veg	0.555	0.617	0.586		2.501	2.689	2.595
	193-WNW	No veg	0.645	0.712	0.679	8.2	2.502	2.555	2.528
		Veg	0.568	0.625	0.596		2.388	2.455	2.422
199	193-W	No veg	0.645	0.712	0.679	11.9	2.745	2.777	2.761
		Veg	0.531	0.588	0.559		2.549	2.726	2.638
	193-WNW	No veg	0.647	0.722	0.685	10.8	2.508	2.701	2.604
		Veg	0.550	0.603	0.577		2.457	2.446	2.452

Table E-20: SWAN 2D results 193-199

Difference H_s SWAN 1D and 2D

Dike location	HC	Input	Significant wave height, H_s [m] including model uncertainty	Significant wave height, H_s [m] including model uncertainty	Difference H_s: SWAN 1D - SWAN 2D [m]
			SWAN 1D	SWAN 2D	
			2075	2075	2075
185	185-NW	No veg	0.835	0.701	13.4
		Veg	0.716	0.641	7.5
	185-WNW	No veg	0.708	0.619	8.9
		Veg	0.635	0.561	7.4
186	185-NW	No veg	0.853	0.751	10.2
		Veg	0.639	0.637	0.2
	185-WNW	No veg	0.644	0.638	0.6
		Veg	0.552	0.546	0.6
187	185-NW	No veg	0.905	0.801	10.4
		Veg	0.574	0.587	-1.3
	185-WNW	No veg	0.751	0.655	9.6
		Veg	0.505	0.494	1.1
188	185-NW	No veg	0.921	0.846	7.5
		Veg	0.575	0.614	-3.9
	185-WNW	No veg	0.901	0.704	19.7
		Veg	0.485	0.507	-2.2
189	190-NW	No veg	0.964	0.846	11.8
		Veg	0.616	0.607	0.9
	190-WNW	No veg	0.945	0.710	23.5
		Veg	0.502	0.507	-0.5
190	190-NW	No veg	0.777	0.734	4.3
		Veg	0.589	0.602	-1.3
	190-WNW	No veg	0.854	0.693	16.1
		Veg	0.569	0.549	2.0
191	190-NW	No veg	0.770	0.723	4.7
		Veg	0.749	0.669	8.0
	190-WNW	No veg	0.853	0.689	16.4
		Veg	0.727	0.622	10.5
192	190-NW	No veg	0.741	0.700	4.1
		Veg	0.707	0.656	5.1
	190-WNW	No veg	0.833	0.671	16.2
		Veg	0.810	0.623	18.7

Table E-21: Difference Hs SWAN 1D and 2D 185-192

Dike location	HC	Input	Significant wave height, H_s [m] including model uncertainty	Significant wave height, H_s [m] including model uncertainty	Difference H_s: SWAN 1D - SWAN 2D [m]
			SWAN 1D	SWAN 2D	
			2075	2075	2075
193	193-W	No veg	0.795	0.695	10.0
		Veg	0.676	0.620	5.6
	193-WNW	No veg	0.839	0.726	11.3
		Veg	0.793	0.657	13.6
194	193-W	No veg	0.816	0.675	14.1
		Veg	0.781	0.613	16.8
	193-WNW	No veg	0.822	0.705	11.7
		Veg	0.732	0.648	8.4
195	193-W	No veg	0.959	0.711	24.8
		Veg	0.959	0.650	30.9
	193-WNW	No veg	0.778	0.717	6.1
		Veg	0.700	0.673	2.7
196	193-W	No veg	0.935	0.706	22.9
		Veg	0.813	0.642	17.1
	193-WNW	No veg	0.721	0.706	1.5
		Veg	0.618	0.653	-3.5
197	193-W	No veg	0.921	0.705	21.6
		Veg	0.791	0.651	14.0
	193-WNW	No veg	0.691	0.700	-0.9
		Veg	0.641	0.656	-1.5
198	193-W	No veg	0.884	0.667	21.7
		Veg	0.605	0.586	1.9
	193-WNW	No veg	0.682	0.679	0.3
		Veg	0.576	0.596	-2.0
199	193-W	No veg	0.895	0.679	21.6
		Veg	0.598	0.559	3.9
	193-WNW	No veg	0.666	0.685	-1.9
		Veg	0.555	0.577	-2.2

Table E-22: Difference Hs SWAN 1D and 2D 193-199

SWAN 2D results 185-NW all dike locations

Dike location	HC	Input	Significant wave height, H_s [m]			Reduction Hs [cm]	Relative peak period, T_p [s]		
			2050	2100	2075	2075	2050	2100	2075
185	185-NW	No veg	0.704	0.698	0.701	5.9	2.719	2.721	2.720
		Veg	0.645	0.638	0.641		2.486	2.478	2.482
186	185-NW	No veg	0.755	0.747	0.751	11.4	2.646	2.654	2.650
		Veg	0.641	0.633	0.637		2.273	2.262	2.267
187	185-NW	No veg	0.807	0.796	0.801	21.4	2.780	2.753	2.767
		Veg	0.591	0.583	0.587		2.083	2.079	2.081
188	185-NW	No veg	0.851	0.840	0.846	23.2	2.895	2.872	2.883
		Veg	0.617	0.610	0.614		2.132	2.121	2.126
189	185-NW	No veg	0.851	0.840	0.846	23.9	2.933	2.898	2.916
		Veg	0.610	0.604	0.607		2.118	2.113	2.115
190	185-NW	No veg	0.855	0.844	0.849	16.2	2.896	2.872	2.884
		Veg	0.691	0.682	0.687		2.698	2.695	2.696
191	185-NW	No veg	0.839	0.828	0.834	6.5	2.813	2.797	2.805
		Veg	0.774	0.763	0.768		2.740	2.734	2.737
192	185-NW	No veg	0.810	0.799	0.804	5.7	2.727	2.721	2.724
		Veg	0.753	0.741	0.747		2.657	2.630	2.644
193	185-NW	No veg	0.818	0.808	0.813	6.9	2.735	2.724	2.730
		Veg	0.749	0.739	0.744		2.597	2.582	2.590
194	185-NW	No veg	0.814	0.803	0.809	6.0	2.653	2.638	2.646
		Veg	0.753	0.743	0.748		2.534	2.524	2.529
195	185-NW	No veg	0.800	0.789	0.795	4.1	2.564	2.556	2.560
		Veg	0.759	0.748	0.753		2.519	2.509	2.514
196	185-NW	No veg	0.782	0.771	0.776	5.2	2.526	2.519	2.522
		Veg	0.729	0.718	0.724		2.495	2.486	2.490
197	185-NW	No veg	0.768	0.759	0.764	4.5	2.516	2.511	2.514
		Veg	0.724	0.713	0.718		2.491	2.481	2.486
198	185-NW	No veg	0.758	0.748	0.753	9.4	2.498	2.494	2.496
		Veg	0.664	0.654	0.659		2.398	2.365	2.381
199	185-NW	No veg	0.747	0.738	0.742	9.8	2.501	2.497	2.499
		Veg	0.650	0.640	0.645		2.466	2.453	2.459

Table E-23: SWAN 2D results 185-NW all dike locations

Vegetation parameters sensitivity analysis

Worst case scenario:

UMW-1			
Height [m]	$\frac{1}{V}\sum_{i=1}^{n} A_i\ [m^{-1}]$	$\widetilde{C}_D\ [-]$	**Vegetation factor:** $\frac{1}{V}\sum_{i=1}^{n} A_i * \widetilde{C}_D\ [m^{-1}]$
0.00-0.50	0.0254	1.0	0.0254
0.50-1.00	0.0301	1.0	0.0301
1.00-1.50	0.0227	1.0	0.0227
1.50-2.00	0.0203	1.0	0.0203
2.00-2.50	0.0186	1.0	0.0186
2.50-3.00	0.0199	1.0	0.0199
3.00-3.50	0.0197	1.0	0.0197
3.50-4.00	0.0339	0.9	0.0305
4.00-4.50	0.0236	1.0	0.0236
4.50-5.00	0.0289	0.9	0.0260
Average vegetation factor: 0.0237			

Table E-24: Vegetation parameters of vegetation area 1

Subarea 1			
Height [m]	$\frac{1}{V}\sum_{i=1}^{n} A_i\ [m^{-1}]$	$\widetilde{C}_D\ [-]$	**Vegetation factor:** $\frac{1}{V}\sum_{i=1}^{n} A_i * \widetilde{C}_D\ [m^{-1}]$
0.00-0.50	0	-	0
0.50-1.00	0	-	0
1.00-1.50	0	-	0
1.50-2.00	0	-	0
2.00-2.50	0	-	0
2.50-3.00	0	-	0
3.00-3.50	0	-	0
3.50-4.00	0	-	0
4.00-4.50	0	-	0
4.50-5.00	0	-	0
Average vegetation factor: 0			

Table E-25: Vegetation parameters of subarea 1

Subarea 2			
Height [m]	$\frac{1}{V}\sum_{i=1}^{n} A_i\ [m^{-1}]$	$\widetilde{C}_D\ [-]$	**Vegetation factor:** $\frac{1}{V}\sum_{i=1}^{n} A_i * \widetilde{C}_D [m^{-1}]$
0.00-0.50	0.0271	1.0	0.0271
0.50-1.00	0.0339	1.0	0.0339
1.00-1.50	0.0350	1.0	0.0350
1.50-2.00	0.0455	1.0	0.0455
2.00-2.50	0.0475	1.0	0.0475
2.50-3.00	0.0527	1.0	0.0527
3.00-3.50	0.0556	1.0	0.0556
3.50-4.00	0.0536	1.0	0.0536
4.00-4.50	0.0436	1.0	0.0436
4.50-5.00	0.0306	1.0	0.0306
Average vegetation factor: 0.0425			

Table E-26: Vegetation parameters of subarea 2

Subarea 3			
Height [m]	$\frac{1}{V}\sum_{i=1}^{n} A_i\ [m^{-1}]$	$\widetilde{C}_D\ [-]$	**Vegetation factor:** $\frac{1}{V}\sum_{i=1}^{n} A_i * \widetilde{C}_D [m^{-1}]$
0.00-0.50	0.0487	0.9	0.0438
0.50-1.00	0.0628	0.9	0.0566
1.00-1.50	0.0658	0.9	0.0592
1.50-2.00	0.0855	0.9	0.0769
2.00-2.50	0.0876	0.9	0.0788
2.50-3.00	0.0933	0.9	0.0840
3.00-3.50	0.0924	0.9	0.0832
3.50-4.00	0.0839	0.9	0.0755
4.00-4.50	0.0613	0.9	0.0552
4.50-5.00	0.0407	0.9	0.0366
Average vegetation factor: 0.0650			

Table E-27: Vegetation parameters of subarea 3

Subarea 4			
Height [m]	$\frac{1}{V}\sum_{i=1}^{n} A_i\ [m^{-1}]$	$\widetilde{C}_D\ [-]$	**Vegetation factor:** $\frac{1}{V}\sum_{i=1}^{n} A_i * \widetilde{C}_D [m^{-1}]$
0.00-0.50	0.0595	0.8	0.0476
0.50-1.00	0.0773	0.8	0.0619
1.00-1.50	0.0812	0.8	0.0649
1.50-2.00	0.105	0.8	0.0843
2.00-2.50	0.108	0.8	0.0861
2.50-3.00	0.114	0.8	0.0909
3.00-3.50	0.111	0.8	0.0887
3.50-4.00	0.0991	0.8	0.0793
4.00-4.50	0.0701	0.8	0.0561
4.50-5.00	0.0457	0.8	0.0366
Average vegetation factor: 0.0696			

Table E-28: Vegetation parameters of subarea 4

Subarea 5			
Height [m]	$\frac{1}{V}\sum_{i=1}^{n} A_i\ [m^{-1}]$	$\widetilde{C}_D\ [-]$	**Vegetation factor:** $\frac{1}{V}\sum_{i=1}^{n} A_i * \widetilde{C}_D [m^{-1}]$
0.00-0.50	0.0703	0.8	0.0562
0.50-1.00	0.0918	0.8	0.0734
1.00-1.50	0.0966	0.8	0.0773
1.50-2.00	0.125	0.8	0.100
2.00-2.50	0.128	0.8	0.102
2.50-3.00	0.134	0.8	0.107
3.00-3.50	0.129	0.8	0.103
3.50-4.00	0.114	0.8	0.0915
4.00-4.50	0.0789	0.8	0.0631
4.50-5.00	0.0508	0.8	0.0406
Average vegetation factor: 0.0815			

Table E-29: Vegetation parameters of subarea 5

UCW			
Height [m]	$\frac{1}{V}\sum_{i=1}^{n} A_i\ [m^{-1}]$	$\widetilde{C}_D\ [-]$	**Vegetation factor:** $\frac{1}{V}\sum_{i=1}^{n} A_i * \widetilde{C}_D [m^{-1}]$
0.00-0.50	0.0276	1.0	0.0276
0.50-1.00	0.0262	0.8	0.0210
1.00-1.50	0.0468	0.8	0.0374
1.50-2.00	0.124	0.8	0.0992
2.00-2.50	0.131	0.8	0.1048
2.50-3.00	0.120	0.8	0.0960
3.00-3.50	0.147	0.8	0.118
3.50-4.00	0.0618	0.9	0.0556
4.00-4.50	0.0666	0.8	0.0533
4.50-5.00	0.101	0.8	0.0808
Average vegetation factor: 0.0694			

Table E-30: Vegetation parameters of UCW

UMW-3			
Height [m]	$\frac{1}{V}\sum_{i=1}^{n} A_i\ [m^{-1}]$	$\widetilde{C}_D\ [-]$	**Vegetation factor:** $\frac{1}{V}\sum_{i=1}^{n} A_i * \widetilde{C}_D [m^{-1}]$
0.00-0.50	0.132	0.8	0.106
0.50-1.00	0.124	0.8	0.0992
1.00-1.50	0.145	0.8	0.116
1.50-2.00	0.144	0.8	0.115
2.00-2.50	0.151	0.8	0.121
2.50-3.00	0.154	0.8	0.123
3.00-3.50	0.155	0.8	0.124
3.50-4.00	0.145	0.8	0.116
4.00-4.50	0.164	0.6	0.0984
4.50-5.00	0.165	0.6	0.0990
Average vegetation factor: 0.112			

Table E-31: Vegetation parameters of UMW-3

Best case scenario:

UMW-1			
Height [m]	$\frac{1}{V}\sum_{i=1}^{n} A_i\ [m^{-1}]$	$\widetilde{C}_D\ [-]$	**Vegetation factor:** $\frac{1}{V}\sum_{i=1}^{n} A_i * \widetilde{C}_D\ [m^{-1}]$
0.00-0.50	0.0700	1.2	0.0840
0.50-1.00	0.0709	1.2	0.0851
1.00-1.50	0.0625	1.2	0.0750
1.50-2.00	0.0560	1.2	0.0672
2.00-2.50	0.0512	1.2	0.0614
2.50-3.00	0.0517	1.2	0.0620
3.00-3.50	0.0538	1.2	0.0646
3.50-4.00	0.0701	1.1	0.0771
4.00-4.50	0.0585	1.2	0.0702
4.50-5.00	0.0619	1.1	0.0681
Average vegetation factor: 0.0715			

Table E-32: Vegetation parameters of vegetation area 1

Subarea 1			
Height [m]	$\frac{1}{V}\sum_{i=1}^{n} A_i\ [m^{-1}]$	$\widetilde{C}_D\ [-]$	**Vegetation factor:** $\frac{1}{V}\sum_{i=1}^{n} A_i * \widetilde{C}_D\ [m^{-1}]$
0.00-0.50	0	-	0
0.50-1.00	0	-	0
1.00-1.50	0	-	0
1.50-2.00	0	-	0
2.00-2.50	0	-	0
2.50-3.00	0	-	0
3.00-3.50	0	-	0
3.50-4.00	0	-	0
4.00-4.50	0	-	0
4.50-5.00	0	-	0
Average vegetation factor: 0			

Table E-33: Vegetation parameters of subarea 1

Subarea 2			
Height [m]	$\frac{1}{V}\sum_{i=1}^{n} A_i\ [m^{-1}]$	$\widetilde{C}_D\ [-]$	**Vegetation factor:** $\frac{1}{V}\sum_{i=1}^{n} A_i * \widetilde{C}_D [m^{-1}]$
0.00-0.50	0.0709	1.2	0.0850
0.50-1.00	0.0916	1.2	0.110
1.00-1.50	0.0960	1.2	0.115
1.50-2.00	0.125	1.2	0.150
2.00-2.50	0.128	1.2	0.153
2.50-3.00	0.136	1.2	0.163
3.00-3.50	0.134	1.2	0.161
3.50-4.00	0.121	1.2	0.145
4.00-4.50	0.0877	1.2	0.105
4.50-5.00	0.0580	1.2	0.0696
Average vegetation factor: 0.126			

Table E-34: Vegetation parameters of subarea 2

Subarea 3			
Height [m]	$\frac{1}{V}\sum_{i=1}^{n} A_i\ [m^{-1}]$	$\widetilde{C}_D\ [-]$	**Vegetation factor:** $\frac{1}{V}\sum_{i=1}^{n} A_i * \widetilde{C}_D [m^{-1}]$
0.00-0.50	0.136	1.1	0.150
0.50-1.00	0.178	1.1	0.196
1.00-1.50	0.188	1.1	0.207
1.50-2.00	0.244	1.1	0.268
2.00-2.50	0.248	1.1	0.273
2.50-3.00	0.259	1.1	0.285
3.00-3.50	0.249	1.1	0.274
3.50-4.00	0.219	1.1	0.241
4.00-4.50	0.149	1.1	0.164
4.50-5.00	0.0954	1.1	0.105
Average vegetation factor: 0.216			

Table E-35: Vegetation parameters of subarea 3

Subarea 4			
Height [m]	$\frac{1}{V}\sum_{i=1}^{n} A_i\ [m^{-1}]$	$\widetilde{C}_D\ [-]$	**Vegetation factor:** $\frac{1}{V}\sum_{i=1}^{n} A_i * \widetilde{C}_D [m^{-1}]$
0.00-0.50	0.169	1.0	0.169
0.50-1.00	0.222	1.0	0.222
1.00-1.50	0.234	1.0	0.234
1.50-2.00	0.303	1.0	0.303
2.00-2.50	0.308	1.0	0.308
2.50-3.00	0.321	1.0	0.321
3.00-3.50	0.306	1.0	0.306
3.50-4.00	0.268	1.0	0.268
4.00-4.50	0.180	1.0	0.180
4.50-5.00	0.114	1.0	0.114
Average vegetation factor: 0.242			

Table E-36: Vegetation parameters of subarea 4

Subarea 5			
Height [m]	$\frac{1}{V}\sum_{i=1}^{n} A_i\ [m^{-1}]$	$\widetilde{C}_D\ [-]$	**Vegetation factor:** $\frac{1}{V}\sum_{i=1}^{n} A_i * \widetilde{C}_D [m^{-1}]$
0.00-0.50	0.202	1.0	0.202
0.50-1.00	0.265	1.0	0.265
1.00-1.50	0.280	1.0	0.280
1.50-2.00	0.363	1.0	0.363
2.00-2.50	0.368	1.0	0.368
2.50-3.00	0.383	1.0	0.383
3.00-3.50	0.364	1.0	0.364
3.50-4.00	0.317	1.0	0.317
4.00-4.50	0.211	1.0	0.211
4.50-5.00	0.133	1.0	0.133
Average vegetation factor: 0.289			

Table E-37: Vegetation parameters of subarea 5

UCW			
Height [m]	$\frac{1}{V}\sum_{i=1}^{n} A_i\ [m^{-1}]$	$\widetilde{C}_D\ [-]$	**Vegetation factor:** $\frac{1}{V}\sum_{i=1}^{n} A_i * \widetilde{C}_D [m^{-1}]$
0.00-0.50	0.149	1.2	0.179
0.50-1.00	0.142	1.0	0.142
1.00-1.50	0.159	1.0	0.159
1.50-2.00	0.235	1.0	0.235
2.00-2.50	0.236	1.0	0.236
2.50-3.00	0.215	1.0	0.215
3.00-3.50	0.239	1.0	0.239
3.50-4.00	0.154	1.1	0.169
4.00-4.50	0.150	1.0	0.150
4.50-5.00	0.186	1.0	0.186
Average vegetation factor: 0.191			

Table E-38: Vegetation parameters of UCW

UMW-3			
Height [m]	$\frac{1}{V}\sum_{i=1}^{n} A_i\ [m^{-1}]$	$\widetilde{C}_D\ [-]$	**Vegetation factor:** $\frac{1}{V}\sum_{i=1}^{n} A_i * \widetilde{C}_D [m^{-1}]$
0.00-0.50	0.365	1.0	0.365
0.50-1.00	0.343	1.0	0.343
1.00-1.50	0.401	1.0	0.401
1.50-2.00	0.397	1.0	0.397
2.00-2.50	0.417	1.0	0.417
2.50-3.00	0.427	1.0	0.427
3.00-3.50	0.428	1.0	0.428
3.50-4.00	0.401	1.0	0.401
4.00-4.50	0.455	0.8	0.364
4.50-5.00	0.457	0.8	0.366
Average vegetation factor: 0.391			

Table E-39: Vegetation parameters of UMW-3

F. Quickscan

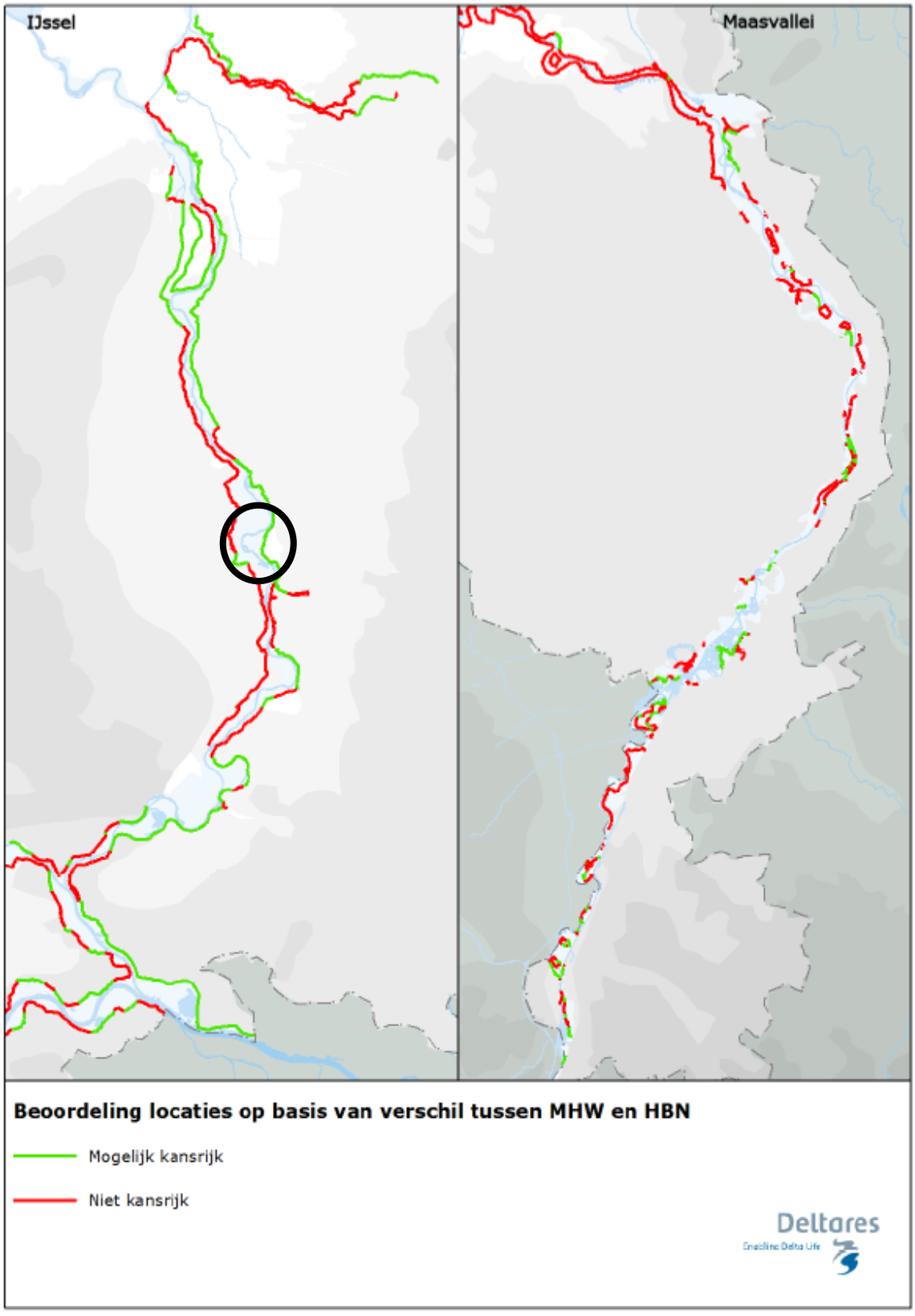

Figuur A.1 – Beoordeling locaties op basis van het verschil tussen MHW en HBN voor de IJssel en Maasvallei

Figure F-1: Assessment locations for promising wave damping foreshores river IJssel and Meuse. Duursche Waarden is outlined black.

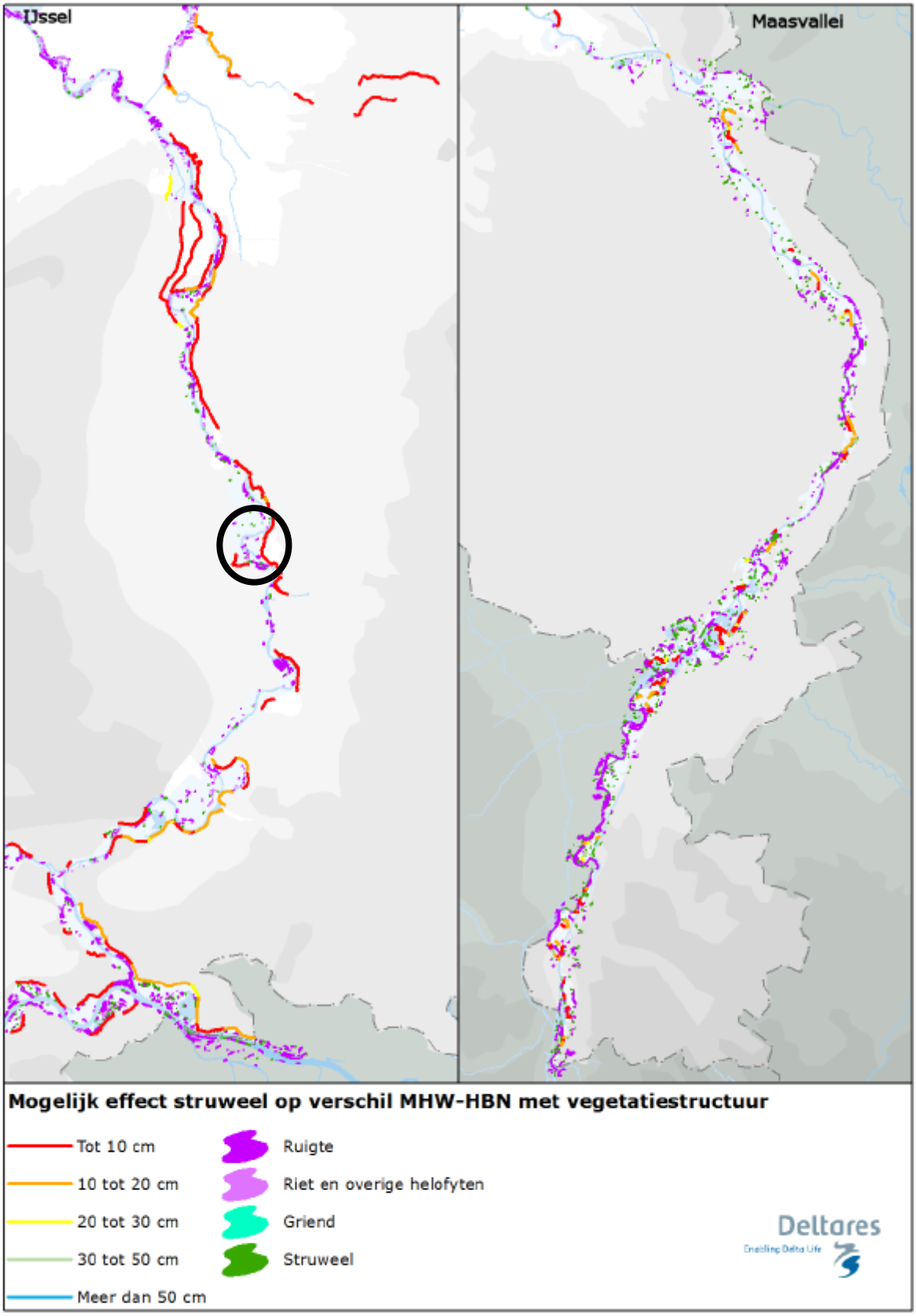

Figuur A.3 Mogelijk effect van struweel op het verschil tussen MHW en HBN, samen met een overzicht van de momenteel aanwezige vegetatietypen in de IJssel en Maasvallei.

Figure F-2: Possible effect for promising wave damping foreshores river IJssel and Meuse. Duursche Waarden is outlined black.